GEOLOGICAL ANALYSIS OF PARTS OF THE SOUTHERN ARABIAN SHIELD BASED ON LANDSAT TM IMAGERY

by

Mohammed Yousef Hedaytullah T. QARI

A thesis
submitted for the degree of
Doctor of Philosophy

Department of Geological Sciences
University College London
1990

ABSTRACT

This thesis examines the capability and applicability of Landsat multispectral remote sensing data for geological analysis in the arid southern Arabian Shield, which is the eastern segment of the Nubian-Arabian Shield surrounding the Red Sea. The major lithologies in the study area are Proterozoic metavolcanics, metasediments, gneisses and granites.

Three test-sites within the study area, located within two tectonic assemblages, the Asir Terrane and the Nabitah Mobile Belt, were selected for detailed comparison of remote sensing methods and ground geological studies. Selected digital image processing techniques were applied to full-resolution Landsat TM imagery and the results are interpreted and discussed. Methods included: image contrast improvement, edge enhancement for detecting lineaments and spectral enhancement for geological mapping. The last method was based on two principles, statistical analysis of the data and the use of arithmetical operators. New and detailed lithological and structural maps were constructed and compared with previous maps of these sites.

Examples of geological relations identified using TM imagery include: recognition and mapping of migmatites for the first time in the Arabian Shield; location of the contact between the Asir Terrane and the Nabitah Mobile Belt; and mapping of lithologies, some of which were not identified on previous geological maps. These and other geological features were confirmed by field checking.

Methods of lineament enhancement implemented in this study revealed structural lineaments, mostly mapped for the first time, which can be related to regional tectonics.

Structural analysis showed that the southern Arabian Shield has been affected by at least three successive phases of deformation. The third phase is the most dominant and widespread. A crustal evolutionary model in the vicinity of the study area is presented showing four stages, these are: arc stage, accretion stage, collision stage and post-collision stage.

The results of this study demonstrate that Landsat TM data can be used reliably for geological investigations in the Arabian Shield and comparable areas, particularly to generate detailed geological maps over large areas by using quantitative remote sensing methods, providing there is prior knowledge of part of the area.

This Thesis is dedicated to my dear father, respected mother, wife, son Jihad, daughters Abrar and Anwaar, and to my dear brothers and sisters.

ACKNOWLEDGMENTS

TABLE OF CONTENTS

LIST OF FIGURES

LIST OF PLATES

LIST OF TABLES

CHAPTER ONE   INTRODUCTION

1.1 BACKGROUND

1.2 LOCATION

1.3 PHYSIOGRAPHY

1.4 CLIMATE AND VEGETATION

1.5 ARABIAN SHIELD GEOLOGY

    1.5.1 Introduction

    1.5.2 History and stratigraphy

    1.5.3 Evolution of ideas for the Arabian Shield

    1.5.4 Summary of Arabian Shield evolution

1.6 PURPOSE OF PRESENT STUDY

1.7 STRUCTURE OF THE THESIS

1.8 METHODS OF INVESTIGATION

1.1 BACKGROUND

Remotely sensed data in the form of aerial photographs have been used for many years as a major tool for field geologists. The photographic remote sensing spectral region is the wavelength range from ultraviolet (UV) 0.3 μm to infrared (IR) 0.9 μm. The aerial photographs record light reflected by a surface, which is determined by the property called "albedo", which is the radiant reflectance of a surface, and is the ratio of the reflected to the incident energy. So, light surfaces have a high albedo and dark surfaces have a low albedo. The disadvantage of air photography is the radial optical distortion.

Saudi Arabia is one of the few countries in the world with complete aerial photographic coverage. Some areas have been rephotographed for different applications.

Since NASA's first Earth Resources Technology Satellite (ERTS-1), now changed to LANDSAT, was launched into orbit in July 1972 and followed by Landsat series, satellites have delivered high-resolution and multispectral images of the earth providing new sources of geological information. Landsat 4 and 5 are now in operation with improved spatial and spectral resolution. They carry a four-channel Multi-Spectral Scanner (MSS) and a seven band multispectral scanner, which is known as Thematic Mapper (TM).

Saudi Arabia is covered by Landsat MSS and TM imagery, though quality of imagery varies from one location to another. In addition, a satellite receiving station has been in operation since January 1987 in Riyadh, which is equipped to receive from different satellites.

The result of integrating the spectral imagery capability and the digital image processing was a significant turn away from the use of standard photo interpretation techniques on aerial photographs to an expanded use of the spectral properties of surface materials for mapping and discrimination (Goetz and Rowan, 1981).

Interpretation of Landsat images has been widely accepted by the geological community. Excellent interpretations of regional structures can be made from the satellite images (e.g. Blodget et al., 1978; Sultan et al., 1988). The results described in this study are primarily concerned with the applications of remote sensing in the visible,

near-, and mid-infrared wavelength regions (0.45 - 2.35 µm), mainly using multispectral data recorded by the Landsat TM sensor.

An arid region such as the Precambrian Arabian-Nubian Shield, provides an excellent area to test the capabilities of remote sensing data for geological studies. It includes a wide variety of rock types and structures. Individual rock units are exposed in large and fairly homogeneous bodies. Due to the arid climate there is little chemical weathering and most of the area is nearly devoid of vegetation.

1.2 LOCATION

The study area, located within the southern part of the Arabian Shield, is a part of the Asir quadrangle (Brown and Jackson, 1959). The area lies within latitudes 18°-20°N and longitudes 42°-44°E (Fig. 1.1). However, Landsat satellite image boundaries are not parallel to the latitudes and longitudes mentioned. A Landsat scene covering the study area is shown in Figures 1.1 and 1.2, where the scene centre point is at 18°47'N and 43°00'E. The area is 185x185 km, which is the approximate coverage of one full Landsat scene.

The aim of the study was to use full-resolution enhancement techniques to verify and evaluate the applicability of Landsat Thematic Mapper (TM) sensor digital imagery for geological investigations. The study area is very large, about 34,000 km^2, and therefore it was necessary to select test areas within the study area. Three test areas were selected, these are called 1, 2, and 3 (Fig. 1.3).

The selection of these three test-sites was based on the excellent exposure of a diverse suite of igneous and metamorphic rocks, interesting structural pattern, location of the test-site within the tectonic assemblages of the southern Arabian Shield (Asir Terrane and Nabitah Mobile Belt), and the availability of detailed geological studies conducted on the ground, particularly for the test-site area No.1. The availability of detailed ground study of the test-site No.1 provided a unique test-site for Landsat data and their ability to detect variation in the geology.

The study area is easily accessible in most parts, especially in the southwestern quarter and along the north-south asphalt roads in the middle of the area, where cities and towns are located. Test-sites No.1 and 2 are easily accessible via asphalt roads and/or
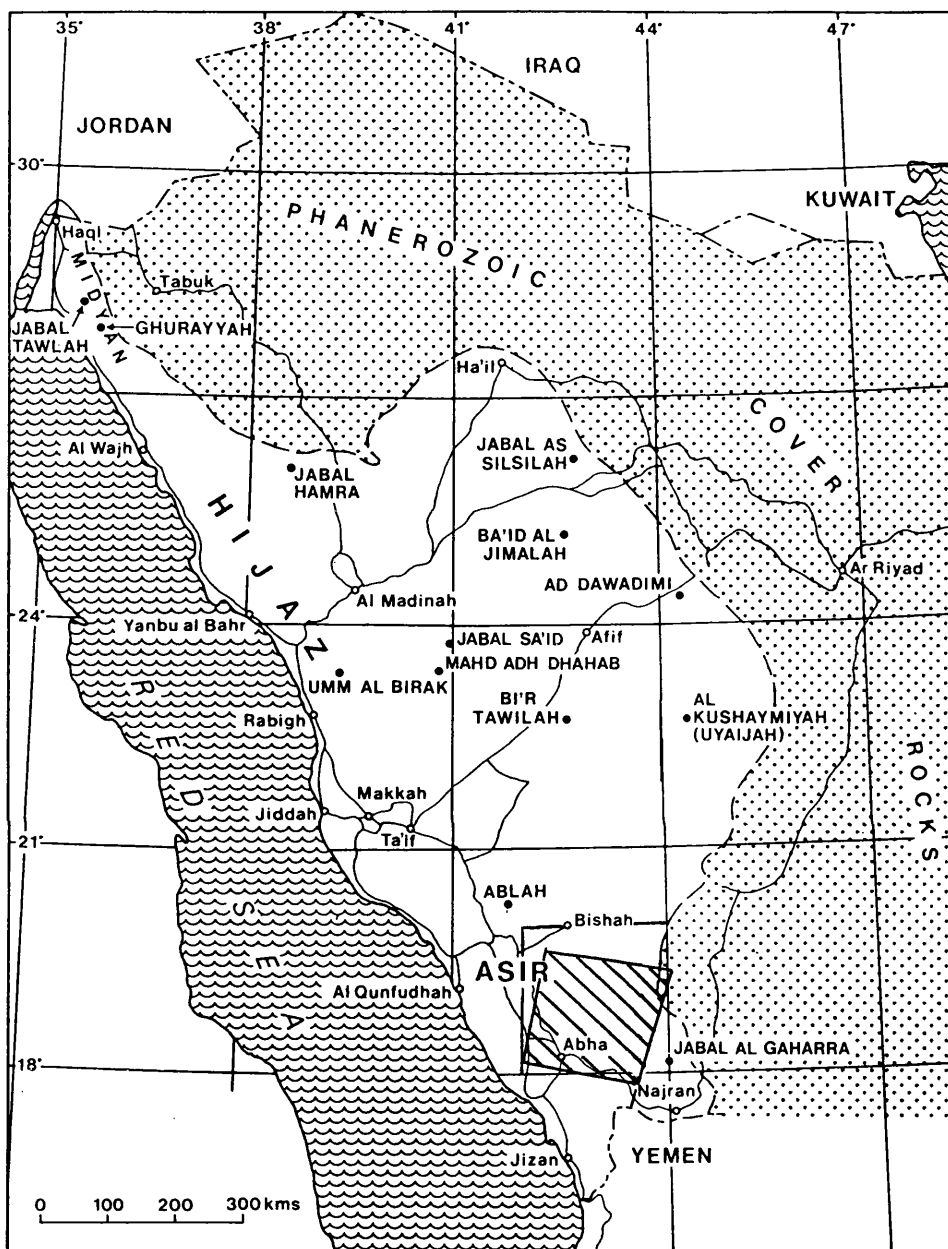
Fig. 1.1 Location map of the study area.
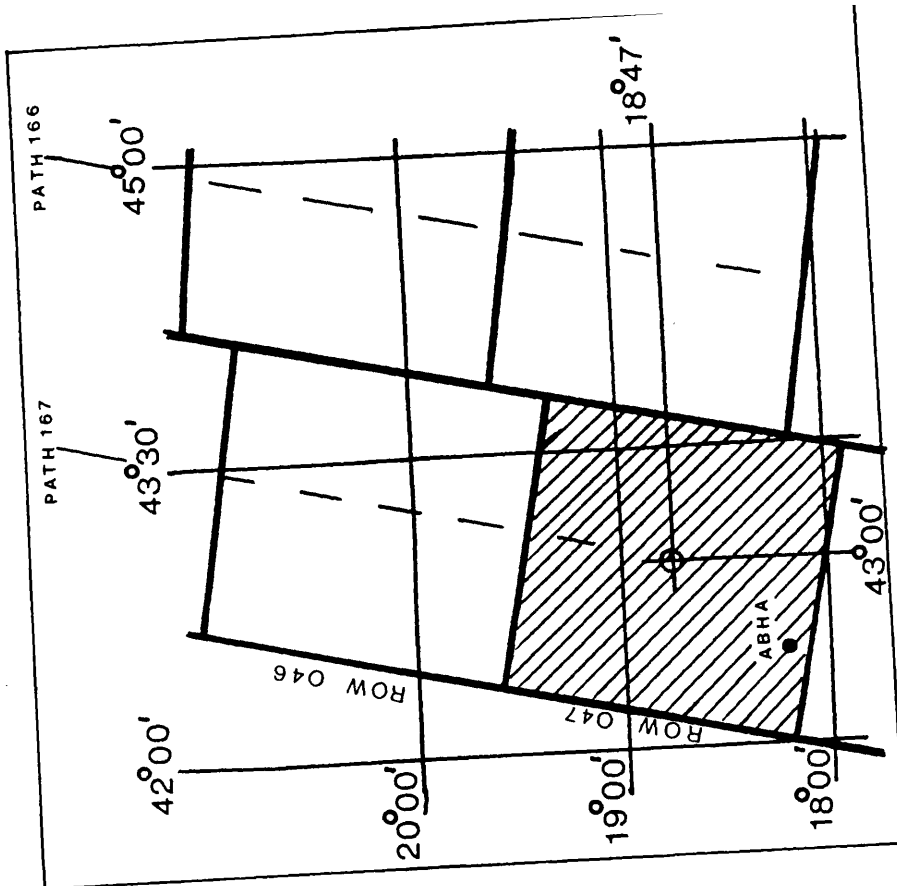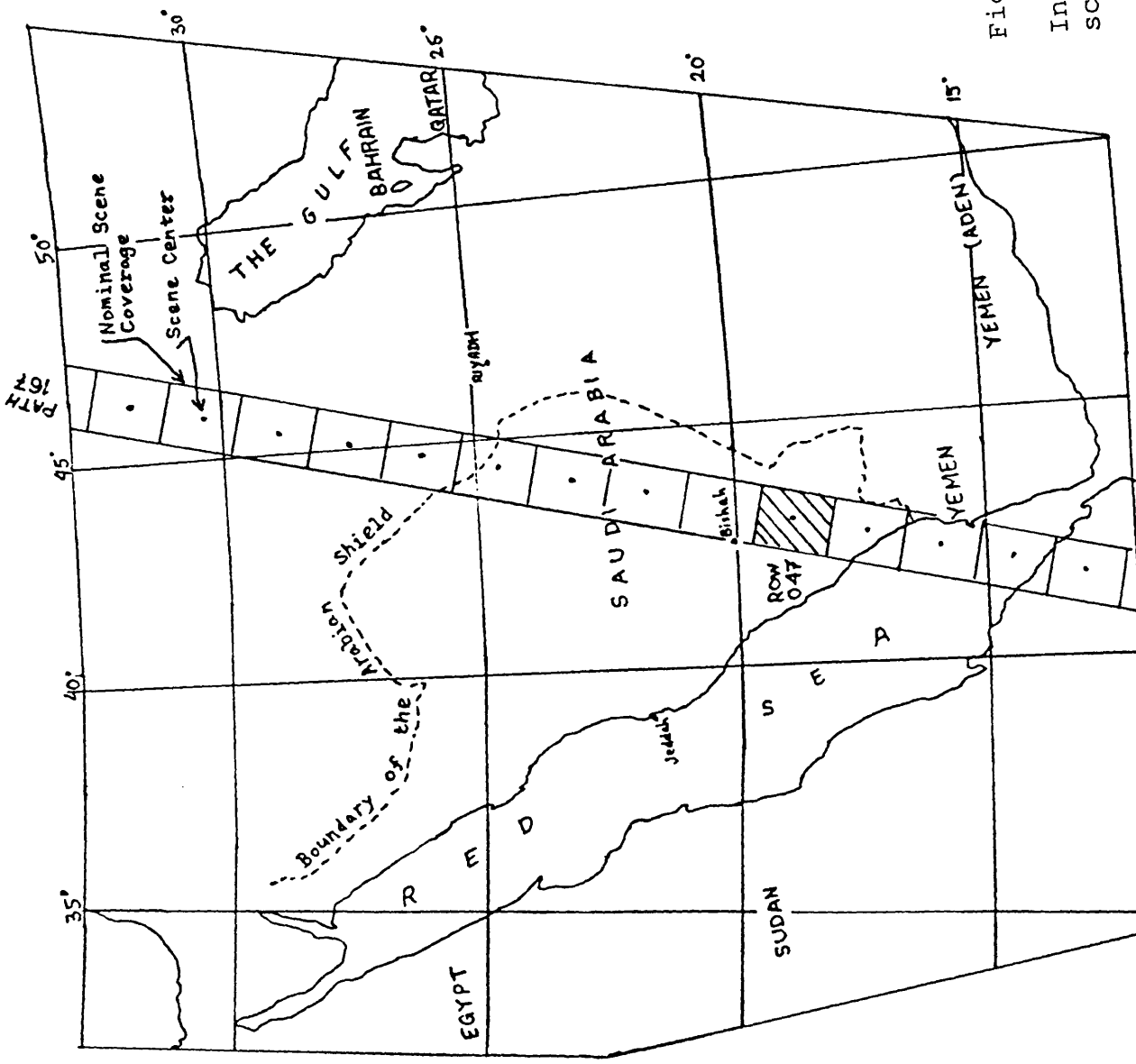
Fig. 1.2

Index and enlarged map showing Landsat 4/5 WRS
scene centers of Path 167 in the Arabian Peninsul

5
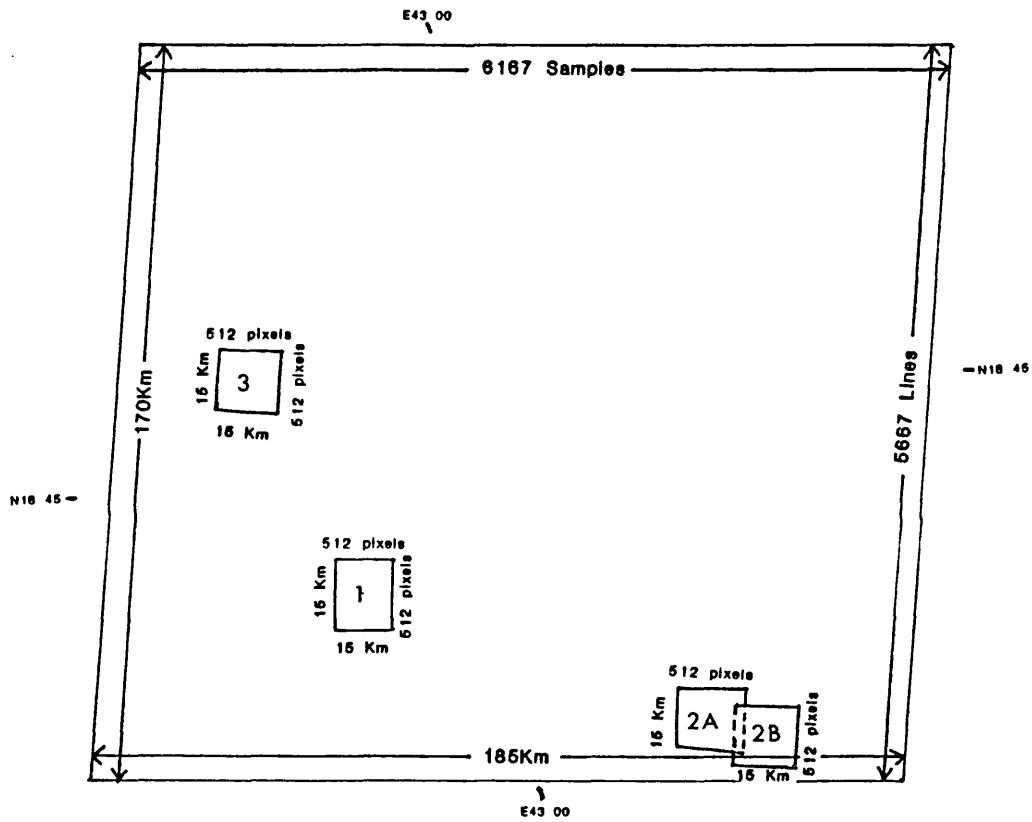
Fig. 1.3 The location of the three test-sites selected for full-resolution studies within the study area (Full TM scene, WRS 167/47).

desert tracks, whereas test-site No.3 can be reached only via rough desert tracks.

1.3 PHYSIOGRAPHY

The Arabian Shield of western Saudi Arabia is on the eastern flank of the Arabian-Nubian Shield which is split by the Red Sea depression and rift.

The study area is a part of Asir province which is geographically the southwestern segment of the Kingdom of Saudi Arabia. Topographically, the area consists of, from southwest to northeast, Tihamah or the Coastal Plain, the Asir Escarpment, and the Hijaz Plateau. The Hijaz Plateau slopes gradually to the east (towards the Arabian Gulf) merging with the Najd Pediplane in the centre of the Arabian Peninsula. The escarpment, where elevations reach 3000 metres above mean sea level, has resulted from uplift of the shield associated with the formation of the Red Sea rift which began about 20 Ma ago, and is the watershed of the Arabian Peninsula between the Red Sea and the Arabian Gulf (Plate 1).

The major drainage channels in the study area flow north into the interior of the shield. In the northeastern corner a dendritic drainage pattern is developed on Phanerozoic sandstones (Wajid Sandstones) overlying the crystalline rocks of the shield. In the southwestern corner, the drainage pattern from the Asir Escarpment is completely different, with steep, narrow, structurally controlled wadis running westward towards the Red Sea Coastal Plain (Plate 1).

1.4 CLIMATE AND VEGETATION

The climate is cool during summer and cold in winter due to the high elevation in the western half of the study area. The daily and seasonal temperature variations are significant and average about 15°C. The eastern half of the area is also cold in winter but it is generally hot in summer. The rainy season is normally between June and October. During this season, short grass appears on the slopes of hills and small bushes in low lands. Many fruit and vegetable plantations are established in the villages and towns along the wadis.

1.5 ARABIAN SHIELD GEOLOGY

1.5.1 Introduction

This study area is part of the southern Arabian Shield, which has been the subject of many geological studies since the 1950s. The Arabian Shield is a region of Precambrian crystalline and metamorphic rocks forming the basement of the western part of the Arabian Peninsula. It covers an area of about 670,000 km² (one-third of the Arabian Peninsula), and is separated from the Nubian Shield in the west by the Red Sea graben (Fig. 1.4). These rocks are overlain in the north and east by a Phanerozoic sedimentary cover; these are thickest in the Arabian Gulf area (sedimentary rocks exceeding 6000 metres).

1.5.2 History and stratigraphy

Richter-Bernburg and Schott (1954), von-Gartner and Schurenberg (1954) made the earliest geological reconnaissance exploration surveys in the shield. Karpoff (1957a and 1960) was the earliest to describe the region as a shield. In 1955, under an agreement between Saudi Arabia and the United States Department of State, the Arabian American Oil Company (ARAMCO) began a major geological mapping programme. This programme of photogeological interpretation and field work resulted in the publication of a series of 1:500,000-scale geological maps covering the whole Arabian Peninsula. The first sheet, published in 1959, covered the Asir quadrangle (Brown and Jackson, 1959). By presenting their map and conclusions at the 21st International Geological Congress in Copenhagen, Brown and Jackson (1960) provided the first significant discussion of the geology of the Arabian Shield in English. They noted that the structural trend in the southern part of the shield is north to northeast, parallel to the faulting.

In the late 1960s, a half-degree 1:100,000-scale mapping programme was started by the Saudi Arabian Directorate General of Mineral Resources (DGMR). This programme aimed to unravel and understand the Precambrian geological history of Saudi Arabia so that economic studies could be set in a regional framework (Schmidt et al., 1972). About seventeen of the 1:100,000-scale map sheets cover the study area (Fig. 1.5) [Anderson (1977; 1979); Coleman (1973a; 1973b); Cornwall (1973), Greenwood (1979a; 1979b; 1980); Overstreet (1978); Prinz (1975); Ratte and Andreasen (1974); Simmons (1980); Stoeser (1984); Warden (1982)].
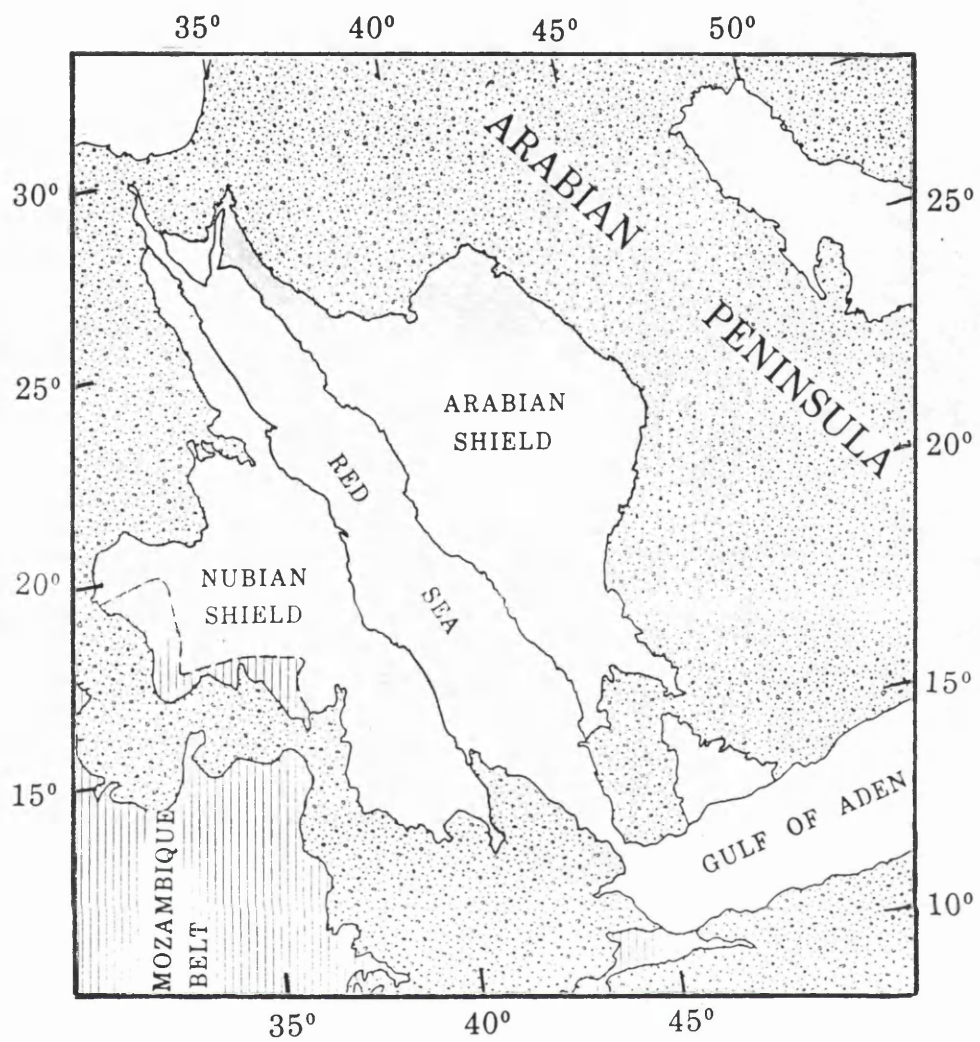
Fig. 1.4 Location of the Arabian and the Nubian Shields.

Subsequently, a one and half-degree compilation-map series programme at 1:250,000-scale by the DGMR began in 1970. About six of these maps (Fig. 1.6) cover the study area [Fairer (1985); Greenwood (1985a; 1985b; 1985c); Greenwood et al. (1986); Sable (1985)].

Following the publication of the Arabian Peninsula geological map by Brown and Jackson (1963), Brown studied the tectonic framework of the area and evaluated the then current interpretations of tectonics in order to compile a tectonic map of the Arabian Peninsula. His tectonic map was published in 1972. In addition to the map (Brown, 1972), Brown and Coleman (1972) presented a paper about the tectonic framework, in which the concept of tectonic cycles was applied to the Arabian Shield for the first time. Their study of the plutonic rocks made an essential contribution to the development of geotectonic models of the shield.

They recognised, from oldest to youngest, the Kibaran cycle, the Hijaz cycle, and the Najd orogeny. The Kibaran cycle was named after the Kibaran Orogeny in Africa because the radiometric data available indicated a correlation with a plutonic episode in the Arabian Shield at about 1000 Ma. During this cycle, basement gneisses, believed to represent the oldest rocks in the shield, and their overlying greenstones, were deformed and metamorphosed. In some places the gneisses form diapiric intrusions along northwest trending transverse faults, and in others they appear to have been remobilized during later orogenies.

The Hijaz cycle is the most widely represented and longest-lasting orogenic event, particularly in the southern part of the shield. It is characterized by metamorphism of eugeosynclinal rocks to the greenschist and amphibolite facies, and also the development of north- to north-northeast-trending folds and faults. The cycle includes syn-tectonic and granodioritic gneisses of 800-500 Ma, and late-tectonic calc-alkalic granites of 650-600 Ma.

The Najd orogeny, which affects the region outside the study area, is characterized by strike-slip faulting with left-lateral displacement of about 240km, calculated from the amount of offset of ophiolites along a north-trending suture, the "Nabitah Suture". Late- to post-tectonic granites, intruded during the climax of the Najd orogeny, are about 570 Ma old. At this time the tensional evaporite basin of the Hormuz Salt Formation developed on the far eastern side of the shield.
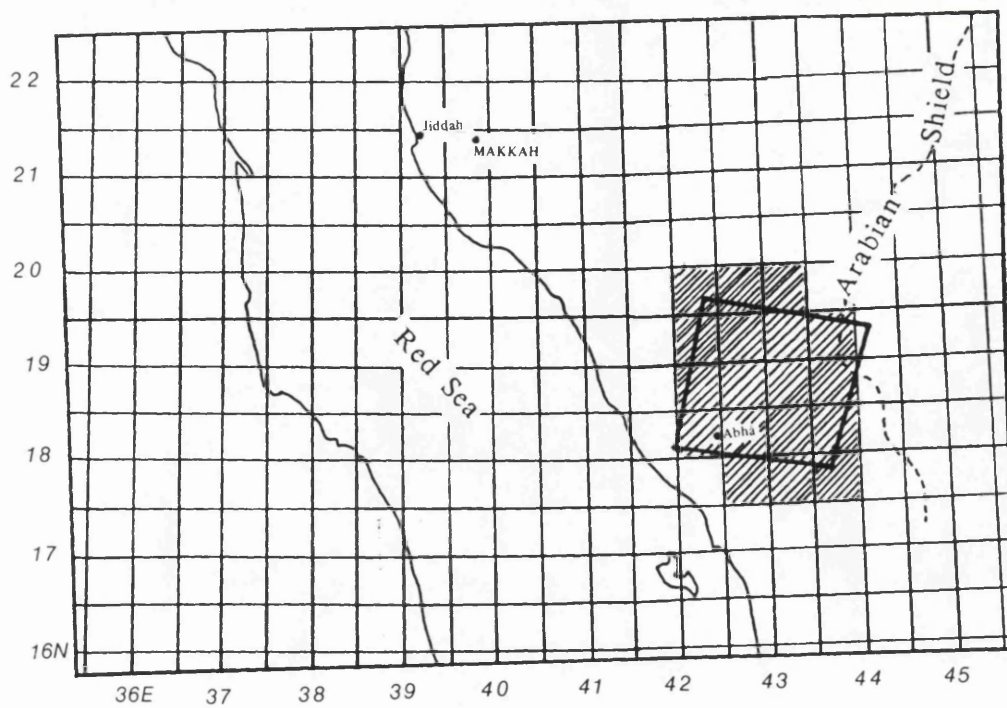
Fig. 1.5 Show the study area and the coverage of the
1:100,000-scale maps.
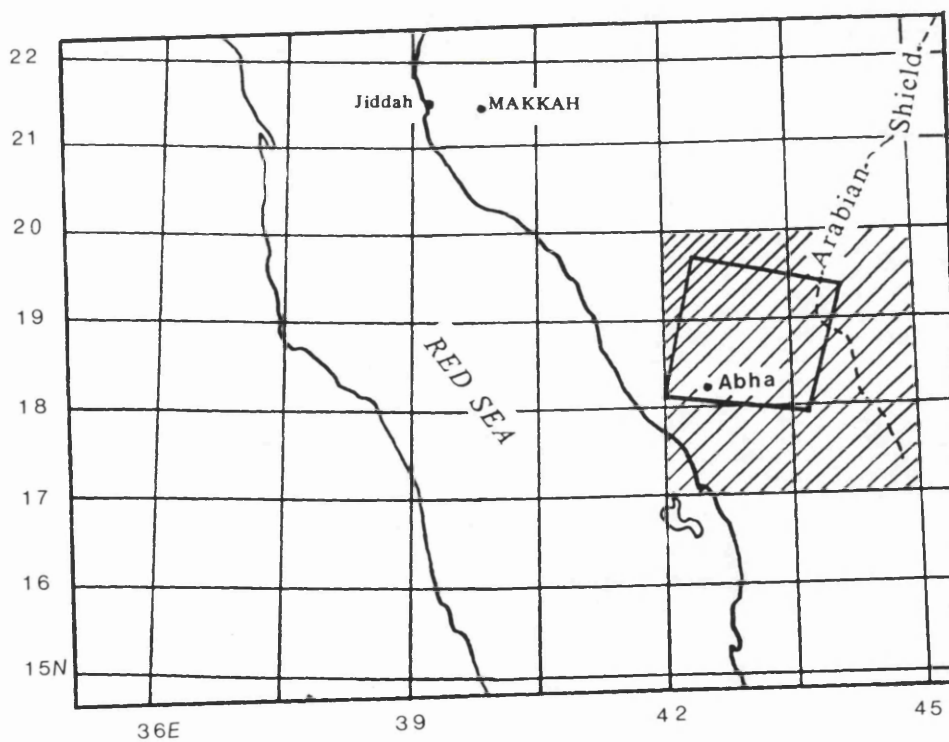
Fig. 1.6 Show the study area and the coverage of the
1:250,000-scale maps.

In June 1971, a field conference was held and led to a major publication by Schmidt et al. (1973), entitled "Stratigraphy and tectonism of the southern part of the Precambrian Shield of Saudi Arabia". The oldest rocks identified were the Khamis Mushayt ortho- and para-gneisses (KMG). These were considered to be a possible basement complex underlying the younger layered metamorphic rocks. Three new orogenies, newly defined stratigraphical units, and several additional deformational and plutonic episodes were recognized and named, based on lithology, degree of metamorphism and structural complexity (Table 1.1). Among the newly defined units were the Baish and Bahah Groups, believed to be older than 1000 Ma; the Jiddah Group; and the Halaban Group. These units are intruded by mafic to felsic igneous rocks and unconformably overlain by Cambro-Ordovician rocks. Seven tectonic episodes were recognized by phases of deformation, metamorphism, and intrusion (Table 2, Schmidt et al., 1973).

The 1:100,000-scale map sheets covering the study area were published between 1973 to 1984, and display the belief that the KMG is the basement complex of the shield (Schmidt et al., 1973; Coleman, 1973a; 1973b). Coleman divided the Precambrian rocks of the Asir mountains, which represent the deepest erosional level of the Arabian Shield, into two units: the Basement Complex (infrastructure) which shows a complex deformational history and forms a large plunging antiform with concordant contact with the surrounding rocks, and the Younger Metamorphic Series (suprastructure) with steep, isoclinal, north-south folds. According to Coleman, the dominant rock type of the KMG is orthogneiss which has in part a migmatitic appearance. The composition is tonalitic to granodioritic with quartz, oligoclase, microcline, biotite, hornblende, and epidote in various proportions. Minor intercalations of paragneiss and amphibolites are frequent. However, detailed structural studies (Amlas, 1983; Qari, 1985) revealed no structural discordance or stratigraphic break between the 'infrastructure' and the surrounding 'suprastructure' rocks which would support the contention that the former is basement to the latter. To the west of the study area, most contacts between the groups of rocks are faults, whereas major unconformities are not apparent (Ratte and Andreasen, 1974).

Publication of the 1:250,000-scale compilation map series for the study area during the years 1985 and 1986, resulted in renaming of some rock units shown on previous maps in order to understand the geological history of the region.

1.5.3 Evolution of ideas for the Arabian Shield

Around the middle of the 1970s, a number of geologists introduced plate-tectonic models to interpret the evolution of the Arabian Shield. Greenwood et al. (1976), presented their report entitled "Late Proterozoic cratonization in southwestern Saudi Arabia". They: (1) abandoned the inferred basement unit of Schmidt et al. (1973) viewing it as the metamorphic equivalent of other layered units, (2) defined one major tectonic cycle for the whole area containing several orogenic events, and (3) they clearly described the development of the southern shield in terms of plate tectonics and the cratonization of volcanic arcs. They concluded that the geochemistry, strontium-isotope initial ratios, and rock types indicated that the volcanic and associated plutonic rocks of the southern shield developed during the Hijaz cycle, within intraoceanic island arcs related to a north-dipping subduction zone. The cycle ended with the consumption of the ocean plate between the island arcs and Gondwanaland, to the southwest, and the collision and accretion of the arcs to the continent.

Greenwood et al. (1980) explicitly argued for a plate-tectonic model of the shield. By revising the stratigraphy developed previously, they believed that the shield was formed by basaltic to dacitic volcanism, associated sedimentation, and gabbroic to granitic magmatism in one or more intra-oceanic island arcs between about 1170 and 550 Ma ago. These events comprise what they called the Hijaz tectonic cycle. They regrouped the units into three lithostratigraphic assemblages (Table 1.2): (1) a metabasalt-greywacke-chert assemblage (Baish and Bahah Groups); (2) a meta-andesitic assemblage (Jiddah, Ablah, Halaban, and Murdama Groups); (3) a nonmetamorphosed assemblage of felsic volcanic rocks (Shammer Group) and taphrogeosynclinal volcanic rocks (Jubaylah Group). In addition, the biotite schist-amphibolite-orthogneiss assemblage, which is not shown on their table, includes rocks assigned to the Hali Group and KMG previously and are now known to be metamorphosed equivalents of rocks of the Baish Group and younger groups.

Among these rocks, there is no sign of a basement; instead the volcanic rocks resemble those formed in intraoceanic island arcs, and the associated plutons display a temporal progression from diorite to trondhjemite and granite, typical of island arcs, and are inferred to reflect a progressive thickening of the crust. It is believed that the island arcs developed over northeast-dipping subduction zones and resulted in a series of northwest-trending, overlapping belts. From southwest to northeast, across the southern shield, an evolutionary geochemical pattern was discerned, comprising early tholeiitic

14

DEPOSITIONAL UNITS	TECTONIC EPISODES	PLUTONIC ROCKS	RADIOMETRIC AGES (millions of years)
Jubaylah Group	**Najd wrench faulting** Northwest-southeast, left-lateral shear zones	Granite to granodiorite and subordinate syenite; late- and postfaulting	520
Shammar Group	**Shammar depression** Basins formed penecontemporaneously with Shammar volcanism	Granite to granodiorite	560
Murdama Group	**Bishah orogeny** Folding about north-south axes and slight metamorphism of rocks of the Murdama Group. Continued north-south wrench faulting	Granite to granodiorite and subordinate syenite	570
Halaban Group Jiddah Group	**Hijaz orogeny** Folding and lower-greenschist-facies metamorphism of Jiddah and Halaban rocks. Extensive north-south left-lateral wrench faulting during volcanism and folding. Emplacement of gneiss domes	Diorite and quartz diorite to granite plutonism related to Jiddah-Halaban volcanism. Subordinate gabbro. Intrusion perhaps related to north-south wrench faulting	665 1,000
Bahah Group Baish Group	**Tihama orogeny** Folding and generally greenschist-facies metamorphism of Baish and Bahah rocks	Plutonism not recognized	
Hali Group	**Asir tectonism** Folding and metamorphism of Hali rocks, chiefly to amphibolite facies	Tonalite; ultimately orthogneiss	
Khamis Mushayt Gneiss	**Basement tectonism (inferred)** Migmatites and quartzo-feldspathic gneisses possibly older than the Hali rocks. Basement tectonism not distinguished from Asir tectonism		

Table 1.1 Precambrian tectonic history for the Arabian Shield (after Schmidt et al., 1973).

ASSEMBLAGES	UNITS	MAJOR ROCK TYPES	TECTONISM EPISODES		PLUTONISM	RADIOMETRIC AGES (m.y.)
Nonmetamorphosed rocks (included with meta-andesitic asemblage on plate 1)	Jubaylah Group	Clastic rocks, minor volcanic rocks, and marine limestone	Najd faulting: Northwest-trending left-lateral wrench faulting		Granite to granodiorite	~530
	Shammar Group	Rhyolite, Trachyte, and minor clastic	—?—		Granite to granodiorite	570(?)
Meta-andesitic	Murdama Group	Conglomerate and graywacke, minior andesite and rhyolite, locally thick marble	Bishah orogeny: Folds and faults, north trends; greenschist metamorphism	CYCLE	Quartz monzonite, subordinate diorite, gabbro, granite	550–570
	Halaban Group	Andesite to rhyolite volcanic and pyroclastic rocks and volcaniclastic rocks	Yafikh orogeny: Folds and faults, north trends; greenschist metamorphism		Quartz monzonite, subordinate diorite, gabbro, granite	600–650
	Ablah Group	Basalt to rhyodacite, volcanic and pyroclastic rocks and volcaniclastic rocks, locally thick marble	Ranyah orogeny: Folds and faults, north and northeast trends; greenschist metamorphism; late gneiss doming and amphibolite to granulite facies metamorphism	TECTONIC	Granodiorite gneiss Second diorite series; gabbro gabbro to trondjhemite, mainly diorite and quartz diorite	~750 ~835
	Jiddah Group	Basalt to dacite volcanic, pyroclastic, and volcaniclastic rocks, minor rhyodacite	Agig orogeny: Folds and faults, north and northeast trends; greenschist metamorphism	HIJAZ	First dioritic series; gabbro to trondjhemite, mainly diorite and quartz diorite	890
Metabasalt-graywacke-chert	Bahah Group	Graywacke, chert, minor marble, and tuff, all locally graphitic, and minor basalt				
	Baish Group	Mafic volcanic rocks, mafic tuff, graywacke, and minor chert and marble			Quartz porphyry orthoschist, diabase	1165

Table 1.2 Summary of Precambrian rock units, tectonism, plutonism, and volcanism in the Arabian Shield (after Greenwood et al., 1980).

basalt, through rocks of tholeiitic and calc-alkalic composition, to young sequences, predominantly of rhyolite. Towards the end of the Hijaz tectonic cycle the ocean crust west of the island arcs was consumed by the northeast-dipping subduction, and the arcs collided with the continental margin of the African craton (Greenwood et al., 1980).

The publications of Greenwood et al. (1976; 1980) created a great deal of interest in Saudi Arabian Shield geology, both in scientific communities in universities in England, Germany and elsewhere, and in the growing geological community in the Saudi Arabian universities, particularly in Jeddah. The divergent basement-tectonic and plate-tectonic viewpoints furthered the development of ideas and concepts about the shield. The plate-tectonic approaches recognised the significance of ophiolites, postulated various east-, west-, or northeast-dipping subduction zones, hypothesized traces of suture zones, and attempted to determine the number and original location of island arcs [Bakor et al. (1976), Greenwood et al. (1976; 1980; 1982), Frish and Al-Shanti (1977), Gass (1977; 1979), Delfour (1979), Shackleton (1979), Kroner et al. (1979), Schmidt et al. (1979), Fleck et al. (1980), Nasseef and Gass (1980), Engel et al. (1980), Bokhari and Kramers (1981), Duyverman et al. (1982), Schmidt and Brown (1982), Darbyshire et al. (1983), Roobol et al. (1983), Al-Shanti and Gass (1983), Johnson (1983), Stacey and Stoeser (1983), Camp (1984), Claesson et al. (1984), Stacey and Hedge (1984), Stoeser et al. (1984), Stoeser and Camp (1985), Vail (1985), Stacey and Agar (1985), Kroner (1985), Scheibner (1986), Almond (1986), Bohannon (1986), Pallister et al. (1987), and Stoeser and Stacey (1988)].

Frish and Al-Shanti (1977) described five ophiolitic belts, particularly the northern half of the Hulayfah-Hamdah belt (known to be as "Nabitah Suture"). This belt trends north-south in the centre of the shield, offset by Najd faulting, and the subduction zone is interpreted to have dipped eastward, the trace of which is the Nabitah Fault Zone (Plate 2). They concluded that the shield was formed as several island arcs were swept together and amalgamated.

Utilizing a field traverse as a basis, Nasseef and Gass (1980) proposed an evolutionary model which hypothesized three episodes of sea-floor spreading, and the development of marginal basins adjacent to intraoceanic island arcs. They also indicated the presence of two, or possibly four, east-dipping Proterozoic subduction zones, and they concluded again that the island arcs had been swept together and the process of cratonization completed by the end of the Pan-African event. The Pan-African tectono-thermal event

was originally proposed by Kennedy (1964) to explain the dominance of 450-650 Ma K-Ar ages for the non-cratonic Upper Precambrian. Since then, the term "Pan-African" has been used to describe the time span of 1200-450 Ma, although some restrict the term to rocks of 450-650 Ma.

Greenwood et al. (1982) presented one of the most detailed plate-tectonic models for the southern part of the Arabian Shield. The age and facies relations of the rocks were discussed, and it was proposed that arcs trending southeast-northwest developed above subduction zones that possibly dipped southwest most of the time. Reviewing the geochronological data, they concluded that two arc complexes are present in the region: an older ensimatic arc, 1100 to 800 Ma old, and a younger marginal-arc, which formed 800 to 690 Ma ago. The older arc is composed of tholeiitic basic to intermediate volcanic rocks and volcaniclastic sedimentary rocks. The composition of the volcanic rocks and Rb-Sr isotope studies indicate that the complex was formed on oceanic crust. Dioritic rocks, intruded the complex between 900-810 Ma. The activity of the younger arc began about 800 Ma ago, with calc-alkalic volcanics and clastic sediments, which locally rest on rocks of the older arc, possibly in fault-controlled troughs which represent a marginal-arc complex. The rocks of this early phase of the younger arc development were deformed and metamorphosed by intrusions of tonalite to granite gneiss between 800-760 Ma. The arc continued to develop with tholeiitic and calc-alkalic volcanism to the east of the shield in an ensimatic environment. Later, the shield was involved in the Pan-African episode when post-tectonic granites were emplaced in the southern shield (Greenwood et al., 1982).

Camp (1984) described two sutures and volcanic-arc complexes in the western part of the Arabian Shield: the older Asir complex (900-700 Ma), and the Hijaz arc (800-700 Ma). He suggested that 700 Ma ago these arcs collided and accreted along a suture through "Bir Umq". This suture represents the traces of the Asir subduction zone (Camp, 1984).

A recent microplate accretion model for the Pan-African evolution of the Arabian Shield was proposed by Stoeser and Camp (1985). They divided the late Proterozoic Arabian Shield into five geologically distinct terranes (microplates), separated by four ophiolite-bearing suture zones (Fig. 1.7).

In the west of the shield there are three ensimatic island-arc terranes (Midyan, Hijaz
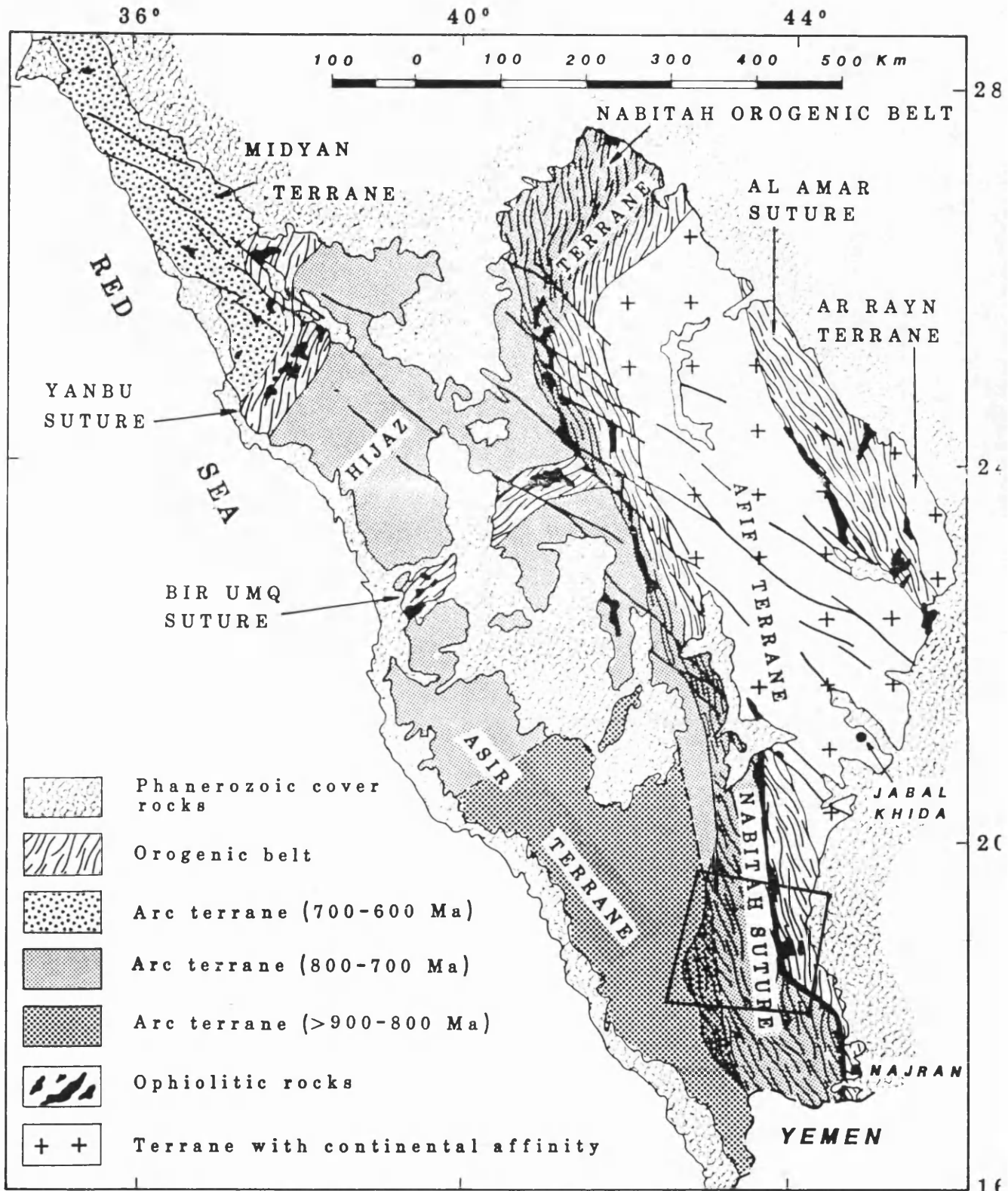
Fig. 1.7 Tectonic sketch map of the Arabian Shield showing
terranes and suture zones. Northwest-trending solid
lines indicate fractures of the Najd fault system
(after Stoeser & Camp, 1985). Study area is shown
by the rectangle.

and Asir), separated by two suture zones (Bir Umq and Yanbu), whereas the two terranes in the eastern shield (Afif and Ar-Rayn) have ensialic affinities. These two terranes are separated by the Al-Amar suture zone. The Nabitah Mobile/Orogenic Belt (NMB) defines a 100 to 200 km wide zone of crustal deformation, remobilization, and plutonism along the margins of the Asir, Hijaz, and Afif terranes. The southern part of the NMB contains ophiolitic complexes along a suture zone (Nabitah Suture Zone) which was interpreted (Stoeser and Camp, 1985) as the site of collision between the eastern and the western terranes of the shield. Accretion of the five terranes to form an Arabian neocraton occurred between 715 and 630 Ma, during the Pan-African event.

1.5.4 Summary of Arabian Shield evolution

The formation of the Arabian Shield can be divided into five phases (Stoeser and Camp, 1985), these are:

-Rifting of the African craton (1200-950 Ma).

-Ensimatic island-arc development ($\approx$950-715 Ma).

-Formation of the Arabian-Nubian neocraton by microplate accretion and continental collision (715-640 Ma).

-Collision-related intracratonic magmatism, tectonism, and the development of the Najd fault zone (640-550 Ma).

-Epicontinental subsidence (<550 Ma), regional peneplaning, and onlap of Wajid Sandstones on to the neocraton.

An evolutionary model for the shield is shown in Figure 1.8.

The Phanerozoic stratigraphic record shows that the Arabian neocraton remained stationary relative to the African craton until Red Sea rifting began during Tertiary time (Powers et al., 1966).

1.6 PURPOSE OF PRESENT STUDY

The study area is situated within the Asir Terrane and the Nabitah Mobile Belt (Fig. 1.7). Detailed geological and/or structural information is not available for the general region, except for a few small parts. Such detailed regional information is essential in understanding the evolution of this part of the Arabian Shield, and hence, the entire shield.

Remote sensing is a new tool used nowadays in many disciplines including geology.
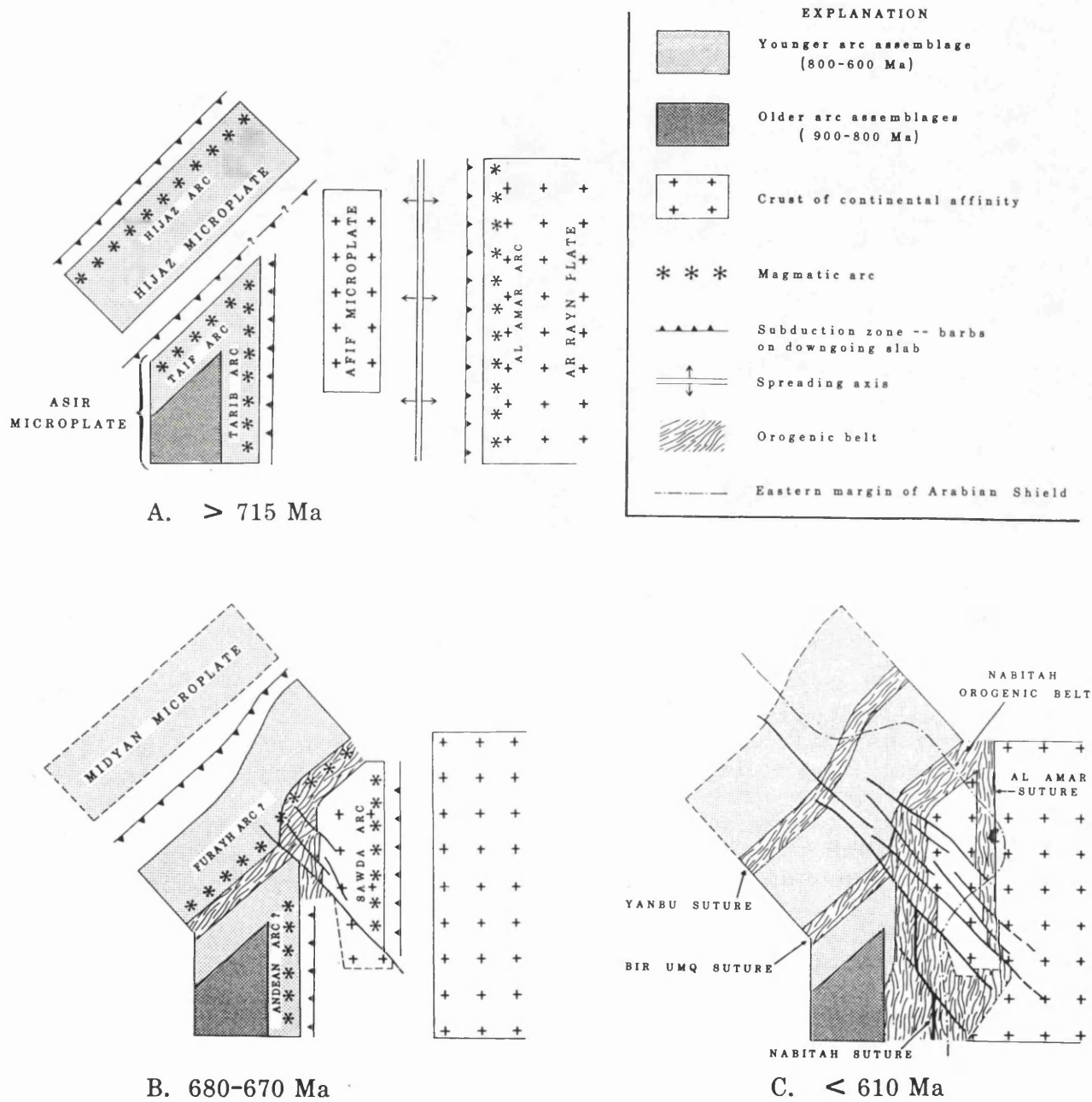
Fig. 1.8 Schematic tectonic diagrams showing evolutionary
stages of Arabian Shield development. A:formation
of younger magmatic arcs, B:terrane accretion, and
C:intracratonic deformation. Northwest-trending
solid lines are fractures of the Najd fault system
(after Stoeser and Camp, 1985).

Unfortunately, there were very few remote sensing applications using Landsat TM sensor data in the Arabian Shield and in the Arabian Peninsula [e.g. Bayer and Kaufmann (1986); Rothery (1987a); Al-Hinai (1988); Kaufmann and Pfeiffer (1988); Sultan et al. (1988); Al-Sari (1989); Pontual (1990)]. Al-Hinai (1988) studied the Quaternary aeolian sand mapping in Saudi Arabia using different remote sensing data, including Landsat TM, whereas Al-Sari (1989) investigated geologically the multispectral remote sensing data, including Landsat TM, for two mining districts in western Saudi Arabia. Utilizing remote sensing technology in such regional geological study will save power and time and will reflect the suitability of this kind of study for geological investigations, particularly in arid desert type of lands.

The Arabian Shield with its vast area composed of different lithologies and structures, is a unique area for testing and evaluating the Landsat data, particularly the study area which is situated in the southern part of the shield. The aims and objectives of this study were to test the capability and ability of Landsat multispectral remote sensing data for geological mapping. Specifically the objectives were as follows:

1-To test and evaluate the ability of Landsat multispectral remote sensing techniques covering the visible, near- and mid-infrared portion of electromagnetic spectrum to map different lithologies in the three test-sites selected for detailed full-resolution study and in the study area as a whole.

2-To compare and interpret the results obtainable by different remote sensing techniques applied throughout the study.

3-To prepare different geological maps, utilizing remotely sensed- and field-data.

4-To determine and evaluate the utility of remotely sensed data and image analysis for delineation of geological elements.

5-To interpret structural features in terms of the tectonic evolution of the area.

1.7 STRUCTURE OF THE THESIS

The thesis is structured for readers interested in remote sensing and geological studies of the Precambrian southern Arabian Shield. The thesis contains nine chapters.

Chapter 1 introduces the study area and the evolution of the Arabian Shield. Chapter 2 briefly describes the Landsat digital imagery and also presents spectral characteristics of rock types in the study area.

Chapters 3, 4 and 5, the main body of the thesis, are concerned with three test-sites within the study area which were selected for detailed comparison of remote sensing methods and ground geological studies. Selected digital image processing techniques were applied and results are interpreted and discussed. Full-resolution images of each of the test-site have been used.

Chapter 6 presents geological conclusions obtained as a result of this study. Chapter 7 contains a regional geological view discussion and interpretation for the entire study area. Based on selected techniques of image processing applied on the entire study area using Landsat MSS data, results are discussed in Chapter 8. The thesis ends with a summary and recommendations (Chapter 9). Figure 1.9 illustrates the thesis structure.

1.8 METHODS OF INVESTIGATION

Literature review commenced in 1987. The preparation of the compiled geological map (Plate 2) was started in late 1987. Initial field work was carried out during February and March 1988, when a reconnaissance study was conducted throughout the area, followed by systematic traverses across the lithological/structural domains identified. 'Ground truth' of the structures recognized by preliminary image enhancement session of the satellite data was also evaluated.

Three test areas were selected within the study area and image enhancement session was conducted prior to the final field work. These test-sites are full-resolution sub-scenes; i.e. 512x512 pixels in size, which is the size available in the image processing video monitor.

During the final field work, the preliminary geological interpretations were very helpful. Mapping was carried out on aerial photo-mosaics and satellite images. More than 170 observation points were visited during both periods of field work (Plate 3) in order to study the geology, measure the available structural data, and evaluate the remote sensing techniques applied previously. Samples were also collected for petrological verification if needed.

Interactive satellite image processing in this study was performed using two systems. The International Imaging Systems (IIS) at the Geography Department, University College London (UCL) and at the Faculty of Earth Sciences, King Abdulaziz University

GEOLOGICAL ANALYSIS OF PARTS OF THE SOUTHERN ARABIAN SHIELD BASED ON LANDSAT TM IMAGERY

Chapter I
INTRODUCTION

Chapter II
REMOTE SENSING STUDIES: PROLOGUE

APPLICATION OF METHODS

Chapter III
I. TEST-SITE No.1
(KHAMIS MUSHAYT AREA)

Chapter IV
II. TEST-SITE No.2
(AL-KHABT & AL-FAYD AREA)

Chapter V
III. TEST-SITE No.3
(JABAL DUHAYYAH AREA)

Chapter VI
GEOLOGICAL CONCLUSIONS

Chapter VII
REGIONAL GEOLOGICAL VIEW

Chapter VIII
REGIONAL ENHANCEMENT USING LANDSAT MSS

Chapter IX
SUMMARY AND RECOMMENDATIONS

Fig. 1.9 Thesis structure.

(KAU), Jeddah, Saudi Arabia. These two systems are similar in configuration, having a tape drive to load images from CCT tapes, a computer to store and process the image, a terminal at which one controls the processing, and a colour monitor on which the processed image displayed.

However, the two systems use two different computers. The IIS at UCL is connected to VAX 11/750 computer, whereas at KAU is connected to MASSCOMP H6800 computer. The image processing facility at KAU was found to be more practical and faster. One more advantage of the IIS at KAU is that it is linked to a film recorder (MATRIX 4007 COLOUR CAMERA) capable of reading an image from the IIS system to produce a hard copy of the processed images. This process is very important if a good interpretation of an image free of photographic distortions is required.

CHAPTER TWO   REMOTE SENSING STUDIES: PROLOGUE

2.1 LANDSAT DIGITAL IMAGERY

2.2 GENERAL SPECTRAL FEATURES

2.3 SPECTRAL CHARACTERISTICS OF ROCK
     TYPES EXPOSED IN THE STUDY AREA

2.4 DIGITAL IMAGE PROCESSING

2.5 SUMMARY

The area of the Arabian Shield is covered by different types of remotely sensed imagery, which includes Landsat Thematic Mapper (TM) and Multi-Spectral Scanner (MSS) line scanned images.

This chapter presents a simple introduction to the:

-digital imagery used throughout study,

-spectral reflectance characteristics of rocks exposed in the study area based on published laboratory- and field-work.

2.1 LANDSAT DIGITAL IMAGERY

A digital image is recorded by an array of discrete values, known as Digital Numbers (DN), at discrete spatial coordinates. Each element of this array is called a picture element or pixel. Each pixel value records the amount of energy reflected from an area whose size defines the spatial resolution of the scanner system, in this case, the Thematic Mapper (TM) of the Landsat system. Each pixel is described by one byte (eight bits) with grey levels ranging from 0 to 255. A multiband digital image consists of several overlapping arrays of pixels, with each pixel representing the same scene in a different spectral band.

The TM scanner records six bands of the reflected visible and infrared spectrum, with image element dimensions of 30 by 30 metres on the ground, and one thermal infrared band with image element dimensions of 120 by 120 metres on the ground (Fig. 2.1). The thermal band, which is named band 6, is not dealt with in any part of this study. The other six bands, i.e. 1-5 and 7 are the ones which will be treated during the course of the study because they are spectrally and spatially significant for geological applications. Landsat MSS description is deferred to Chapter 8.

Digital Landsat-4 TM scanner imagery from the Arabian winter season (1 Mar 1984) was obtained for the purpose of the present quantitative remote sensing study. The sub-scenes for the selected test-sites No.1 and No.3 are 512x512 picture elements (pixels) in size (Fig. 1.3), which is approximately 15 by 15 kilometres, i.e. 225 square kilometres in area. The test-site No.2 is composed of two 512x512 sub-scenes with an overlap area. This larger area was used because of the interesting structural geometry which could not be confined as a single full-resolution 512x512 pixels image. Hence the test-site No.2 is composed of 2A and 2B (Fig. 1.3).
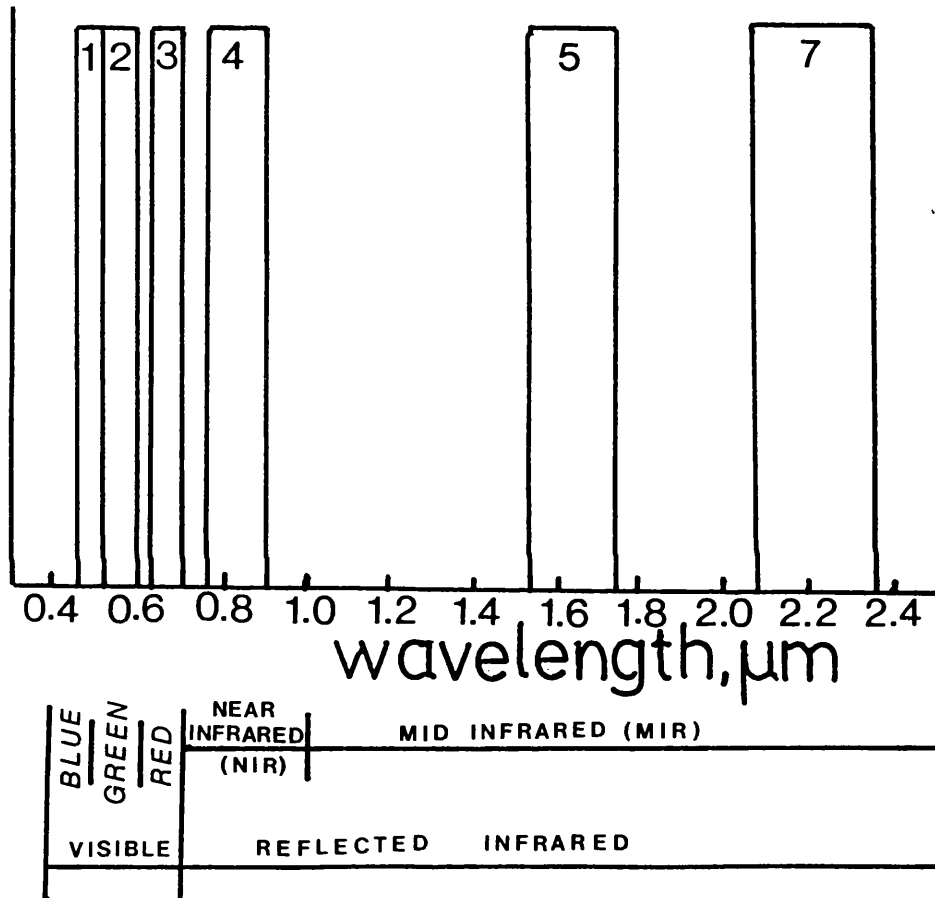
Fig. 2.1 Landsat TM bands and its spectral region. Thermal
       infrared band 6 is not shown (10.4-12.5 μm).

2.2 GENERAL SPECTRAL FEATURES

The spectral distribution of reflectance from an earth material is often the most useful property measured by remote sensing methods for geological studies. Spectral reflectance is a measure, within specific wavelength intervals, of the amount of sunlight reflected by a material. In our case the material concerned is rock or regolith, and the spectral reflectance is expressed as the tone or colour of photographic images. The reflectance is a consequence of the chemical and mineral composition of the material and also its structure. All these may be modified by environmental factors.

Several studies, especially in hydrothermal alteration zones, have demonstrated that spectral properties can be used to recognize and map the occurrence of particular minerals in different geological settings. Understanding of the spectral reflectance of certain minerals in the visible, near- and mid-infrared portion of the electromagnetic spectrum (0.4 - 2.5 μm) has significant application to terrestrial remote sensing.

Rocks are assemblages of minerals, and so the reflectance spectrum of a rock is a composite of the individual spectra of its constituent minerals. The features which characterise the spectral signatures of minerals and rocks in the visible, near-, and mid-infrared spectrum are produced as a result of either electronic transitions or vibrational processes (Hunt and Salisbury, 1970). These two types of process require different amounts of energy, and thus evidence for their occurrence appears in different regions of the spectrum.

Electronic transitions require more energy than vibrational processes, and evidence for their occurrence appears in the form of band and slope changes primarily in the visible range. Electronic transitions are associated particularly with the transition elements, of which iron is the most abundant. It is present as a principal constituent in many minerals; Fe^{2+} and Fe^{3+} substitute with some facility into octahedral Al^{3+} and Mg^{2+} sites, and occasionally into tetrahedral Si^{4+} sites. The ready solubility of the ions in water accounts for their widespread distribution in terrestrial materials.

Fundamental vibrational processes are evident in the mid- and far-infrared region, particularly the region between 2.0-2.5 μm (≈Landsat TM band 7), which provides more diagnostic spectral information about the composition of minerals and rocks than the

visible and near-infrared region. Here, sharp, highly diagnostic spectral absorptions are caused by vibrational processes, especially in hydroxyl-bearing minerals. Al-OH absorption bands occur near 2.2 µm in minerals such as muscovite, 2.208 µm and montmorillonite, 2.205 µm. A similar band, related to the Mg-OH association occurs near 2.3 µm, e.g. in phlogopite at 2.33 µm and chlorite at 2.32 µm. Fe-OH minerals, such as jarosite, have a spectral band centred at 2.264 µm.

2.3 SPECTRAL CHARACTERISTICS OF ROCK TYPES EXPOSED IN THE STUDY AREA

As part of a laboratory study of spectroscopic remote sensing techniques, the visible and near-infrared spectral behaviour of rocks and minerals has been evaluated by Hunt and Salisbury (1970; 1976b) and Hunt et al. (1973a; 1973b; 1974). Spectra of mineral and rock samples were recorded using a spectrometer fitted with equivalent specially constructed bi-directional reflectance attachments in both sample and reference beams. The attachments allow bi-directional measurements to be made of particulate samples by allowing the beam to impinge from above on horizontal sample (Hunt and Salisbury, 1970).

The results of their laboratory evaluation of visible and near-infrared reflectance spectra behaviour of minerals and rocks is presented in Figs. 2.2 to 2.7. Figure 2.2 shows reflectance spectra for selected silicate minerals and indicates the positions where significant absorption features may occur in relation to the spectral bands detected by the Landsat TM scanner. Figures 2.3 and 2.4 present the reflectance spectra of gabbro (basic igneous rock) and granite (acidic igneous rock), respectively. Figures 2.5 and 2.6 exhibit the reflectance spectra of slates, phyllites, and schistose rocks (metamorphic rocks). Finally, Figure 2.7 shows the laboratory reflectance spectra of different gneissic rocks.

Rocks are assemblages of minerals, and so the spectrum of a rock is a composite of the individual spectra of its constituent minerals. Minerals that have low, flat spectral reflectances are defined as "opaque phases" by Hunt et al. (1971). The abundance of opaque phases in a rock has been shown by Hunt et al. (1974) to be a useful rock type discriminator. They found that mafic rocks generally have lower spectral reflectances than other igneous rock types, due to the relatively high abundance of the opaque phases. In addition, whether we consider fresh or weathered surfaces of igneous or
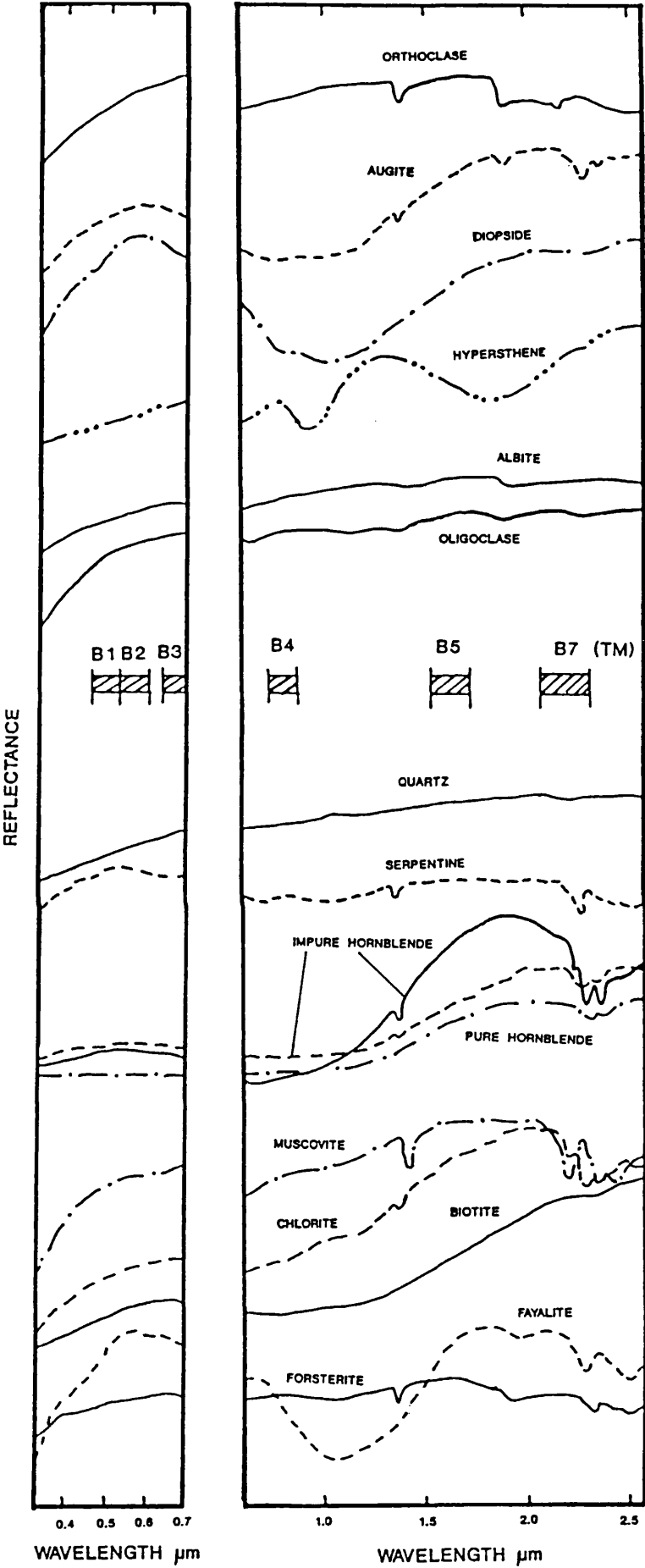
Fig. 2.2 Visible and near-infrared spectra obtained in the laboratory (Hunt & Salisbury, 1970; Hunt et al., 1973a). The spectra are offset vertically for clarity.
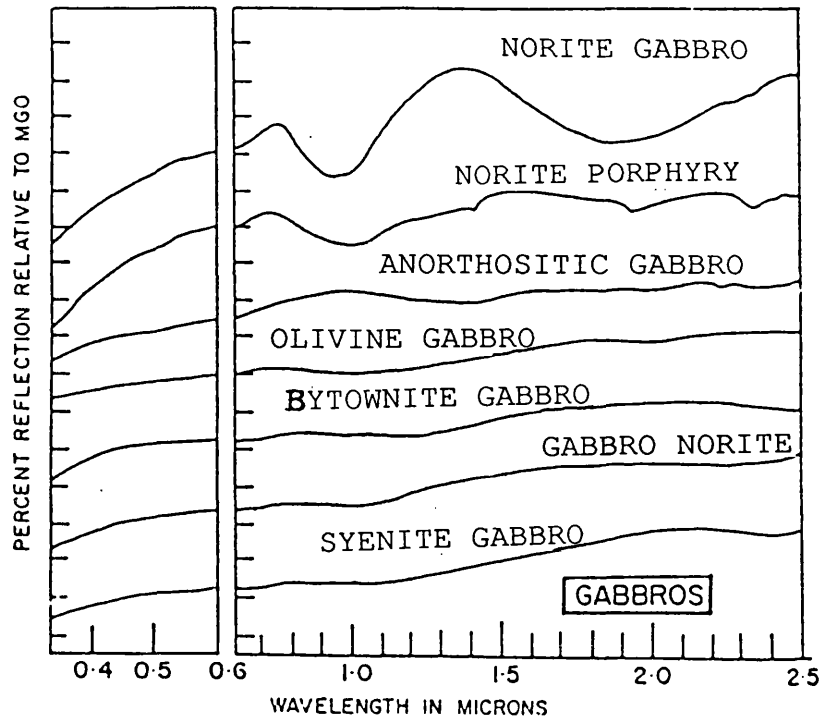
Fig. 2.3 Reflectance spectra of gabbroic rocks (Hunt et al., 1974). The spectra are displaced vertically and the percent reflectance markers are separated by 10%.
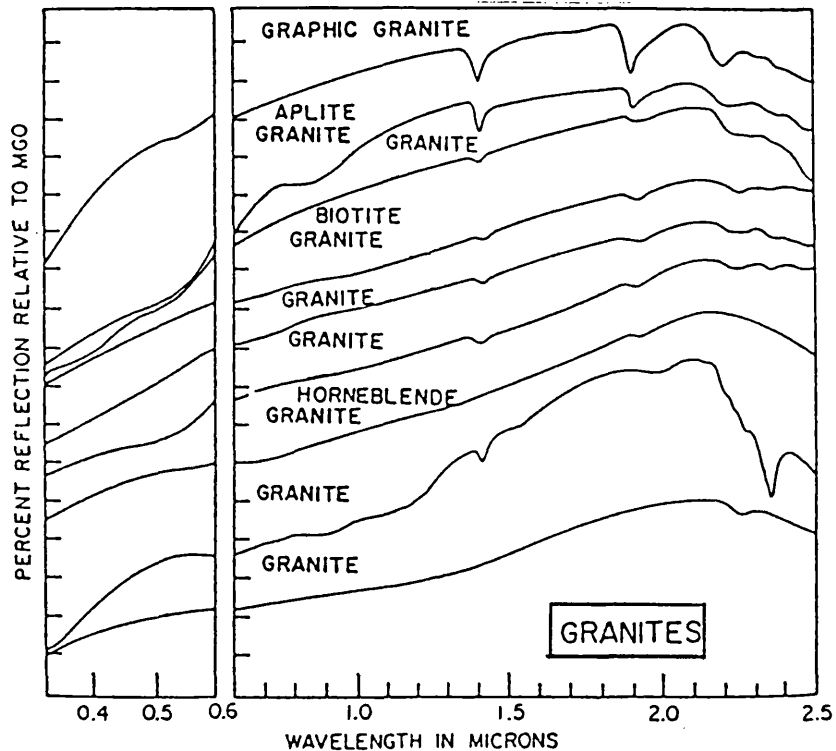
Fig. 2.4 Reflectance spectra of granitic rocks (Hunt et al., 1973b). The spectra are displaced vertically and the percent reflectance markers are separated by 10%.
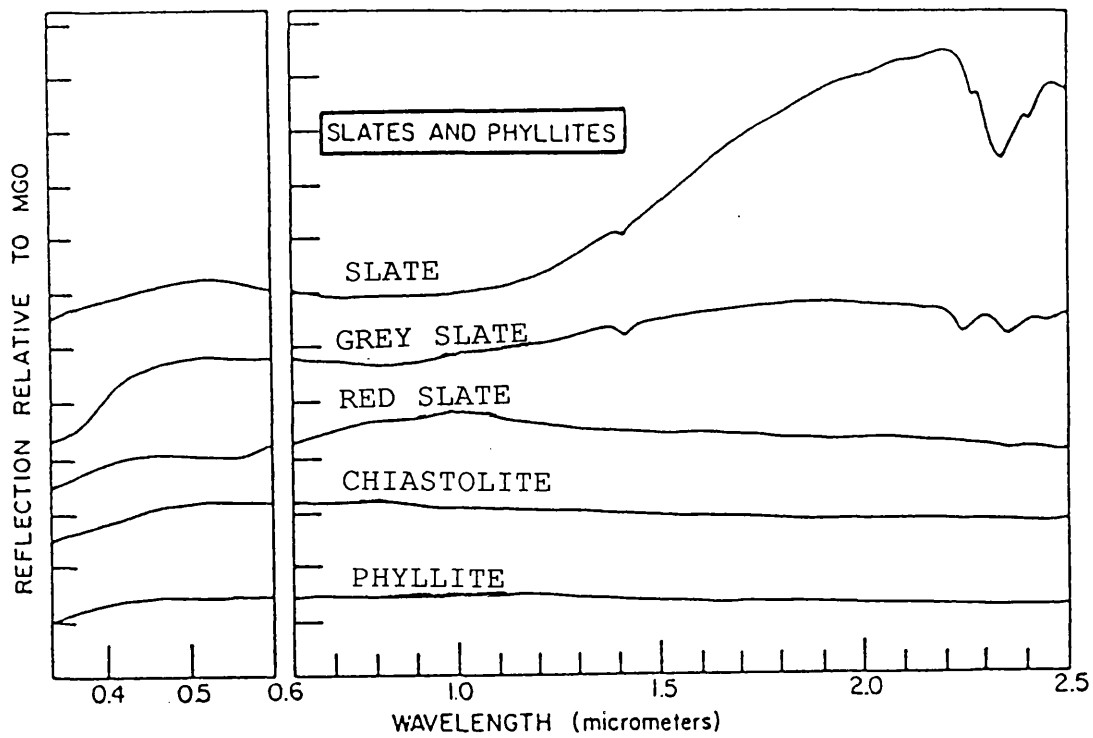
Fig. 2.5 Reflectance spectra of slates and phyllites (Hunt and Salisbury, 1976b). The spectra are displaced vertically and the reflectance markers are separated by 10%.
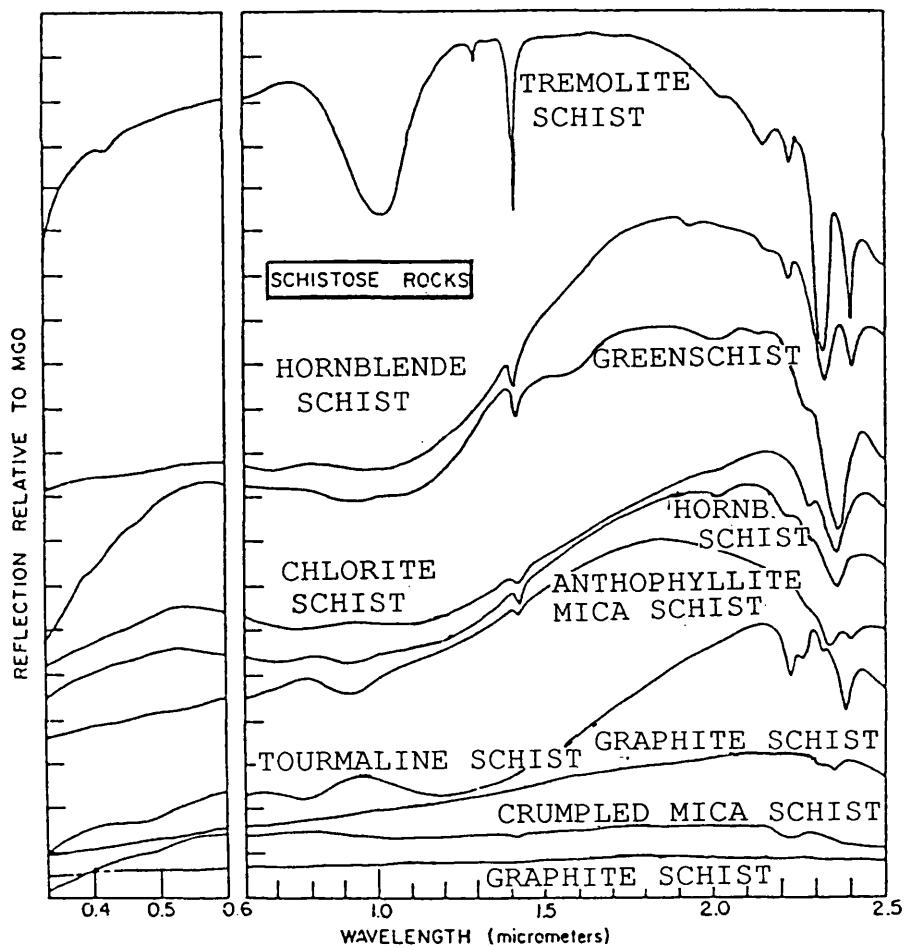
Fig. 2.6 Reflectance spectra of schistose rocks (Hunt and Salisbury, 1976b). The spectra are displaced vertically and the percent reflectance markers are separated by 10%.
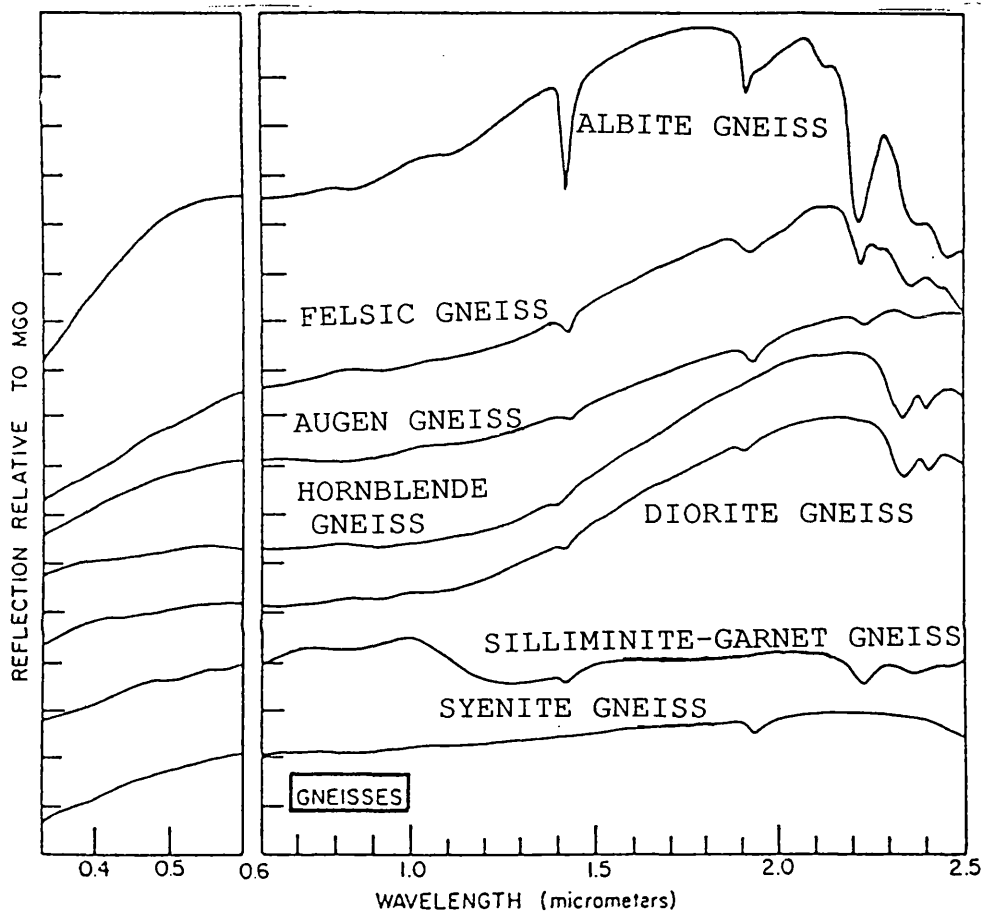
Fig. 2.7 Reflectance spectra of gneissic rocks (Hunt and
Salisbury, 1976b). The spectra are displaced
vertically and the percent reflectance markers
are separated by 10%.

metamorphic rocks, the only metallic element causing strong absorption in the visible and near-infrared region is iron (Hunt et al., 1971 and 1974; Hunt and Ashley, 1979; Hunt and Salisbury, 1976b; Blom et al., 1980).

A study relevant to this has been carried out recently by Sultan et al. (1987), using digital TM images of the Eastern Desert of Egypt on part of the Nubian Shield to evaluate the capabilities of TM imagery in lithological mapping of the Meatiq dome area, latitude 26°00'N and longitude 33°45'E. They found that:

(a) Mafic rocks (massive amphibolite and mafic mylonite) could be distinguished from other rock types largely on the basis of the high content of Fe-bearing aluminosilicates revealed in the reflectance spectra.

(b) Coarse- and fine-grained granites, granite gneiss, and tonalite could only be mapped as a group together because variations in opaque, hydroxyl-bearing, and Fe-bearing aluminosilicate phases were too small to permit separation. Finer subdivisions were possible where detailed field traverses provided local verification.

(c) Quartzofeldspathic mylonite, quartz phyllonite, and biotite schist, could be mapped on the basis of their relatively high content of hydroxyl-bearing phases and/or opaque phases.

They also determined bi-directional spectral reflectance curves both for the outcrops and rock powders acquired from their test-site (Figs. 2.8 and 2.9). In addition, they demonstrated the effect of the desert varnish on the spectral reflectances of the underlying rocks in arid regions by suggesting that the ubiquitous varnish modulates, but does not obscure, the spectral reflectance of the underlying rocks.

The crustal rocks of the Arabian Shield and the Nubian Shield are grossly similar in petrology, chemistry, structure, and age. Across both shields, the crustal rocks were made and cratonized in about 450 m.y., from about 1,000 m.y. to about 550 m.y. (Brown et al., 1989). The area studied by Sultan et al. (1987) is similar to the present study area: both areas are structurally complex and consist of conformable sequences of low to high amphibolite facies rocks which are intruded by various igneous bodies, and the age of these units is late Proterozoic. Both are parts of the Arabian-Nubian Shield, and have been subjected to the same sequence of orogenic events, and display intrusive and extrusive igneous rock units of the same age. The rock types in the present study area are almost exactly like the rock types appearing in the Eastern Desert of Egypt, and hence their spectral characteristics are identical.
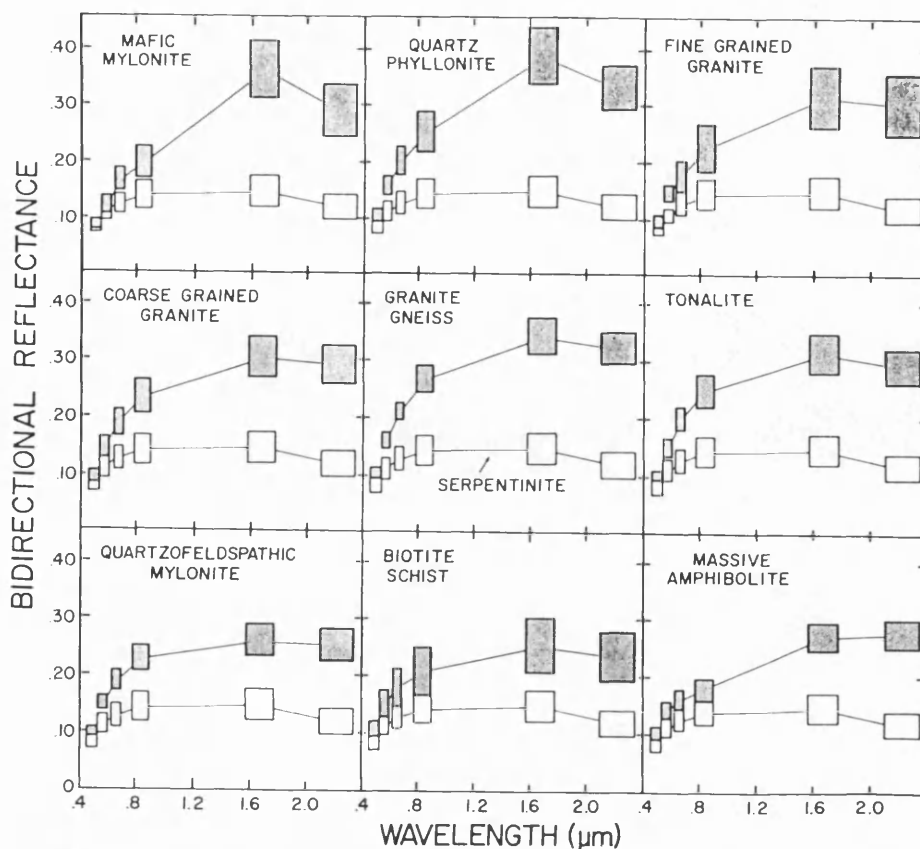
Fig. 2.8 Representative TM spectral reflectance data for the major rock units (In the test-site outcrops of Sultan et al., 1987).
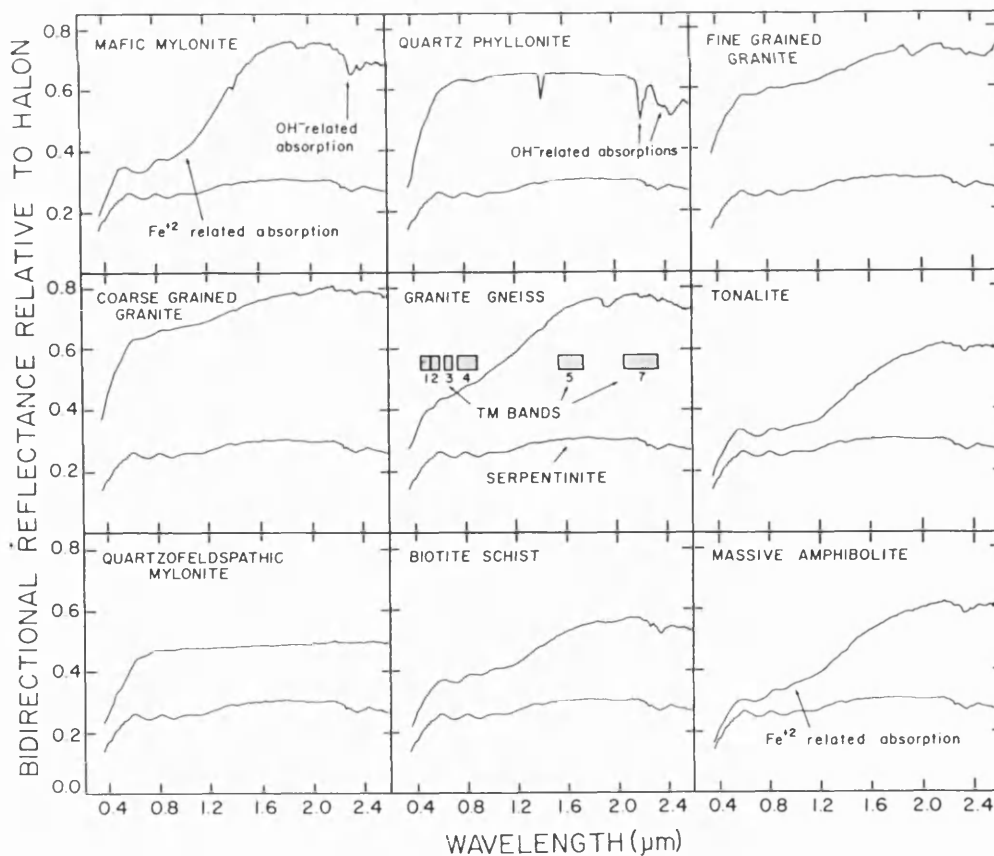
Fig. 2.9 Bi-directional spectral reflectance curves for rock powders (after Sultan et al., 1987).

2.4 DIGITAL IMAGE PROCESSING

Numerous authors reviewed the theory and practice of digital image processing (e.g. Condit and Chavez, 1979; Gillespie, 1980; Schowengerdt, 1983; Sabins, 1978; 1987; Drury, 1987). The processing of a digital image serves two main purposes, these are: enhancement, which improves the quality and appearance of the image for visual interpretation, and the extraction of information from the image. The essential advantages of digital processing methods are their versatility, repeatability and the preservation of the original data precision (Sabins, 1978).

Image processing methods which are normally performed on image data prior to visual interpretation are grouped into three main categories in this study. These are:
(1) contrast manipulation for improving image contrast,
(2) edge enhancement for detecting lineaments,
(3) spectral enhancement for geological mapping.
The spectral enhancement techniques are based on two principles, statistical analysis of the data and the use of arithmetical operators. The next three chapters are mainly devoted to the application of these methods in parts of the southern Arabian Shield.

2.5 SUMMARY

In this chapter a review of Landsat TM digital imagery, general spectral features of earth materials, spectral characteristics of rock types exposed in the study area and the methods applicable to the study area were presented. Detailed description of methods and interpretation of the results are deferred to later chapters.

CHAPTER THREE   APPLICATION OF METHODS:
I. TEST-SITE No.1
(KHAMIS MUSHAYT AREA)

3.1 INTRODUCTION

3.2 GEOLOGY OF THE TEST-SITE

3.3 REMOTE SENSING TECHNIQUES

   3.3.1 Introduction

   3.3.2 Contrast enhancement

   3.3.3 Spectral enhancement techniques

     (a) Arithmetic operation techniques

        SE1 Technique

        SE2 Technique

     (b) Statistical analysis based technique

        SE3 Technique

   3.3.4 Edge enhancement techniques

     (a) Introduction

     (b) Image enhancement

     (c) Lineament trend interpretation of Landsat images

     (d) Conclusion

3.1 INTRODUCTION

This chapter and the following two chapters are mainly devoted to an evaluation of the applicability of the Landsat Thematic Mapper (TM) sensor digital imagery to geological investigations in arid regions, particularly for lithological discrimination and structural analysis. The Arabian Shield, and in particular the three test-sites (Fig. 1.3) includes a wide variety of rock types. The test-sites are located within or on the border of two tectonic assemblages of the southern Arabian Shield (Stoeser and Camp, 1985); these are the Asir Terrane (AT) and the Nabitah Mobile Belt (NMB) (Fig. 1.7).

These sites were chosen because of the excellent exposure of a diverse suite of igneous and metamorphic rocks, and because there were previous geological studies of them.

Three main categories of technique were applied during image processing (enhancement) of the digital imagery from/of the three test-sites. The categories are: contrast manipulation, edge detection (filtering) and spectral enhancement. The last category is based on two principles: statistical analysis of the data (imagery), and the use of arithmetical operators. The results of the image processing are displayed in this thesis as photographic prints of Cathode-Ray-Tube (CRT) monitors at the remote sensing laboratories, and these were used for visual interpretation. Interpretation utilizing photographic colour composites were performed on the original photographs produced by the laboratories. All colour references in the text refer to the original colour composites. Much care was taken in reproducing the original photographs for the thesis as colour photocopies, but there may be some differences in colour reproduced on the photocopies in regard to the originals.

The first test-site was selected because of the excellent exposure of different lithological units, interesting structural pattern, availability of detailed geological studies and the approximate location on the border between the Asir Terrane and the Nabitah Mobile Belt.

The only detailed geological studies conducted on the ground during the past few years for this test-site, two M.Sc. theses describing adjacent areas approximately covering the test-site (Amlas, 1983 and Qari, 1985). Apart from these two detailed studies, the only source of geological information for the test-site is the 1:100,000 map of Coleman (1973b), which makes broad lithological discriminations, based on photo-interpretation

and field checking of some localities (Fig. 3.1).

3.2 GEOLOGY OF THE TEST-SITE

The geology of the test-site is complex because of a history of polyphase deformation and igneous activity. The major lithologies are granites, gneisses, metasediments, amphibolites and gabbroic rocks.

Granite intrusions are distributed randomly in the area of the test-site. Gneisses and other layered metamorphic rocks occupy a large portion. Gabbro is present in two places only. One is to the southwestern corner and the other is in the core of the synform between the dome and the mushroom structures in the southeastern quarter of the site (Fig. 3.1).

The area has been affected by four phases of deformation. The southeastern quarter of the area is composed of dome-, synform-, and mushroom-like structures (Amlas, 1983), and the outcrop pattern in the western half also displays fold interference patterns structures (Qari, 1985).

3.3 REMOTE SENSING TECHNIQUES

3.3.1 Introduction

As mentioned before, three main types of image processing have been performed on this test-site. These are: contrast-, edge-, and spectral-enhancements. The last category is most suitable for lithological mapping and was performed on the basis of either statistical analysis of the data (imagery) or using arithmetic operations in the available Image Analysis System. The prime target was to produce high quality hardcopy images suitable for geological interpretations. Afterwards, important decisions such as locating lithological boundaries and structural elements could be performed. The contrast enhancement method will be presented first, followed by spectral enhancement techniques and finally the edge enhancement techniques. It is logical to start with the simplest technique used for interpretation purposes.

3.3.2 Contrast enhancement

Enhancement processes for improving image contrast are widely used among digital image users.

E42°40'

N18°25'

N18°25'

E42°40'

2   0   2 km
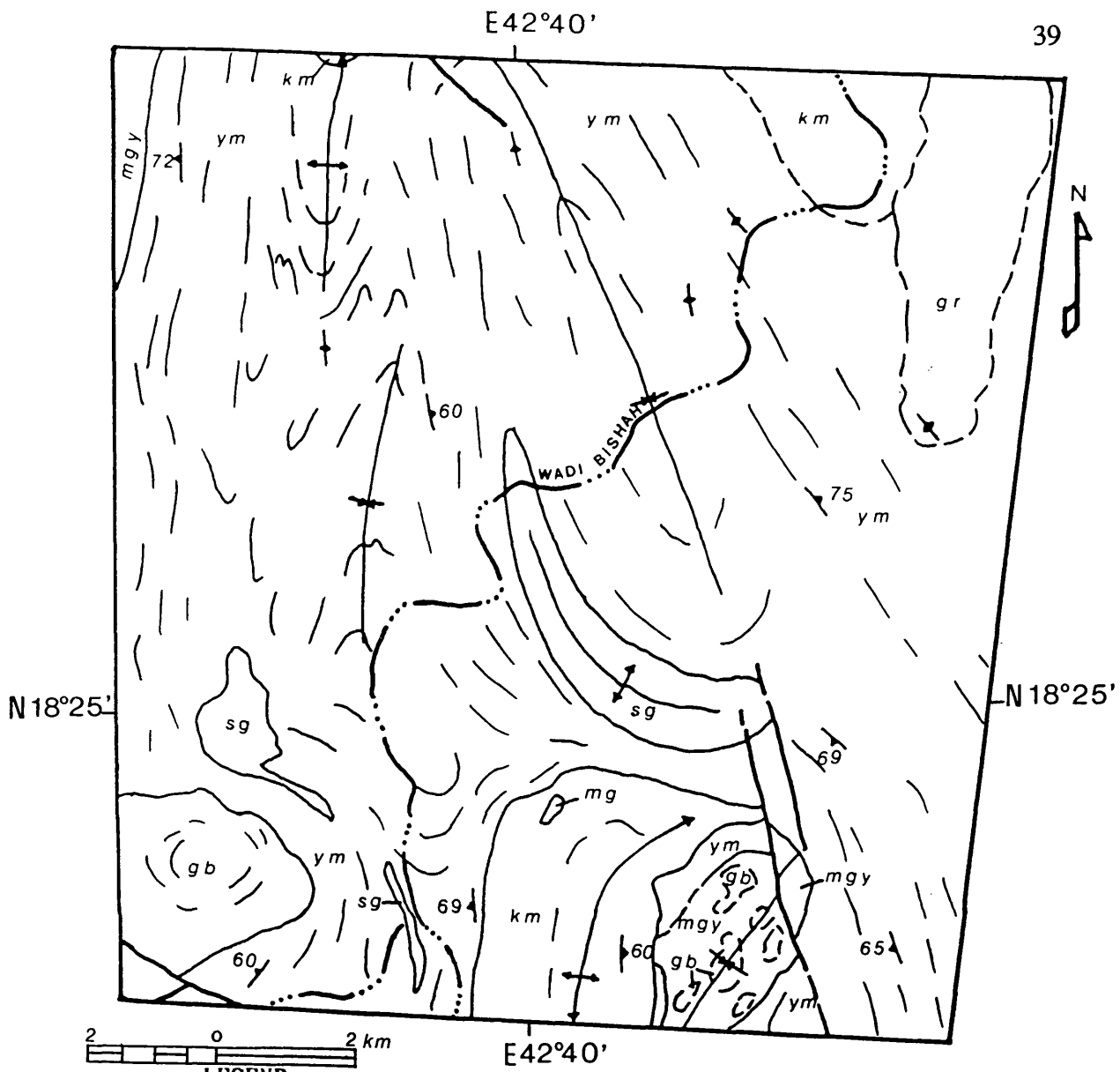
LEGEND

gr	Quartz monzonite and granodiorite
gb	Gabbro and metagabbro
sg	Syntectonic granitic rocks
mgy	Complex synform of 'ym' and intrusive gabbro
mg	Metagabbro
ym	Young metamorphic rocks
km	Khamis Mushayt gneiss

⌁···⁻ Wadi with alluvium
⌒ Lithological contact, dashed where inferred
— Fault
⊣→ Antiform—showing direction of plunge
⊣— Synform
⤬ Vertical foliation
69⤬ Strike and dip of foliation
⦚ Trend lines in bedded rocks and fractures in igneous rocks

Fig. 3.1 Geological published map of the test-site No.1
         (after Coleman, 1973b).

The basis of these contrast enhancement processes is that the CRT monitor expresses brightness value or Digital Number (DN) in a stepped range of intensities from 0 (black) to 255 (white). The image processing system can change or transform any DN in an image to any of these 256 intensity levels. So, contrast enhancement is a pixel-by-pixel transformation or stretching that is designed to enhance visual discrimination of low contrast image features. Only two types of contrast stretching were applied to test-site No.1. These are linear- and nonlinear-contrast stretching.

Linear contrast stretching

Simple linear contrast stretching enhancement (scaling) was routinely used throughout this study to increase the contrast of a displayed image by expanding the original grey level to fill the dynamic range of the display device. This means that a DN value in the low end of the original histogram is assigned to extreme black, and a value at the high end is assigned to extreme white. The remaining pixel values are distributed linearly between these two extremes. Figure 3.2A shows the raw Landsat TM band 5 data, while Figure 3.2B shows the linearly contrast stretched Landsat TM band 5 data for the test-site No.1. It is obvious that linear contrast stretching enhancement shows more details.

Nonlinear contrast stretching

To avoid the loss of contrast in the tails of the original histogram inherent in linear contrast stretch enhancement, nonlinear contrast stretching is used. Here, the raw data (Fig. 3.2A) is taken to resemble a normal distribution (Gaussian), producing a bell-shaped histogram, and this process is known as a Gaussian stretch. Improvement of contrast in the very light and dark ranges of the image is obtainable. Figure 3.2C shows Gaussian contrast stretching of Landsat TM band 5 data for test-site No.1.

3.3.3 Spectral enhancement techniques

(a) Arithmetic operation techniques

Two techniques have been applied in this study; the method of Sultan et al. (1987), herein called SE1, and the method of Loughlin and Tawfiq (1985), herein called SE2.

SE1 Technique

The rugged nature of the test-site and the fluctuation in the topographic relief require
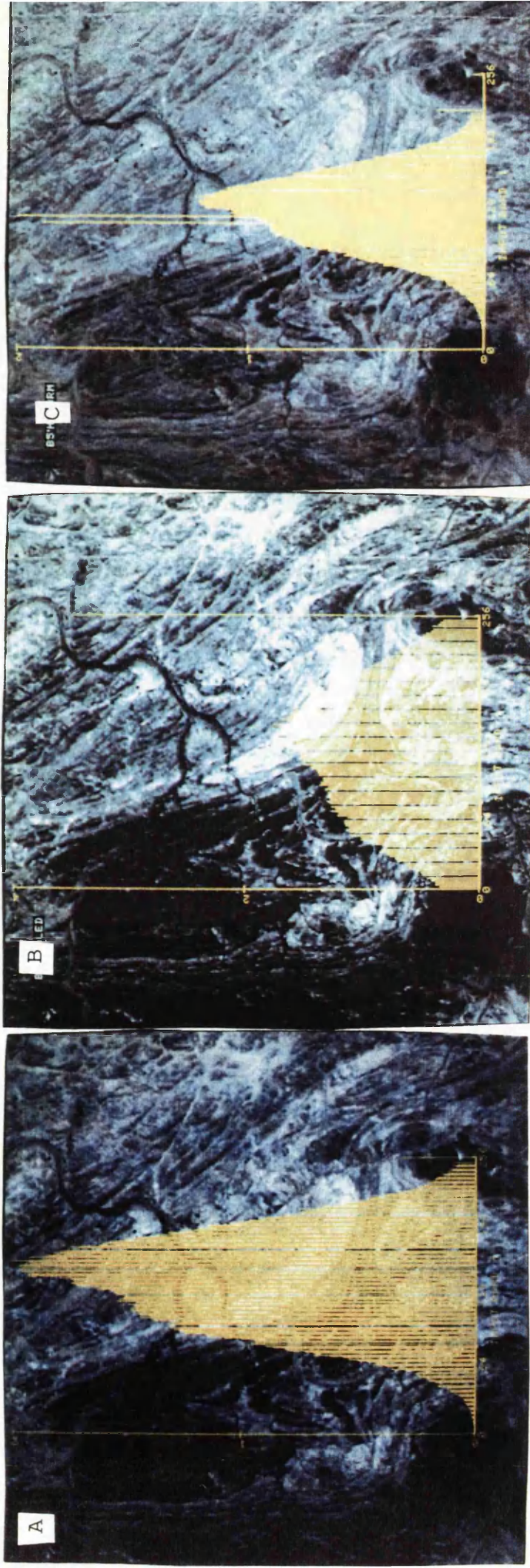
Fig. 3.2 A:Landsat TM band 5 subscene for the test-site
No.1; B:the linearly contrast stretched image;
C:the Gaussian contrast stretched image.

an enhancement technique that suppresses these variations. Reflectance ratios have been found to suppress variations due to topography and overall reflectance, while emphasizing differences in shapes of spectral reflectance curves (Abrams et al., 1977; Blodget and Brown, 1982). Therefore, ratioing (dividing) of TM bands was chosen in order to create a Colour Ratio Composite (CRC) image for later interpretations.

Method:

The TM bands selected were 1,3,4,5 and 7, whilst the ratio combinations (arithmetic operations) which were applied were:

- TM BAND 5/1, to portray rocks rich in opaque phases which have low band-5 and band-1 values. Figure 3.3A shows the TM band 5/1 image. Bright areas correspond to regions deficient in opaque phases.

- TM BAND 5/7, as a measure of the intensity of the hydroxyl absorptions in the 2.2-2.4 μm region, i.e. band 7. Figure 3.3B shows the TM band 5/7 image. The slightly brighter areas correspond to regions with high OH contents.

- TM BAND (5/4 x 3/4), was used to emphasize and discriminate the iron-bearing aluminosilicates. Figure 3.3C shows the TM band (5/4 x 3/4), where bright areas correspond to regions rich in Fe-bearing aluminosilicates, whereas the dark areas correspond to the granitic, gneissic, layered metamorphic and gabbroic rocks.

Rock units defined on enhanced imagery:

Gabbroic rock outcrops and amphibole-rich metamorphic rocks were identified in the TM band 5/1 ratio image because these rocks' constituent minerals have low reflectance values, i.e. low DN values. The greater the DN value, the brighter the pixel is. Again, gabbro and amphibolites were distinguished from other rock units observed in the test-site area on the TM band 5/7 ratio image. Amphibolites could be separated effectively from other lithological units on the TM band (5/4 x 3/4) imagery, where they show as bright areas.

The rock types mentioned have unique brightness patterns on the ratio images and should have unique colours on a CRC image. The granitic and the gneissic rock types have similar brightnesses on the three ratio images which will result in a similar colours on the CRC. The separation between the granitic and the gneissic rock types is difficult, but field knowledge helped in distinction of these types.

Fig. 3.3 SE1 Technique images for the test-site No.1.
A:TM band 5/1 ratio image ; B:TM band 5/7 ratio
image; C:TM band (5/4x3/4) ratio image.

43

The lithological information contained in the three TM band ratio images is integrated into one image. The resultant contrast-stretched CRC constructed is shown in Figure 3.4. The TM band 5/7 image was assigned the red component; the TM band 5/1 image, the green component; and the TM band (5/4 x 3/4) image, the blue component. Table 3.1 indicates the way of predicting the colours on the CRC, based on the mineralogical controls for each of the ratio images discussed previously. For example, the gabbroic rocks or the gabbroic regolith (sections H9 and C9, Fig. 3.4), have a high abundance of opaque phases, and a relatively high abundance of hydroxyl-bearing phases, and are deficient in Fe-bearing aluminosilicates (e.g. hornblende and biotite). Thus, gabbroic rock types will be red on the CRC. Similarly, granitic rocks (section F6, Fig. 3.4) and gneisses (sections G8, F9, E2, F5, J5, and J3, Fig. 3.4) are deficient in opaque, hydroxyl-bearing phases and Fe-bearing aluminosilicates and will appear as green colour on the CRC. Because the gneiss is mixed with other rock type; e.g. amphibolites, this is reflected in the colour of the granitic gneiss on the CRC (blue patches and/or bands in a green colour).

The sediments in the wadis consist primarily of mechanically weathered rock fragments that have been transported a short distance. Where the sediments are compositionally similar to the adjacent mountains, the wadis become spectrally indistinguishable on the CRC, e.g. the small wadis in the granite (section F6, Fig. 3.4). On the other hand, where the source rock of the sediments in the wadis is compositionally different from the adjacent mountains, the wadis preserve the spectral characteristics of their source rock and are thus spectrally distinguishable on the CRC (e.g. Wadi Bishah, sections F4-G2, Fig. 3.4).

A detailed geological map of the test-site area was constructed (Fig. 3.5) based on the CRC image. Field observations were used to supplement remote sensing interpretations in making decisions during the construction of the geological map. Comparing the geological map constructed from the TM image with the geological information contained in the earlier map of Coleman (1973b), it is clear that although there is a good correspondence between the two maps, there is more detail in the TM-based map. For example, the area which is mapped by Coleman as 'young metamorphic rocks' can be resolved into three distinct lithological units: amphibolites, schistose amphibolites and intercalated metasediments, amphibolites and granitic rocks.

There were four successive phases of tectonic deformation which affected the rock

Fig. 3.4 A contrast-stretched CRC of TM band 5/7 in red,
band 5/1 in green, and band (5/4x3/4) in blue
for the test-site No.1.

ROCK TYPE	B 5/7 image bright = RED	B 5/1 image bright = GREEN	B 5/4 × 3/4 image bright = BLUE	COLOUR IN CRC IMAGE
Granitic rocks	dark—moderate	bright	dark	Green
Granitic gneiss	dark	bright	dark—moderate	Bluish-green
Amphibolites	moderate—dark	moderate—dark	bright	Bright Reddish-blue
Schistose amphibolites	dark	dark	moderate—dark	Dark Blue
Gabbroic rocks	bright	dark	dark	Red
Intercalated layered metamorphic rocks	moderate—bright	moderate—bright	moderate—bright	Bluish-white

Table 3.1 Explanation of relative colour values in Fig. 3.4.

GEOLOGICAL MAP

0 _____ 2.5km

LEGEND

Granitic rocks

Granitic gneiss mixed with amphibolite

Amphibolites

Schistosed amphibolite

Gabbroic rocks

Intercalation of metasediments, amphibolites, and granitic rocks

Wadi with alluvium

Lithological contact

Fault, arrows show sense of movement

Strike and dip direction of foliation

Strike of vertical foliation

WADI BISHAH

N

Fig. 3.5 Geological map constructed from the CRC for the test-site No.1.

types exposed in the test-site area during Proterozoic time. These four phases produced folds, foliations and lineations. The four generations have been distinguished from each other in ground-based studies on the basis of their style, orientation and geometrical relationships to one another on various scales (Amlas, 1983; Qari, 1985).

The third phase of deformation was the dominant one, and the resultant geological structures are the most prominent and widespread in the test-site area. Numerous F3 folds are observed throughout the area, and also some F2 folds.

The strike directions of foliation can be delineated on the CRC imagery, particularly in the gneissic and the layered metamorphic lithologies.

Several structures could be easily detected on the CRC imagery. Second-, third-, and fourth-phase folds (F2, F3, and F4), were clearly detectable in interference folding patterns (Qari, 1989). Several F2 antiformal fold axial traces (Fig. 3.4, sections D5, D6, E7, and A4), and several F3 antiformal and synformal fold axial traces were mapped throughout the area. The F3 axial traces strike approximately N-S. Major F4 folds were not easily located although many minor F4 structures were observed on the ground (c.f. Amlas, 1983 and Qari, 1985). The structural map revealed an F4 regional doming pattern (Fig. 3.6). The axial trace of the F4 dome strikes E-W. Micro- and meso-scale folds were not detectable or extendable on the CRC imagery because their wavelengths are less than the resolution of the imagery. The criterion on which these folds and their axial traces were identified is the change of the geometry of the foliation planes.

Faults were also easily detectable and extendable on the CRC imagery. For example, the gabbroic synformal structure (sections H8 and H9, Fig. 3.4), has been faulted by a left-lateral strike-slip fault (Fig. 3.6).

SE2 Technique

Loughlin and Tawfiq (1985), found that for general geological interpretation in arid terrains, a False Colour Composite (FCC) using TM bands 7, 4 and 2 in red, green and blue respectively is the best choice, whereas one using bands 7, 5 and 2 is excellent for discriminating clay and ferruginous alteration products. They also suggested the CRC (7/5,5/4,4/2) in red, green, blue respectively as a useful combination for general lithological discrimination which suits the varied topographic conditions.

STRUCTURAL MAP

0   2,5km

LEGEND

Foliation/lithological layering

Fold axial trace

Direction of plunge of fold axes

F2 Antiform

F3 Antiform

F3 Synform

F4 Doming

Strike and dip direction of foliation

Fault, arrows show sense of movement

Oval/circular igneous body
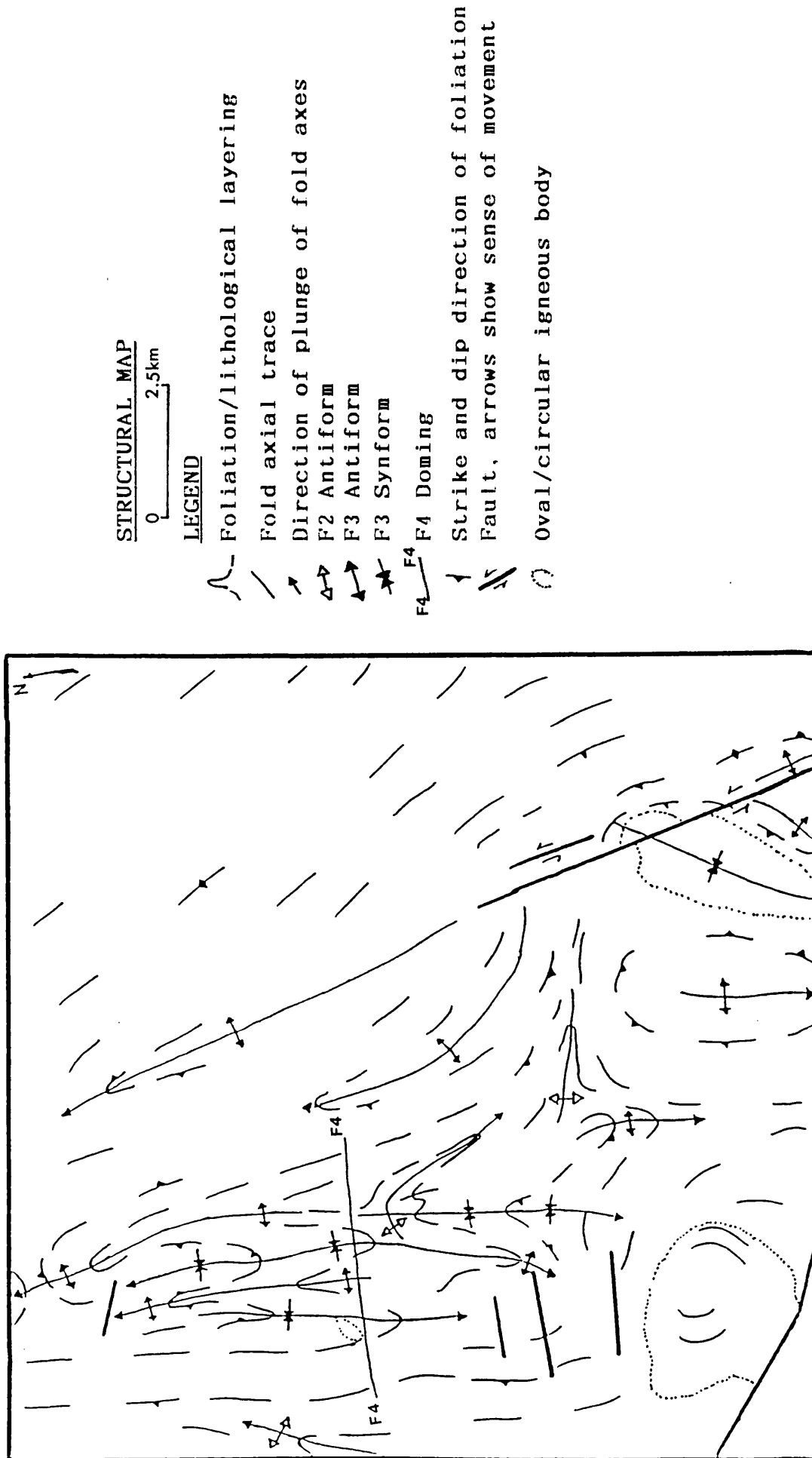
Fig. 3.6 Structural map constructed from the CRC for the test-site No.1.

Method:

The TM bands selected were 2,4,5 and 7, whereas the ratio combinations which were obtained after applying a contrast stretching were:

- TM BAND 7/5. Although TM band 5/7 is widely used for the detection of clay alteration and as a measure of the intensity of hydroxyl absorptions, Loughlin and Tawfiq suggested its inverse, the ratio 7/5. They do not explain why. This produces a negative image compared with the 5/7 ratio image, with moderately dark areas corresponding to regions rich in OH content (Fig. 3.7A).

- TM BAND 5/4. This emphasizes and discriminates Fe-bearing aluminosilicates. Figure 3.7B shows that the bright areas correspond to regions rich in these minerals, whereas the darker areas correspond to the other rock units presented in the area.

- TM BAND 4/2 (NIR/Visible green). This is used for the detection of iron-staining. Such areas are shown as dark in Figure 3.7C.

Rock units defined on enhanced imagery:

Granites were identified easily as the brightest areas on the TM band 4/2 ratio image (Fig. 3.7C), because their opaque-phases content is very low compared to the other units, i.e. gabbro and metavolcanics. The gneissic unit could also be identified as relatively brighter areas. On the TM band 5/4 ratio image (Fig. 3.7B), rock units rich in Fe-bearing aluminosilicates, i.e. amphibolites, could be discriminated reliably. They show a particularly strong contrast with the darker background which facilitates lithological contact verification. The schistose amphibolites were less easy to identify than the massive amphibolites in this ratio image.

The rock types mentioned have unique brightness patterns on the ratio images, which are reflected in the CRC image as well. Here, the separation between the granitic and gneissic rock types is much easier than that obtained by the SE1 technique both on the 4/2 ratio image and the CRC image.

The lithological information contained in the three TM band ratio images has been integrated into one image. The resultant FCC is shown in Figure 3.7D, where the TM band 7/5 image was assigned the red component; the TM band 5/4 image, the green component; and the TM band 4/2 image, the blue component. This FCC image was not acceptable for interpretation purposes. Therefore, one further linear contrast stretch was applied in order to enhance the FCC. The resultant CRC imagery is shown in Figure
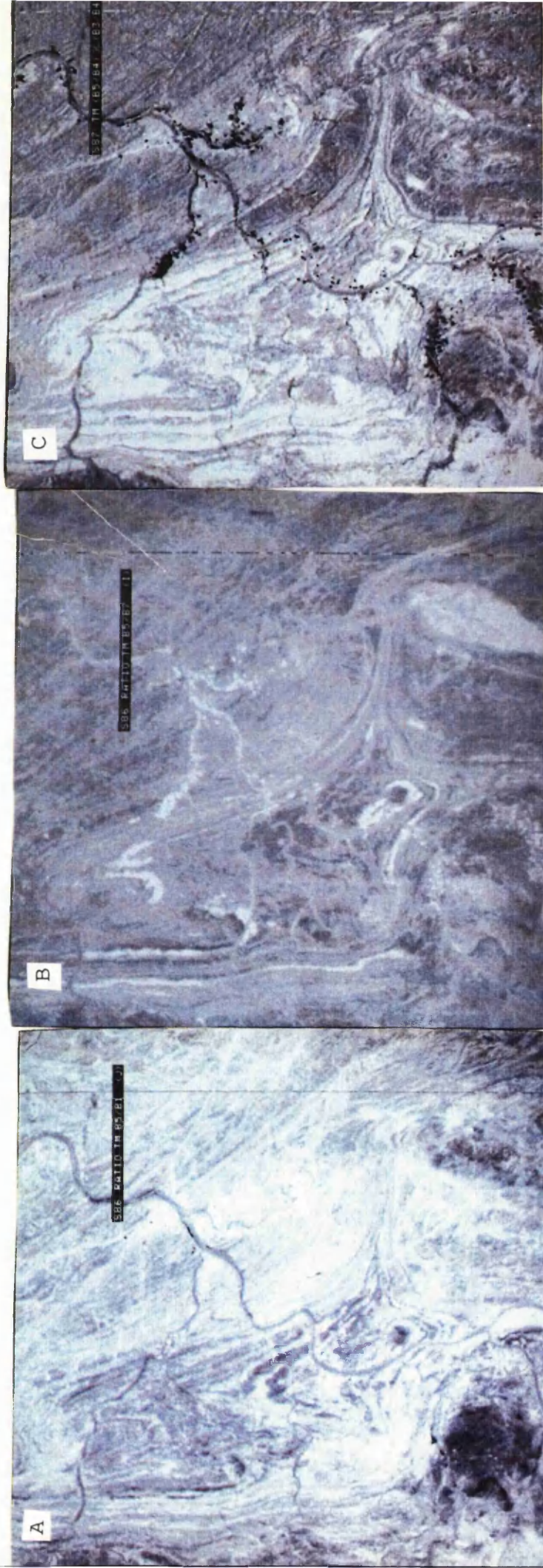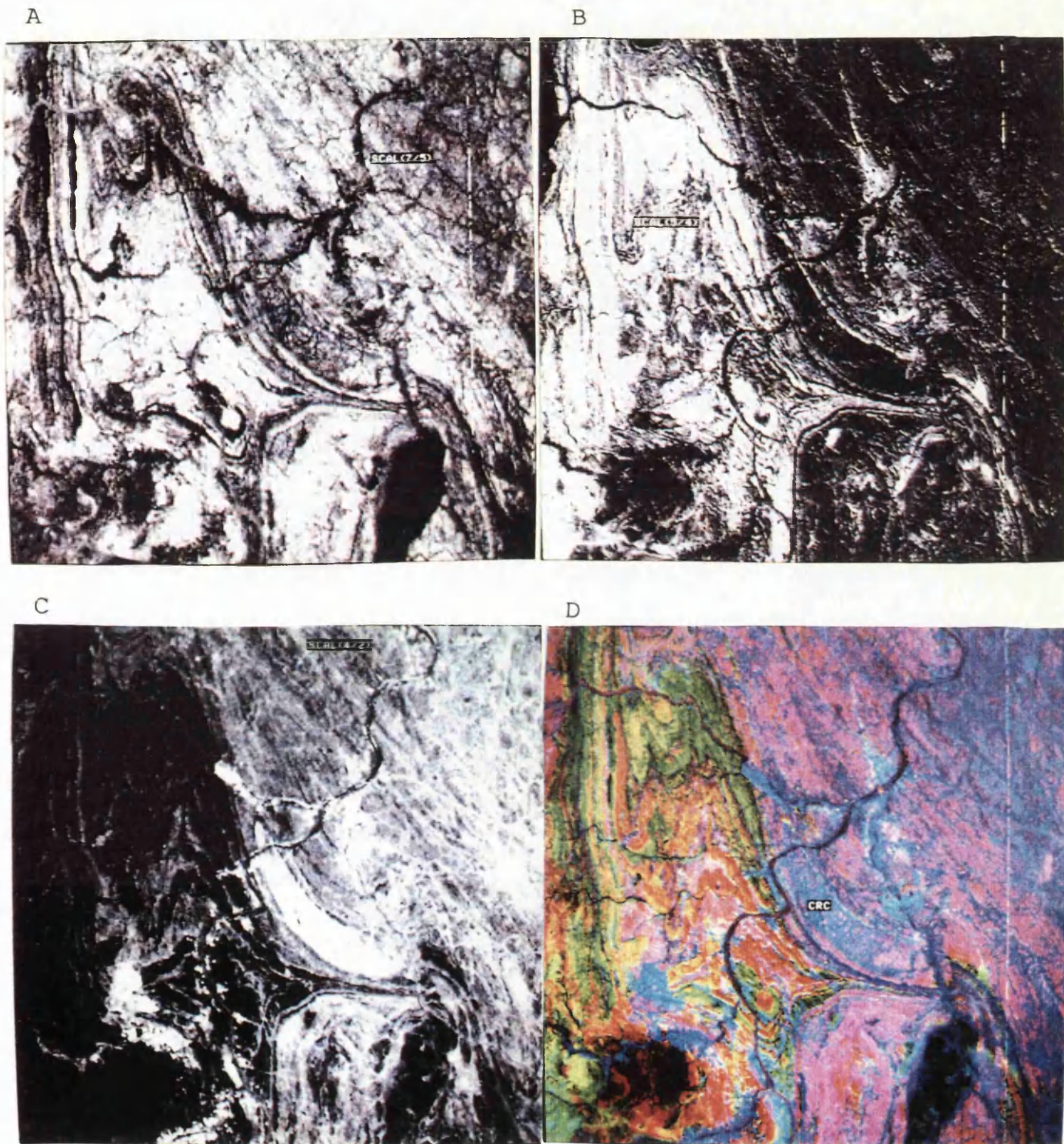
Fig. 3.7 SE2 Technique images for the test-site No.1.
A:TM band 7/5 ratio image; B:TM band 5/4 ratio
image; C:TM band 4/2 ratio image; D:FCC image.

3.8, and this was then suitable for the later interpretations.

After comparing the results obtained by this technique and those by the SE1 technique, it was found that the results of both techniques were mostly identical. However, gabbroic rocks are much easier to identify by the SE1 technique, and granitic rocks are also easier to identify in this technique.

The geological map constructed using the SE1 technique (Fig. 3.5), could alternatively be constructed using information from the CRC obtained by the SE2 technique. For structural mapping, the SE2 technique and the SE1 technique yield identical results.

(b) Statistical analysis based technique

Principal-components analysis (PCA), originally known as the Karhunen - Loeve transformation, has been used for many years in various applications including remote sensing.

Typically, for any pixel in a multispectral original image, the DN values are highly correlated from band to band. This correlation means that there is much redundancy in the data set.

PCA is used to compress multichannel image data by calculating a new coordinate system, i.e. by determining a linear transformation that can condense the scene variance in the original data into a new set of variables, which are called principal components. Its aim is to produce decorrelated images in which most of the image variance is confined in the first few PC's. Normally, the first, second, and third principal component (PC) images will contain appreciably more information than any of the raw channels. If a FCC is generated from the first three PCs by assigning each PC image to red, green and blue respectively, it is not possible to make much fuller use of colour space. This problem can be overcome by producing a decorrelation stretched image (Soha and Schwartz, 1978).

Decorrelation stretching is becoming widely used in geological remote sensing, and is proving very effective in supplying geological information (Abrams et al., 1985; Drury, 1987; Gillespie et al., 1986; Rothery, 1987a; 1987b; 1988). The technique is called SE3, following the procedures described by Rothery (1988).

Fig. 3.8 Linearly contrast stretched CRC of TM band 7/5 in red, band 5/4 in green, and band 4/2 in blue for the test-site No.1.

SE3 Technique

Method:

Rothery (1987a) has demonstrated that it is better to enhance the colour information in a three-band colour composite, because this enables the geologist to appreciate and interpret the significance of each colour. The three spectral bands used should be those which, in combination, perform the best discrimination between surface types. Thus TM bands 7, 5 and 4 were selected. The technique is described in Rothery (1988), with one emphasis, i.e. the final decorrelation stretched image must be scaled to render it displayable and interpretable.

Rock units defined on enhanced imagery:

A TM band 7,5,4 red, green, blue decorrelation stretched FCC image of the test-site area is shown in Figure 3.9. The gabbroic rocks display blue colour hues (sections B9, B10, C9, and C10), which must not be confused with the blue patches along wadis, which are areas of vegetation. Granite is the best discriminated lithological unit. The granitic outcrops are shown in bright white hues (e.g. sections E5, F7, and I2), while the amphibolitic rocks display a mixture of colours (greenish, brownish and reddish brown). The schistose amphibolite differs from the amphibolitic unit in that the colour is mostly pure reddish brown (sections D5 and D6). The granitic gneiss tends to be white in colour, but because it is mixed with amphibolites, it often also includes brownish reddish hues on a white background (e.g. sections E1, E3, F8, and I8). Where it is intercalated with units rich in metasediments, it displays yellow hues (e.g. sections A10, B1, B6, and C5). The main wadis are well distinguished on the FCC, because they are different in composition from the surroundings and hence differ in spectral characteristics (e.g. Wadi Bishah, sections F4 and G2).

The geological map (Fig. 3.5) constructed for the test-site area based on the FCC image is identical to that produced using the techniques described earlier.

Similarly, the geological structures recognized using this technique are similar to those recognized with the SE1 technique.

3.3.4 Edge enhancement techniques

(a) Introduction

Landsat images are especially suited for lineament analysis in relatively high relief areas

Fig. 3.9 TM band 7,5,4 red,green,blue scaled decorrelation
stretched FCC image for the test-site No.1.

where fractures are highlighted by shadowing and appear on the images as linear boundaries. The boundaries mark changes from one range of DN to another, and this is represented by a steep or even vertical gradient, giving rise to edges. These may be shadow effects giving information on topographic features, or may be tectonic features, such as faults or joints. Some edges are boundaries between rocks with different properties, but they have been explicitly excluded from this analysis. Lineaments can be defined as "mappable, simple or composite linear features of a surface, whose parts are aligned in a rectilinear or slightly curvilinear relationship and which differ distinctly from the patterns of adjacent features and presumably reflect a subsurface phenomenon" (O'Leary et al., 1976).

Edge enhancement, edge detection or filtering (high-pass) is a valuable image enhancement technique for detecting lineaments. By suppressing very low frequencies in an image, a harsher contrast stretch may be applied to the image data, because the linear features are often very subtle on Landsat images. This allows increased discrimination of fine detail, and also may reveal some structures that were obscured by albedo changes in the unfiltered image. A certain amount of subjectivity is inevitable in defining and drawing the lineaments. Filtered images should be used and examined carefully to avoid misinterpreting other artifacts similar to lineaments, such as scene detail. Also, images produced in this way must not be used for any processing other than visual interpretation, and even then with some care.

(b) Image enhancement

Edge enhancement is often used to bring out geological structure, especially lineaments or fractures, but other structural features which may appear on imagery, such as foliations, bedding planes and compositional layering, may also benefit from this enhancement. A variety of edge enhancement algorithms in the literature have been tested on the test-site area image. These include: Laplacian, Prewitt, Roberts, Sobel and other box filters with different kernel sizes.

Edge enhancement was achieved by high-pass filtering in order to emphasize higher spatial frequencies. This was done using a convolution operation which is useful for increasing contrast differences for the enhancement of lineaments. Convolution is the movement (pixel by pixel and line by line) of a filter window through an image. Successive elements of the original image are multiplied by values within the window, and the products are summed to form the resulting filtered (enhanced) image. Contrast

stretching (scaling) is very important after each convolution to render it displayable.

Any TM band of digital data can be directionally enhanced, but TM band 5 (1.55 - 1.75 μm) is generally selected for this purpose, because bare rock has a relatively uniform grey tone on band 5 images and because atmospheric haze penetration is better in this part of electromagnetic spectrum. Winter season (low sun-elevation) images are best for the detection of lineaments because of the shadow caused by the topographic steps or tones along the lineaments. A sun elevation of 35 to 45 degrees, for example, is near optimum for slightly rolling terrain (Moore and Waltz, 1983).

The method used here has been developed from the technique described by Moore and Waltz (1983). The Landsat TM digital image of the test-site area has been processed using three high-pass directional digital filters to enhance linear features oriented along the north, northeast and northwest directions. These directions are found to be the most informative in this part of the Arabian Shield, where most rocks are well exposed and there are no human alterations over most of the ground.

A three-step procedure was performed for lineament enhancement. The first step in the procedure was to increase the contrast of edges that have trends in approximately the selected directions by making the dark side of an edge segment darker and the light side lighter relative to the background. The resulting filtered images are shown in Figures 3.10A, B and C.

In the second step, all three filtered images were added together and one more contrast stretching (scaling) was applied (Fig. 3.10D). The product of this step was regarded as appropriate for visual drawing of the lineaments or fractures. However, a better image was obtained by adding this scaled filtered image to the original image, and this was the last step of the procedure. The product is shown in Figure 3.11, which is the directionally enhanced image for the test-site area, which was used for the identification and tracing of lineaments. The steps followed are summarised in Table 3.2. Similar results could be obtained following the procedure described in Appendix B.

The lineaments were identified by visual inspection, recorded on transparent overlay as ruled straight lines. A conventionally compiled fracture map (Fig. 3.12), has been constructed, which was used as the data-set for further geological interpretation.
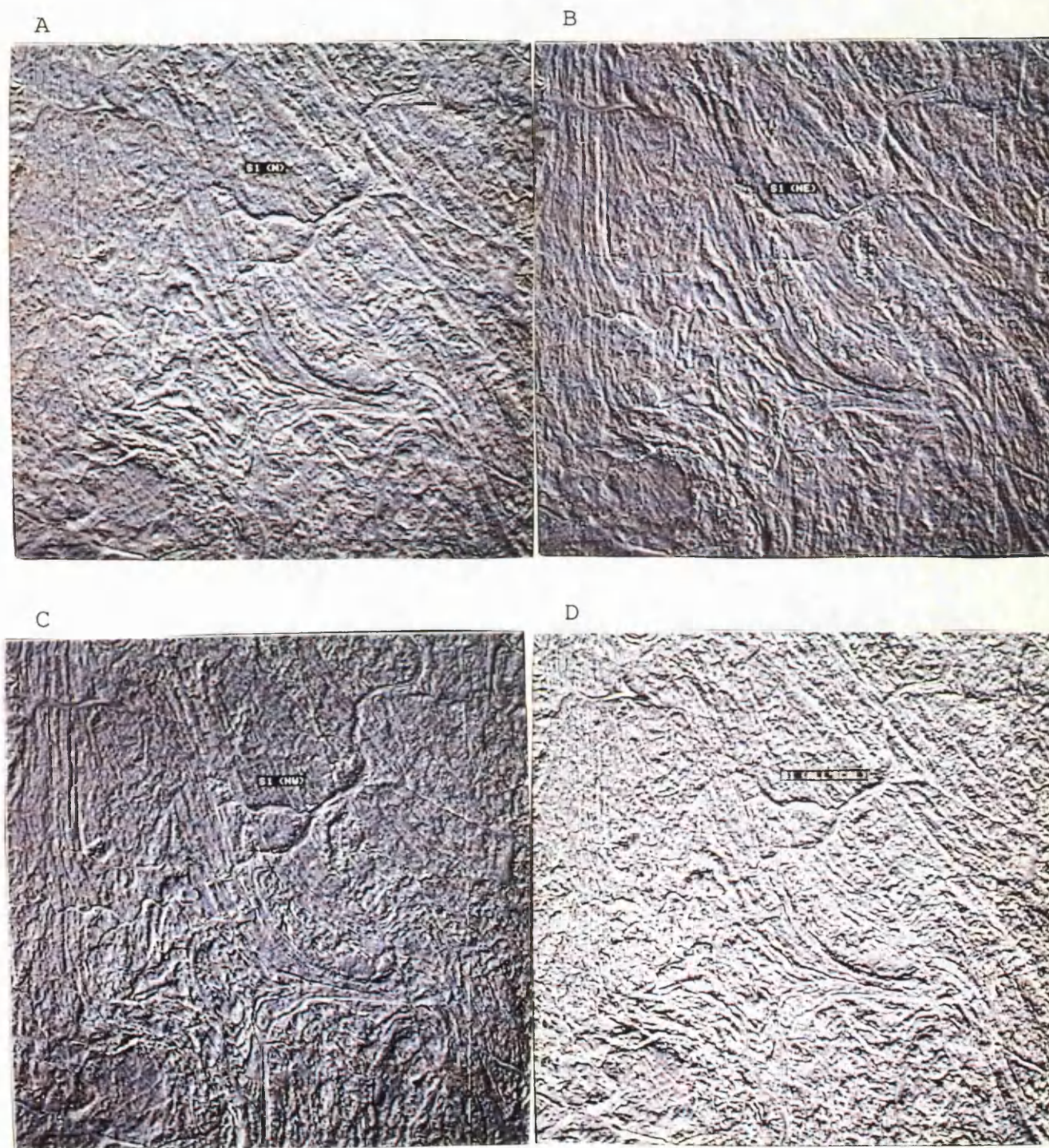
Fig. 3.10 Edge enhancement technique images for the test-
site No.1. A:north directional high-pass filtered
image; B:northeastern directional high-pass filtered
image; C:northwestern directional high-pass filtered
image; D:all these three filtered images added
together with additional scaling.

Fig. 3.11 Directionally enhanced image superimposing TM band 5 for the test-site No.1.

STEP 1: Derive directional components from original TM band 5.
Each pixel in the window is multiplied by the digital value, the final value for the central pixel being the sum of these products. Apply linear stretching (scaling) to each individually.

NORTH-WEST

1	1	1
1	-2	-1
1	-1	-1

NORTH

1	1	1
1	-2	1
-1	-1	-1

NORTH-EAST

1	1	1
-1	-2	1
-1	-1	1

STEP 2: Add the previous directionally derived components (filtered images) and apply scaling.
Scaling is a procedure where the lowest digital value is set at 0, and the highest at 255, all intermediate values being distributed through this range.

STEP 3: Superimpose (add) directional components of Step 2 to the original TM band 5 image for display and interpretation.

Table 3.2 A three-step procedure for producing directionally enhanced images.

PRELIMINARY LINEAMENT MAP

0   2.5 km

▬▬▬ Dominant lineament

——— Weak lineament

) Oval/circular igneous body

N
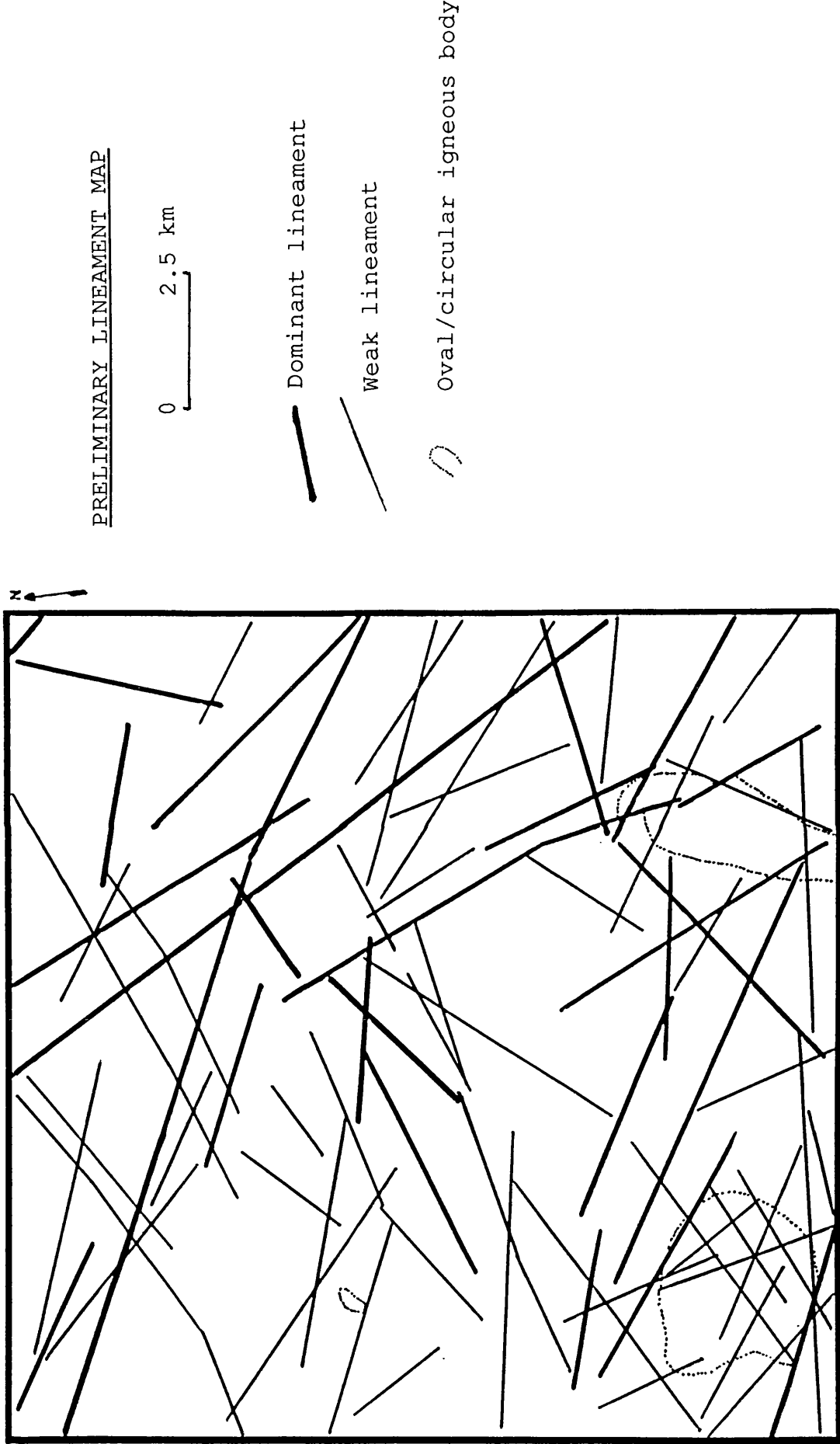
Fig. 3.12 Preliminary lineament map for the test-site No.1.

The lineaments, particularly the longer ones, are composite, i.e. defined by more than one type of feature such as linear tonal contrast, straight segments of valleys, ridges and topographic escarpments.

Lineaments running parallel or subparallel to the sun azimuth of the Landsat on the acquired date will hardly be detectable. With a 57 degrees sun elevation, shadow enhancement will be at a minimum for lineaments running parallel or subparallel to the sun azimuth direction, which is in the 101° direction. Consequently, the 280 - 290° direction will be under-represented on the Landsat imagery. Directions perpendicular to the sun azimuth direction, the 10 - 20° direction, will be additionally enhanced. To overcome this, the three directional filters previously mentioned were found to solve the problem. Structural geological knowledge, based upon work in the field, has been applied to arrive at a fracture map with a different emphasis. This map (Fig. 3.13), was produced by using the resulted image from the edge enhancement procedures as an input together with the resultant images of the previously described techniques, i.e. ratio and decorrelation stretching techniques. This map is used as the basis for discussion of lineaments and fractures. Ground inspection and geological significance of lineaments were considered before preparing the map. When extracting the lineaments, what remains relatively constant and reproducible is the azimuth of the line drawn rather than its precise location. Thus, the present analysis emphasizes lineament trends rather than the absolute locations of lineaments. Figure 3.14 shows the successive logical course followed for obtaining the remotely sensed geological fracture map.

(c) Lineament trend interpretation of Landsat images

The synoptic, equal-illumination images provided by Landsat present an ideal opportunity for examining the structural fabric of an area. Unfortunately, not many workers have mapped lineaments from Landsat data in the Arabian Shield, and particularly the southern part where the test-site area is situated. A few regional studies are available, mainly covering central Saudi Arabia (Moore, 1976; Norman, 1980a; Al-Khatieb, 1981; Al-Khatieb and Norman, 1982). Norman (1980a) discussed the tectonic structure of the cover rocks in Saudi Arabia and studied the statistics of the orientations of straight lineaments in the Arabian Shield based on a Landsat Multi-Spectral Scanner (MSS) 1:2,000,000 mosaic. Figure 3.15 is his rose diagram for lineaments in the basement areas of Saudi Arabia (Arabian Shield). It can be seen that there are several preferred directions. The implication is that a stress field caused the activation or a reactivation of old lines of failure, in the basement rocks (Al-Khatieb and Norman,

REMOTELY SENSED GEOLOGICAL
FRACTURE MAP

0   2,5km

——— Lineament (mainly joints)

▬▬ Observed faults

⌒ Oval/circular igneous body

N
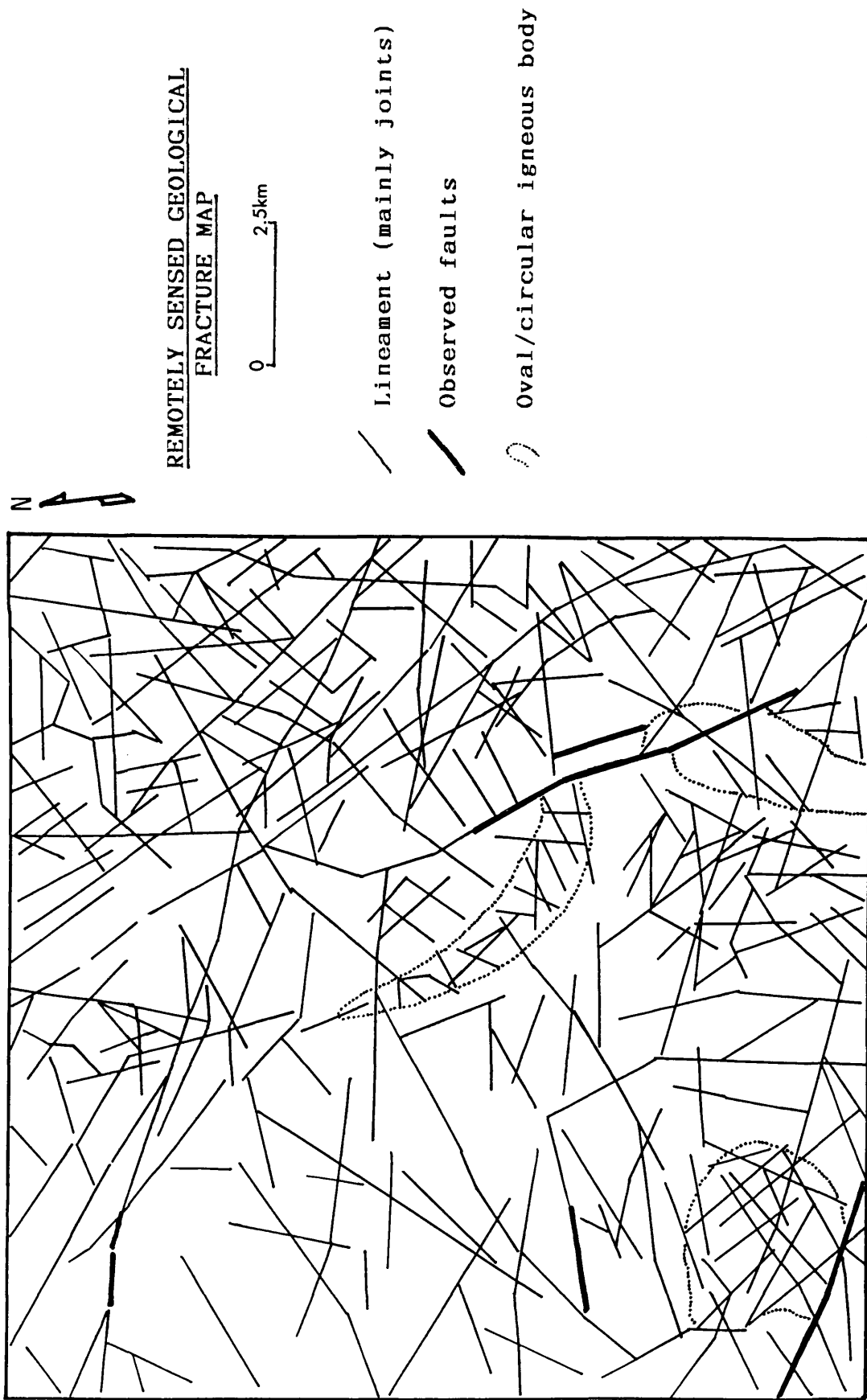
Fig. 3.13 Remotely sensed geological fracture map for the
test-site No.1.
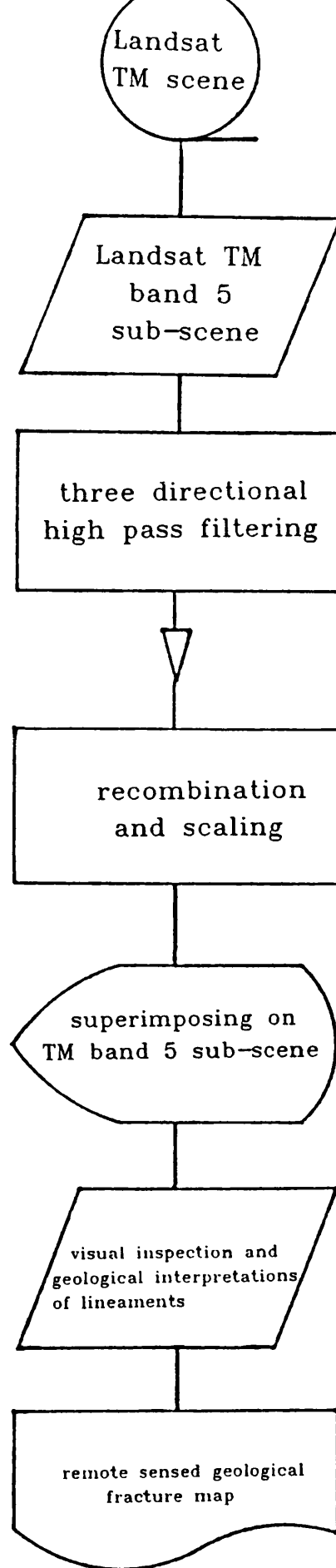
Fig. 3.14 Successive logical procedures of obtaining
a remotely sensed geological fracture map.
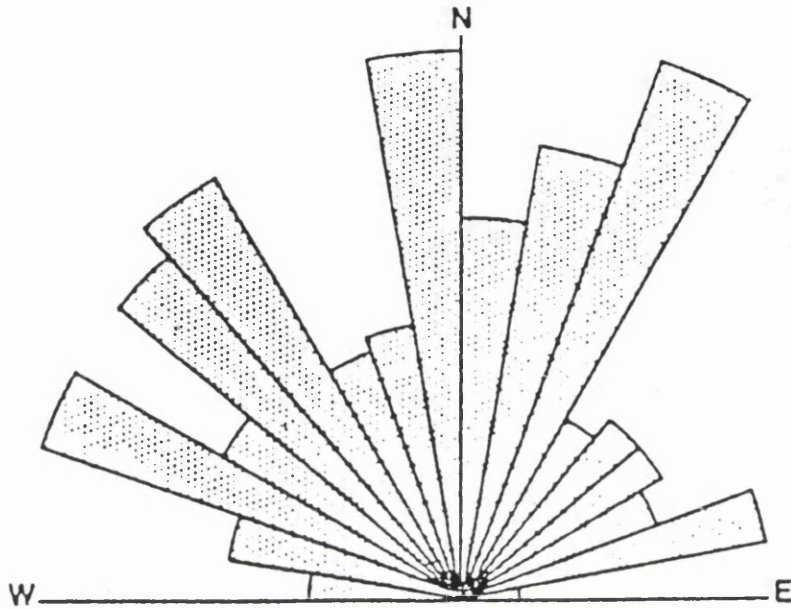
Fig. 3.15 Relative directional frequency of lineaments in the basement of Saudi Arabia (Norman, 1980a).

1982).

Computer processing of lineament data provides an objective method of interpretation. Often, visual inspection fails to reveal significant trends on a lineament map. The significance of the lineaments interpreted from images was analyzed by using directional frequency rose diagrams with a 10 degree azimuth class interval.

Initially, the conventionally constructed fracture map (Fig. 3.12), includes weak and dominant lineaments, where the dominant ones are the wider and more easily detected lineaments. Separate rose diagrams for each category (Figs. 3.16A and 3.16B) were plotted as well as a combined diagram for both categories (Fig. 3.16C). Two trends stand out above the background: N 55° W and N 65° E; neither could be correlated with the earlier study of Norman (Fig. 3.15).

Study of the detailed fracture map (Fig. 3.13), shows that lineament frequency is greater in areas of exposure of granitic gneisses and granites (granitoid rocks) (Fig. 3.5). Therefore, the test-site area was divided roughly into two domains: a domain of granitoid rocks and a domain of non-granitoid rocks, based on the rock units exposed. Two rose diagrams were plotted separately for these two domains (Figs. 3.17A and 3.17B). In the granitoid domain there is no obvious preferred orientation of lineaments, whereas in the non-granitoid domain there are broad concentrations orientation. A broadly NE-SW, E-W, a weaker WNW-ESE and N 25° W directions are visible in the combined domain rose diagram (Fig. 3.17C). Although E-W lineaments were not recorded by Norman (c.f. this analysis), some directions were observed in both studies, e.g. N 65° W. This is because Norman was dealing with the entire shield area, mostly concentrating in the central part, whereas the test-site area is very small compared to that of Norman. In addition, the study area lies in the southern Arabian Shield where the structural grain may well be different from the central part of the shield.

The lineaments shown on Figure 3.13 were counted on a 2.5- by 2.5-km grid, and the total density was contoured (Fig. 3.18) to examine the pattern of concentration and to assess how it might relate to the other studies. The number of lineaments/6.25km^2 varies from 2 to 21. Several locations of high concentrations of lineament density are quite apparent. There is a high lineament frequency in the granitoid domain, particularly the two concentrations (>15) to the upper right of the map (Fig. 3.18).
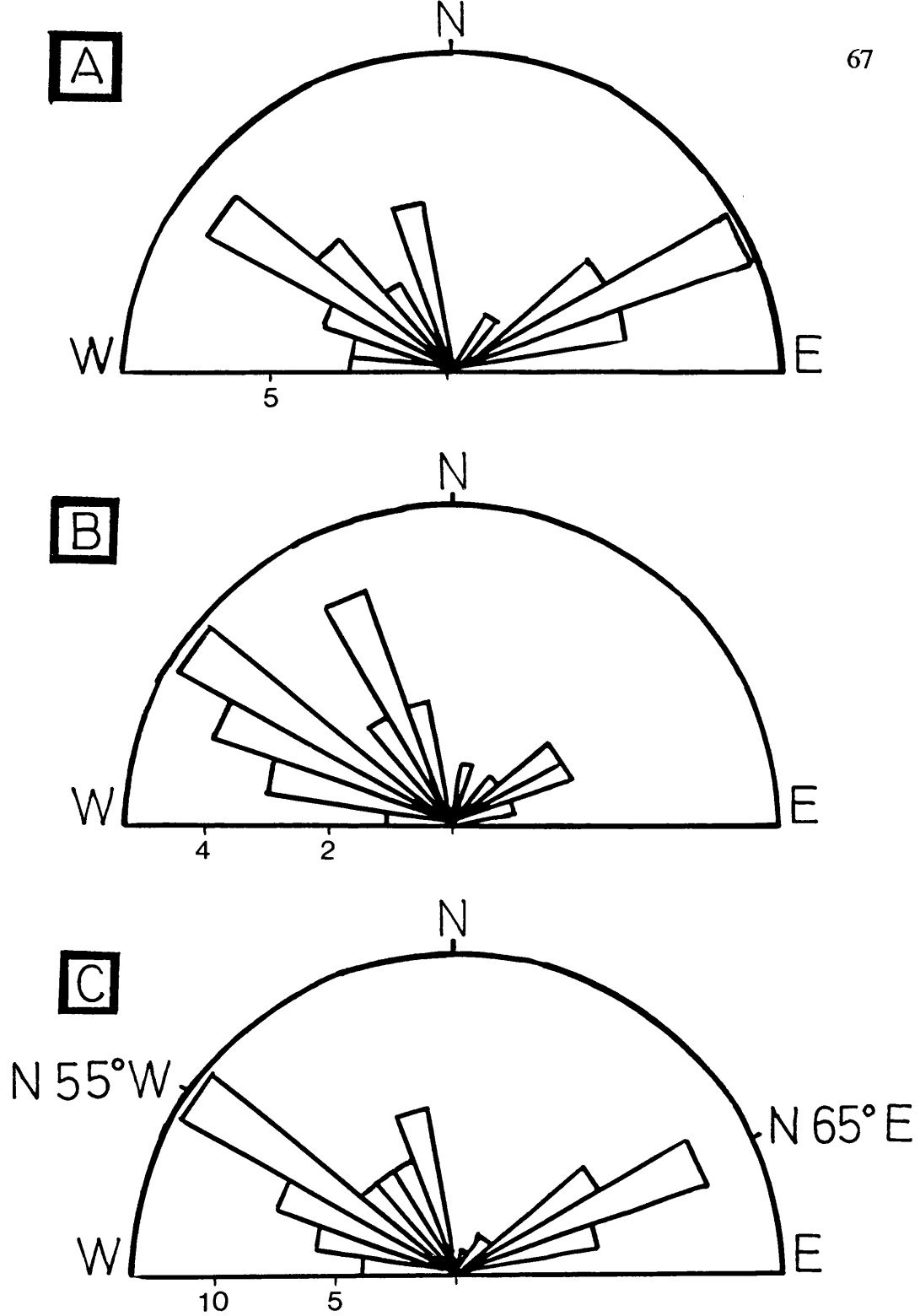
Fig. 3.16 Rose diagrams summarising strike-frequency
distribution of the lineaments in Fig. 3.12.
A:weak lineaments; B:dominant lineaments; C:84
lineaments of A and B.

(This, and the following diagrams, plot number of
lineaments but do not consider lineament length)
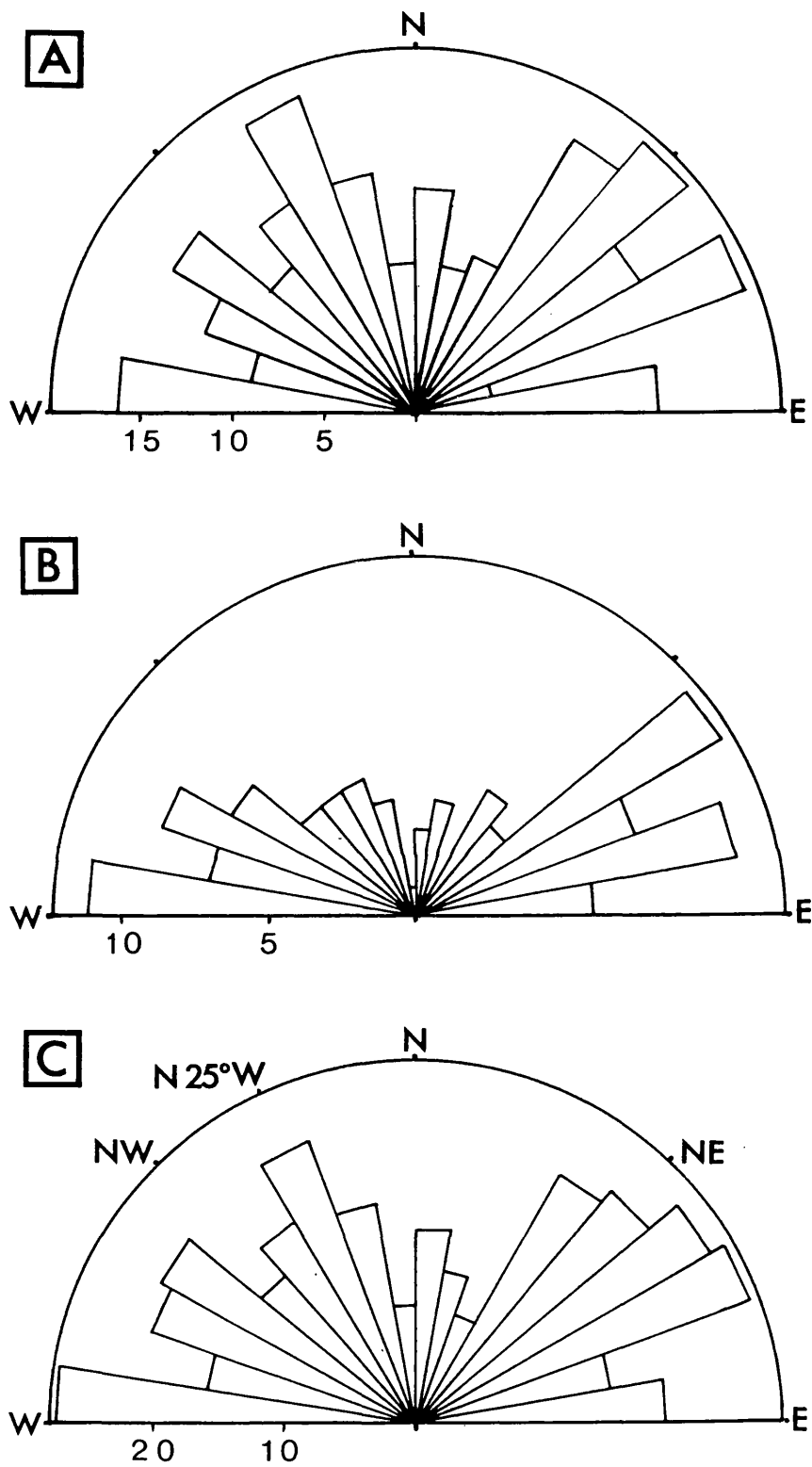
Fig. 3.17 Rose diagrams summarising strike-frequency
distribution of the lineaments in Fig. 3.13.
A:granitoid rocks domain; B:non-granitoid rocks
domain; C:336 lineaments of the two domains.
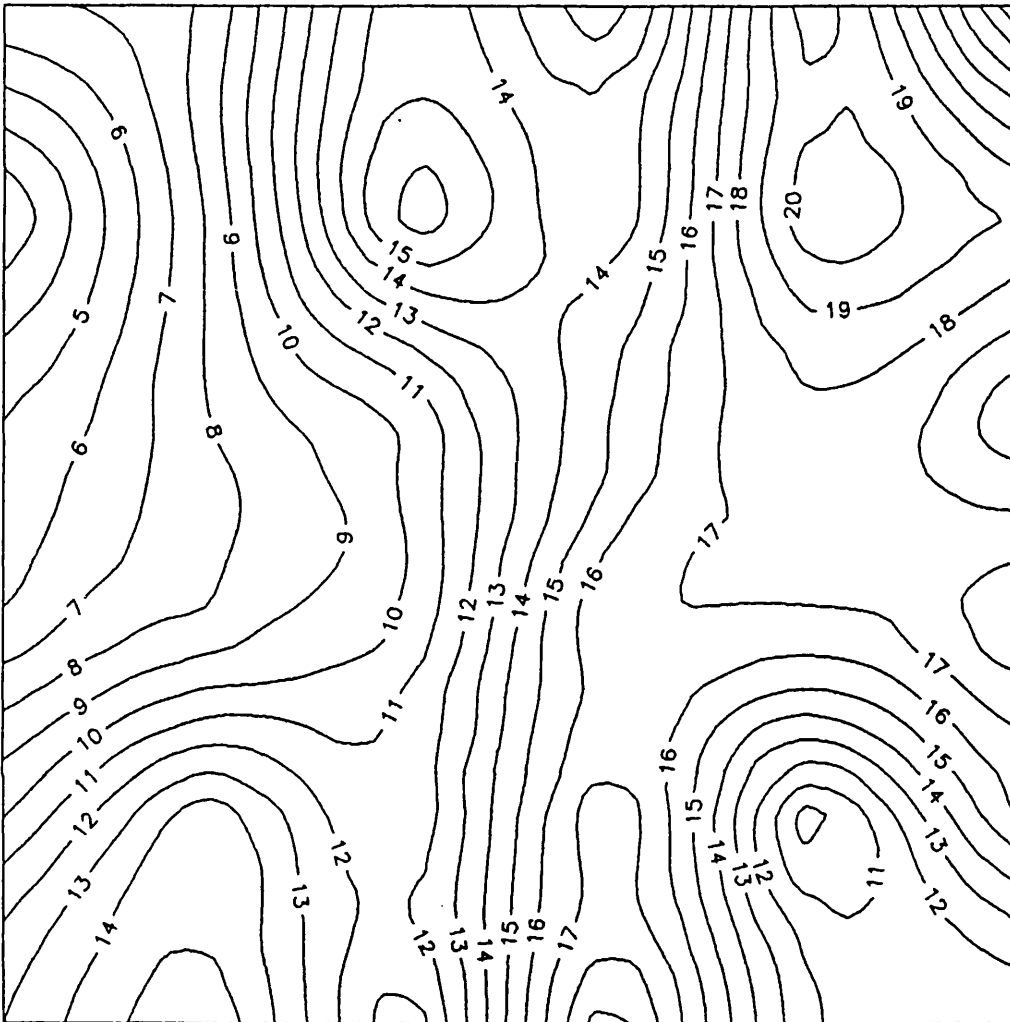
Fig. 3.18 Fracture density isopleth map. Fracture density is expressed in number of fractures/6.25 km^2.

An attempt was also made to correlate the observed lineaments (Fig. 3.13) and mapped faults, using the detailed available geological maps of Amlas (1983) and Qari (1985). Many lineaments were found to accord with mapped faults, and field work indicates that other lineaments correspond to joint sets which have not previously been mapped in the ground surveys.

An important conclusion is that image analysis is a very objective and effective method of mapping lineaments and that lineament interpretation should not be based solely on ground studies. Ground studies can complement space-borne imagery in order to obtain fruitful results.

(d) Conclusion

Landsat TM imagery proved particularly useful for revealing lineaments which can be correlated with fractures within the test-site area. Some of these structures were known or suspected from ground studies, but the majority were revealed for the first time during the Landsat TM investigations. The edge enhancement technique was found to be more useful in detecting edges in dark coloured areas on unprocessed images (low DN values).

Quantitative examination of the lineaments showed that the test-site area has several preferential directions, these are E-W, NE-SW, WNW-ESE and N 25° W. The application of the procedures followed in this technique to the entire research area, should reveal significant trends in relation to the regional tectonics. It would be a good idea to include the interpretation of aeromagnetic maps in such regional analysis.

Although the images produced by edge enhancement techniques were very useful for the study of lineaments, one can detect most of the lineaments (about 80%) from images prepared by previously mentioned enhancement techniques.

CHAPTER FOUR   APPLICATION OF METHODS:
II. TEST-SITE No.2
(AL-KHABT AND AL-FAYD AREA)

4.1 INTRODUCTION

4.2 GEOLOGY OF THE TEST-SITE

4.3 REMOTE SENSING TECHNIQUES

    4.3.1 Introduction

    4.3.2 Contrast enhancement

    4.3.3 Spectral enhancement techniques

        SE1 Technique

        SE2 Technique

        SE3 Technique

    4.3.4 Edge enhancement techniques

    (a) Image enhancement

    (b) Lineament trend interpretation of Landsat images

    (c) Conclusion

4.1 INTRODUCTION

The second test-site was selected because of the interesting structural character, diverse lithology and the location within the Nabitah Mobile Belt in contrast to test-sites No.1 and No.3, which are located approximately on the border between the Asir Terrane and the Nabitah Mobile Belt. Again, there is excellent exposure of lithological units as in test-site area No.1.

Because of the interesting structural geometry of the test-site which could not be displayed and processed in one 512x512 pixels sub-scene, it was necessary to handle this test-site as two separate 512x512 pixels sub-scenes in order to utilize the full-resolution criterion, so that no data element from the Landsat TM imagery is ignored. Hence, these test-sites are called 2A and 2B respectively (Fig. 1.3), with an area of overlap to help in the preparation of the geological analysis.

The only detailed geological studies available for this test-site are four 1:100,000 quadrangle maps (Anderson, 1979; Greenwood, 1980; Stoeser, 1984), where broad lithological discriminations were based on photo-interpretation and field checking of some localities (Fig. 4.1). Apart from these maps, Blodget (1977) used early Landsat MSS digital imagery for lithological mapping of crystalline shield test-sites in western Saudi Arabia. He used the False Colour Composite (FCC) images and contrast-stretched ratio images in his study. The difference between the two studies are:
-the resolution of the images used, i.e. 80m for the MSS and 30m for the TM.
-Blodget used only one technique for lithological mapping, i.e. standard MSS ratio technique, whereas this study deals with three techniques for lithological discrimination.
-Blodget's test-sites covered a large area, hence there was loss of data due to sub-sampling of the scene, whereas this study deals with full-resolution analysis with no omission of any data element of the TM digital imagery.

4.2 GEOLOGY OF THE TEST-SITE

The geology of the test-site is complex due to folding, intense faulting and intrusions. The major lithologies are: Tertiary volcanic rocks, Precambrian metamorphic and plutonic rocks. Reconnaissance geological mapping at 1:100,000 scale was carried out by the Directorate General of Mineral Resources (DGMR) personnel (Anderson, 1979; Greenwood, 1980; Stoeser, 1984). This was followed by a regional 1:250,000 scale

73

SCALE 1:100 000

N

AL FAYD
TONALITE

SUWAYDAH GNEISS

HADABAH
DOME
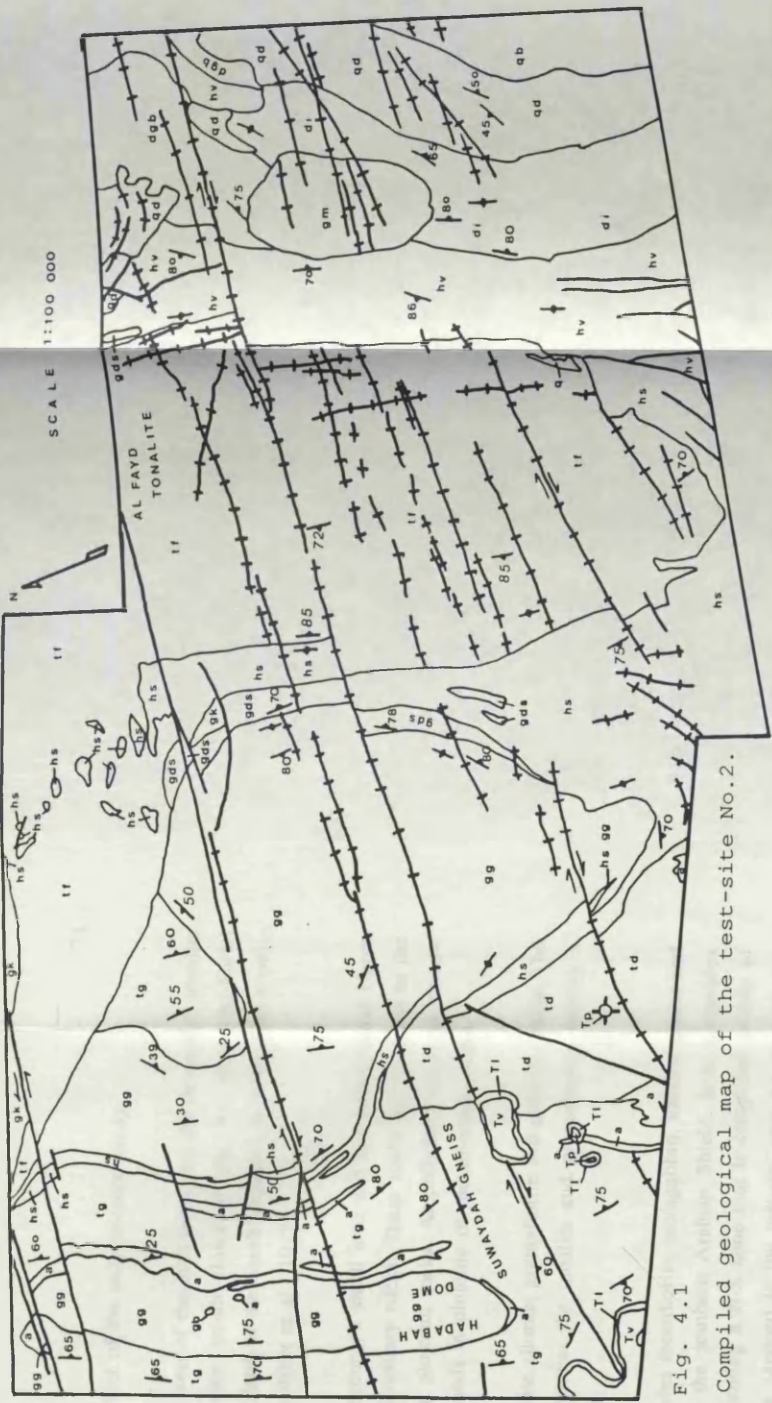
Fig. 4.1

Compiled geological map of the test-site No.2.

LEGEND

Tv	Volcanic rocks (basalt flow)
Tl	Laterite
Tp	Basalt pipes
q	Quartz pods
gm	Monzogranite
gb	Gabbro
gk	Khaniqah granite (biotite monzogranite)
td	Mafic tonalite and quartz diorite
gg	Granodiorite gneiss
tf	Al Fayd tonalite
tg	Tonalite gneiss
di	Metadiorite and metagabbro

ggb	Gabbro, diorite and quartz diorite (metamorphosed)
gds	Granodiorite sills
qd	Quartz diorite
qb	Quartz monzonite
a	Amphibolite
hs	Metasedimentary rocks (Halaban Group)
hv	Metavolcanic rocks (Halaban Group)

Lithological contact
Fault, arrows indicate relative horizontal displacement
Fault--intruded by mafic dyke
Vertical foliation
⊢86 Strike and dip of foliation

compilation. These maps are the product of the only detailed study.

The volcanic rocks are situated in the west of the area overlying the Suwaydah tonalite gneiss. They are Tertiary alkali-olivine basalt flows of the As Sirat (As-Sarat) mountains (Coleman et al., 1977). The base of the basalt sequence is marked by a well-developed sub-lateritic palaeosol (Overstreet et al., 1977).

The Precambrian metamorphic rocks occupy a small area and are well-foliated Upper Proterozoic metavolcanic and metasedimentary rocks. These rocks are assigned to the Halaban Group, and they are intruding plutonic rocks. Amphibolites occur as narrow septa between plutons or as isolated bands in plutonic or metamorphic rocks.

The plutonic rocks include granite, tonalite, diorite, granodiorite and gabbroic rocks. The granitic rocks occupy a small area, whereas the tonalite and granodiorites occupy a large portion of the test area (Fig. 4.1).

The Wadi Tarib (Tareeb) batholith includes metadiorite, metagabbro, tonalite gneiss and the Al Fayd tonalite and is located in the southern Arabian Shield. It is a complex batholith 70km wide by 150km long forming a N-S zone that is composed mostly of quartz diorite and tonalite. All tonalites exposed in the test-site area are part of this batholith. One of the older plutonic units of the batholith is the Suwaydah biotite-hornblende tonalite gneiss. The gneiss has a uniform massive appearance, typically weathering into large, smooth, rounded blocks. The foliation strikes to the north and generally dips steeply towards the east (Stoeser et al., 1982). This gneiss is intruded by a syn-tectonic granodioritic gneiss, which forms the core of asymmetric overturned antiform with an eastward dipping axial plane. This structure was named the Hadabah dome (Fig. 4.1). The granodiorite is weakly foliated, medium grained, and leucocratic (Stoeser et al., 1982). A large synformal pluton east of the Hadabah dome is composed of a similar granodiorite. This synformal pluton is called here the Al Khabt synformal phacolith, after Al Khabt village (Fig. 4.2). The gneiss is also intruded by several basalt pipes related to the Tertiary As-Sarat volcanic field. The dome and the nearby synclinal phacolithic pluton are typical of syn-tectonic forceful emplacement (Agar, 1986).

The post-tectonic Khaniqah granite is a large complex pluton, located to the north of the test-site area (Fig. 4.1). It is petrographically inhomogeneous with dykes apparently concentrated near the margin of the pluton. The granite is a medium grained
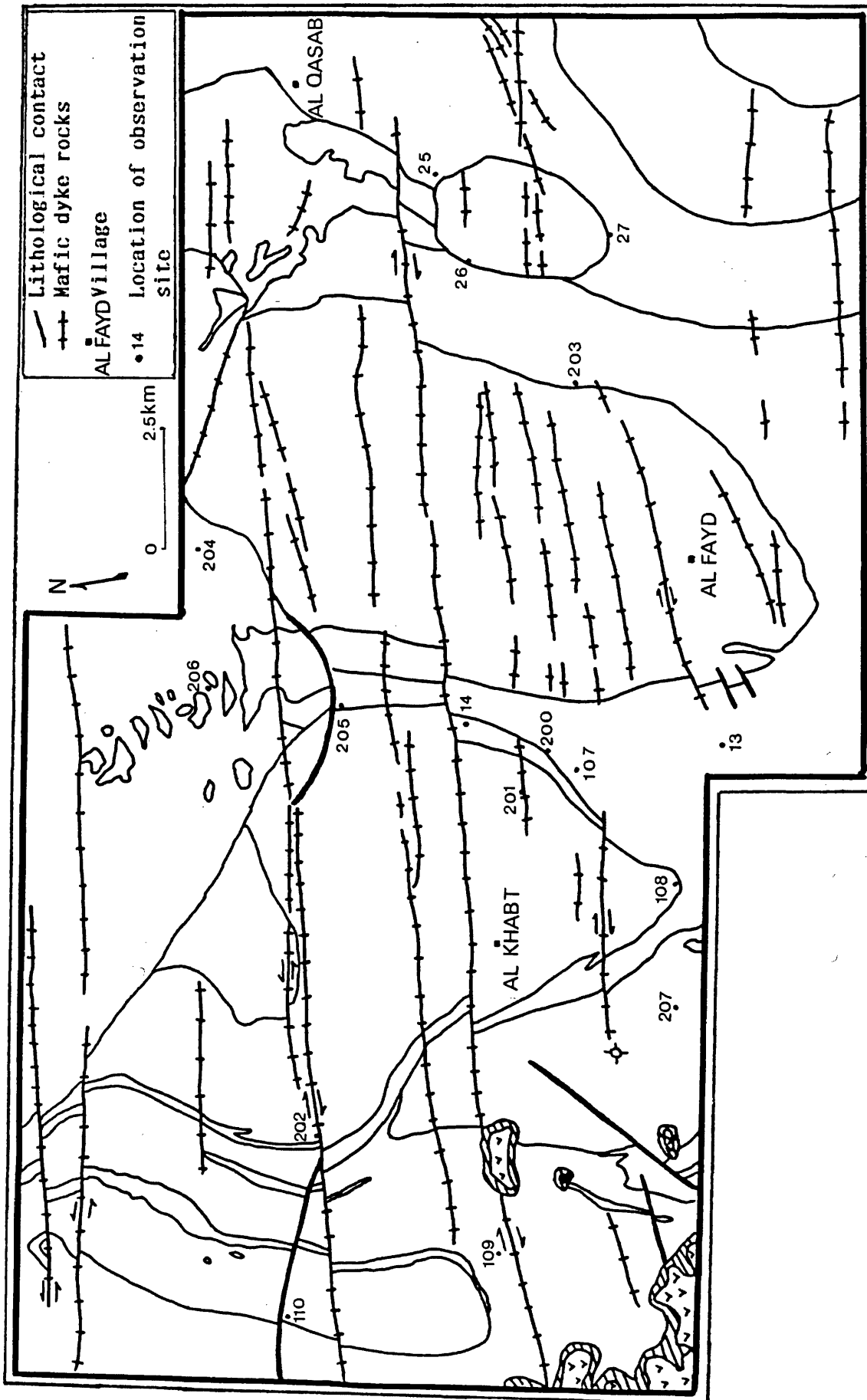
Fig. 4.2 Location map of observation sites for the test-site area No.2.

equigranular to microcline-porphyritic biotite monzogranite with rare hornblende.

A major group of E-W striking faults were mapped which extends in some cases for distances over 20km. These are mostly right-lateral strike-slip faults and commonly have mafic dykes emplaced along portions of their length. The dykes are fine grained hornblende dolerites (Stoeser, 1984).

4.3 REMOTE SENSING TECHNIQUES

4.3.1 Introduction

The three main types of image processing techniques have been performed on each sub-scene covering this test-site area, i.e. test-site numbers 2A and 2B, separately. The two hardcopy images produced by each method were used to produce a single interpretive map; the overlap area allowed safe correlation of units from one subscene to the other. The three image processing methods are: contrast-, spectral- and edge-enhancements.

4.3.2 Contrast enhancement

As in the previous test-site, only two types of contrast stretching were applied. These are linear- and nonlinear-contrast stretching.

Simple scaling was applied to each sub-scene of this test-site. Figures 4.3A and B shows the raw Landsat TM band 5 data for the test-sites No.2A and 2B, respectively, while Figures 4.4A and B shows the linearly contrast stretched Landsat TM band 5 data for the test-sites No.2A and 2B, respectively. It is obvious that linear contrast stretching enhancement shows more details.

To produce a bell-shaped histogram; i.e. Gaussian stretch, to improve the contrast in the light and dark ranges of the image, nonlinear contrast stretching was applied. Figures 4.5A and B shows Gaussian contrast stretching of Landsat TM band 5 data for the test-sites No.2A and 2B.

4.3.3 Spectral enhancement techniques

SE1 Technique

As previously described in section 3.3.3(a), the technique of ratioing TM bands 1, 3,
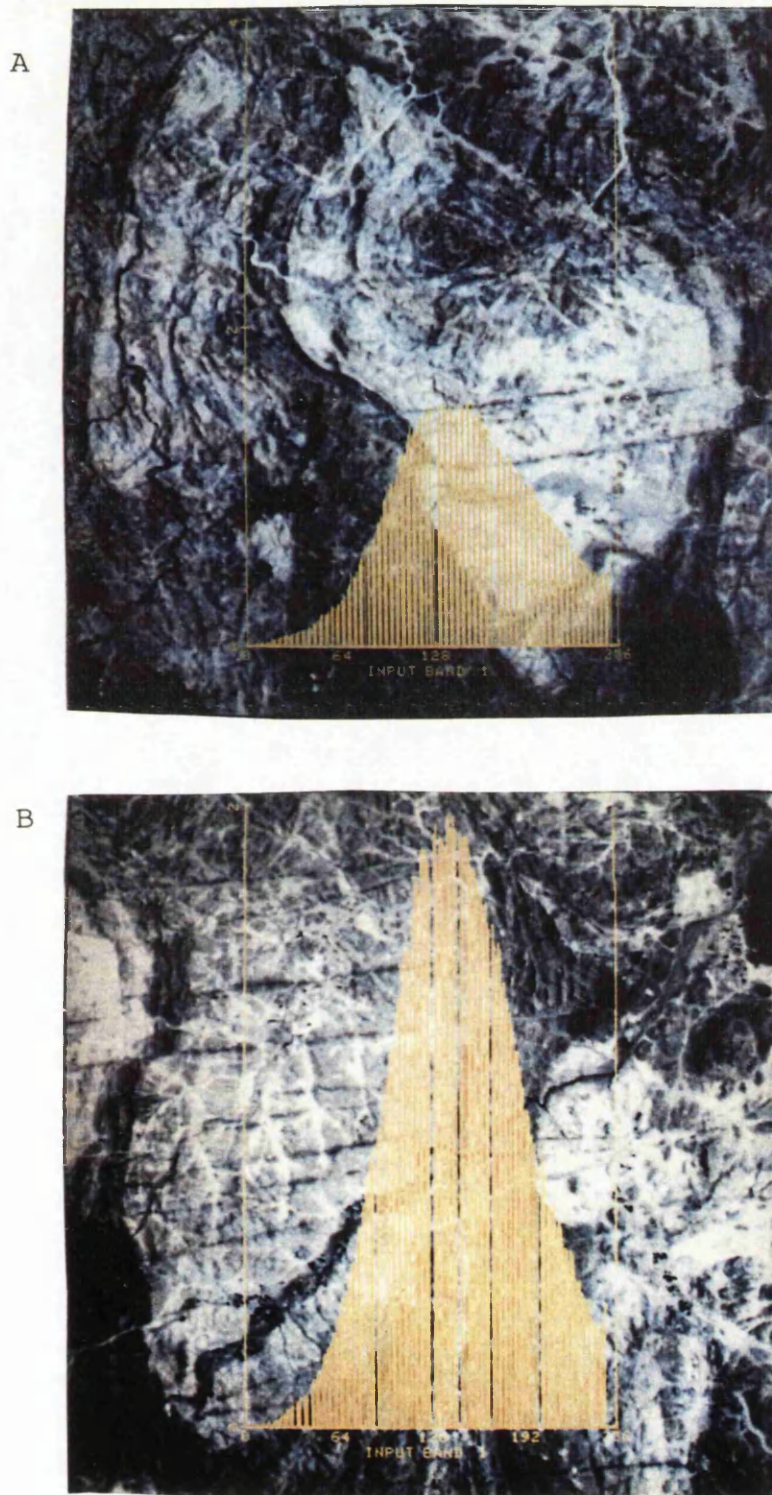
Fig. 4.3 Landsat TM band 5 subscenes. A:for test-site 2A;
B:for test-site 2B.
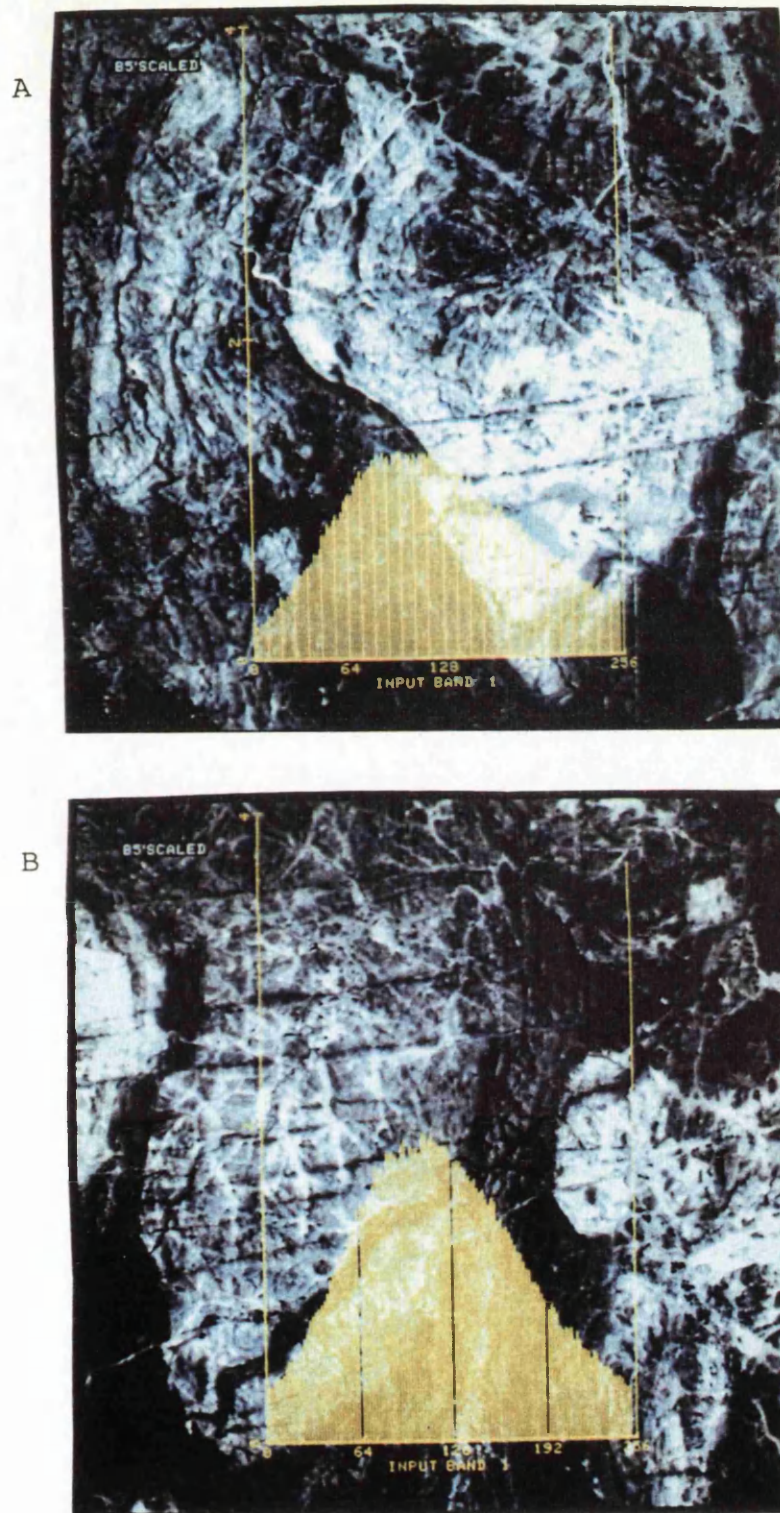
Fig. 4.4 Linearly contrast stretched images. A:for test-site 2A; B:for test-site 2B.
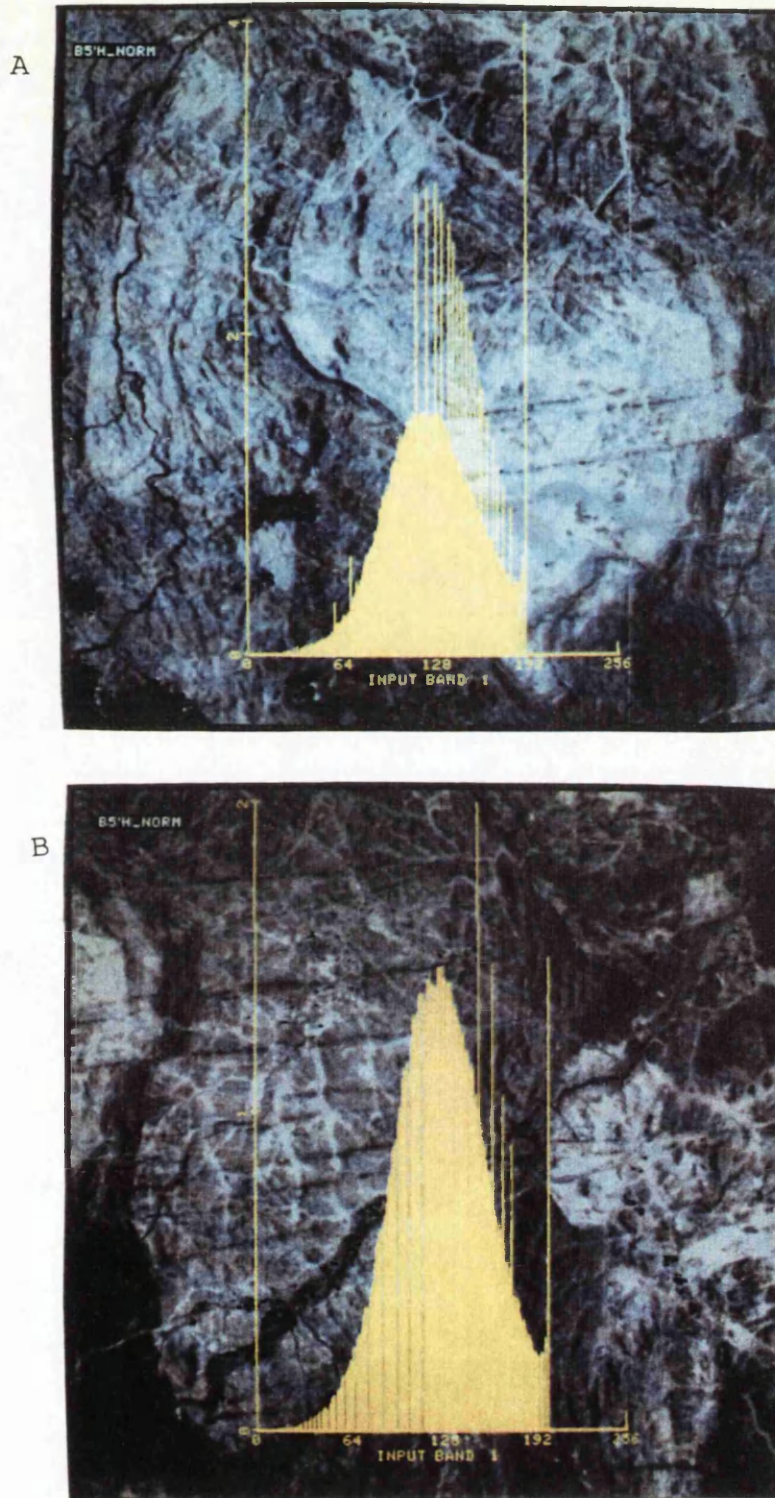
Fig. 4.5 Gaussian contrast stretched images.
A:for test-site 2A; B:for test-site 2B.

4, 5 and 7 was applied on test-sites No.2A and 2B individually.

Method:

-TM BAND 5/1, was used to distinguish rocks rich in opaque phases which have low band-5 and band-1 values. Figures 4.6A and B shows the TM band 5/1 image for both test-sites 2A and 2B. Bright areas correspond to regions deficient in opaque phases.

-TM BAND 5/7, provides a measure of the intensity of the hydroxyl absorptions in the 2.2-2.4 μm region, i.e. band 7. Figures 4.7A and B shows the TM band 5/7 image. The slightly brighter areas correspond to regions with high OH contents.

-TM BAND (5/4 x 3/4), was used to emphasize and discriminate the iron-bearing aluminosilicates. Figures 4.8A and B shows the TM band (5/4 x 3/4), where bright areas correspond to regions rich in Fe-bearing aluminosilicates and the nonbright areas correspond to the granitic, gneissic, tonalitic and volcanic rocks.

Rock units defined on enhanced imagery:

Volcanic rocks in the southwestern part of the test-site No.2A can be easily identified in the TM band (5/4 x 3/4) ratio image because these rocks are not rich in Fe-bearing aluminosilicates. The layered metamorphic rocks were also identified in the TM (5/4 x 3/4) ratio image because these rocks are very rich in Fe-bearing aluminosilicates. The granitoid rocks in both test-sites No.2A and 2B can be distinguished as bright ares on the TM band 5/1 ratio image due to their deficiency in opaque phases. The mafic dyke rocks are also easily identifiable as dark areas, particularly in test-site No.2B, because they are rich in opaque phases.

The resultant contrast-stretched Colour Ratio Composites (CRCs) constructed are shown in Figures 4.9A and B. The TM band 5/7 image was assigned the red component; the TM band 5/1 image, the green component; and the TM band (5/4 x 3/4) image, the blue component. The rock types mentioned have unique brightness patterns on the ratio images and should have unique colours on a CRC images. For example, the post-tectonic granitic pluton in the test-site No.2B (section H6, Fig. 4.9B) is deficient in opaque phases which show up as bright areas and will be green on the CRC. The basaltic rocks (sections B10 and E9, Fig. 4.9A), the mafic dyke rocks which fill the E-W faults and the materials in the wadis (e.g. Wadi Al Fayd, sections E7 and J3, Fig. 4.9B) are a distinct greenish-red colour in the CRC. This is because these rocks are rich in opaque phases. The source for most wadi alluvium is the As-Sarat volcanic field, located to the west of the test area No.2, and these shows up as red areas on the
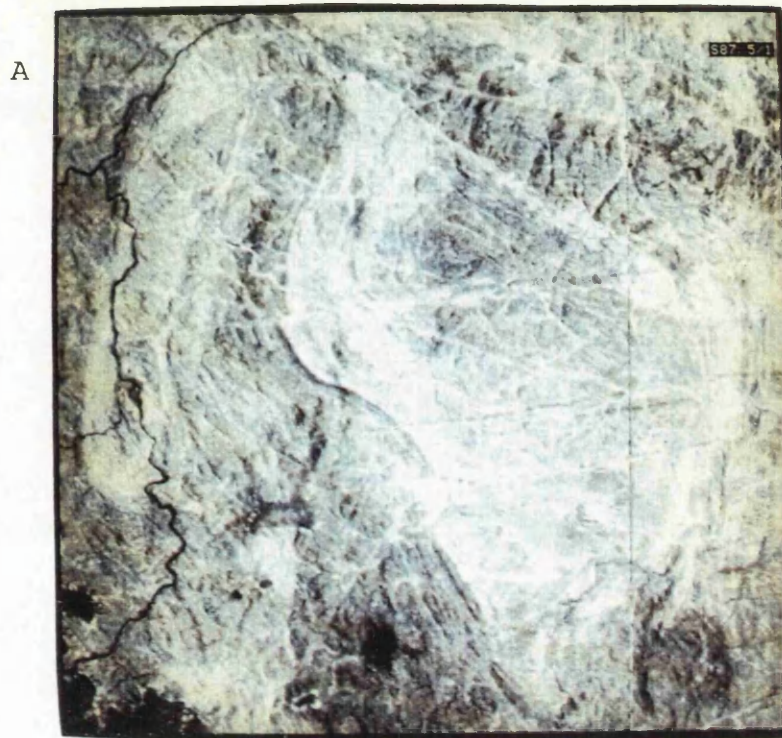
Fig. 4.6 SE1 Technique TM band 5/1 ratio images.
A:for test-site 2A; B:for test-site 2B.

Fig. 4.7 SE1 Technique TM band 5/7 ratio images.
A:for test-site 2A; B:for test-site 2B.

Fig. 4.8 SE1 Technique TM band (5/4x3/4) ratio images.
A:for test-site 2A; B:for test-site 2B.

Fig. 4.9 A contrast-stretched CRCs of TM band 5/7 in red, band 5/1 in green and band (5/4x3/4) in blue. A:for test-site 2A; B:for test-site 2B.

CRC image. In contrast, where sediments in the wadis are not of basaltic composition the colour is not red (sections G8 and H7, Fig. 4.9A). Because the Al Khabt synformal phacolith granodioritic gneiss includes tonalite gneiss, it also can be distinguished on the CRC. The granodioritic gneiss is greenish in colour (sections E4 and G6, Fig. 4.9A), because it is rich in OH, hence appears as bright areas on the TM band 5/7 ratio image. The tonalite gneiss is a reddish-blue colour (section G4, Fig. 4.9A), because it is less rich in OH but richer in opaque phases; it therefore forms darker areas on the TM band 5/1 ratio image. The metamorphic layered rocks are also easily recognized on the CRC. They show burgundy-bluish hues (e.g. sections I10 and J9, Fig. 4.9A; G4 and C10, Fig. 4.9B), because they are rich in Fe-bearing aluminosilicates, and are bright areas in the TM band (5/4 x 3/4) ratio images (Figs. 4.8A and B).

A detailed geological map of the test-site area No.2 was constructed (Fig. 4.10) from the CRC images. Field observations were used to supplement remote sensing interpretations in making decisions during the construction of the geological map, particularly in the northern granitic unit (Khaniqah granite). Comparing the geological map constructed from the TM image (Fig. 4.10) with the geological information contained in the earlier maps of the DGMR personnel, it is clear that although there is a good correspondence between the two maps, the area which is mapped as Al Fayd tonalite in the previous published maps can be resolved into two lithologies, which are the Al Fayd tonalite and a granitic unit with dyke complex. Particular attention was given to this area during fieldwork (Fig. 4.2).

There is no detailed structural analysis available for this test area such as that for the test area No.1. But, Stoeser (1984) reported that:

-all major units show evidence of deformation,

-the granodioritic gneiss units were emplaced under conditions of major regional plastic deformation, and show phacolithic morphology rather than normal penetrative plutons,

-the folding and deformation associated with the granodioritic gneiss units appear to have had a westward-directed component. This is indicated by the strong asymmetry of the Hadabah antiform with its eastward-dipping axial plane and the general eastward dip of the foliation of the layered rocks and tonalite gneiss,

-the late to post-tectonic group of plutons are characterized by a general lack of foliation,

-significant regional crustal deformation continued after the emplacement of the "post-tectonic" plutonic rocks. This deformation may relate to strain associated with faults

GEOLOGICAL MAP

LEGEND

0   2.5 km

Volcanic rocks—Alkali-olivine basalt flow

Laterite

Granite with dyke complex

Monzogranite

Granodiorite gneiss

Mafic tonalite

Al Fayd tonalite

Tonalite gneiss

Metadiorite and metagabbro

Granodiorite and tonalite s

Undivided felsic and mafic schists

Basalt pipe

Lithological contact

Faults. arrows show sense of movement in faults

Mafic dyke rocks

Strike and dip of foliation

A B   Test-site No. 2A and 2B

N

AL FAYD TONALITE

AL KHABT SYNFORMAL PHACOLITH

HADABAH DOME

SUWAYDAH GNEISS
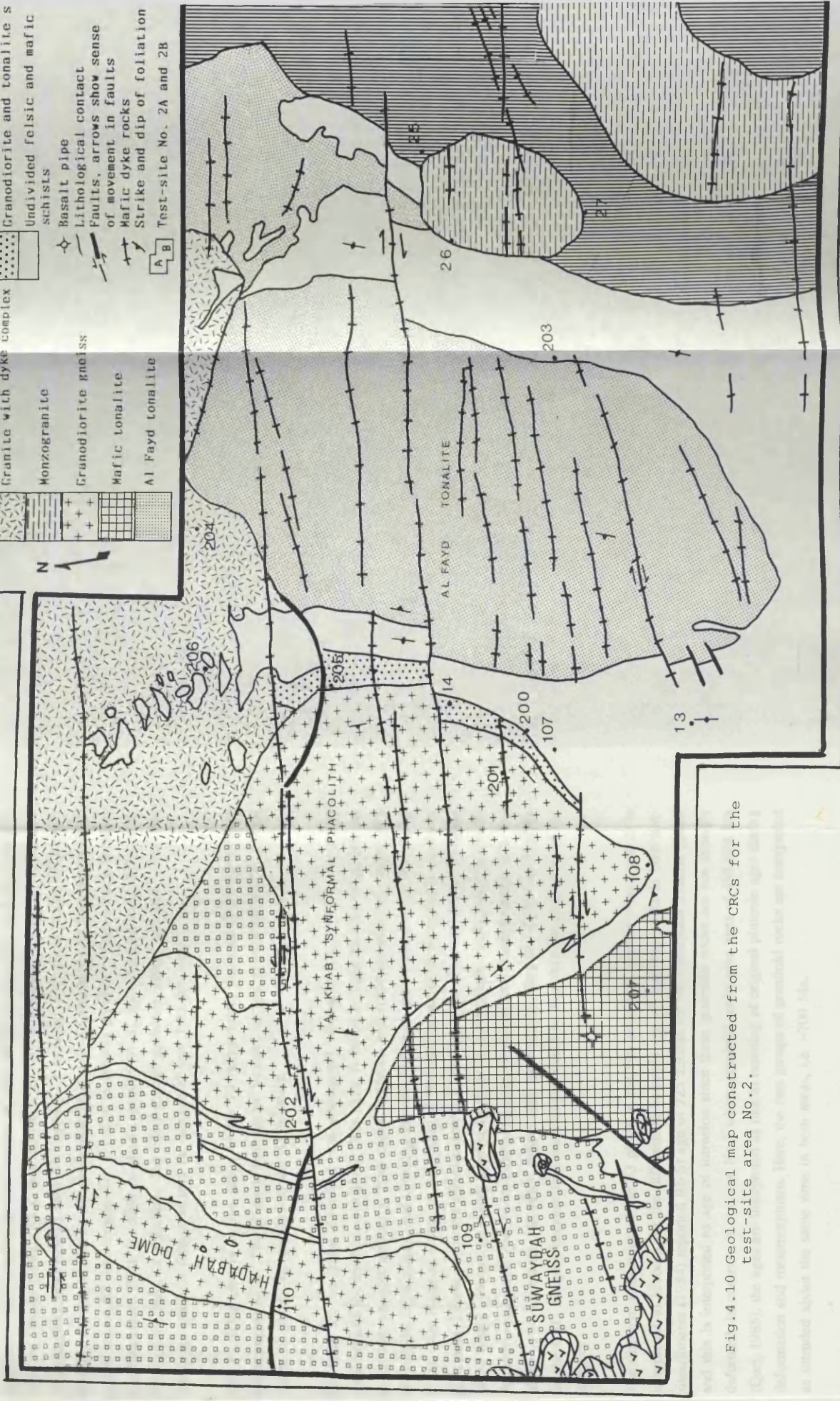
Fig. 4.10 Geological map constructed from the CRCs for the test-site area No. 2.

which cut all these units or may relate to some unknown episode of deformation.

The structural map (Fig. 4.11) for test-site area No.2 is based on field studies, correlation with detailed ground studies of test-site No.1, the CRC and the available work of Stoeser (1984). As in test-site No.1, all rock units and in particular the layered metamorphic rocks exhibit well developed S1,2 foliation. This axial planar foliation is strongly developed fabric and easily distinguishable as schistosity or fracture cleavage across minor F2 fold hinges. The foliation is broadly parallel to the contacts between the lithologies. This foliation is almost parallel to S1 foliation and thus difficult to distinguish from S1 foliation. The S2 foliation generally strikes between north and northeast and it is folded around the hinges of later fold generations.

The F2 folds present in the limbs of the F3 major folds, particularly in the layered metamorphic rocks. This phase is represented by tight, upright asymmetrical folds where the axial planes are parallel to the S2 foliation.

F3 folds are the most dominant and widespread structures and defining the major structures of the test-site area No.2. This phase is found as tight- to open-asymmetrical folds with variable geometry. Four major antiforms and synforms with steep, generally NNE-SSW axial planes, and plunging towards the south are assigned to F3 folds (Fig. 4.11). The Hadabah dome is the result of two antiforms found plunging in opposite directions. Linear structures associated with F3 folding were observed around the hinge of Al Khabt synform as strong mineral lineation in the schistose rocks trending mostly towards south with low to moderate plunges, which is in correspondence with the plunge of the synform. However, micro- and meso-scale folding would be undetectable on the CRC imagery because fold wavelength would be less than the resolution of the imagery.

The different intensities of the F3 phase in the two areas (i.e. test-site Nos.1 and 2) is interpreted to account for the different radiometric age of granitoid rocks in both test-sites. Stoeser (1984) reported Rb-Sr age of 725 ±30Ma for the Suwaydah tonalite gneiss and this is interpreted as age of intrusion since these granitoid rocks are not strongly deformed. In contrast, in test-site No.1 where granitoid rocks give ages of 495-624 Ma (Qari, 1985), the ages are interpreted as due to resetting of original plutonic ages during deformation and metamorphism. Here, the two groups of granitoid rocks are interpreted as intruded about the same time in both areas, i.e. ≈700 Ma.

Fig. 4.11

Structural map for the test-site area No. 2. For lithological units, see Fig. 4.10.

0   2.5 km

LEGEND

⌒ Lithological contact

⌒ Fault

╫ Fault, filled with mafic dyke rocks

↕ F3 Synform, direction of plunge is shown

↕ F3 Antiform, direction of plunge is shown

↕ F3 Dome

▓ Post-tectonic emplacement

▓ Syn-tectonic emplacement

▓ Pre-tectonic emplacement

▓ Earlier layered metamorphic rocks

⟋ Strike and dip direction of foliation

⊢ Strike of vertical foliation
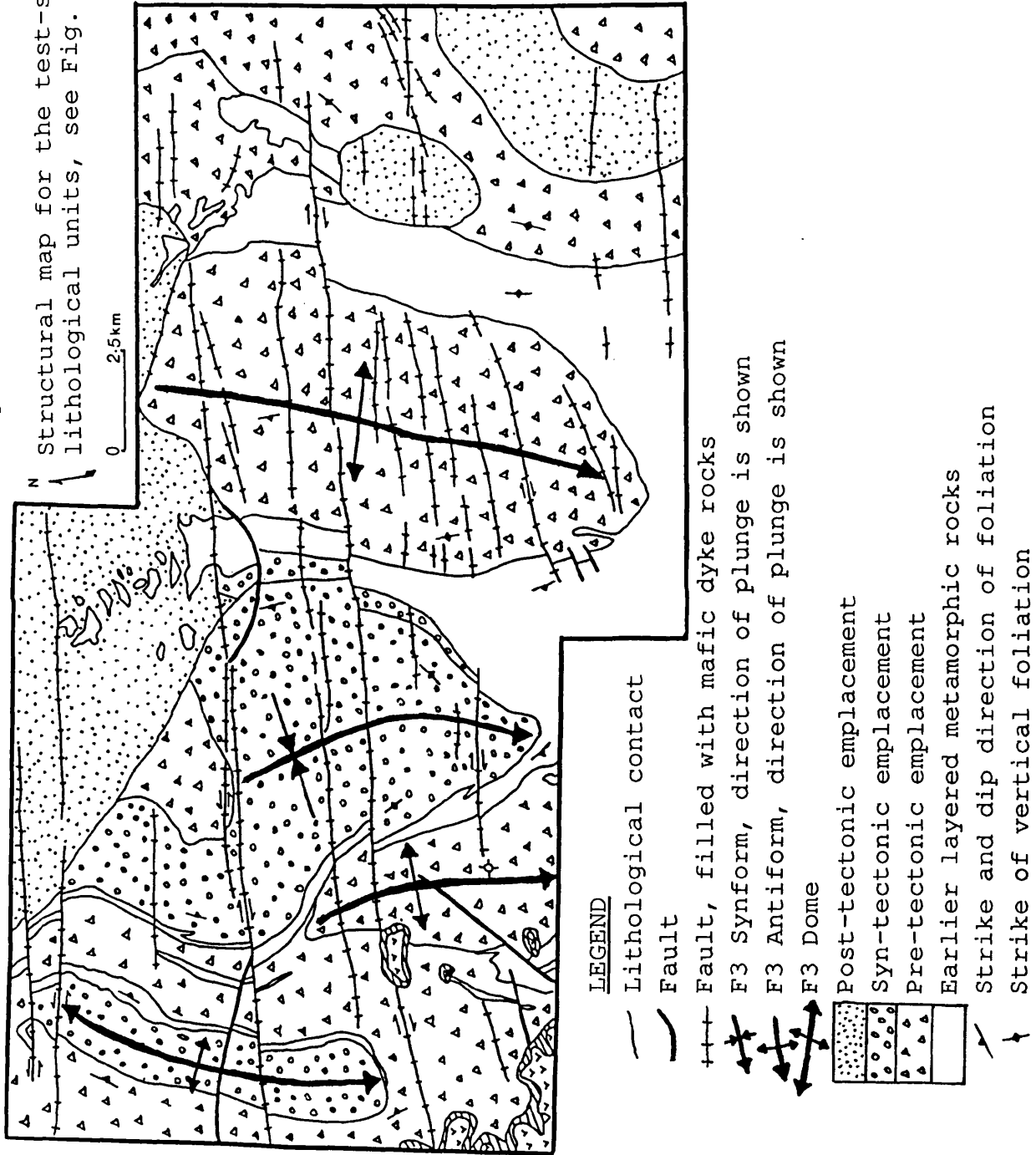
Faults are very prominent in test-site No.2 (Plate 4). They are easily detectable on the CRC imagery (e.g. sections D5 and F7, Fig. 4.9A; B4 and G4, Fig. 4.9B). Most of these E-W faults are right-lateral strike-slip faults intruded by mafic dyke rocks. Some of these faults can be traced into the Tertiary As-Sarat volcanic field (west of the test-site area) which suggests that they may have been rejuvenated during the Tertiary (Stoeser, 1984). A close investigation will probably indicate that these E-W faults are associated with the formation of the Red Sea, west of the study area.

SE2 Technique

As described earlier in section 3.3.3(a), the TM CRC (7/5,5/4,4/2) in red, green, blue was applied for general lithological discrimination for each sub-scene covering the test-site area No.2.

Method:

The ratio combinations which were obtained after applying a contrast stretching were:
-TM BAND 7/5 distinguishes the area rich in OH. Figures 4.12A and B shows these areas as moderately dark.
-TM BAND 5/4 emphasizes and discriminates rocks rich in Fe-bearing aluminosilicates. Figures 4.13A and B show very bright areas which correspond to regions rich in such minerals (layered metamorphic rocks), whereas the darker areas correspond to the other rock units in the test-site such as granitoid and basaltic rocks.
-TM BAND 4/2 used for the detection of surface iron-staining. Such areas are shown as dark in Figures 4.14A and B.

Rock units defined on enhanced imagery:

Monzogranites and granodioritic gneiss were identified as the brightest areas on TM band 4/2 ratio images (Figs. 4.14A and B), because their opaque-phases content is very low compared to the other units. The sub-lateritic palaeosol is also identified on these ratio images as bright bands surrounding the basaltic flow areas. On the TM band 5/4 ratio images (Figs. 4.13A and B), rock units rich in Fe-bearing aluminosilicates, i.e. metavolcanics and metasediments, could be discriminated reliably. They show a strong contrast with the darker background which facilitates lithological contact verification. The tonalitic composition rock types are shown as brighter areas in the TM band 7/5 ratio images (Figs. 4.12A and B).
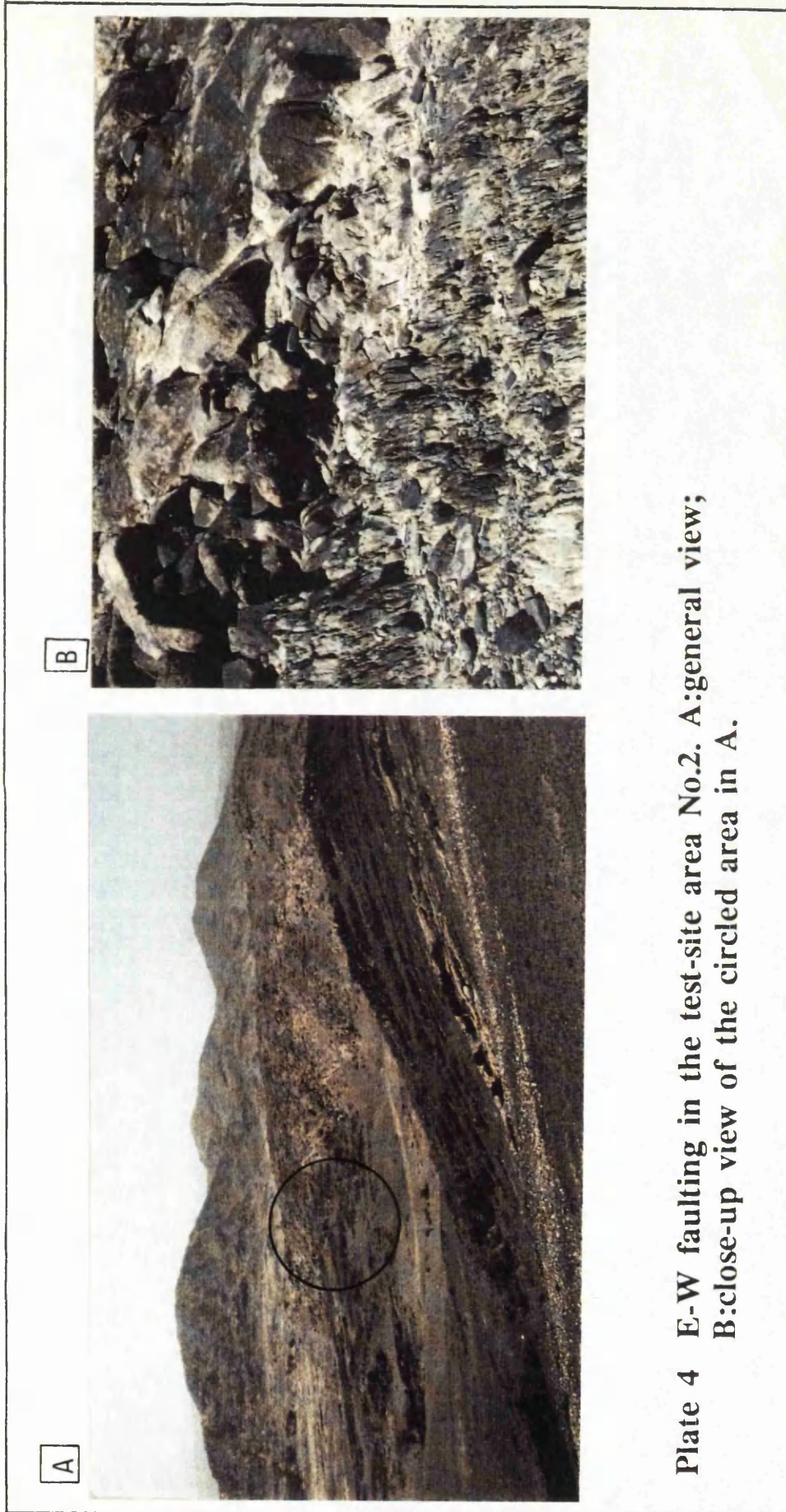
Plate 4 E-W faulting in the test-site area No.2. A:general view; B:close-up view of the circled area in A.

Fig.4.12 SE2 Technique TM band 7/5 ratio images.
A:for test-site 2A; B:for test-site 2B.
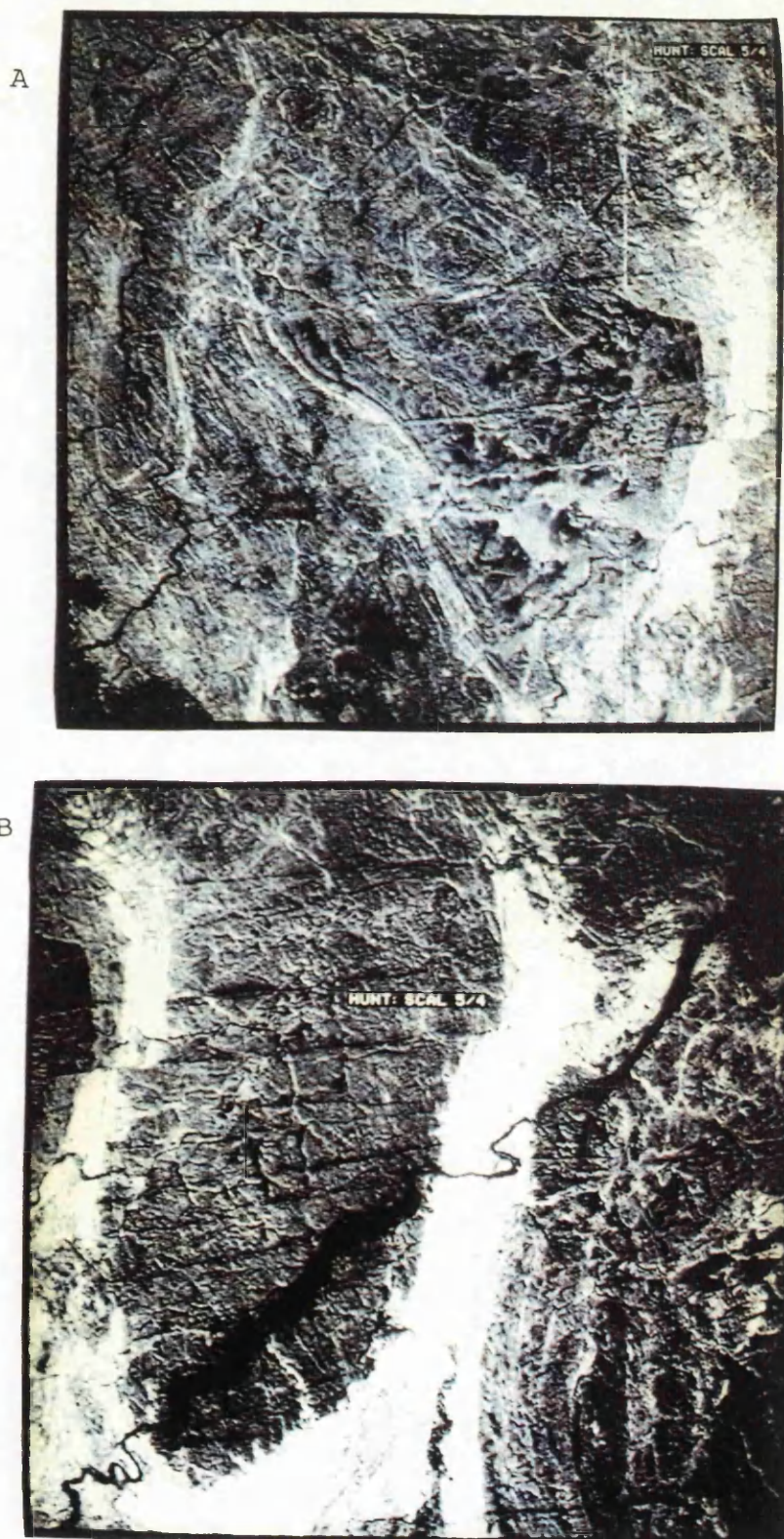
Fig.4.13 SE2 Technique TM band 5/4 ratio images.
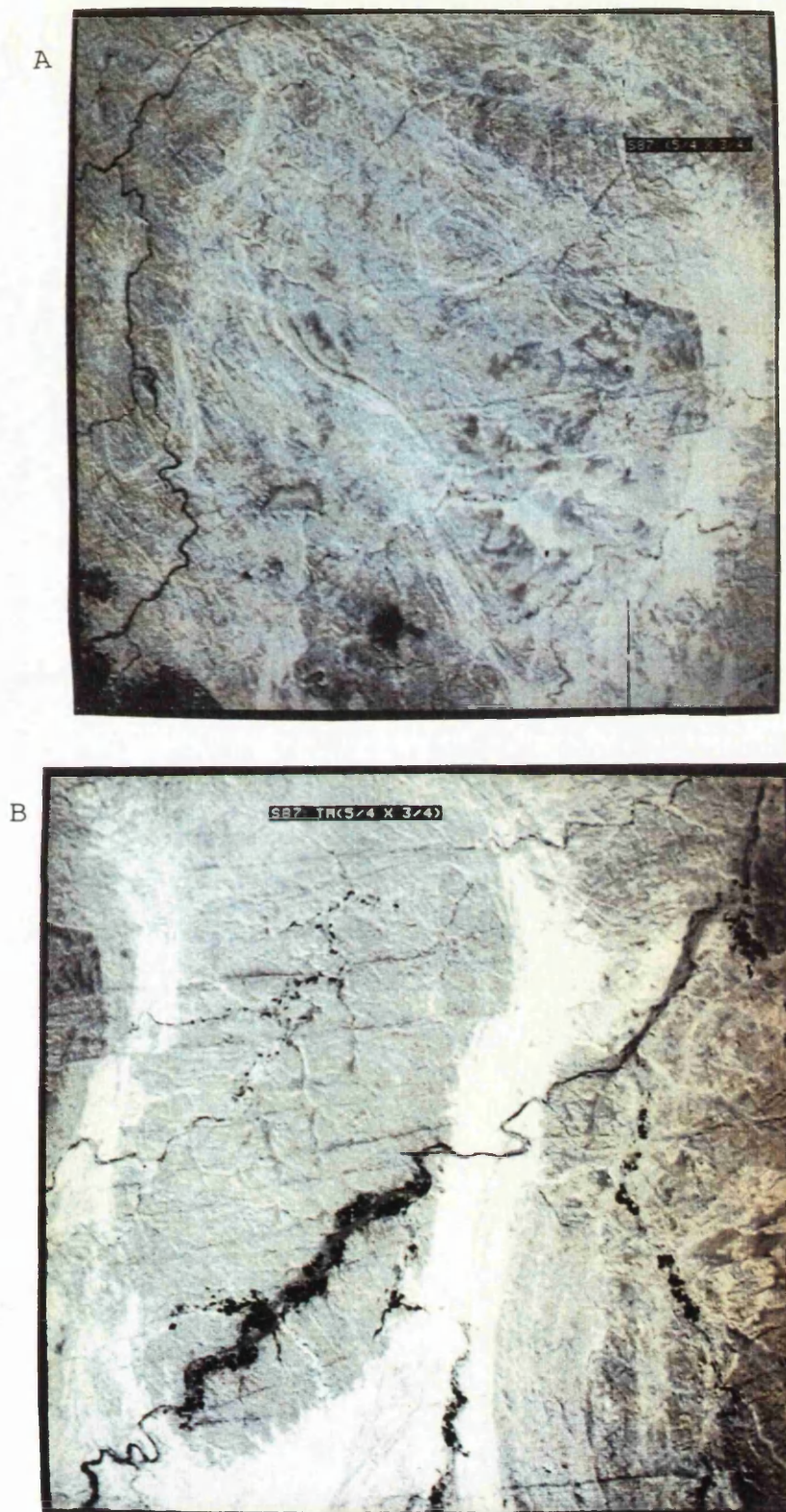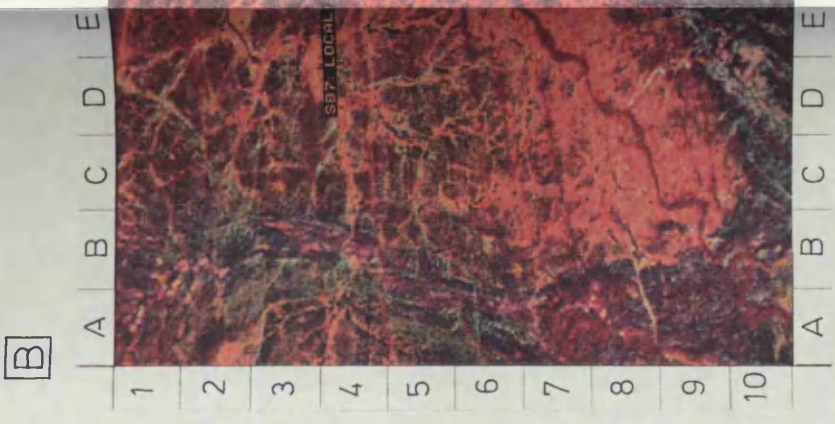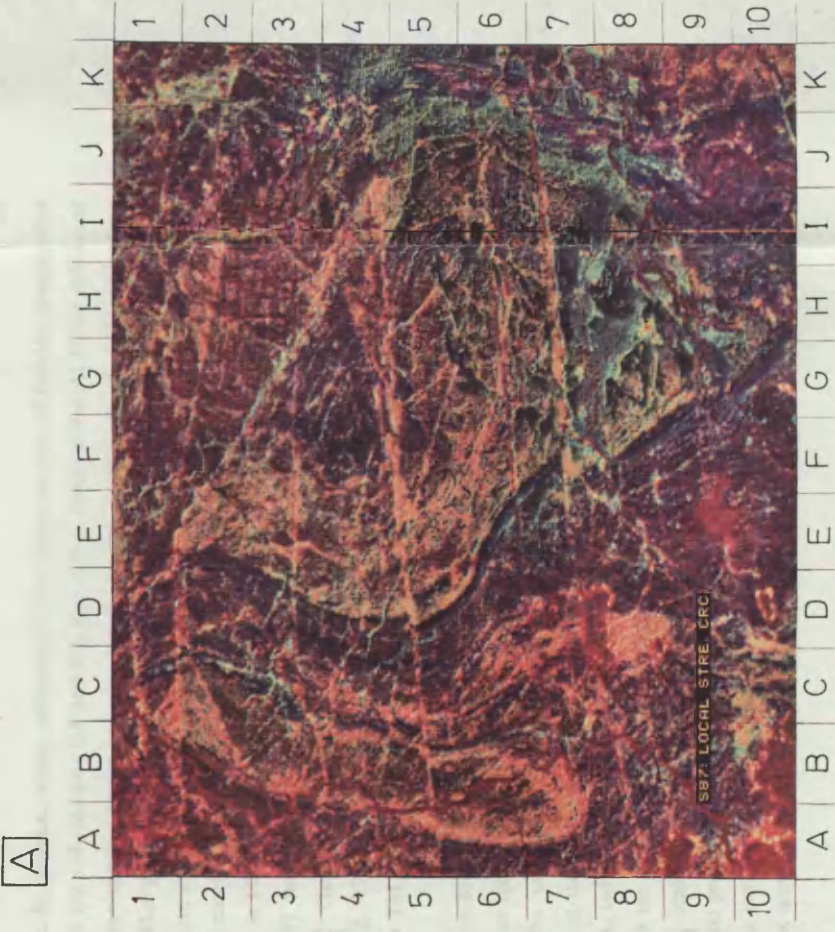A:for test-site 2A; B:for test-site 2B.
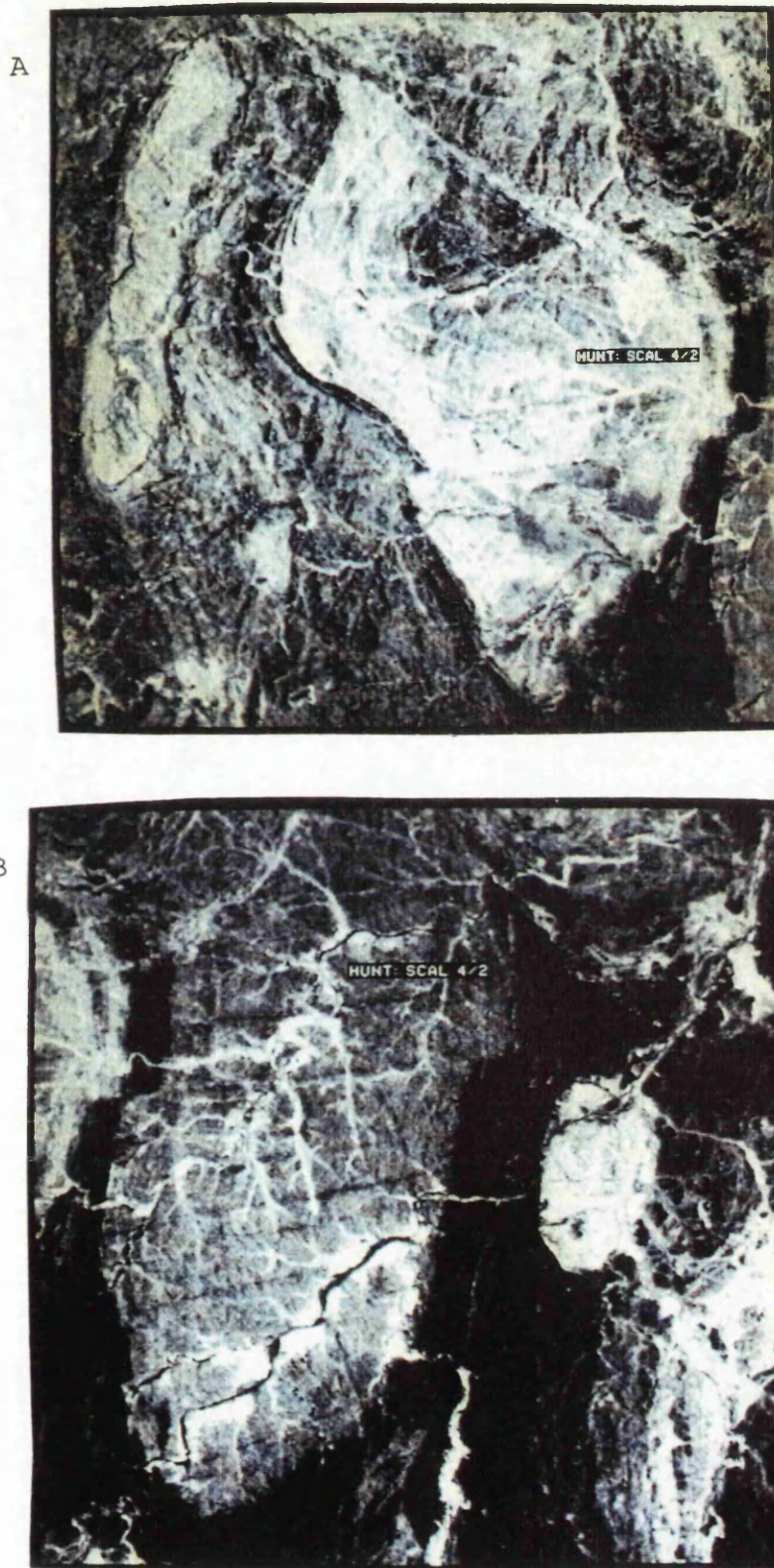
Fig.4.14 SE2 Technique TM band 4/2 ratio images.
A:for test-site 2A; B:for test-site 2B.

The rock types mentioned have unique brightness patterns on the ratio images observed on the CRC images as well. The colours are more prominent than those in the SE1 technique which facilitates lithological discrimination.

The lithological information contained in the three TM band ratio images for each sub-scene composing the test-site area has been integrated into one image. The resultant FCCs are shown in Figures 4.15A and B: the TM band 7/5 image was assigned the red component; the TM band 5/4 image, the green component; and the TM band 4/2 image, the blue component. An additional linear contrast stretch was applied in order to enhance the FCCs. The resultant CRCs are shown in Figures 4.16A and B, which was used for the later interpretations. Table 4.1 indicates the way of predicting the colours on the CRC, based on the mineralogical controls for each of the ratio images discussed previously.

The lateritic palaeosol is shown as a light blue colour in the CRC (e.g. sections B10, D8 and A9, Fig. 4.16A) surrounding the basaltic flow. This blue colour should not be confused with the blue colours of the granodioritic and monzogranitic units. The mafic dykes (Plate 5) which are filling the E-W, mostly right-lateral, faults are also clear as dark blue colours on the CRCs. The non-blue areas in the Al Khabt synformal phacolith and the eastern monzogranitic units (e.g. sections H8 and I5, Fig. 4.16A; J7 and H6, Fig. 4.16B) are due to low ground covered with white sand. The alluvium in the wadis is largely derived from the As-Sarat basaltic flow, and hence produces a dark blue colour (e.g. sections A10, C9, and G6, Fig. 4.16B). Where the alluvium is not basaltic material, the colour on the CRC is not blue (e.g. sections G8, H8 and I8, Fig. 4.16A).

The metamorphic layered rocks which are exposed as small patches within the northern granitic unit (Plate 6) display pronounced green and yellow colours (sections A1 and B2, Fig. 4.16B).

Although the Al Fayd tonalite and the tonalite gneiss (which is included in Al Khabt phacolith) are similar in colour compared with the northern granitic unit, there is an inhomogeneity in the red colour of the granitic unit. This is due to the fact that this unit is invaded by a dyke complex, which is mostly of tonalitic composition. Field checking showed that there is a contact between these units which is shown on the
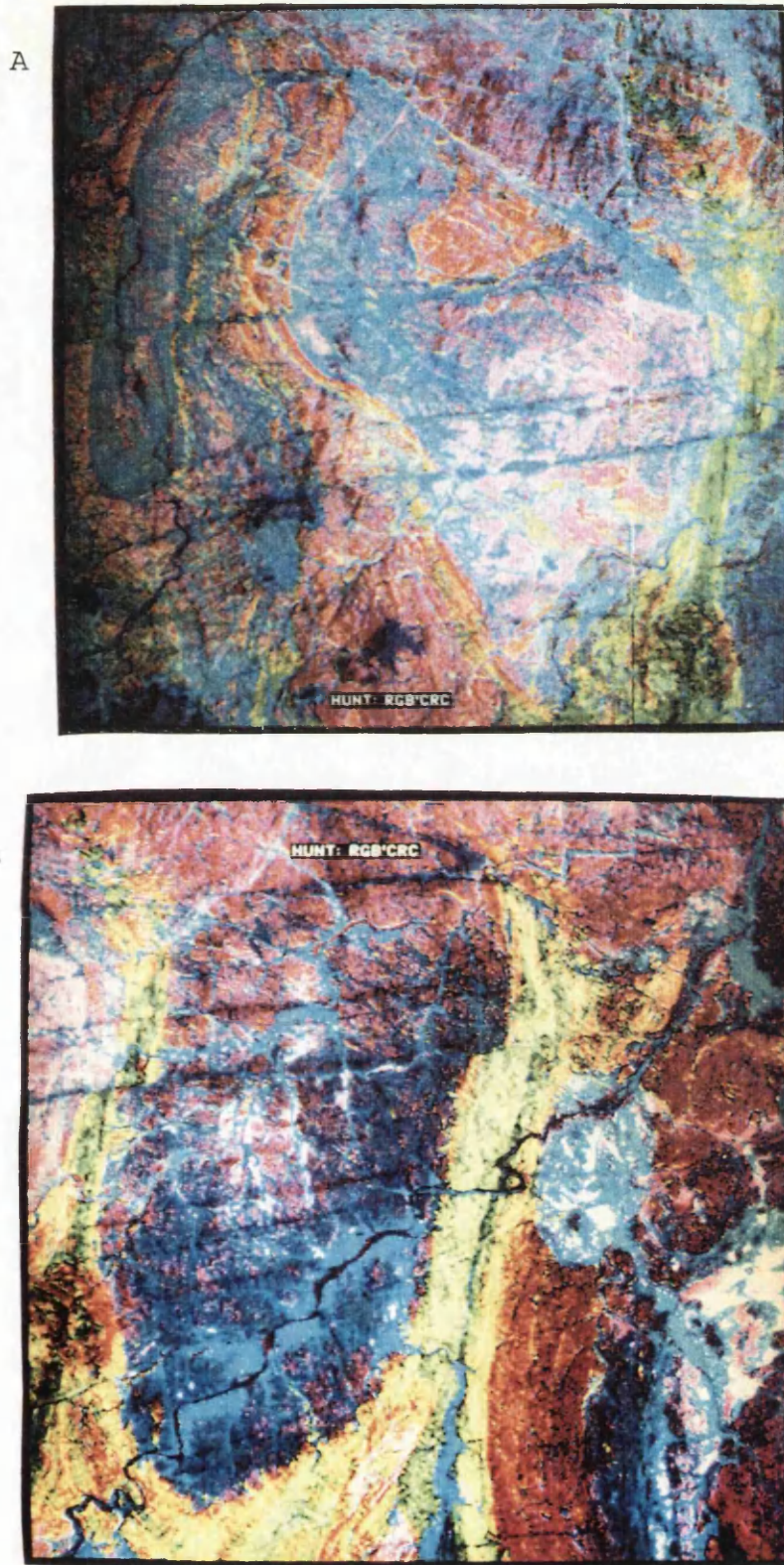
Fig.4.15 SE2 Technique FCC images. A:for test-site 2A;
B:for test-site 2B.
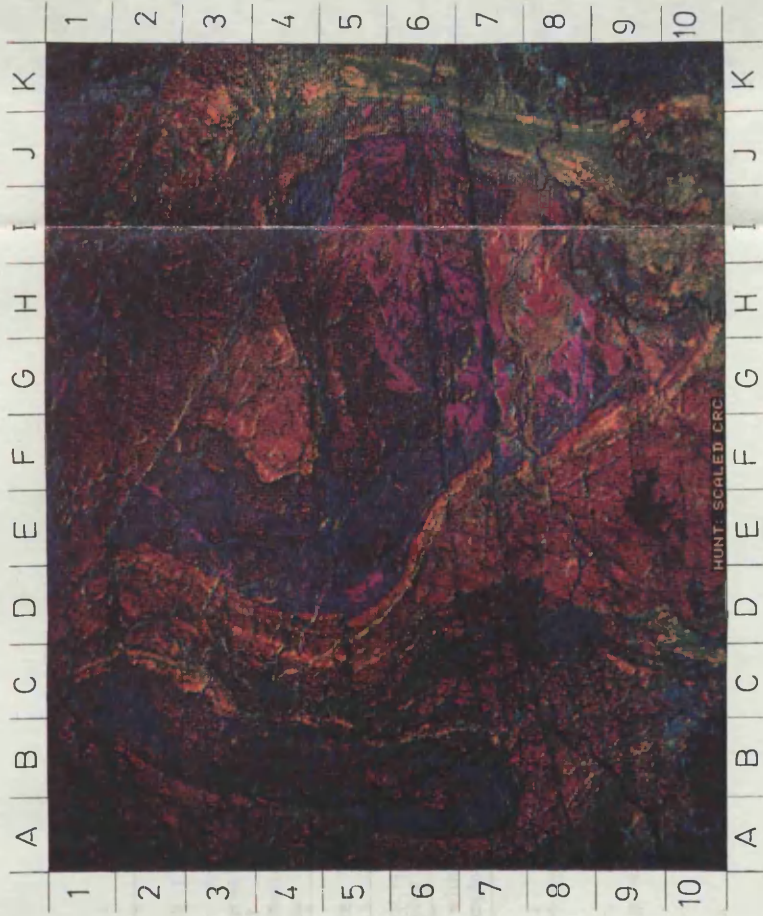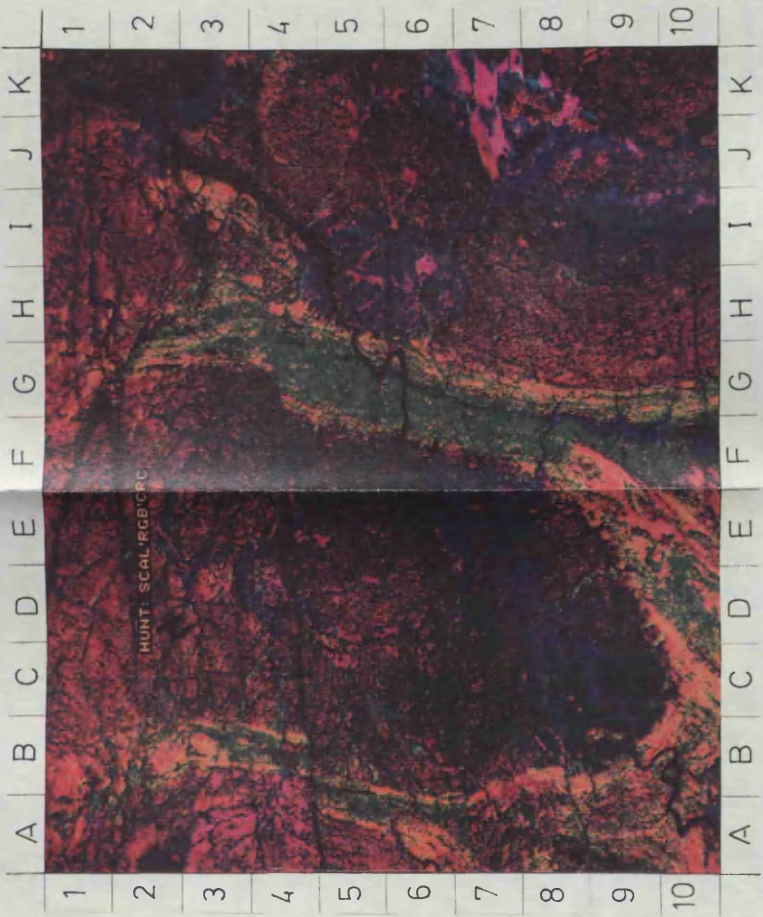
Fig.4.16 Linearly stretched CRCs of TM band 7/5 in red, band 5/4 in green and band 4/2 in blue. A:for test-site 2A; B:for test-site 2B.

ROCK TYPE	B 7/5 image bright=RED	B 5/4 image bright=GREEN	B 4/2 image bright=BLUE	COLOUR IN CRC IMAGE
Monzogranite and granodiorite gneiss	Moderate - dark	Moderate - dark	Bright	Blue
Tonalites	Bright	Dark - moderate	Dark	Red
Undivided layered metamorphic rocks	Dark - bright	Bright	Dark	Green and yellow
Granite with dyke complex	Moderate - bright	Moderate - dark	Moderate	Yellowish red
Basalt	Dark - moderate	Dark - moderate	Moderate - bright	Reddish blue

Table 4.1 Explanation of relative colour values in Figs. 4.16A and B.
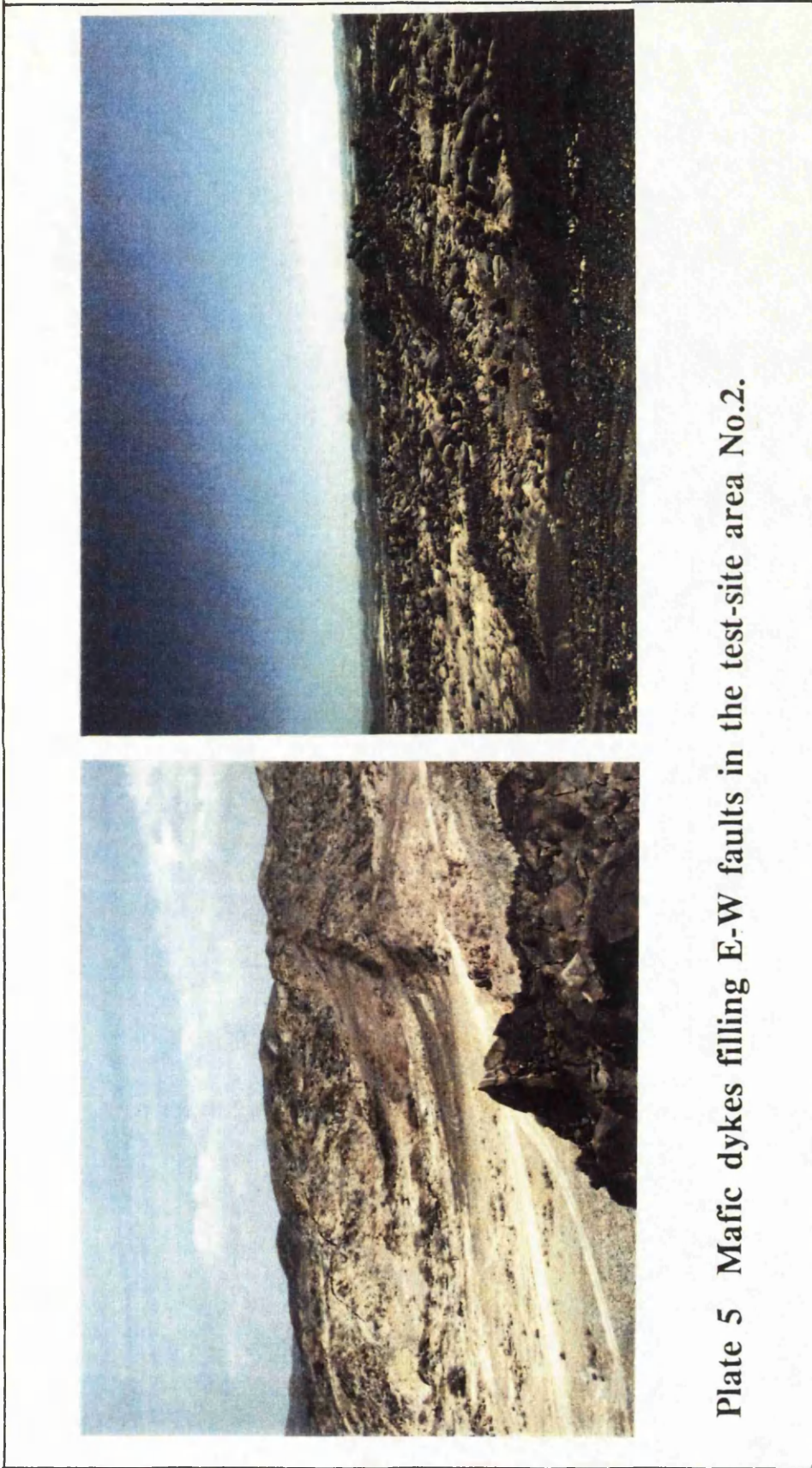
Plate 5 Mafic dykes filling E-W faults in the test-site area No.2.
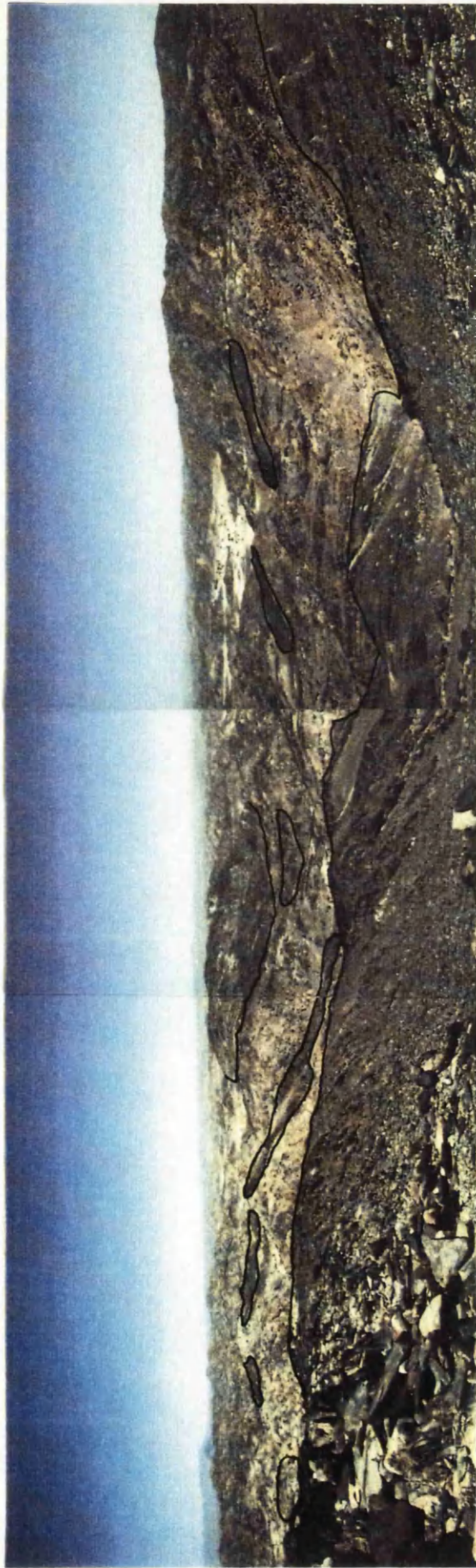
Plate 6   Panorama view of the area north of location No.206 (test-site No.2A). The metamorphic layered rocks patches are shown as grey colour within the northern granitic unit (light colour).

geological map (Fig. 4.10).

Comparison of the results obtained from the SE2 technique and that of the SE1 technique, showed that they were similar. However, it is preferable to use the SE2 technique for first interpretations since the SE2 images have stronger and a greater variety of colours, which correspond to different lithologies. The geological map (Fig. 4.10) was interpreted more easily using information obtainable from the CRCs obtained by this technique. For structural mapping, both techniques (SE1 and SE2) yield identical results.

SE3 Technique

Method:

As described earlier in section 3.3.3(b), the TM bands 7, 5 and 4 were selected to produce the decorrelated stretched images for the test area No.2. The final decorrelation stretched (DS) images were scaled to render them displayable and interpretable.

Rock units defined on enhanced imagery:

TM band 7,5,4 red, green, blue DS FCC images of the test-site area No.2 are shown in Figs. 4.17A and B. The basaltic rocks in the southwestern corner of the test-site No.2A (sections A10 and B10, Fig. 4.17A) display blue hues, which should not be confused with the blue colour patches along wadis, which are areas of vegetation (e.g. Wadi Al Fayd, sections C9, D8, and E7, Fig. 4.17B). Because the basaltic flow of the As-Sarat volcanic field, located to the west outside the test-site area, is high in elevation, the material transported to most of the wadis in the test area is of basaltic composition and is displayed as a blue colour filling these wadis (e.g. sections B4, B8, H10 and K8, Fig. 4.17A; B9, F6 and H5, Fig. 4.17B). Where the alluvium in the wadis is not of basaltic composition, the colour is not blue (e.g. sections H7 and H8, Fig. 4.17A). An obvious contact was detected on the DS images between most of the lithologies, such as the Hadabah dome, Al Khabt synclinal phacolith, Al Fayd tonalite, and the post-tectonic monzogranitic pluton (sections H5 and H6, Fig. 4.17B). The granitoid rocks are shown mostly in bright white hues, whereas the metamorphic layered rocks display a mixture of colours (red, brown and green). The mafic dyke rocks which intrude the E-W faults are also very distinctive. A contact between the Suwaydah gneiss and the mafic tonalite is also clear in the DS image in test-site area No.2A.

Fig. 4.17 TM band 7,5,4 red,green,blue scaled decorrelation stretched FCC images. A:for test-site 2A; B:for test-site 2B.

The geological map (Fig. 4.10) constructed for the test area based on the FCC images is identical to that produced using the techniques described earlier. Similarly, the geological structures recognized using this technique are similar to those recognized with the previous techniques.

4.3.4 Edge enhancement techniques

(a) Image enhancement

As previously described, the Landsat images are suitable for lineament analysis by applying high-pass filtering on the data image TM band 5.

Edge enhancement was achieved by high-pass filtering in order to emphasize higher spatial frequencies. TM band 5 was selected for the application of the method in this study, which described in section 3.3.4 (test-site area No.1). The Landsat TM digital image of the test-sites No.2A and 2B has been processed using three high-pass directional filters to enhance linear features oriented in north, northeast, and northwest directions only, because these were found to yield the most useful information after comprehensive testing using different filters.

The three-step procedure (Table 3.2) performed for lineament enhancement was as follows:

-an increase in the contrast of edges that have trends in approximately the selected directions was achieved by making the dark side of an edge segment darker and the light side lighter relative to the background. The resulting filtered images for both test-sites 2A and 2B are shown in Figs. 4.18 and 4.19, respectively.

-in the second step, all three filtered images were added together and additional scaling was applied (Figs. 4.18D; 4.19D). The product of this step was appropriate for visual definition of lineaments or fractures.

-a better image was obtained by adding these scaled filtered images to the original image, and this was the last step of the procedure. The product is shown in Figs. 4.20A and B for the test-site areas No.2A and 2B respectively. This product was used for the identification and tracing of lineaments. Similar results could be obtained following the procedure described in Appendix B.

Lineament identification (recorded on transparent overlay) for this test area followed the procedure described earlier in section 3.3.4 for test-site No.1. Ground inspection was
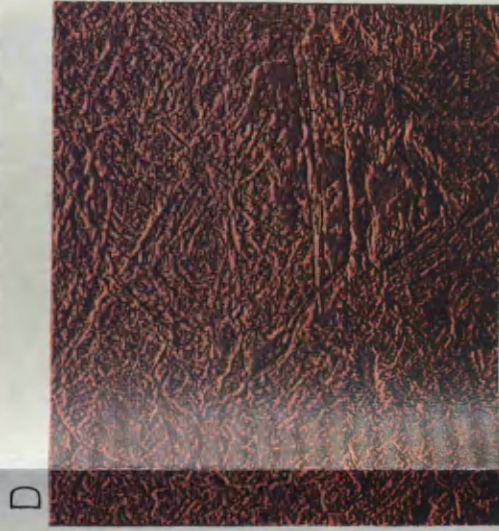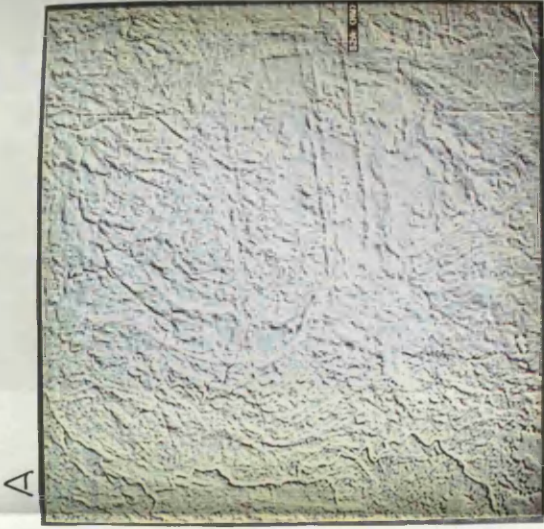
Fig.4.18 Edge enhancement technique images for the test-site
No.2A. A:northwestern directional high-pass filtered
image; B:north directional high-pass filtered image;
C:northeastern directional high-pass filtered image;
D:all these three filtered images added together with
additional scaling.
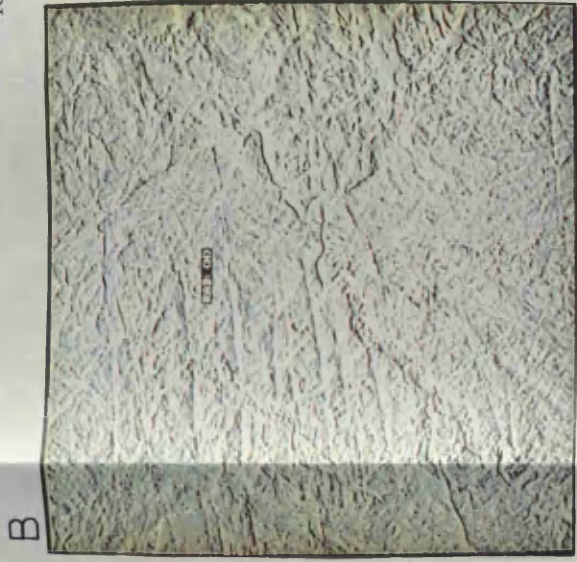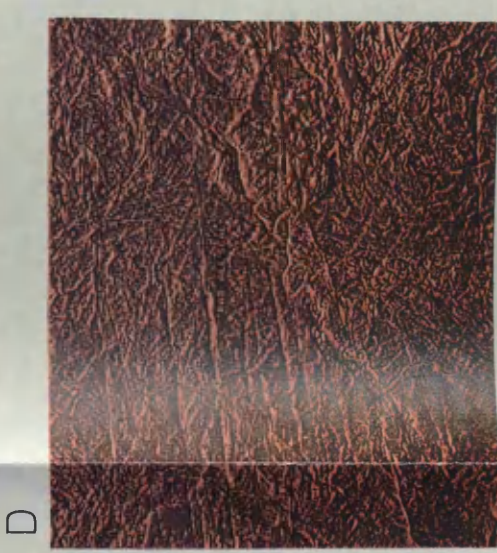
Fig.4.19 Edge enhancement technique images for the test-site No.2B. A:northwestern directional high-pass filtered image; B:north directional high-pass filtered image; C:northeastern directional high-pass filtered image; D:all these three filtered images added together with additional scaling.
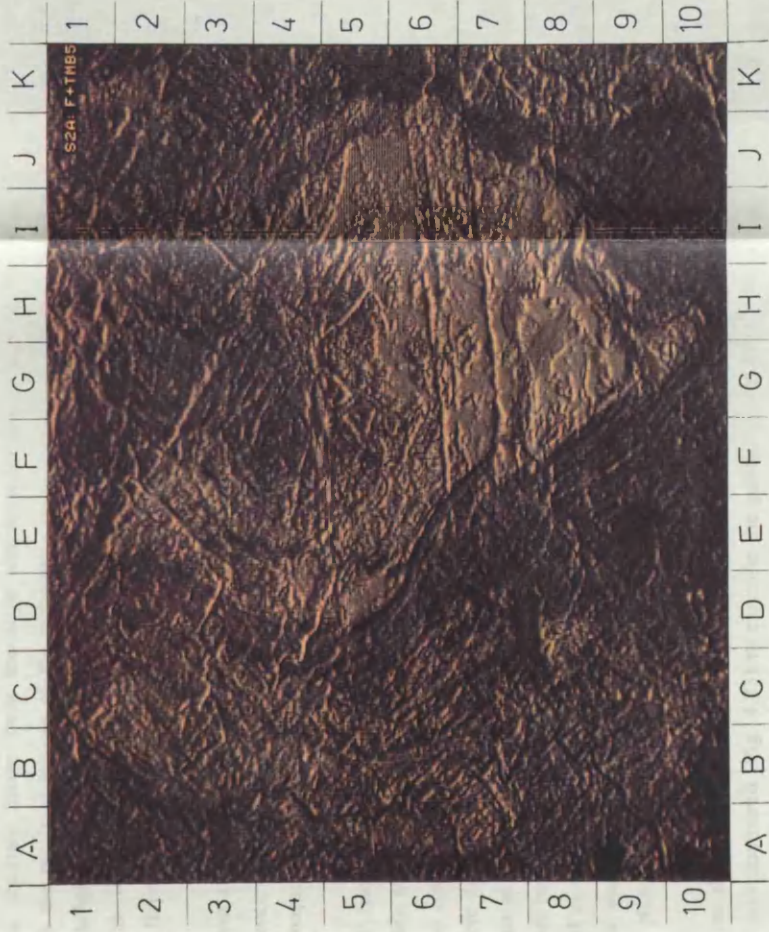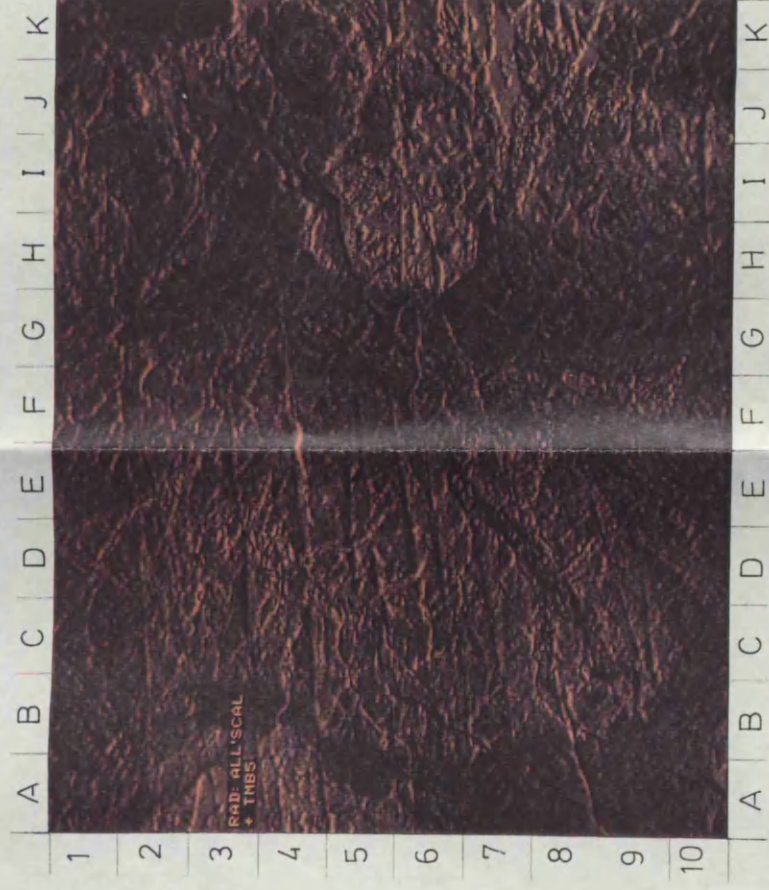
Fig.4.20 Directionally enhanced image superimposing TM band 5.
A:for test-site 2A; B:for test-site 2B.

utilized in constructing the geological fracture map (Fig. 4.21). This map was produced by using the resultant image from the edge enhancement procedures as an input together with the resultant images of the techniques previously described, particularly the SE3 technique. This map is used as the basis for discussion of lineaments and fractures. The lineament analysis emphasizes the trends rather than the absolute locations of lineaments.

(b) Lineament trend interpretation of Landsat images

The significance of the lineament trends interpreted from images was analyzed by using directional frequency rose diagrams with a 10 degree azimuth class interval.

The detailed fracture map (Fig. 4.21), shows that lineament frequency is generally constant within test area No.2. This area is composed of two test-sites (2A and 2B) and therefore two rose diagrams were plotted separately (Figs. 4.22A and B). In test-site area 2A, there is no obvious preferred orientation of lineaments, although there are concentrations at NE-SW, N 25° W, N 50° W and E-W directions. In contrast, test-site 2B shows two concentrations: E-W and NW-SE trend. If these two rose diagrams are combined as test-site No.2 (Fig. 4.22C), two orientation concentrations are obvious. These are in the NW-SE and E-W directions. Although E-W lineaments were not recorded by Norman (1980a), the NW-SE trend was observed by him.

The lineaments shown on Figure 4.21 were counted on a 2.5- by 2.5-km grid, and the total density was contoured (Fig. 4.23) to examine the pattern of concentration and to asses how it might relate to the other studies. The number of lineaments/6.25 km² varies from 2 to 21. Several concentrations of lineaments are quite apparent throughout test-site No.2, particularly in the Al Khabt synformal phacolith and Al Fayd tonalite.

An attempt was also made to correlate the observed lineaments (Fig. 4.21) and mapped faults, using the available 1:100,000 geological maps. Many lineaments were found to accord with mapped faults, whereas lineaments corresponding to joint sets have not previously been mapped in ground surveys.

(c) Conclusion

Landsat TM imagery is very useful for revealing lineaments which can be correlated with fractures within the test-site area. Many of these fractures were revealed for the first time during this TM investigation. Here, numerous continuous long lineaments

Lineament (mainly joints)

Igneous rocks

0   2.5 km

N
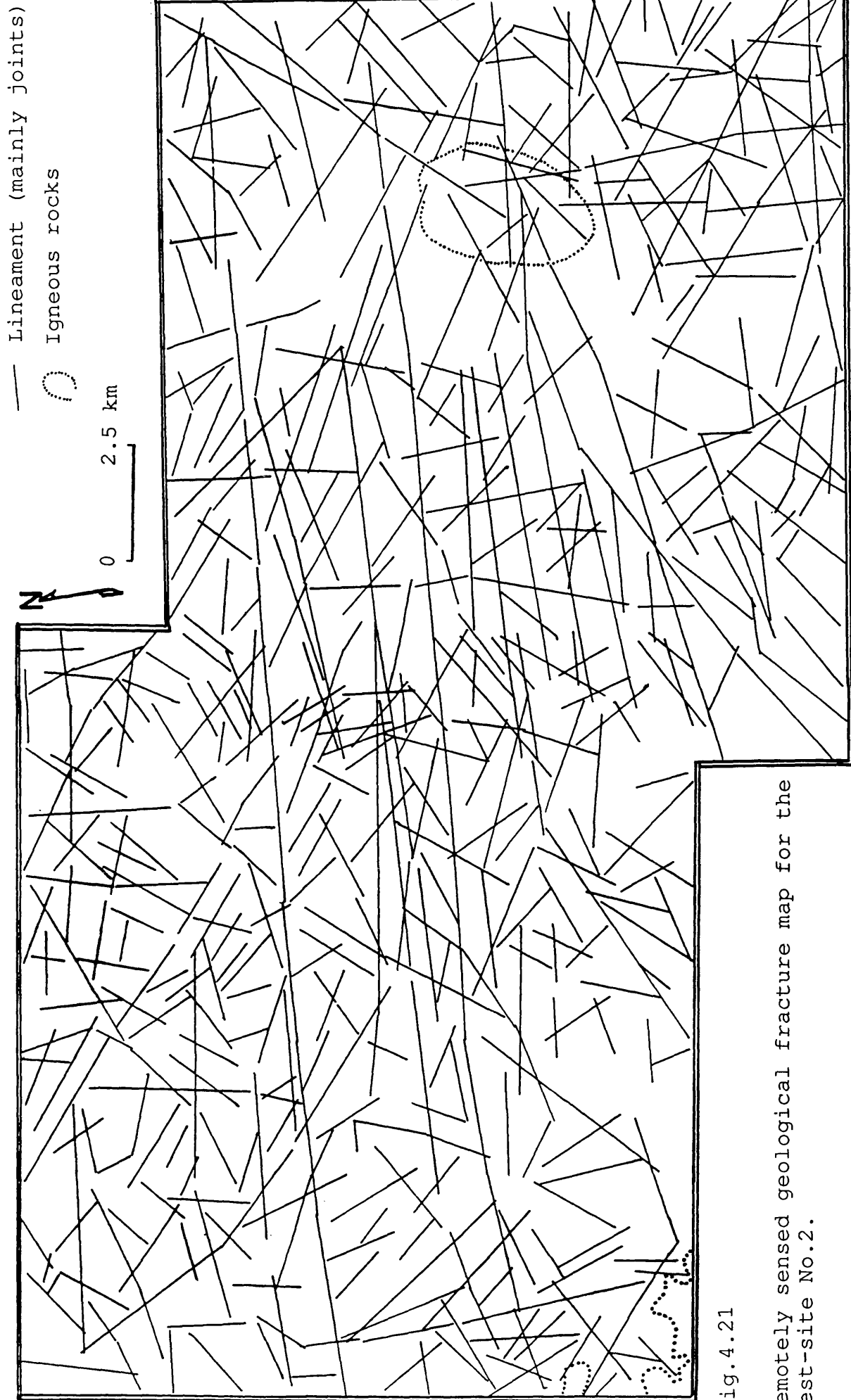
Fig. 4.21

Remotely sensed geological fracture map for the
test-site No.2.
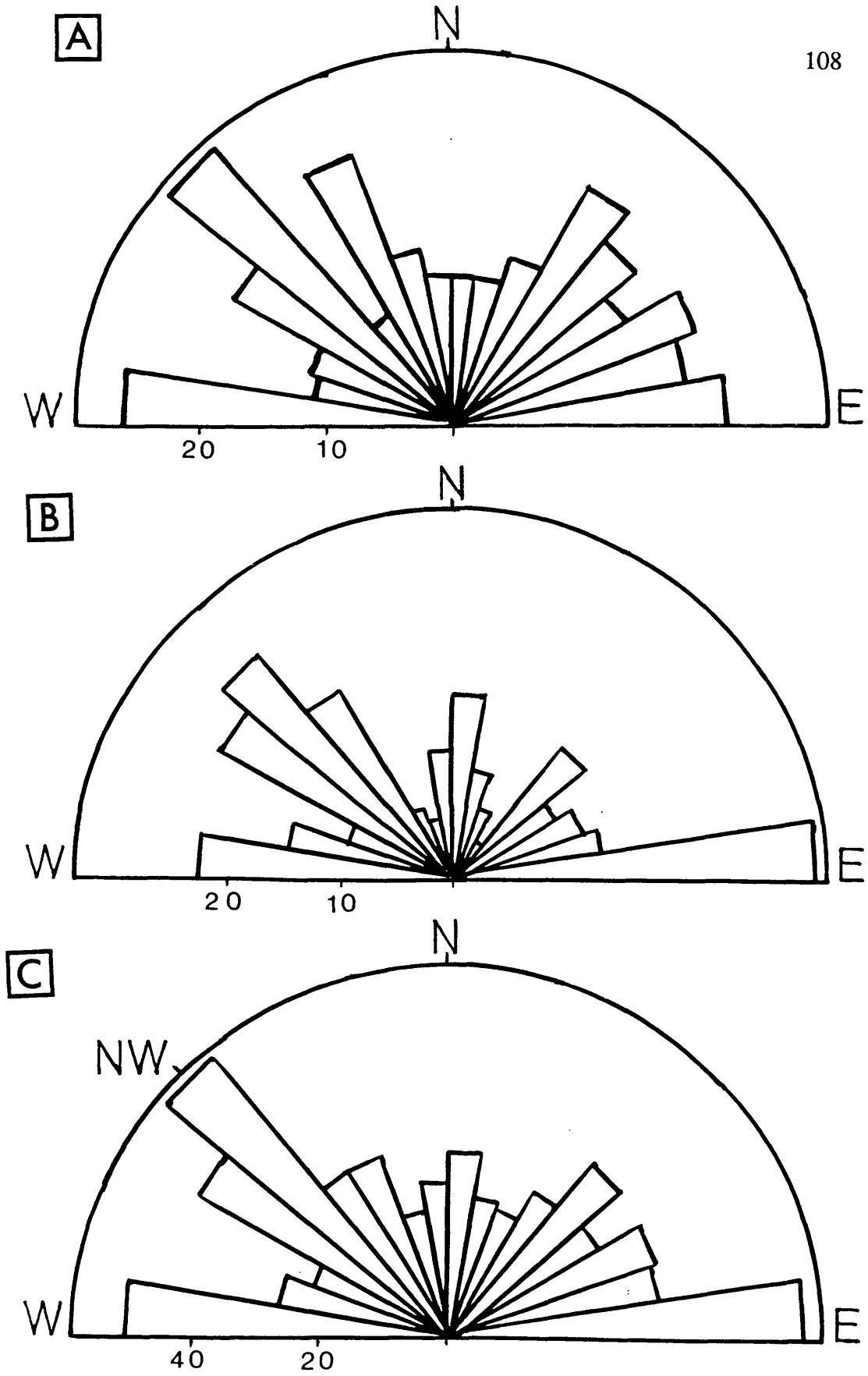
Fig.4.22 Rose diagrams summarising strike-frequency
distribution of the lineaments in Fig. 4.21.
A:test-site No.2A; B:test-site No.2B; C:583
lineaments of the test-site area No.2.

Fig.4.23 Fracture density isopleth map for the test-site area No.2. Fracture density is expressed in number of fractures/6.25 km².
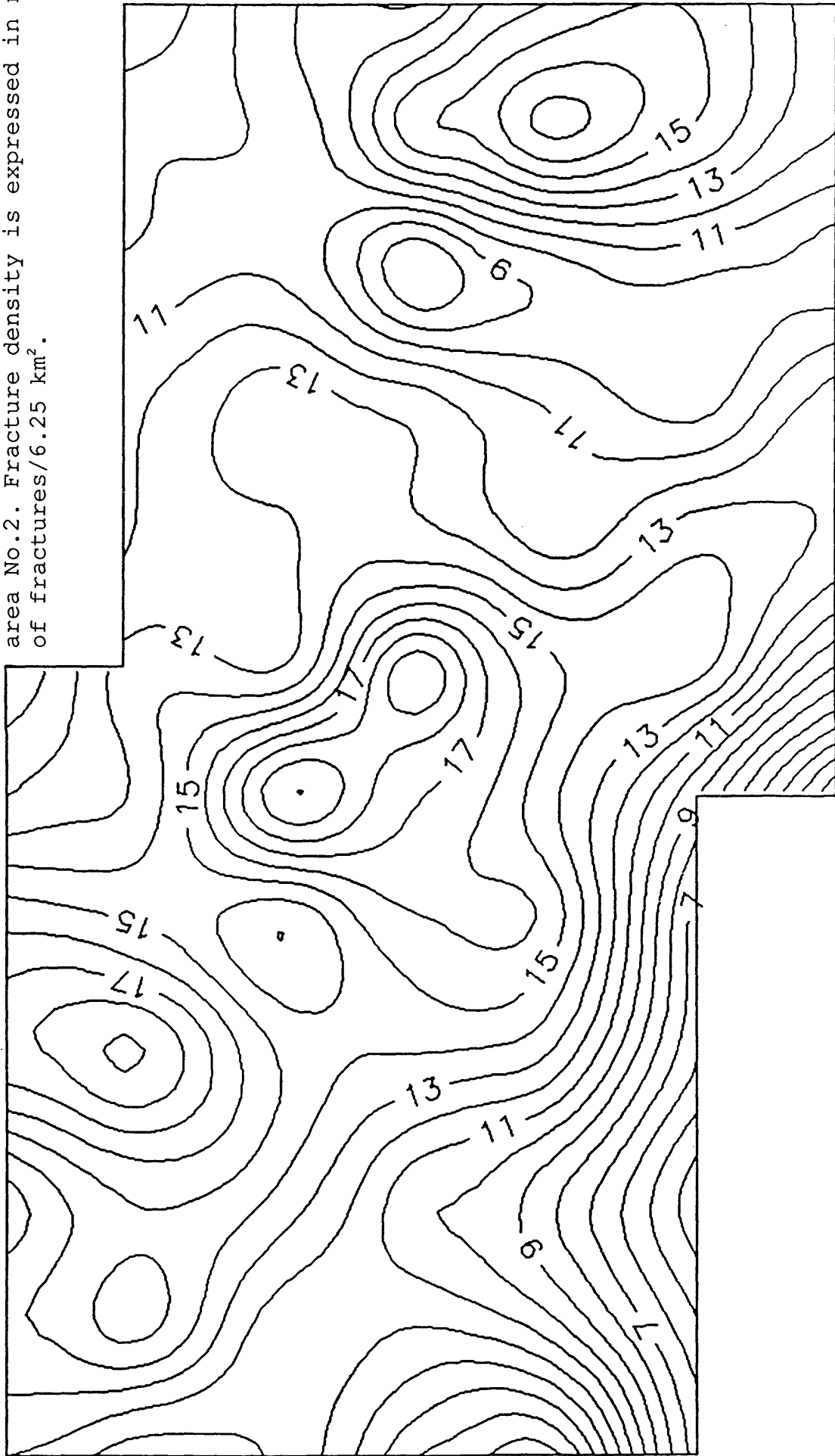
were observed in contrast with the test-site No.1.

Quantitative examination of the lineaments showed that the test-site area has two preferential directions, these are E-W and NW-SE.

Although the images produced by edge enhancement techniques were very useful for the study of lineaments, most of the lineaments (about 70%) can be detected on images prepared by previously mentioned enhancement techniques, particularly the SE3 technique.

CHAPTER FIVE APPLICATION OF METHODS:
III. TEST-SITE No.3
(JABAL DUHAYYAH AREA)

5.1 INTRODUCTION

5.2 GEOLOGY OF THE TEST-SITE

5.3 REMOTE SENSING TECHNIQUES

    5.3.1 Introduction

    5.3.2 Contrast enhancement

    5.3.3 Spectral enhancement techniques

        SE1 Technique

        SE2 Technique

        SE3 Technique

    5.3.4 Edge enhancement techniques

    (a) Image enhancement

    (b) Lineament trend interpretation of Landsat images

    (c) Conclusion

5.1 INTRODUCTION

The third test-site was selected because of the interesting folding pattern, diverse igneous and metamorphic rocks, location on the border between Asir Terrane (AT) and Nabitah Mobile Belt (NMB) (Fig. 5.1) and the excellent exposure of the assorted lithological units.

There were no previous detailed geological studies for this test-site as for the test-site No.1, but the test-site is within the area of two published 1:100,000 reconnaissance geological maps of Coleman (1973a) and Prinz (1975), where broad lithological discriminations were based on photo-interpretation and field checking of some localities (Fig. 5.2).

The test-site is accessible to the east of Wadi Aya, but it is difficult to reach the exposures of Asir Terrane to the west of Wadi Aya due to the rugged terrain produced by strongly foliated metamorphic rocks of the Asir escarpment.

Wadi Aya has a running water throughout the year, wild mint plantations are extensive and the area is inhabited by many bedouins.

5.2 GEOLOGY OF THE TEST-SITE

The geology of the test-site is complex since it is located at the border between two tectonic assemblages (Asir Terrane and Nabitah Mobile Belt). The major lithological units of Precambrian age are: plutonic rocks, gneisses and layered metamorphic rocks. Reconnaissance geological mapping at 1:100,000 scale was carried out by DGMR personnel (Coleman, 1973a and Prinz, 1975). This was followed by a regional 1:250,000 scale compilation (Greenwood, 1985c). These maps are the results of the only detailed available study.

The plutonic rocks includes quartz monzonites, granites, tonalites and granodiorites. These intrude older metamorphic rocks. Small gabbroic intrusives cut the granitoid rocks of the Jabal Duhayyah.

The Khamis Mushayt Gneiss (KMG) consists of orthogneiss, paragneiss, migmatite, amphibolite and marble. The KMG has been plastically folded and records a very
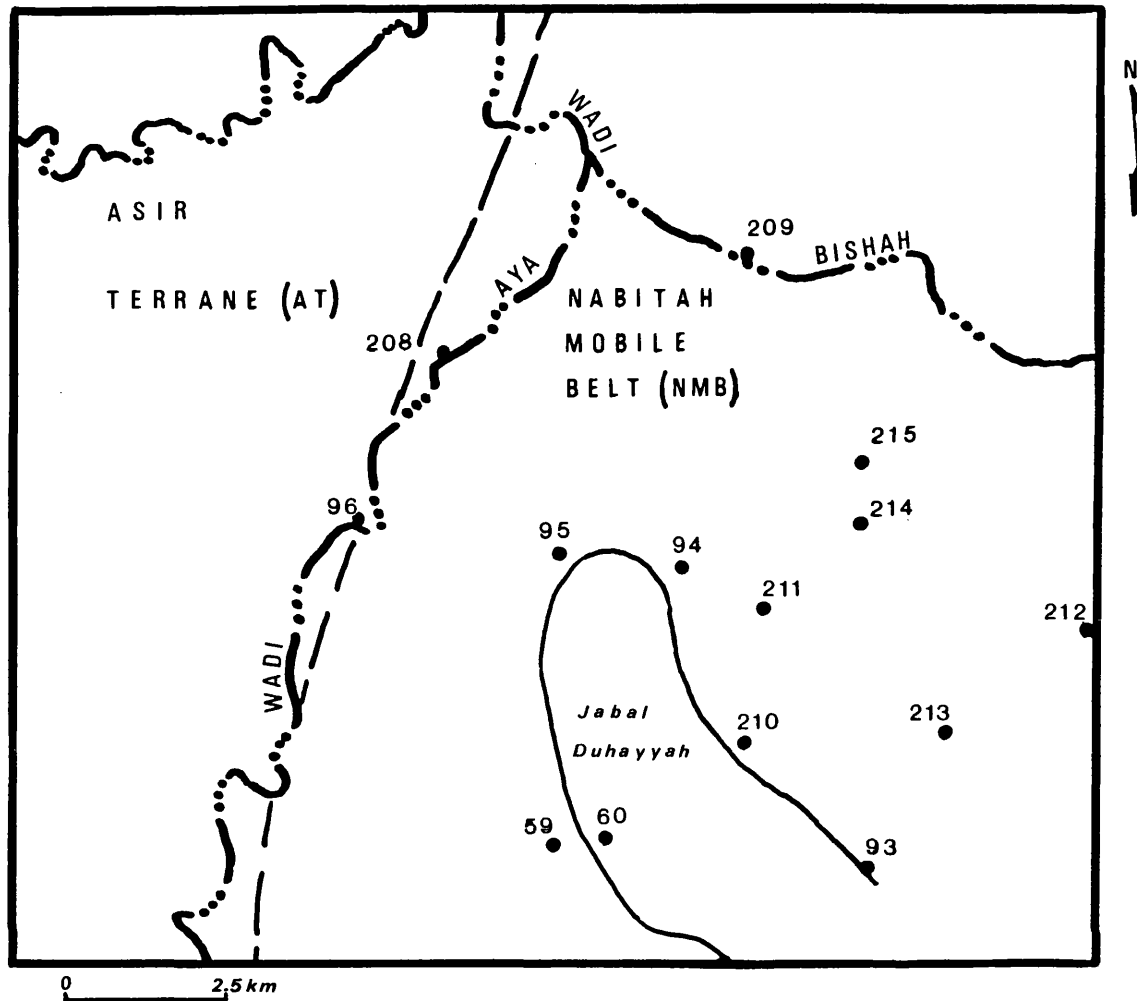
Fig. 5.1 Location map of observation sites for the
        test-site No.3.
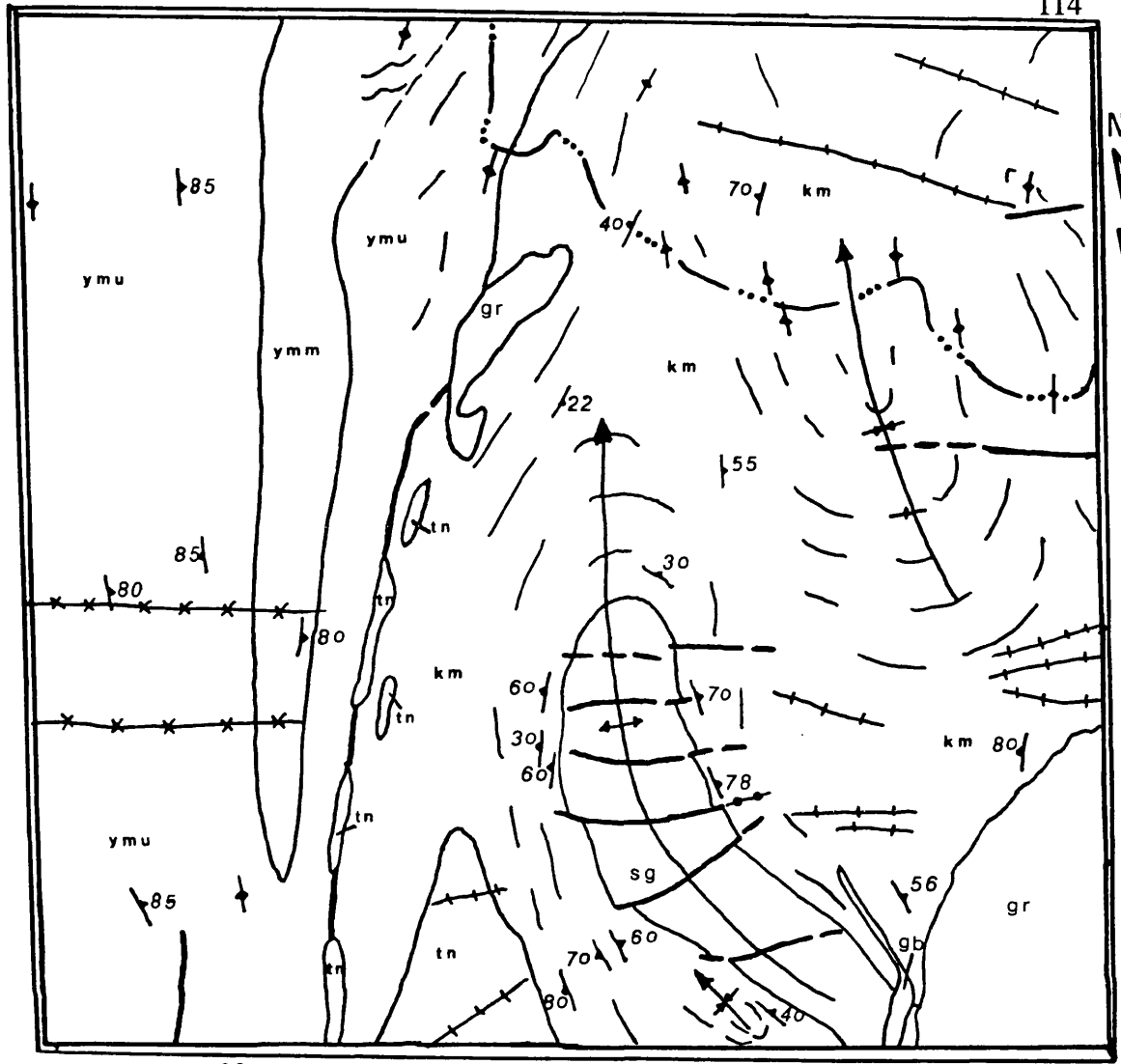
SCALE 1:100000

LEGEND

—•—•— Basalt and andesite dykes

—+—+—+— Granite and aplite dykes

—×—×—×— Dolerite dykes

gr	Quartz monzonite
gb	Gabbro and metagabbro
sg	Quartz monzonite, granodiorite and granite
tn	Tonalite to granodiorite
km	Khamis Mushayt Gneiss
ymu	Young metamorphic rocks-upper unit
ymm	Young metamorphic rocks-middle unit

—...— Wadi Bishah

——— Lithological contact, dashed where inferred

——— Fault, dashed where inferred

Antiform—showing crestline and direction of plunge

Synform—showing troughline and direction of plunge

Strike of vertical foliation

80 Strike and dip of inclined foliation

Trend lines observable on aerial photographs

Fig. 5.2 Compiled geological map of the test-site No.3.

complex history of metamorphism and plutonism (Coleman, 1973a).

The layered metamorphic rocks of the test-site are assigned to the Hali Group (Prinz, 1975). This group of metamorphosed sedimentary rocks is divided into three units. Only the upper and the middle units are exposed in test-site No.3. The upper carbonate-rich unit consists of calcareous green phyllite and actinolitic schist, grey-to-brown to reddish-brown marble and interbedded clastic rocks. The carbonate-poor middle unit consists predominantly of fine- to medium-grained metamorphosed clastic rocks (quartzite, metasiltstone, slate and phyllite). The colour of the middle unit varies from white to black, the coarser clastic rocks being generally light coloured, and the slate and phyllite dark.

Structurally, Coleman (1973a) proposed that the area could be divided into two distinct structural units:(1) the basement complex (infrastructure) and (2) the younger metamorphic rocks (suprastructure). The infrastructure shows a complex deformational history.

5.3 REMOTE SENSING TECHNIQUES

5.3.1 Introduction

The three main types of image processing techniques; contrast-, spectral- and edge-enhancements; have been performed on the sub-scene of this test-site. Each technique yields a hardcopy image which was used later for interpretation.

Because Jabal Duhayyah is high in elevation and because the sun elevation was 57° and the sun azimuth 101° from the north, there is shadow on the western flank of Jabal Duhayyah. This affects the results of image processing in this test-site. This should be remembered when considering the resultant images used for this test-site.

Field observations were used extensively to supplement remote sensing interpretations during the construction of the geological maps, particularly the area mapped as KMG by Coleman (1973a) and the contact between Asir Terrane and Nabitah Mobile Belt (Plate 7).

5.3.2 Contrast enhancement

Simple linear contrast stretching enhancement (scaling) was applied to the sub-scene of
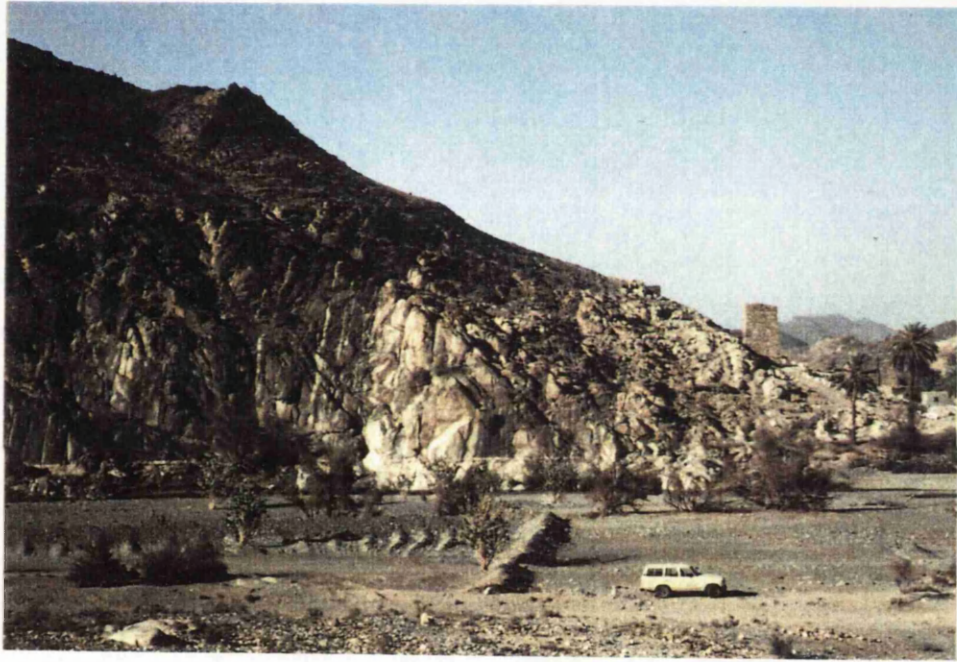
Plate 7 NW Steeply dipping contact zone between AT (dark coloured rocks) and NMB.

this test-site. Figure 5.3A shows the raw Landsat TM band 5 data, while Figure 5.3B shows the linearly contrast stretched Landsat TM band 5 data for the test-site No.3. It is obvious that such enhancement shows more detail.

5.3.3 Spectral enhancement techniques

SE1 Technique

As described earlier in section 3.3.3(a) for test-site No.1, this technique of ratioing TM bands 1,3,4,5 and 7 was performed on test-site No.3 in order to create a CRC image for later interpretations.

Method:

-TM BAND 5/1, was used to distinguish rocks rich in opaque phases which have low band-5 and band-1 values. Figure 5.4A shows the TM band 5/1 image. Bright areas correspond to regions deficient in opaque phases.

-TM BAND 5/7, provides a measure of the intensity of the hydroxyl absorptions in the 2.2-2.4 μm region, i.e. band 7. Figure 5.4B shows the TM band 5/7 image. The slightly brighter areas correspond to regions with high OH contents.

-TM BAND (5/4 x 3/4), was used to emphasize and discriminate the iron-bearing aluminosilicates. Figure 5.4C shows the TM band (5/4 x 3/4), where very bright areas correspond to regions rich in Fe-bearing aluminosilicates, whereas the darker areas correspond to the granitic, tonalitic, gneissic and parts of the young metamorphic rocks.

Rock units defined on enhanced imagery:

Granitoid rocks of Jabal Duhayyah, a small portion of the southeastern granitic pluton and the gneisses which are intercalated with the schistose rocks surrounding Jabal Duhayyah were identified in the TM band 5/1 ratio image because these rocks' constituent minerals have high reflectance values and they are deficient in opaque phases. The small body of gabbroic composition intruding the granitoid rocks of the southern Jabal Duhayyah and all other rock types (except the granitoid rocks) are also identified on the TM band 5/1 ratio image because these rocks' constituent minerals have low reflectance values, because they are rich in opaque phases although with different proportions in each rock type.

In the TM band 5/7 ratio image several lithologies were distinguished, including quartz
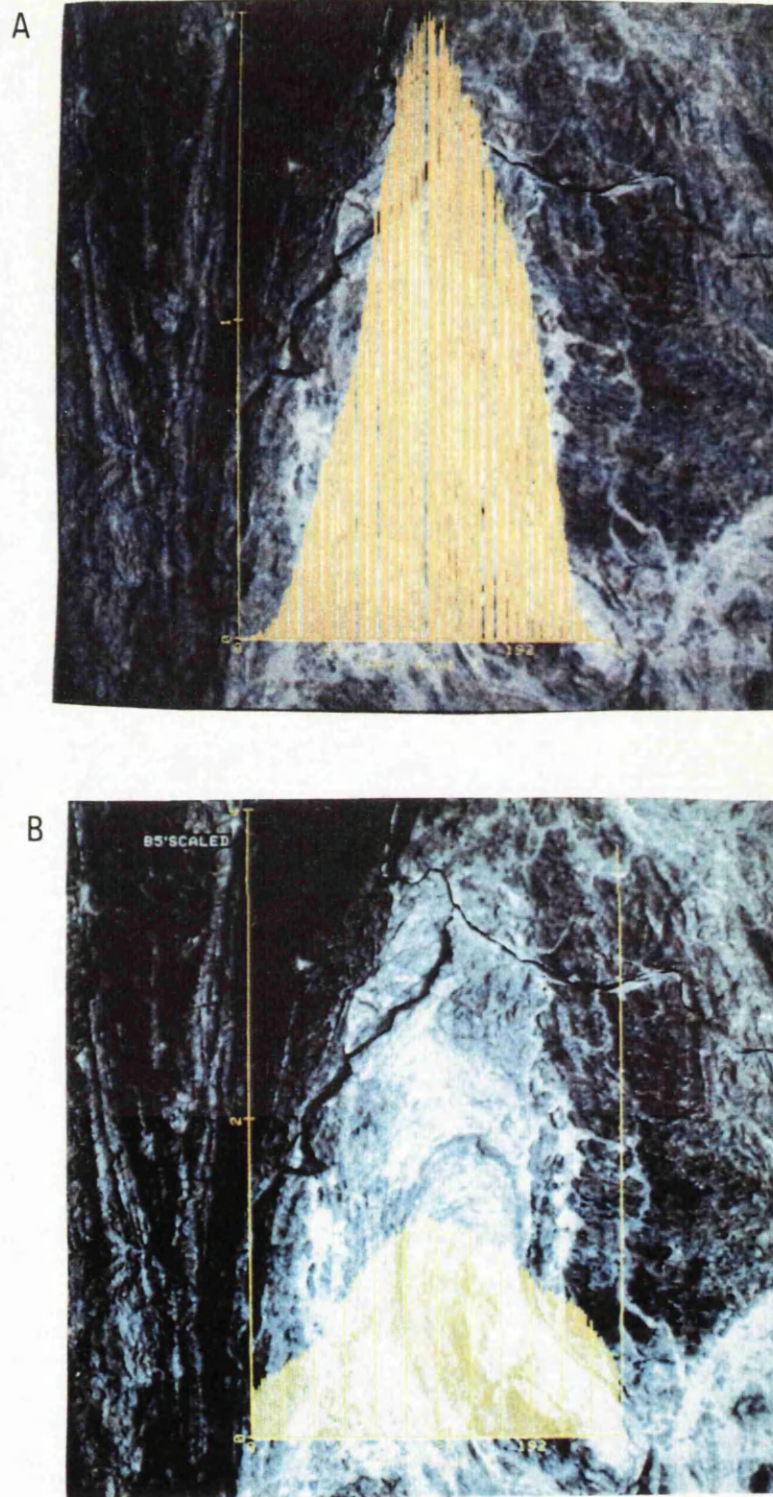
Fig. 5.3 A:Landsat TM band 5 subscene for the test-site
No.3; B:the linearly contrast stretched image.
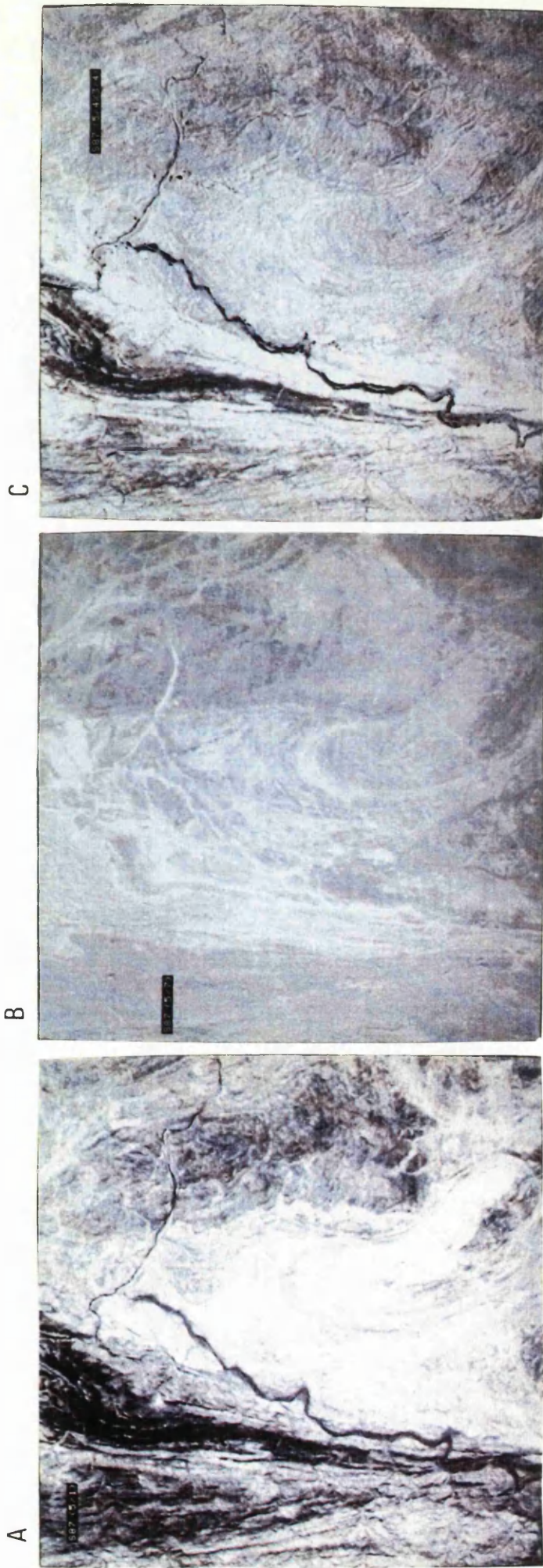
Fig. 5.4 SE1 Technique images for the test-site No.3.
A:TM band 5/1 ratio image; B:TM band 5/7 ratio
image; C:TM band (5/4x3/4) ratio image.

monzonite, metagabbro, migmatites and granitoid rocks. The granitoid and the gneissic rock types have similar brightnesses on the three ratio images resulting in similar colours on the CRC. The separation between those rock types is difficult, but field checking helped in the distinction of these types.

The resultant contrast-stretched CRC is shown in Figure 5.5. The TM band 5/7 image was assigned the red component; the TM band 5/1 image, the green component; and the TM band (5/4 x 3/4) image, the blue component. Although the rock types mentioned above have unique brightness patterns on the ratio images and should have unique colours on a CRC image, this technique allowed only a broad lithological discrimination between the layered metamorphic rocks, quartz monzonite, metagabbro and the granitoid rock types. The layered metamorphic rocks of Asir Terrane (e.g. sections B2, C6 and E1, Fig. 5.5) and the quartz monzonite and metagabbro (e.g. sections I8, J6 and J7, Fig. 5.5) are bluish-red colours. The granitoid rocks in the test-site No.3 are green on the CRC, because of the deficiency in opaque phases which produce bright areas on the TM band 5/1 ratio image. This green colour of the granitoid rocks is the same as that in test-site No.1. The sharp contact between migmatites and the schist and gneiss outcrops to the east of the contact between Asir Terrane and Nabitah Mobile Belt is very well exhibited (e.g. sections G2-H2, G4-H4 and G6-H6, Fig. 5.5). This contact was not previously reported or mapped. The contact is also distinguished on the ratio images, particularly the TM band 5/1 and 5/7 ratio images.

The sediments in the wadis consist primarily of mechanically weathered rock fragments that have been transported a short distance. Where the sediments are compositionally similar to the adjacent mountains, the wadis become spectrally indistinguishable on the CRC, e.g. Wadi Aya (sections C9 and D5, Fig. 5.5). In contrast, if they are compositionally different from the adjacent mountains they are spectrally distinguishable on the CRC (e.g. Wadi Aya, sections E4 and F3, Fig. 5.5).

Although geological maps could be constructed for the test-site area based on the CRC image obtained by the SE1 technique, the SE2 technique was preferred.

SE2 Technique

As shown earlier in section 3.3.3(a), the results obtainable from this technique are

Fig. 5.5 A contrast-stretched CRC of TM band 5/7 in red,
band 5/1 in green, and band (5/4x3/4) in blue
for the test-site No.3.

useful for lithological discrimination. Therefore, the TM CRC (7/5,5/4,4/2) in red, green and blue was created.

Method:

-TM BAND 7/5. Distinguishes areas rich in OH content. Figure 5.6A shows these areas as moderately dark.

-TM BAND 5/4. Emphasizes and discriminates rocks rich in Fe-bearing aluminosilicates. Figure 5.6B shows very bright areas which correspond to regions rich in such minerals.

-TM BAND 4/2. This is used for the detection of surface iron-staining. Such areas are shown as dark in Figure 5.6C.

Rock units defined on enhanced imagery:

The layered metamorphic rocks forming the Asir Terrane, a small area to the northeast and the area surrounding Jabal Duhayyah, were identified easily as the darkest areas on the TM band 4/2 ratio image (Fig. 5.6C), because they are strongly iron-stained compared to the other rock units. Migmatites and gabbroic rocks are also identified using the same criterion. The granitoid rocks and the schist and gneiss exposures in the test-site are distinguished by their lack of iron-staining. They show as bright areas on the TM band 4/2 ratio image. The migmatitic rocks were identified as the brightest areas on the TM band 7/5 ratio image, because of their low OH content, and they should not be confused with the bright areas resulting from the shadows of Jabal Duhayyah. The amphibolitic rocks could be reliably discriminated as particularly strong bright areas on the TM band 5/4 ratio image.

The rock types mentioned have unique brightness patterns on the ratio images, which are reflected in the CRC image as well. The colours are more variable and prominent in this technique than in the SE1 technique which helps in the preparation of the lithological map.

The lithological information contained in the three TM band ratio images for the test-site has been integrated into one image. The resultant FCC is shown in Figure 5.6D, where the TM band 7/5 image was assigned the red component; the TM band 5/4 image, the green component; and the TM band 4/2 image, the blue component. One additional linear contrast stretch was applied in order to enhance the FCC. The resultant CRC imagery is shown in Figure 5.7, which was used for further interpretations.
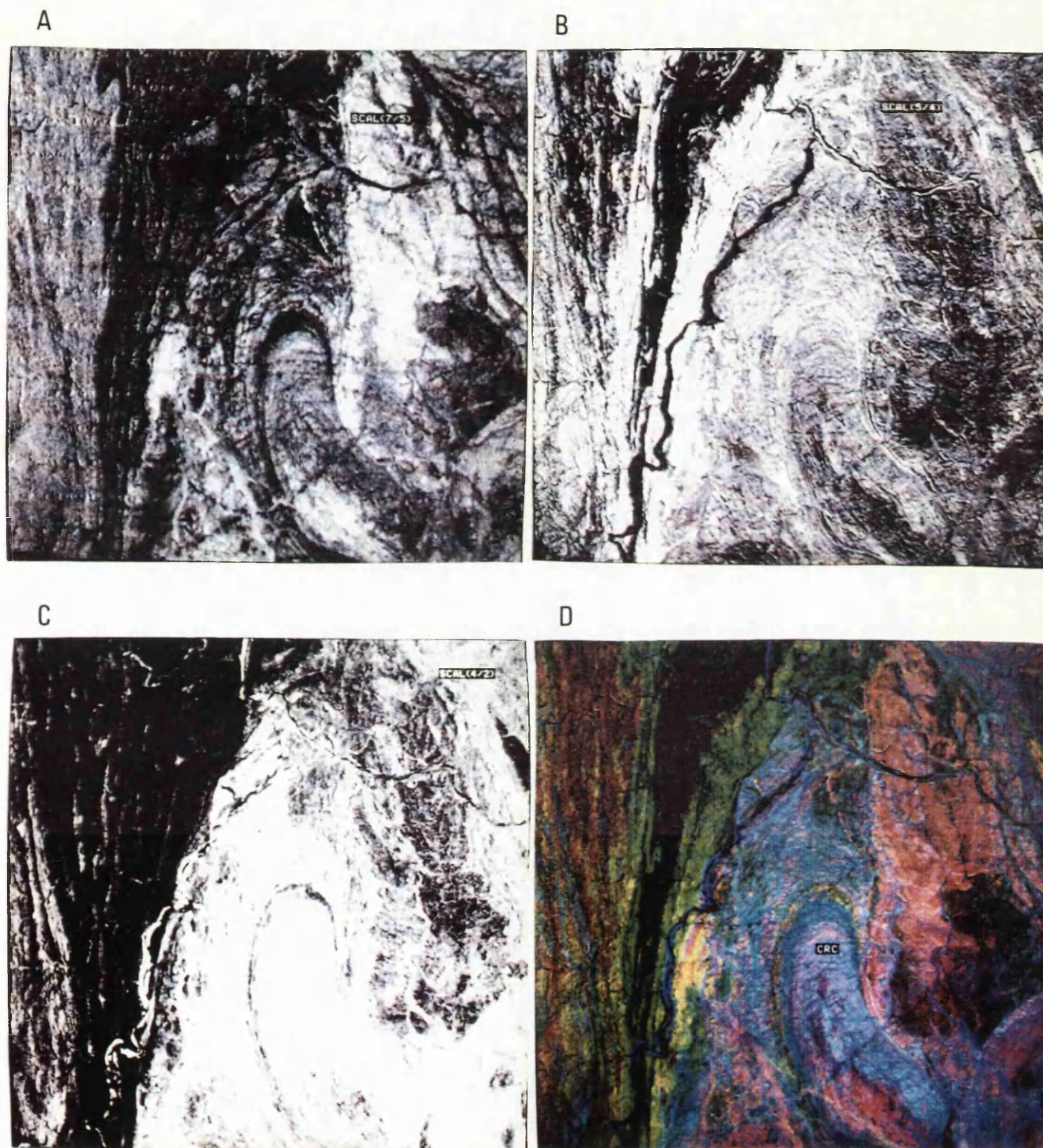
Fig. 5.6 SE2 Technique images for the test-site No.3.
A:TM band 7/5 ratio image; B:TM band 5/4 ratio
image; C:TM band 4/2 ratio image; D:FCC image.

Fig. 5.7 Linearly contrast stretched CRC of TM band 7/5 in red, band 5/4 in green, and band 4/2 in blue for the test-site No.3.

The granitoid rocks have reddish-blue hues (e.g. sections E10, F3, G8, H9, J9 and K8, Fig. 5.7) on the CRC, but field knowledge was used in addition in order to differentiate these rocks. Green and yellow colour combinations indicate amphibolitic rocks as observed earlier in section 3.3.3(a) (test-site No.1) (e.g. sections C1, C9, D6, E3, G6 and K3, Fig. 5.7). The tonalitic pluton to the west of Jabal Duhayyah contains abundant inclusions of amphibolitic country rock, hence the yellowish green colour patches identified within this tonalite (sections D10 and E10, Fig. 5.7).

Migmatites, metagabbros and quartz monzonites, which were mapped earlier as a single unit, are very easily discriminated on the CRC prepared by this technique. A thorough field check (Nos. 209 to 215, Fig. 5.1) and thin section studies were utilized in locating the contacts of these rocks. The quartz monzonitic rock unit is shown as a blood-red colour on the CRC (sections H8 and I8, Fig. 5.7), whereas metagabbro has a blood-red colour background mixed with green (sections J6 and K7, Fig. 5.7). This colour is also noticed in the gabbroic rocks to the southwestern corner of the test-site No.1 (Fig. 3.8). Gabbroic xenoliths were found in the quartz monzonite. The migmatites were easily identified in the field along Wadi Bishah and also to the north of the metagabbroic rocks. The word migmatite is used here following definitions given by Dietrich and Mehnert (1960) and Mehnert (1968). Where these migmatites appear, they are generally coarsely crystalline and intensely invaded by veins and dykes of varied composition. The migmatites vary in appearance, texture and composition. Some are regularly layered, veined and schlieren in texture, but mostly agmatitic (Plate 8). This migmatitic zone is thought to be developed within the older schist and gneiss unit. The migmatites have a distinct orange/red colour on the CRC image (e.g. sections H2, H4, H6 and I4, Fig. 5.7).

The schist and gneiss unit was previously called Khamis Mushayt Gneiss by Coleman (1973a). This unit displays a variety of colours on the CRC, because it is composed of many lithologies. Gneiss, amphibole- and mica-rich schists are the most abundant lithologies, but gneiss is most common (bluish hues, e.g. sections E7, F5, J1, K1 and K2, Fig. 5.7). A foliation and a strong lineation are present.

The Asir Terrane layered metamorphic rocks in the test-site No.3 were previously mapped as two units, the upper and the middle units of the Hali Group (Prinz, 1975). The upper carbonate-rich unit consists of calcareous green phyllite and actinolite schist,

Plate 8　Migmatites in test-site No.3.

marble and interbedded clastic rocks. The carbonate-poor middle unit consists predominantly of metamorphosed clastic rocks (quartzite, metasiltstone, slate and phyllite). It was difficult to check these lithological identifications, except along Wadi Aya, because of the rugged terrain. Prinz (1975) reported low metamorphic grades (green-schist) with rock types generally actinolite-, muscovite- and biotite-rich schists in addition to phyllite and slate. Quartzite was also found. The middle unit displays a dark brownish-red colour on the CRC (e.g. sections C3, C6 and D1, Fig. 5.7), whereas the upper unit shows up as a mixture of yellow, green and brownish-red colours (e.g. sections A1, A9, B2, B5 and B9, Fig. 5.7).

The granitoid rocks were discriminated based on the CRC image, field knowledge and previously published information. Table 5.1 indicates the way of predicting the colours of these granitoid rocks on the CRC based on the texture, mineralogy and surface colour. This nomenclature was used later on the geological maps.

The sediments in the wadis consist primarily of mechanically weathered rock fragments that have been transported a short distance. If the sediments are compositionally similar to the adjacent mountains, the wadis become spectrally indistinguishable on the CRC (e.g. sections C9, D1 and D2, Fig. 5.7). On the other hand, where the source rock of the fragments in the wadis is compositionally different, the wadis are spectrally distinguishable in the CRC (e.g. section C5; Wadi Aya, sections C7, E4 and F3; Wadi Bishah, sections G3, H3 and K4, Fig. 5.7).

A detailed geological map of test-site No.3 area was constructed (Fig. 5.8) from the CRC image and field knowledge. Field observations were used extensively in the interpretations throughout the area. Comparing the geological map constructed from the TM image with the geological information contained in earlier maps compiled on Figure 5.2, it is very clear that although there is a general correspondence, there is more detail in the TM-based map. For example, the area which is mapped by Coleman (1973a) as Khamis Mushayt Gneiss can be resolved into four distinct lithological units: schist and gneiss, migmatites, metagabbro and quartz monzonite. Another example is the recognition of three rock units in the Asir Terrane instead of the two units mapped by Prinz (1975). Amphibolite, previously not separated on geological maps, was mapped in the east and around Jabal Duhayyah antiform.

There is no detailed structural analysis available for this test-site. An attempt to

ROCK TYPE	TEXTURE	RICH IN MINERALS	COLOUR	REMARKS	COLOUR IN CRC IMAGE	E.G. SECTIONS IN FIG. 5.7
Granodiorite	Fine-medium grained, strongly foliated.	mica	light-grey	Jabal Duhayyah antiformal pluton	Reddish medium blue	G7 and H9
Tonalite	Medium grained, foliated.	biotite-hornblende	greyish	contains abundant inclusions of amphibolitic country rocks	Reddish	E10
Granodiorite-monzogranite	Medium-coarse grained, massive.	biotite-hornblende	grey	part of a big post-tectonic pluton	Red and blue mixture	K8 and K10
Monzogranite	Medium-coarse grained, massive.	biotite	pink-medium grey	uniform body appearing as hills surrounding the big post-tectonic pluton	White reddish blue	J8

Table 5.1 Explanation of relative colour values for the
granitoid rocks in Fig. 5.7.

LEGEND

×× × × × ×× ×	Tonalite containing amphibolites
	Monzogranite
+ + + + +	Granodiorite – monzogranite
□ □ □ □ □ □	Quartz monzonite
	Metagabbro
	Metagabbro **dyke**
	Granodiorite
	Migmatites
	Schist and gneiss
	Metamorphosed clastic rocks (schist)
	Amphibolites
	Metavolcanic rocks (schist)

Lithological contact

Fault

Fault and contact zone between AT and NMB

Strike and dip of foliation
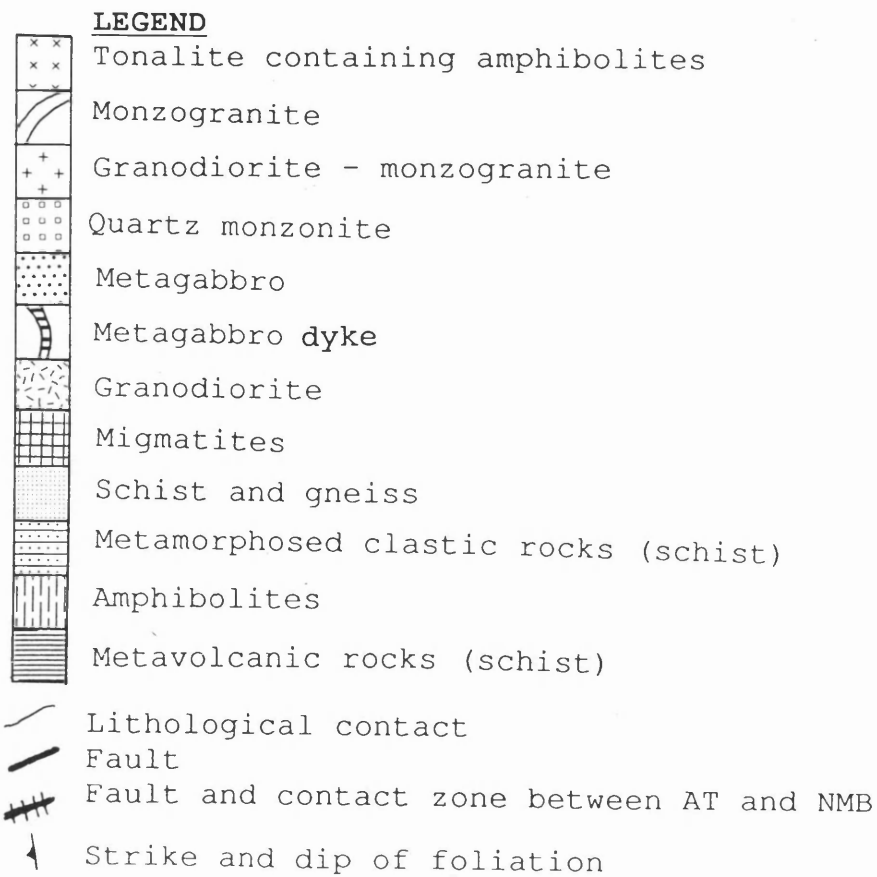
Fig. 5.8 Geological map constructed from the CRC for the test-site No.3.

construct a structural map in block form (Fig. 5.9) for test-site No.3 is based on the CRC image and field studies as well as correlations with the detailed ground studies of test-site No.1. The main phase of deformation is interpreted as F3 by correlation with test-site No.1 as discussed earlier (section 4.3.3), but with a stronger evidence, i.e. this test-site is an extension of the border zone between the Asir Terrane and the Nabitah Mobile Belt from the test-site No.1. F3 folds were detected in the northern part of the metamorphosed clastic rocks (section D1, Fig. 5.7). The Jabal Duhayyah is interpreted as F3 overturned antiform. The criterion on which these folds and their axial traces were identified is the change of the geometry of the foliation planes.

Faults were also easily detectable on the CRC imagery, for example, the left-lateral strike-slip fault in the northern part of Jabal Duhayyah (Fig. 5.8; sections E7 and F7, Fig. 5.7).

SE3 Technique

Method:

As discussed earlier, the TM bands 7, 5 and 4 were selected to create the decorrelated stretched (DS) image for test-site No.3. The final DS image was scaled to render it displayable and interpretable.

Rock units defined on enhanced imagery:

A TM band 7,5,4 red, green and blue DS FCC of the test-site area is shown in Figure 5.10. The migmatitic rocks display red colours (e.g. sections H2, H4 and I4), which should not be confused with the red colour of the Jabal Duhayyah shadow (sections G9 and H10). The wadis are prominent, having a blue colour. Quartz monzonite and metagabbro could be distinguished easily from migmatites (e.g. sections H8, I7, J6 and J7). The non-coloured areas within the granitoid rock types (e.g. sections D9, E9, J9 and K8) are areas of surface gravels of granitic composition. The schist and gneissic unit and the granitoid rock units have almost the same colours, which complicates discrimination between these units. The layered metamorphic rocks within the Asir Terrane are easily distinguished from other rock units based on the colour and N-S striking schistosity.

The geological map (Fig. 5.8) constructed for the test-site based on the FCC image is identical to that based on the SE2 technique but was more difficult to produce.

LEGEND

Granitoid rocks

Quartz monzonite and Metagabbro ⎫ POST-TECTONIC

Jabal Duhayyah granitoid rocks ⎱ SYN-TECTONIC

Migmatites

Schist and gneiss

Layered metamorphic rocks

F3 Antiform, plunging direction is shown
F3 Synform, plunging direction is shown
Fault
AT   Asir Terrane
NMB Nabitah Mobile Belt
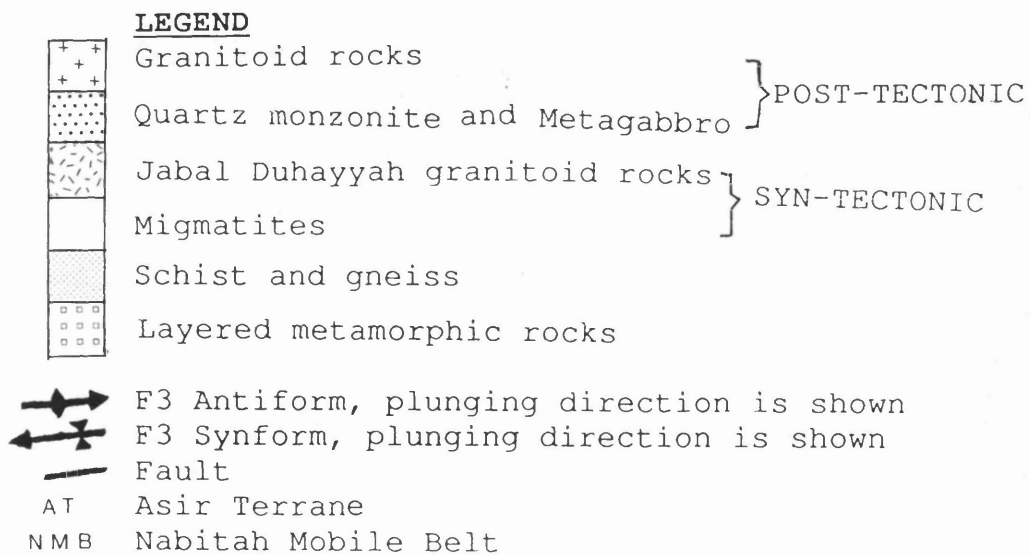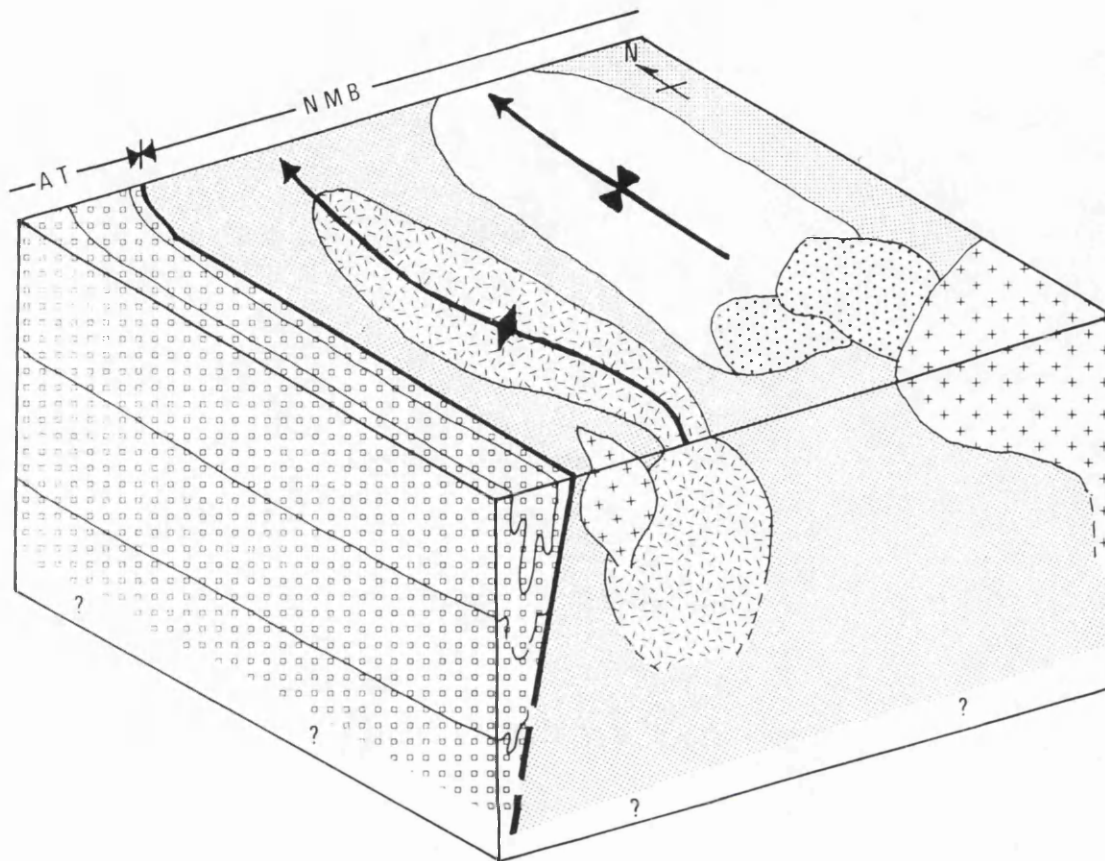
Fig. 5.9 Simplified non-scaled structural block-diagram for
the test-site No.3 based on the CRC image and field
interpretations.

Fig.5.10 TM band 7,5,4 red,green,blue scaled decorrelation
stretched FCC image for the test-site No.3.

5.3.4 Edge enhancement techniques

(a) Image enhancement

Edge enhancement was achieved by high-pass filtering in order to emphasize higher spatial frequencies via a convolution operation. TM band 5 was selected for the application of the method used in this study (described earlier in section 3.3.4). The Landsat TM digital image of the test-site No.3 was processed using three high-pass directional filters to enhance linear features oriented in north, northeast and northwest directions only, because these were found to yield the most useful information. Following the three-step procedure (Table 3.2) performed for lineament enhancement, Figures 5.11 and 5.12 were obtained. Similar results could be obtained following the procedure described in Appendix B.

Lineament identification (recorded on transparent overlay) was achieved as described earlier in test-site No.1. Geological fracture map (Fig. 5.13) was produced utilizing the resulted image from the edge enhancement procedures together with the resultant images of the techniques previously described, particularly the SE2 and SE3 techniques. This map is used as basis for discussion of lineaments and fractures. The lineament analysis emphasizes the trends rather than the absolute locations of lineaments.

(b) Lineament trend interpretation of Landsat images

The significance of the lineaments interpreted from images was analyzed by using directional frequency rose diagram with a 10 degree azimuth class interval.

The study of the fracture map (Fig. 5.13), shows that lineament frequency is generally constant within the test-site No.3, except in the Jabal Duhayyah area where the abundance of lineaments is greater. A rose diagram was plotted for the test-site area (Fig. 5.14), on which one distinct concentration is visible, i.e. N 65° E. Other broad concentrations are visible in directions: NE-SW, WNW-ESE and E-W. Although the E-W and the prominent N 65° E lineaments were not recorded by Norman (1980a), some directions were observed by him, e.g. WNW-ESE.

The lineaments shown on Figure 5.13 were counted on a 2.5- by 2.5-km grid, and the total density was contoured (Fig. 5.15) to examine the pattern of concentration and to assess how it might relate to the other studies. The number of lineaments/6.25 km^2 varies from 4 to 23. There is a high concentration of lineaments in the middle of the
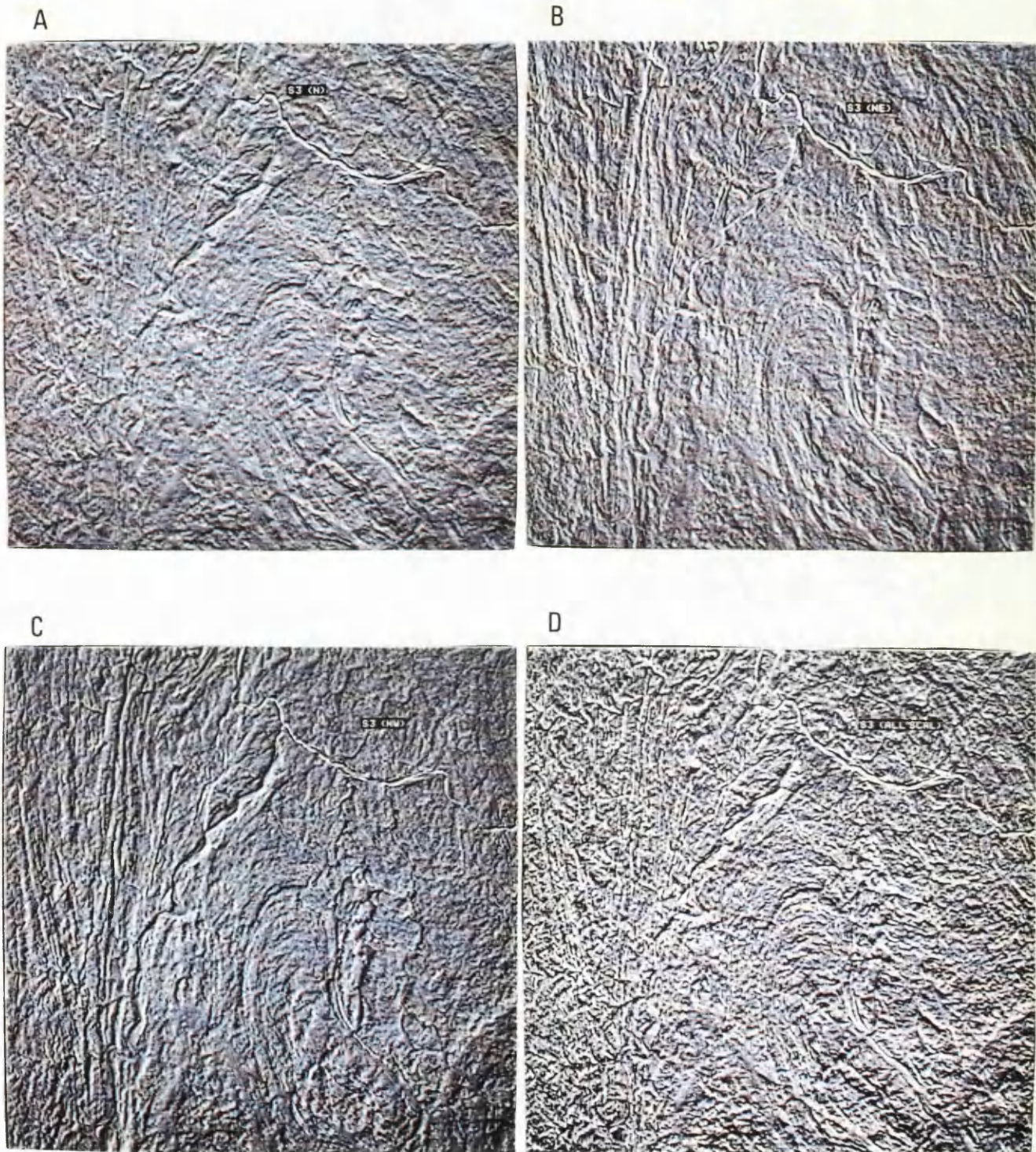
Fig.5.11 Edge enhancement techniques images for the test-site
No.3. A:north directional high-pass filtered image;
B:northeastern directional high-pass filtered image;
C:northwestern directional high-pass filtered image;
D:all these three filtered images added together with
additional scaling.

Fig.5.12 Directionally enhanced image superimposing TM band 5
for the test-site No.3.

0   2.5 km   —— Lineament (mainly joints)

◯ Jabal Duhayyah
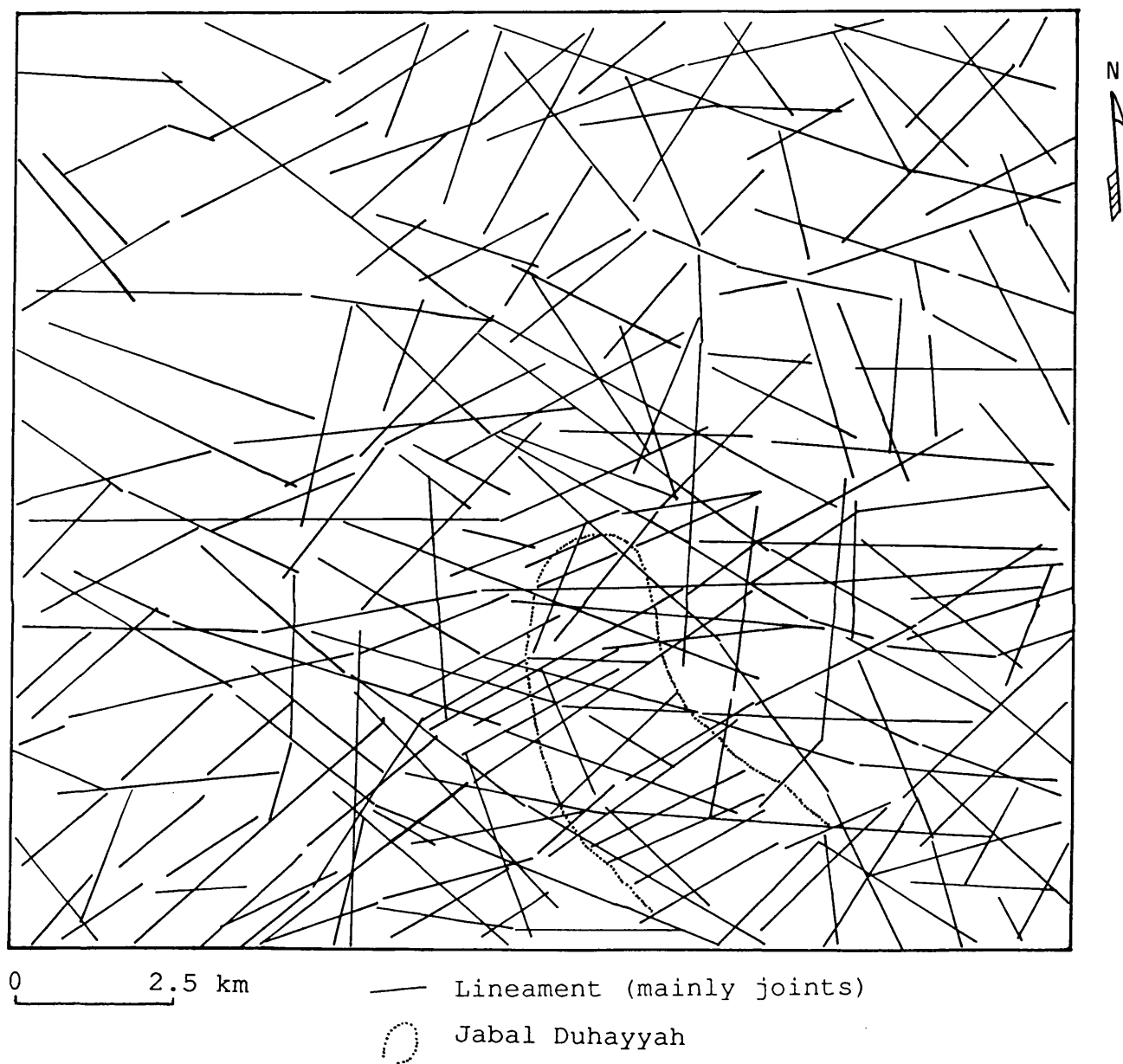
Fig.5.13 Remotely sensed geological fracture map for the
         test-site No.3.
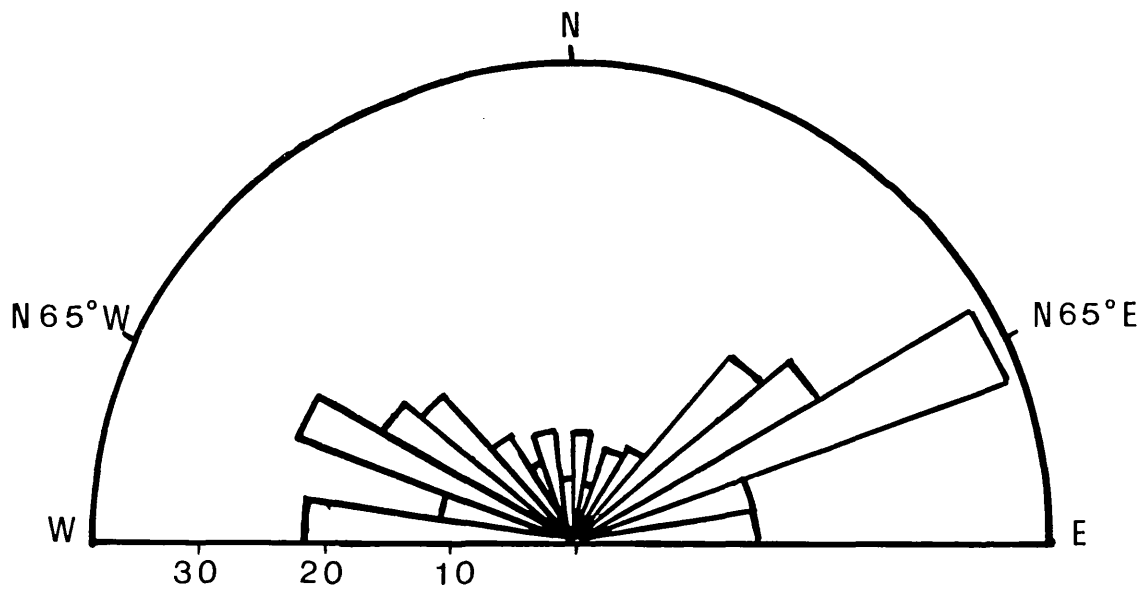
Fig.5.14 Rose diagram summarising strike-frequency distribution
of 264 lineaments in Fig. 5.13.
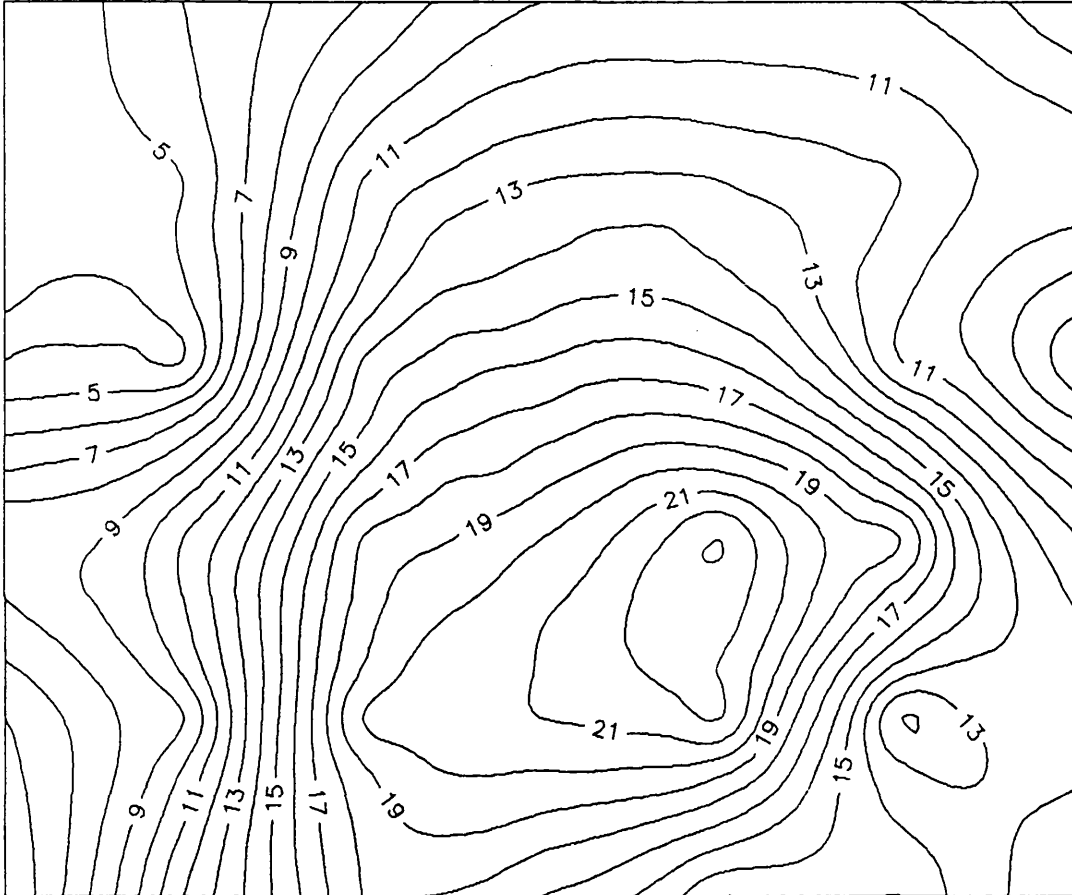
Fig.5.15 Fracture density isopleth map for the test-site
No.3. Fracture density is expressed in number of
fractures/6.25 km^2.

map which corresponds to Jabal Duhayyah area.

An attempt was also made to correlate the observed lineaments and mapped faults, using the compiled map (Fig. 5.2). Many lineaments were found to accord with mapped faults; other lineaments, corresponding to joint sets, have not previously been mapped in any survey.

(c) Conclusion

Landsat TM imagery proved to be useful for revealing lineaments which can be correlated with fractures within the test-site area. The majority of these fractures were revealed for the first time during this TM investigation. The concentration of lineaments is particularly high in the Jabal Duhayyah granitic area.

Quantitative examination of the lineaments showed that the test-site area has one distinct preferential direction (N 65° E), and several broad subsidiary directions: E-W, NE-SW and WNW-ESE.

Although the images produced by edge enhancement techniques were very useful for the study of lineaments, most of the lineaments (about 60%) can be detected on images prepared by other enhancement techniques, particularly the SE2 and SE3 techniques.

CHAPTER SIX GEOLOGICAL CONCLUSIONS

6.1 INTRODUCTION

6.2 THE INFLUENCE OF DESERT VARNISH
 AND WEATHERING

6.3 GEOLOGICAL ADVANCES AS A RESULT
 OF THIS STUDY

6.1 INTRODUCTION

The objective of this chapter is to summarise the results obtained from quantitative remote sensing techniques applied to three test-sites within the southern Arabian Shield in order to determine the extent to which Landsat TM data may be used for lithological and structural studies.

It has been shown in this and other studies that TM data are useful for discriminating different rock types, delineating geological boundaries and studying structures within an area. This is very useful in poorly accessible or inaccessible regions. The synoptic views of the images provided by a satellite, together with the spectral information beyond the visible wavelengths, facilitate geological mapping over such terrain.

In the three test-sites, new and detailed lithological and structural maps were constructed and compared with published maps. As those maps were mostly field/photo-interpretation based, there were parts of them had been mapped by extrapolation of boundaries. Study of the enhanced images, as discussed in Chapters 3, 4 and 5, revealed many more complexities and allowed confident extrapolation of lithologies.

Structural analysis showed that the southern Arabian Shield (including the three test-sites) has been affected by at least three successive phases of deformation. The third phase is the most dominant and widespread.

6.2 THE INFLUENCE OF DESERT VARNISH AND WEATHERING

Rocks of the study area, which is part of the Arabian-Nubian Shield, have been affected by chemical weathering and desert varnishing, which may change spectral signatures. However, vegetation and soil cover that might strongly modulate rock spectral reflectance signatures are absent due to the prevailing arid conditions.

Rock coatings known as desert varnish cover most outcrops in the study area (including the three test-sites). Detailed studies of desert varnish from many arid and semi-arid regions (e.g. Engel and Sharp, 1958) indicate that the coatings are characterised by high concentrations of iron, manganese and magnesium relative to the host rock. Clay minerals with strong hydroxyl-related absorptions are major phases in many desert varnish coatings (Potter and Rossman, 1977).

The only study of desert varnish in the Arabian-Nubian Shield area is that of Sultan et al. (1987). They measured the extent to which the ubiquitous desert varnish obscures the reflectance signatures of underlying rocks in the Meatiq area, Eastern Desert of Egypt (part of the Nubian Shield). They examined thin-sections of coating from each of the major rock types exposed, using transmitted light microscopy and back-scattered electron images. The following textural observations were made:

(1)   rock coatings are generally very thin (0-5 μm), although they may be thicker (up to 50 μm) in local rock surface depressions;

(2)   a sharp contact always separates the coatings from the host rocks;

(3)   coatings are either amorphous or very fine-grained (<1 μm); and

(4)   larger grains (1 to 10 μm) are irregularly distributed in the coatings.

They also determined the extent to which the rock coatings modify the spectral reflectances of fresh rocks by examining bi-directional reflectance measured for powdered and for thickly coated, thinly coated and uncoated surfaces of massive amphibolite and fine-grained granite samples (Fig. 6.1). They found that:

(1)   The broad ferrous-related absorption, near the 1 μm, is not obscured even by the thickest coatings.

(2)   Coated mafic rocks are brighter and have higher spectral contrast as compared to natural uncoated surfaces, whereas coated felsic rocks are generally darker and show lower overall contrast than uncoated surfaces. Thus, thick coatings can obscure differences in overall spectral reflectance and contrast between some uncoated mafic and felsic rocks by increasing the contrast for mafic rocks, but decreasing that of felsic rocks.

(3)   Clay minerals in the coatings strongly absorb in the 2.2-2.35 μm wavelength region and contribute to the hydroxyl-related absorption feature.

One principal conclusion was that the thin discontinuous desert varnish that consists of amorphous to poorly crystalline dioctahedral smectite, iron oxides and/or oxyhydroxides, has a bulk composition independent of the underlying rock type may modify but does not obscure the spectral reflectance of the underlying rocks.

The only other study in the Arabian Peninsula, outside the Arabian Shield, is that of Pontual (1990) who mapped the ophiolitic succession in Oman utilizing Landsat TM
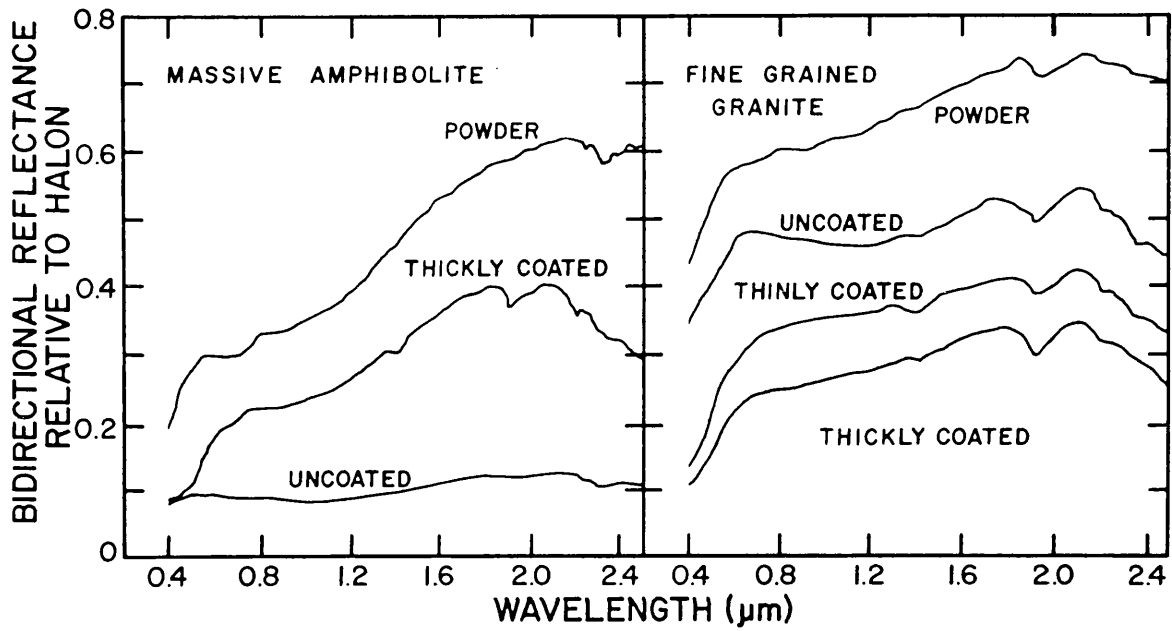
Fig. 6.1 Bi-directional spectral reflectance data relative to
halon for powder, and for thickly coated, thinly
coated and uncoated surfaces from massive amphibolite
and fine-grained granite (after Sultan et al., 1987).

imagery. Pontual noted the 'red-weathered' surfaces which consist entirely of weathered material with a ferric hydroxide impregnation along grain boundaries and fracture surfaces, but observed that the spectra of these surfaces still display characteristic features that are related to the substrate rock mineralogy. The influence of this 'red-weathering' is evident in the visible wavelengths (TM bands 1 to 3) as steep drop-off in reflectance at wavelengths less than 0.75 μm.

Another type of weathering surface that tends to mask the underlying rock spectrum in Oman was named by Pontual as 'dark red-weathering'. The dark red-weathering surfaces are an intimate mixture of patchy varnish coating and a well-developed red-weathering cortex formed from *in situ* weathering of the rock. The effect of this weathering in Oman is to produce spectra with low values in the visible and very near-infrared wavelengths (TM bands 1 to 4) and high values in the near-infrared (TM bands 5 and 7), due to the high reflectance in the near-infrared of the ferric hydroxides in the weathering cortices. Because the 'dark red-weathering' surfaces are developed only in a patchy and discontinuous fashion on rock outcrops, they serve only to modulate the responses of the rock outcrop, hence, the spectral characteristics of the rocks are still apparent. The peridotites display the best developed deep weathering cortices of all the rock types in the Oman and are the most influenced by the effect described (Pontual, 1990).

There are no ophiolitic rocks nor peridotites in the study area. In contrast to the studies of Sultan et al. (1987) and Pontual (1990), neither red-weathering nor dark red-weathering surfaces were observable or detectable in the three test-sites or in the study area as whole. Although desert varnish coatings are thin and discontinuous, they were observed distributed on most rock exposures, particularly the amphibolites and gabbros of the test-site No.1. Area studied by Sultan et al., (1987) is closely comparable in terms of geology and environment to this study area, hence, based on comparision with Sultan et al., (1987) study, it could be concluded that desert varnish does not alter the interpretations reached in this study.

6.3 GEOLOGICAL ADVANCES AS A RESULT OF THIS STUDY

Digital TM data covering the visible and reflected infrared spectrum were evaluated for geological mapping capabilities over three full-resolution test-sites in the arid areas of the Precambrian southern Arabian Shield. The analysis of processed TM data proved

invaluable in the acquisition of new geological information relevant to this study.

In Khamis Mushayt area (test-site No.1), where the geological relationships are well known from previous ground studies (Amlas, 1983; Qari, 1985), geological maps were made using different enhancement techniques. In contrast, in the test-sites No.2 and 3, previous geological maps had been prepared based on photo-interpretation and limited field checking of some localities. In this study, new geological maps were prepared which differed in important aspects from previous maps, based on studies of previous workers, new TM imagery and new fieldwork.

The arithmetical operational spectral enhancement techniques (SE1 and SE2 techniques) were performed on the three test-sites to produce a colour ratio composite. By comparing the results, i.e. rock type identification in different ratioed images, obtainable from these two techniques, it was found that SE2 technique is straightforward, easier to use and interpret and gives the same or better results as the SE1 technique (Table 6.1). Because of the range of colours and their prominency (contrast) using the SE2 technique than using the SE1 technique, this helped in the preparation of the lithological maps (e.g. test-site No.3). The SE2 enhancement techniques resultant colour ratio composite is the ratio of TM bands 7/5,5/4,4/2 in red, green and blue.

Lithological results:

In addition to showing that the TM data contain significant information for visual differentiation, certain interesting geological aspects were identified and geological maps at a scale of $\approx$1:70,000 were reliably created. Geological information of particular value includes the following:

- Comparison of ratioed TM data with field observation shows the following:

  -increasing amounts of Fe-bearing aluminosilicates (e.g. hornblende and amphiboles in general) that absorb in the TM band 4 wavelength region increase the product of the TM ratio band 5 to band 4, and are seen as bright areas in the ratioed images. This allows discrimination of amphibole-rich rocks for example.

  -increasing amounts of Fe-staining minerals (Fe-rich minerals which are Al-poor) that absorb in the TM band 4 wavelength region decrease the product of the TM ratio band 4 to band 2, and are seen as dark areas in the ratioed images. Examples of such minerals are olivine, pyroxene

RATIO IMAGE	SE1 Enhancement Technique			SE2 Enhancement Technique		
	TM bands 5/7	TM bands 5/1	TM bands 5/4x3/4	TM bands 7/5	TM bands 4/2	TM bands 5/4
Reason for preparing Ratio Image	as a measure of the intensity of hydroxyl absorptions	to portray rocks rich in opaque phases	to emphasise and discriminate the Fe-bearing aluminosilicates	as a measure of the intensity of hydroxyl absorptions	for the detection of surface Fe-staining	to emphasise and discriminate the Fe-bearing aluminosilicates
Appearance in the Ratio Image	as moderately bright areas (rich)	as dark areas (rich)	as bright areas (rich)	as moderately dark areas (rich)	as dark areas (rich)	as bright areas (rich)
Rock Types Identified In The Ratio Image						
TEST-SITE No.1	granitoid rocks and metasediments	gabbroic rocks and amphibolites vs. granitoid rocks and metasediments	amphibolites vs. granitoid and gabbroic rocks	granitoid rocks and metasediments	gabbro and amphibolites vs. granitoid rocks generally	amphibolites vs. granitoid and gabbroic rocks
TEST-SITE No.2	granitoid rocks	mafic dyke and basaltic rocks vs. granitoid rocks	layered metamorphic rocks vs. basaltic and granitoid rocks	granitoid rocks vs. basaltic and mafic dyke rocks	basalt, mafic dyke and layered metamorphic rocks vs. granitoid rocks	layered metamorphic rocks vs. basaltic and granitoid rocks
TEST-SITE No.3	granitoid rocks generally vs. metavolcanics	metavolcanics and gabbroic rocks vs. granitoid rocks	amphibolites vs. granitoid rocks	granitoid rocks vs. migmatites	Layered metamorphic rocks, migmatites and gabbroic rocks vs. granitoid rocks	amphibolites vs. granitoid rocks generally

Table 6.1 Comparision of results obtainable from SE1 and SE2 techniques applied on the three test-sites.

and magnetite, which are commonly present in quantity in metagabbros. Thus these rock types can be mapped using this feature.

-increasing amounts of hydroxyl-bearing minerals, such as mica, with hydroxyl-related absorptions in TM band 7 wavelength region, increase the ratio of TM band 5 to band 7. This allows discrimination of the granitoid rocks for example.

-granitoid rocks (e.g. granite, granitic gneiss and granodioritic gneiss) can only be mapped as a group using the TM images because variations in modal minerals contents are too small to permit discrimination. Field information was used for finer subdivisions.

-observation of sediments in the wadis confirms that the TM-based mineralogical inferences used to map crystalline shield rocks can also be applied to mapping alluvial sediments in the same area. For example, alluvium in the wadis in the test-site No.2 is largely derived from the neighbouring As-Sarat basaltic flow, and hence seen as a dark blue colour (e.g. sections A10, C9 and G6, Fig. 4.16B).

• Although the decorrelation stretching enhancement technique used is scene-dependent, it was found to be very useful and yielded the following extra advantages:

-interpretation of the enhanced image is straightforward, as colours can be related to features of the surface materials, such as topography or relief.

-it retains useful topographic information which helped in understanding the fracture distribution within an area.

• A new, detailed lithological map was constructed for the Khamis Mushayt area (test-site No.1), which was compared with detailed ground studies. Comparision showed a good correspondence which saved time and costs. As an example, the M.Sc. field study (Qari, 1985) lasted for two-months in comparision to the TM-based mapping of this study which lasted for a couple of days.

• A new, detailed lithological map was constructed for the composite test-site No.2 (Al-Khabt and Al-Fayd areas). The new geological maps differs in many places from previous maps, and new more precise contacts were established

using TM data, particularly to the north of the test-site and were confirmed by field checking.

• A new, detailed lithological map was constructed for the Jabal Duhayyah area (test-site No.3), where certain interesting geological field relations were identified, these include:

-migmatites were mapped in the Arabian Shield using TM digital data for the first time. Mapping and studying migmatites throughout the shield will contribute to an understanding and appreciation of the metamorphic processes involved in their formation.

-the contact between the Asir Terrane and Nabitah Mobile Belt (two tectonic assemblages) is easily and precisely located using TM digital data. Following the extension of this contact and other contacts within the shield will contribute significantly to improving the tectonic map of the Arabian Shield.

-different rock types were distinguished and hence mapped utilizing TM digital data, some of which were not previously mapped (e.g. quartz monzonite and metagabbro). Field-checking confirmed this. It will be possible to rapidly sample and map these types of plutons at all levels of spatial detail, particularly in remote areas.

• Particular lithologies were shown to have a consistent appearance of colours on colour ratio composites. For example, green and yellow colour combinations in test-sites No.1 and 3 helps in delineating amphibolites. This mean that such lithologies could be reliably identified in different regions even though they were widely separated. Furthermore, the juxtaposition of spectrally contrasting units in the TM images may establish critical field relationships between rock types and structural features present in the scene, even if the lithologies are not known.

Structural results:

Test-site area No.1 had previously been studied on the ground in detail and structural analysis had been carried out (Amlas, 1983; Qari, 1985). However, test-sites No.2 and 3 had previously not been studied in detail and there were no structural studies of these areas. Structural analysis of well exposed outcrops of crystalline bed rock proved to be

possible for the three test-sites using Landsat TM images. Polyphase deformation structures were grouped in generations according to the geometry of the folds, and structural maps were constructed. The following are the conclusions of the structural analysis:

- The sequence of deformational phases recognized is:

  -The first deformational phase, D1 (observed in the test-site No.1) produced isoclinal F1 folds. No large-scale F1 folds were recognized or detected.

  -The second deformational phase, D2 (observed in test-site No.1) produced tight to isoclinal recumbent folds with variable axial directions, which were detected in the Landsat TM data.

  -All rock units and in particular the layered metamorphic rocks exhibit a well developed axial planar foliation which is a strongly developed fabric and easily distinguishable on the TM image. Both S1 and S2 foliations are broadly parallel to lithological contacts and it is not possible to distinguish between them on the TM image or on the ground (Qari, 1985).

  -The third deformational phase (D3) is the dominant phase and responsible for geological structures which are the most prominent and widespread in the three test-sites as well as in the entire study area. The folds of this F3 phase are asymmetrical, tight to open, with steep, generally N-S striking axial planes. Several major antiforms and synforms interpreted as F3 folds in the three test-sites were detected on the Landsat TM images. Linear structures associated with this phase were observed in the three test-sites and throughout the entire study area, observable in the ground as a strong mineral lineation in the schistose rocks.

  -Major folds of the fourth deformational phase (D4) were not easily located using TM data although many minor F4 structures were observed on the ground in test-site area No.1. However, an F4 regional doming pattern was detected in the test-site No.1 using the TM images.

- Many faults, differing in scale and orientation were observed throughout the region and were also easily detectable and extendable on the Landsat TM

images. In particular, faults are very prominent in test-site No.2; mostly are E-W right-lateral strike-slip faults.

- Lineament enhancement was performed on the digital TM image and the

measurements showed that the three test-sites have three principal lineament orientations which can be related to regional tectonics of the Arabian Shield. Most of these lineaments were mapped for the first time during this study. The three principal orientations are (Fig. 6.2):

-An east-west direction. This is conformable with the older east-trending tectonic fabric in the tectonically more complex and possibly older parts of the shield as postulated by Moore (1983).

-A general NW-SE direction. This is part of the Najd fault system which was active in the Arabian Shield at about 530-630 Ma (Moore, 1979), and which also extendeds to the Central Eastern Desert of Egypt (Sultan et al., 1988).

-A general NE-SW direction. This is postulated to be the youngest fault system, possibly representing the extension of transform faults identified in the Red Sea by several geophysical surveys (ARGAS, 1977). An alternative explanation is that this fracture set represents a conjugate set of fractures developed at the same time as the Najd fault system.

Because the first test-site had been studied on the ground in detail, it provided a secure basis on which to compare field geological results with the results obtainable from remote sensing studies. 'Ground truth' has also been checked for the other test-sites. The result of this comparison demonstrates that TM data can be used with reliability for geological applications in the Arabian Shield and comparable areas, particularly to generate detailed geological maps over large areas by using quantitative remote sensing methods, providing there is prior knowledge of part of the area.
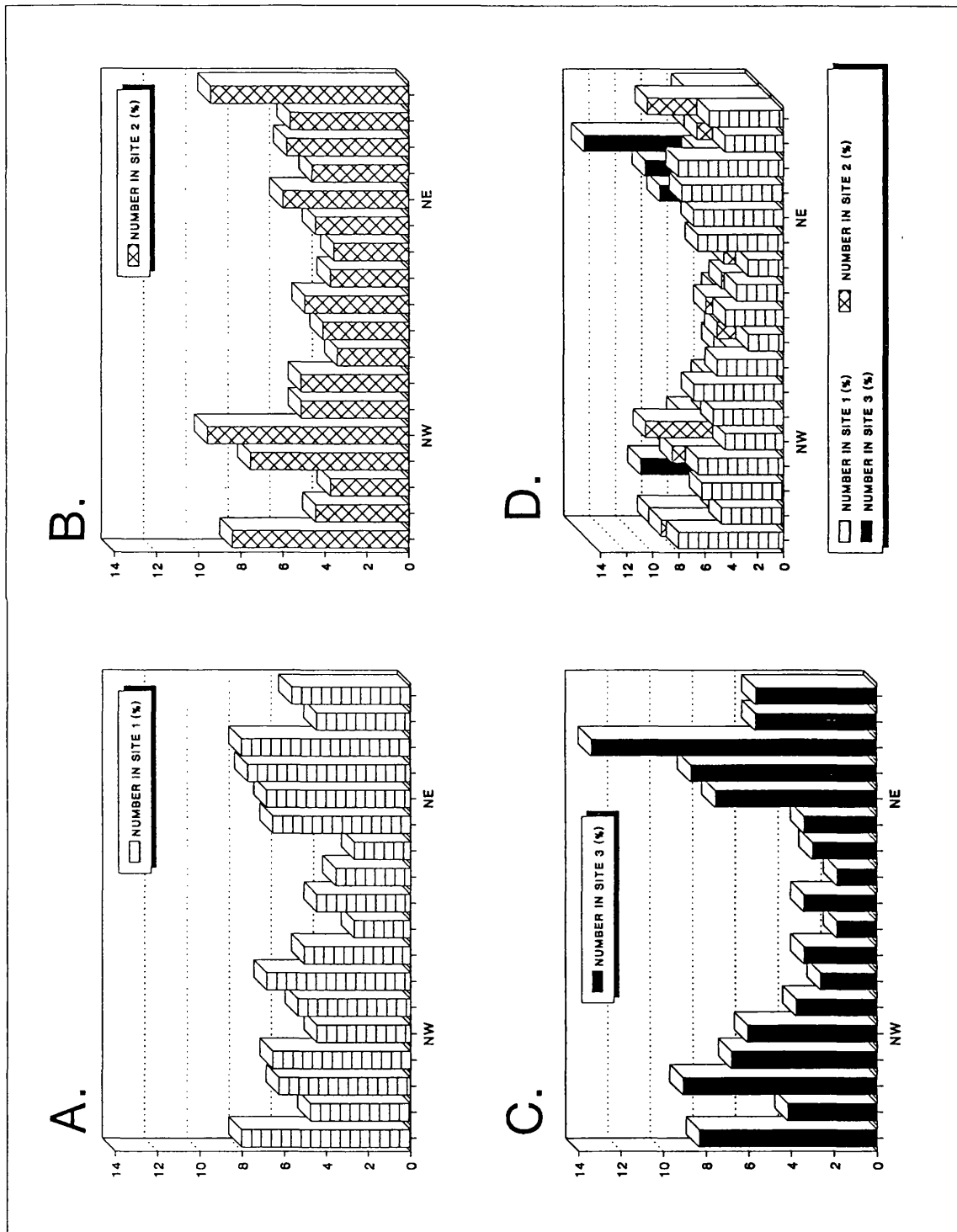
Fig. 6.2 Histograms summarising strike-frequency for lineaments in the three test-sites within the southern Arabian Shield.

CHAPTER SEVEN   REGIONAL GEOLOGICAL VIEW

7.1 INTRODUCTION

7.2 GENERAL GEOLOGY

-Two tectonic assemblages

-Rock types in the study area

7.3 CRUSTAL HISTORY

-Early crustal history

-Late crustal history

-Najd faulting

-Evolution model for the study area

7.4 STRUCTURAL ANALYSIS

7.5 GEOPHYSICAL STUDIES

7.1 INTRODUCTION

In order to provide a context for the geological analysis of parts of the southern Arabian Shield based on the Landsat TM imagery (Chapters 3, 4 and 5) it is necessary to review the geology of the region. Because the study area comprises about one-third of the Late Proterozoic southern Arabian Shield, an understanding of the study area will help to decipher the geology and evolution of the Arabian Shield as whole.

The geological setting is presented first, followed by an account of the crustal history of the shield together with a structural analysis and account of geophysical studies in order to relate this area to neighbouring areas.

7.2 GENERAL GEOLOGY

The study area is located within two tectonic assemblages which are the Asir Terrane to the west and the Nabitah Mobile Belt to the east, and has excellent exposures of a diverse suite of different rocks belonging to different stratigraphic units.

Two tectonic assemblages:

The Asir Terrane (in the study area) includes at least two generations of arc magmatism (Stoeser and Camp, 1985). The older arc assemblage consists predominantly of north-striking belts of intercalated low-potassium tholeiitic basalt and greywacke (Baish, Bahah and Jiddah Groups) (Chapter 1, section 1.5) and dioritic to tonalitic plutonic rocks which formed between 950 to 800 Ma (Bokhari and Kramers, 1981; Fleck et al., 1980). Magmatism of the older island-arc assemblage appears to have terminated about 800 Ma and was followed by orogenesis and synorogenic plutonism from 780-760 Ma (Fleck et al., 1980; Greenwood et al., 1976). Subsequently, the Tarib arc system developed along the margins of the older arc terrane. It is not known if the younger arc assemblage was accreted to, or superimposed upon, the older assemblage. This Tarib arc assemblage, along the terrane's eastern margin, consists of basic to intermediate volcanic and volcaniclastic rocks which were intruded by diorite to tonalite plutons between 760 to 725 Ma (Fleck et al., 1980; Stoeser et al., 1984). The Tarib arc is informally named after the Wadi Tarib batholith, one of the major plutonic complexes of the arc assemblage (Stoeser et al., 1984).

The Nabitah Orogenic/Mobile Belt defines a 100 to 200 km wide zone of crustal

deformation, remobilization and plutonism along the margins of the Asir, Hijaz and Afif terranes (Fig. 1.7). The belt consists of broad, linear complexes of synorogenic, unfoliated to gneissic, granitoid plutonic rocks, separated by regions of middle greenschist- to amphibolite-grade metamorphic rocks (Stoeser et al., 1984). The southern and central parts of the belt contains a north-trending linear belt of ultrabasic and basic rocks (Fig. 1.7), interpreted by Frish and Al-Shanti (1977) as ophiolitic complexes along a suture zone between two juxtaposed arcs. Schmidt et al. (1979) supported this interpretation and referred to this zone as the "Nabitah Suture" (Fig. 1.7).

Stoeser et al. (1984) defined the Nabitah Mobile Belt and interpreted the suture zone and belt as marking the site of collision between the Afif Terrane to the east and the western arc terranes. They showed by U/Pb zircon dating that the synorogenic plutonism within the southern part of the orogenic belt occurred between 680 and 640 Ma. The western part of the belt developed within the western arc terranes and incorporates much of the Tarib arc assemblage of the Asir Terrane in the study area. Similarly, the eastern part of the belt is superimposed over the continental margin of the Afif Terrane (outside study area)(Stoeser and Camp, 1985).

Rock types in the study area:

In the study area, the rocks of the shield can be subdivided into two main assemblages: (1) metasedimentary and metavolcanic layered rocks and (2) plutonic rocks. In addition to these two main assemblages, the Nabitah Suture Zone's ultrabasic rocks and the Wajid Sandstone are exposed mostly in the northeastern part of the area. Tertiary basalt flows are exposed in the middle of the southernmost part of the study area (Plate 2).

The metamorphic layered rocks of the study area (Bahah, Jiddah and Halaban Groups) (Plate 2) consist primarily of basic to intermediate metavolcanic rocks and clastic metasedimentary rocks, and they are thought to predate all of the plutonic rocks (Greenwood, 1980; 1985c).

Brown et al. (1989) classified the plutonic rocks of the study area into pre-, syn- and post-tectonic suites, the last of which includes an early layered gabbroic phase. The major orogeny associated with the late crustal history is called the "culminant orogeny" which began slightly before 650 Ma and extended to about 620 Ma (Brown et al., 1989). The classification of the plutonic rocks was in reference to the culminant

orogeny during which most of the rocks of the early crust were intensely tectonized during the cratonization of the shield (see section 7.3). They also divided the Precambrian plutonic rocks of the study area into two groups, which are the dioritic and the granitic suites. The pre-tectonic dioritic suite consists, in order of decreasing abundance, of diorite, quartz diorite, tonalite, trondhjemite and gabbro. These rocks are commonly medium grained with hypidiomorphic granular textures. Many of the low-density, more silicic rocks of this suite, such as the trondhjemites and some tonalites, are found in large gneiss domes or antiforms, where they have been metamorphosed to amphibolite facies, conspicuously shear foliated and converted to orthogneisses. These gneiss domes rose gravitionally in response to heating and tectonic thickening during the culminant orogeny. These orthogneisses are tectonically associated with migmatitic and plutonic rocks of the granitic suite.

The syn- and post-tectonic granitic suite consists, in order of decreasing abundance, of granodiorite, granite, alkali-feldspar granite and peraluminous-peralkalic granite as well as gabbro. Most of these rocks were emplaced during cratonization after about 675 Ma. Many granitic rocks are slightly to extensively tectonized and partly metamorphosed through pervasive cataclastic shear and are classified as syn-tectonic; these were intruded during the culminant orogeny. Other granitic rocks were intruded in a post-tectonic setting in the interval following the culminant orogeny until about the end of the Precambrian. The syn-tectonic granitic rocks commonly form large batholiths of predominantly biotite granodiorite composition and are typically associated with the large gneiss domes of tonalitic and trondhjemitic orthogneiss. The batholithic granodiorite is mostly conspicuously flow foliated as well as cataclastically sheared in response to late orogenic processes (Brown et al., 1989).

Early in the post-tectonic setting, biotite granite (monzogranite and syenogranite) was intruded as large, irregularly shaped plutons. Presumably with increasing depth of erosion and the resultant ease of brittle fracture at shallow crustal levels, circular plutons of biotite-perthite granite, from a few kilometres across to as much as 10 km in diameter, were emplaced somewhat later, at about 600 Ma. Many of these have a ring structure where they intruded a preexisting structure, or perhaps where some late orogenic forces controlled their emplacement (Brown et al., 1989). In addition, circular layered plutons of gabbro, commonly leucocratic and from a few kilometres to 10 km in diameter, are conspicuous throughout the study area. These gabbroic rocks are late and nonmetamorphosed, and in a few places they can be seen to cut late granite

plutons.

The Wajid Sandstone covers the southeastern edge of the whole Arabian Shield, but occupies only a small parts of the study area. Flat-lying or gently arched, unmetamorphosed, and broken only by Tertiary and Quaternary high-angle tension faults, and until recently considered devoid of fossils, the Wajid Sandstone was assigned only a pre-Permian and post-shield age. A Cambrian-Ordovician age for the Wajid Sandstone was first proposed by Hemer (1968), who found algal forms in well cuttings similar to those described from the lower Palaeozoic in the Russian Baltic region. The lithology of the Wajid Sandstone also suggests such an age is reasonable. The bulk of the sandstone is composed of mature grains and pebbles of quartz and displays large-scale planar crossbedding.

The Jabal As-Sarat, the southernmost Harrat (lava field) extends to the Yemen border. Jabal As-Sarat appears to be a northern remnant of the lower portion of the Yemen Volcanics (Trap Series), with ages from 30.1 ±1 Ma in the lowermost flow to 25.3 ±0.5 Ma in the uppermost flow. Ages from the Yemen Trap Series (29.7 ±0.9 to 20.8 ±1 Ma) and the Northern Ethiopian Plateau volcanics at Adigrat (30 ±0.7 to 19.4 ±0.6 Ma) all range in age from late Oligocene to early Miocene. The As-Sarat flows are picritic basalt at the base and grade up to alkali-olivine basalts and to hawaiite. The 17 to 20 flows of Jabal As-Sarat total 580m in thickness (Coleman et al., 1977), which is considerably less than half the maximum thickness of the Yemen Volcanics. Isolated feeder pipes of basalt crop out as far as 20 km east of the basaltic fields. A deeply weathered lateritic profile representing a post-Mesozoic erosion interval underlies the As-Sarat basalt (Overstreet et al., 1977). Of varying thicknesses ranging from a few centimetres to more than 50m, but mostly 20 to 30m. The profiles are typical of those developed under tropical conditions.

7.3 CRUSTAL HISTORY

The evolutionary history of the Precambrian Arabian Shield must be evaluated across a structural width of more than 1000 km, or a total of more than 1500 km if the Nubian Shield of Egypt and Sudan is included. Across these widths, the crustal rocks of the Arabian Shield and the Nubian Shield are grossly similar in petrology, chemistry, structure and age. Across both shields, the crustal rocks were made and cratonized in about 450 Ma, between about 1,000 Ma and about 550 Ma (Brown et al., 1989).

No continental crust older than about 1 Ga has been reported in the Arabian Shield despite a concerted effort to find "old" continental crustal rocks. In the easternmost part of the shield (outside the study area), a 2,100 Ma old continental crust may be nearby, as recent lead-isotope studies indicate that some of the youthful Precambrian granitoid rocks there contain old leads (Stacey et al., 1981). However, the original emplacement in early Proterozoic time is now established at about 1,630 Ma, with subsequent metamorphism or remobilization at about 660 Ma (Stacey and Hedge, 1984).

Early crustal history:

The early (primary) crust of the Saudi Arabian Shield is a composite of several intraoceanic island arcs and subordinate remnants of oceanic crust (ophiolites). These primary constructional blocks have been combined at different times in different places during several subduction and collisional events from after 900 to about 650 Ma (Fleck et al., 1980; Greenwood et al., 1976; Stacey et al., 1981). Throughout most parts of the shield, compressional structures are consistently north-trending, and it is presumed that the original island arcs trended generally northward and that subduction may have been both westward and eastward under different arcs at different times.

The early (primary) crust consists predominantly of an andesitic assemblage of metavolcanics and metasedimentary rocks and comagmatic plutonic equivalents of the diorite suite. These primary crustal rocks have been well dated in the southern part of the shield (study area) at between about 900 and 700 Ma (Fleck et al., 1980).

In the southern part of the shield, several widely spaced gneiss domes of tonalitic-trondhjemitic orthogneisses are indicative of crustal heating, tectonism, metamorphism and the gravitational rise of less dense plutonic parts of the primary crusts. Syntectonic intrusion of granodioritic batholiths accompanied the rise of orthogneisses (Brown et al., 1989).

Late crustal history:

The late crustal history of the Arabian Shield began sometime after 700 Ma and involved the final combining, consolidation and cratonization of the shield as a whole. The major orogeny associated with this late crustal history is called the "culminant orogeny" which began slightly before 650 Ma and extended to about 620 Ma (Brown et al., 1989). It was the ultimate orogeny involved in the cratonization of the entire

shield. This late crustal history is characterized by many gneiss domes (antiforms), granodioritic batholiths and granitic plutons. During this orogeny, widespread crustal heating caused amphibolite-facies metamorphism in the primary crustal rocks. Under these conditions, large, low-density bodies of trondhjemite and tonalite became gravitionally unstable adjacent to denser rocks, and they rose as orthogneisses in elongated gneiss domes along north-trending axes.

The culminant orogeny (collisional orogeny) resulted in the final combining of the various constructional blocks of the primary crust and in the final tectonic thickening of the combined crust, such that potassic granitic magma was produced in the lower crust and was intruded mostly in circular or elliptical plutons with their principal axis oriented northward parallel to the old structural grain at shallow crustal levels in both syntectonic and posttectonic settings (Brown et al., 1989).

Tectonic remnants of ultrabasic rocks and serpentinite, gabbro, sheeted dyke complexes, tholeiitic metabasaltic rocks and ocean-floor metasedimentary rocks occur in varying combinations in many places in the shield. Many of these have been described as tectonized and deeply eroded ophiolites of either oceanic or back-arc crustal origin (Pallister et al., 1987). Most of the exposed ophiolites of the shield are small remnants because erosion has been deep. The deeply eroded serpentinite belt of Nabitah Suture (within Nabitah Orogenic/Mobile Belt in the study area) is the only remaining component of the former oceanic crust (Frish and Al-Shanti, 1977) in the study area.

Najd faulting:

The Najd faulting was the final tectonic event in the Arabian Shield. East-west compressional forces acted to fracture the cratonized shield along a few great shears. A northwest-trending, left-lateral, transcurrent fault system (Moore, 1979) prevailed over the conjugate northeast-trending right-lateral transcurrent fracturing. Although the shield was displaced sinistrally, mostly along three major northwest-trending fault zones (outside the study area), the effects of the Najd stresses can be found throughout the shield.

Evolution model for the study area:

Based on the geological conclusions presented in Chapter 6 and review of various regional studies (e.g. Stacey and Agar, 1985; Stoeser and Camp, 1985; Stoeser et al., 1984), a Proterozoic crustal evolutionary model in the vicinity of the study area

(c. southern Arabian Shield) is presented (Fig. 7.1). Four principal stages are recognized, these are:

1. Arc Stage (>≈700 Ma)

   The bulk of Asir terrane appears to be an ensimatic arc (Fig. 7.1A) composed of older and younger arcs. The subduction of oceanic lithosphere, volcanism and syn-tectonic pluton emplacement were all approximately contemporaneous and related to arc formation.

2. Accretion Stage (≈700-670 Ma)

   Then followed an accretion or pre-collision stage, during which the Asir and Afif terranes began to suture together (Fig. 7.1B).

3. Collision Stage (<≈670 Ma)

   Continuing from the previous stage, the island-arc Asir terrane completed collision with the Afif continental terrane and the Nabitah Orogenic/Mobile Belt started to appear (Fig. 7.1C). This east-west compressional collision is interpreted as the cause of the second-phase of deformation (D2) which has affected the entire southern Arabian Shield and produced the strong obvious foliation (S2) generally striking in a north-south direction.

4. Post-collision Stage

   After an intense collisional stage, remobilization, intrusion emplacement, folding and faulting successively affected the study area. This stage is interpreted as responsible for structures of the third phase of deformation (D3) which is the most dominant deformational phase observed throughout the study area.

7.4 STRUCTURAL ANALYSIS

Rock units, particularly the layered metamorphic rocks throughout the study area were affected by at least three phases of deformation D1, D2 and D3, which produced F1, F2 and F3 folds, S1, S2 and S3 foliations, and L1, L2 and L3 lineations, respectively. These three generations are distinguished from each other on the basis of their character, orientation and relationship to one another at various scales.

Based on the detailed geological ground studies conducted on the test-site No.1 (Amlas,

C **Collision Stage**

Nabitah Orogenic Belt

ASIR TERRANE

AFIF TERRANE

Nabitah Suture

B **Accretion Stage**

sea level

ASIR TERRANE

AFIF TERRANE

A **Arc Stage**

YOUNGER ARC

sea level

OLDER ARC

AFIF TERRANE

Oceanic crust in A and B, and ophiolitic complex in C.
Fore-arc, trough and shelf sediments.
Crust of continental affinity.
Deformed crust and sediments.
Deformed crust.
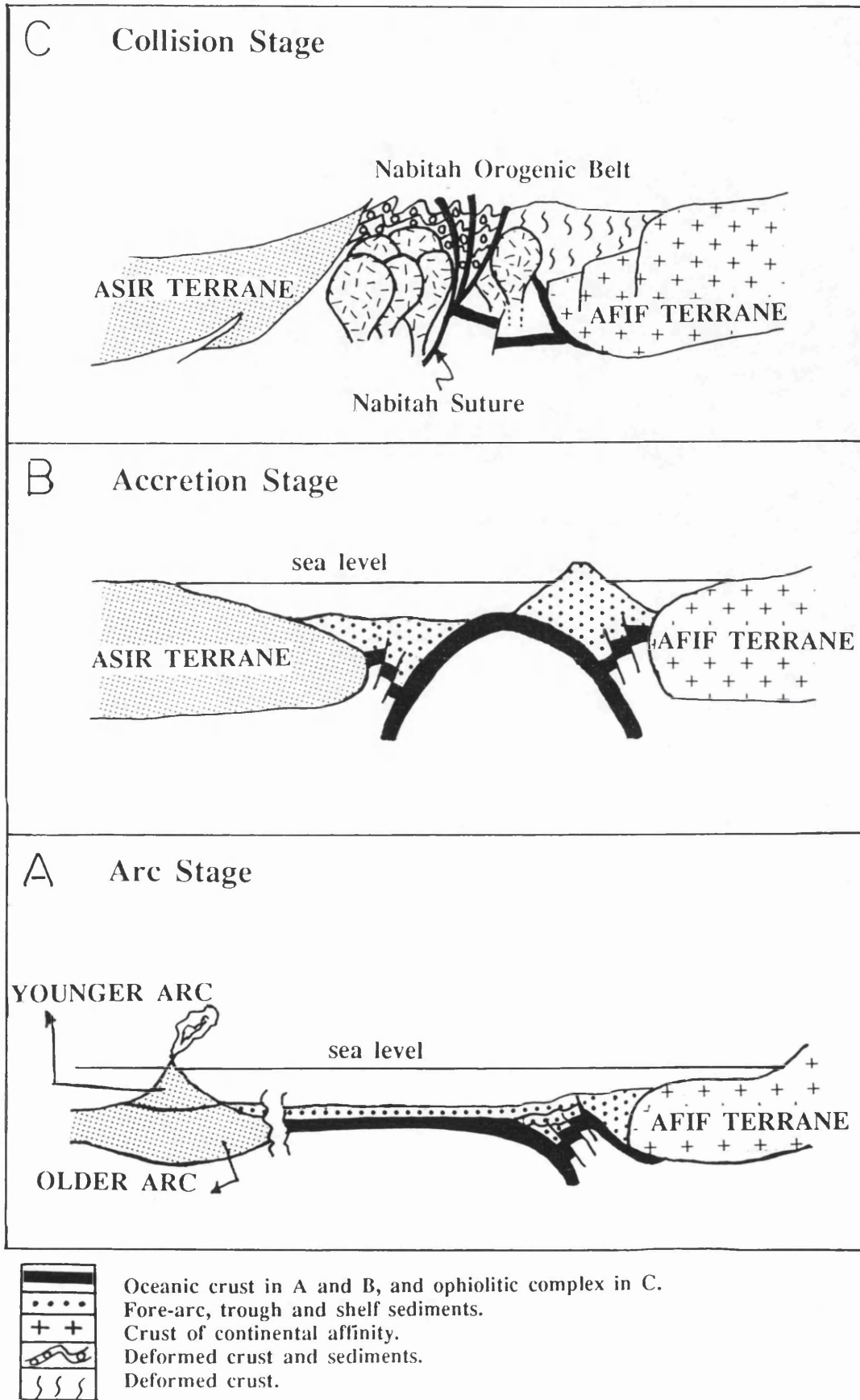
Fig. 7.1 Schematic west-east cartoon-sections tracing the
Proterozoic crustal evolution of the study area.

1983; Qari, 1985, Chapter 3) and during this study of all three test-sites, it can be said that all Precambrian rock units exhibit a well developed S2 foliation, while D1 structures are found locally in metasedimentary rocks in the form of small-scale isoclinal intrafolial folds (Qari, 1985). F2 folds are tight to isoclinal, nearly recumbent and asymmetrical, with variably oriented axial planes (Amlas, 1983; Qari, 1985). D3 structures are the most dominant and widespread throughout the test-site area No.1 as well as the entire study area. F3 folds were found at meso- and macro-scales in the form of open to tight asymmetrical folds with steep, approximately N-S striking, axial planes. Plunges of these F3 fold axes are either approximately towards the north or south, as in the case of the strong and distinctive L3 lineation. Analyses of some of these structures were made during this study.

In the study area (Plate 2), the metamorphic rocks of the Asir Terrane exhibit north-trending, fault-bounded, folded structures. These fold complexes are wide and can be traced parallel to strike for long distances. Geological cross sections shown on previously published 1:100,000 maps commonly represent synclinal structures as being asymmetric and having one limb either partly or wholly eliminated by reverse strike-oblique slip movement on one or both of the high-angle boundary faults (Moore, 1983).

The folded structures of the Asir Terrane and of the three test-sites are interpreted as the F3 phase of folding. In addition, the main wadis in the study area (Plate 1), e.g. Wadi Bishah, Wadi Al Qa'ah, Wadi Tarib, Wadi Al Arin and Wadi Tathlith, have courses running approximately in a N-S direction, which is in fact a zone of weakness resulting from the deformation of the study area, and hence related to the D3 phase of deformation.

There has been no systematic study of faulting in the study area, although faults were identified on published 1:100,000 maps. These faults are products of numerous orogenic and tectonic events that occurred during the long geological evolution of the region. Faulting is well displayed in the study area (Plate 2). There are three principal concentrations of fault orientation, these are north, northwest and northeast. East-west faulting is mainly observed in the southern half of the study area, particularly near to the southeastern corner where the test-site area No.2 is located. Some of these faults can be traced for long distances, particularly within the Asir Terrane (to the west of the study area). These faults are in positions where lineaments interpreted by the edge enhancement techniques have been detected.

The S2 foliation, which is the axial planar schistosity, dominates most rock units in the study area. It is a strongly developed fabric and easily distinguishable as a schistosity or fracture cleavage. Because this foliation is almost parallel to S1 foliation, it is not possible to distinguish between them on the ground (Qari, 1985). The S2 foliation generally strikes north-south and dips towards the east or the west (Fig. 7.2A). These S2 foliations are folded around the hinges of later F3 folds.

Linear structures associated with the F3 generation of folds are pronounced throughout the test-site area No.1 (Amlas, 1983 and Qari, 1985) and also throughout the entire study area within the southern Arabian Shield. These linear structures are defined dominantly by strong mineral lineations trending towards north or south generally with low to moderate plunges (Fig. 7.2B).

The character of the L3 lineation varies. It includes such features as oriented elongate minerals or elongate domains of mineral grains, intersections of S-surfaces, axes of crenulations, mullions and quartz and feldspar rodding. This L3 lineation is parallel to the axes of the F3 folds.

In the test-site area No.1, the lineation associated with the F3 folding is certainly folded around the E-W hinge of regional folds assigned to F4 (Qari, 1985).

7.5 GEOPHYSICAL STUDIES

The southern Arabian Shield is covered by different gravity and magnetic surveys, and a variety of anomaly maps have been produced (e.g. Blank et al., 1980; Gettings, 1983).

Gettings et al. (1986) interpreted the trends of the gravity anomaly map to fall into four distinct directional sets: east, north, northeast and northwest (Fig. 7.3). The ranges of each trend set are fairly narrowly defined, especially for the east and north sets. The north and east sets seem to be the oldest, as they are systematically interrupted or offset by the northeast and northwest trending sets. They interpreted the northwest set to be associated with the late Precambrian Najd tectonic event because of their direction and their coincidence with mapped Najd faults. The northeast set of trends is presumably the signature of a conjugate set of fractures developed at the same time.
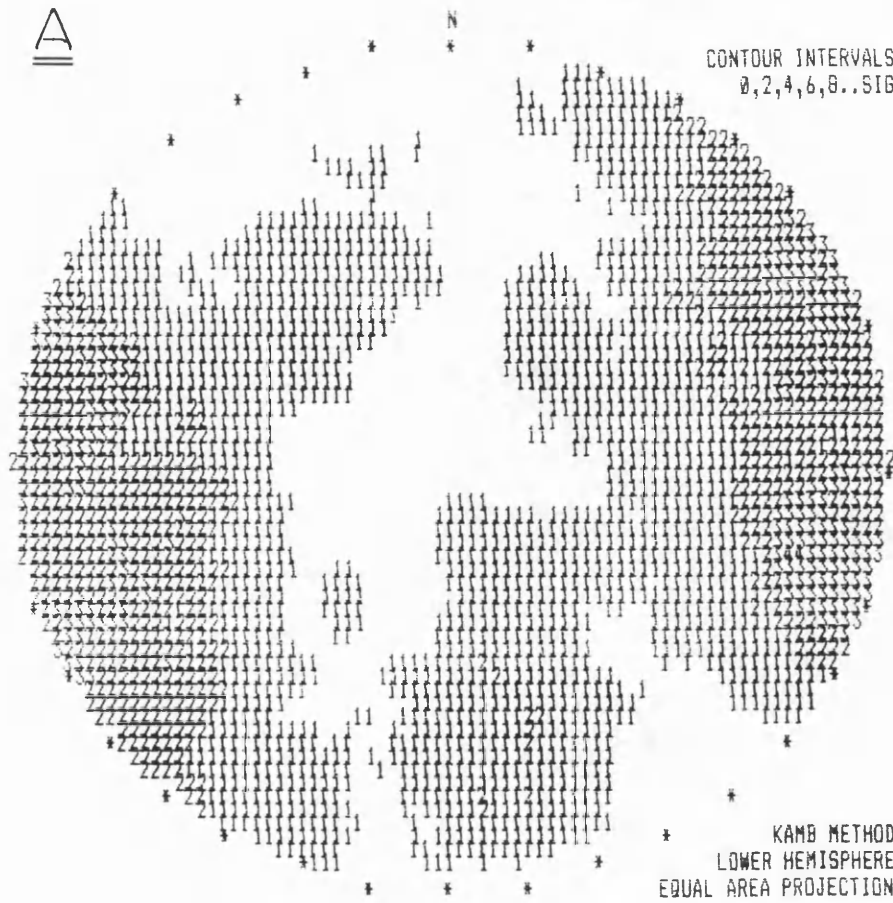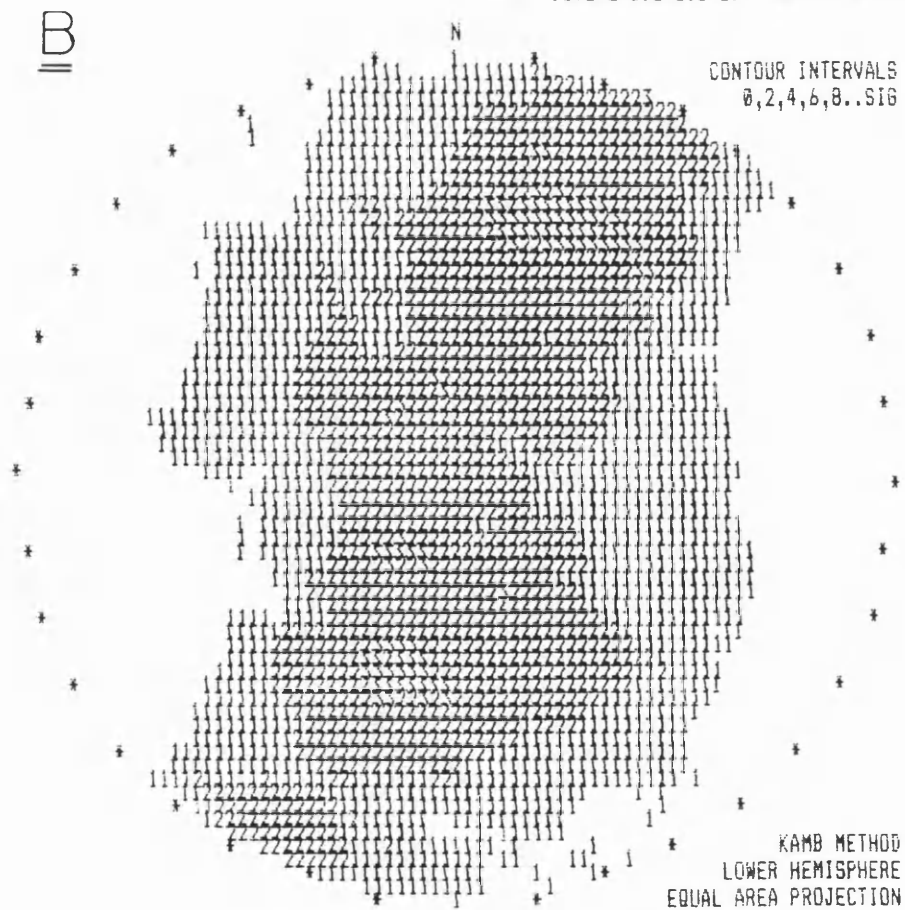
Fig. 7.2 A:Contour diagram for 126 poles to S2 foliation
in the study area; B:Contour diagram for 89 L3
lineations in the study area. See Appendix A for
the preparation of diagrams.
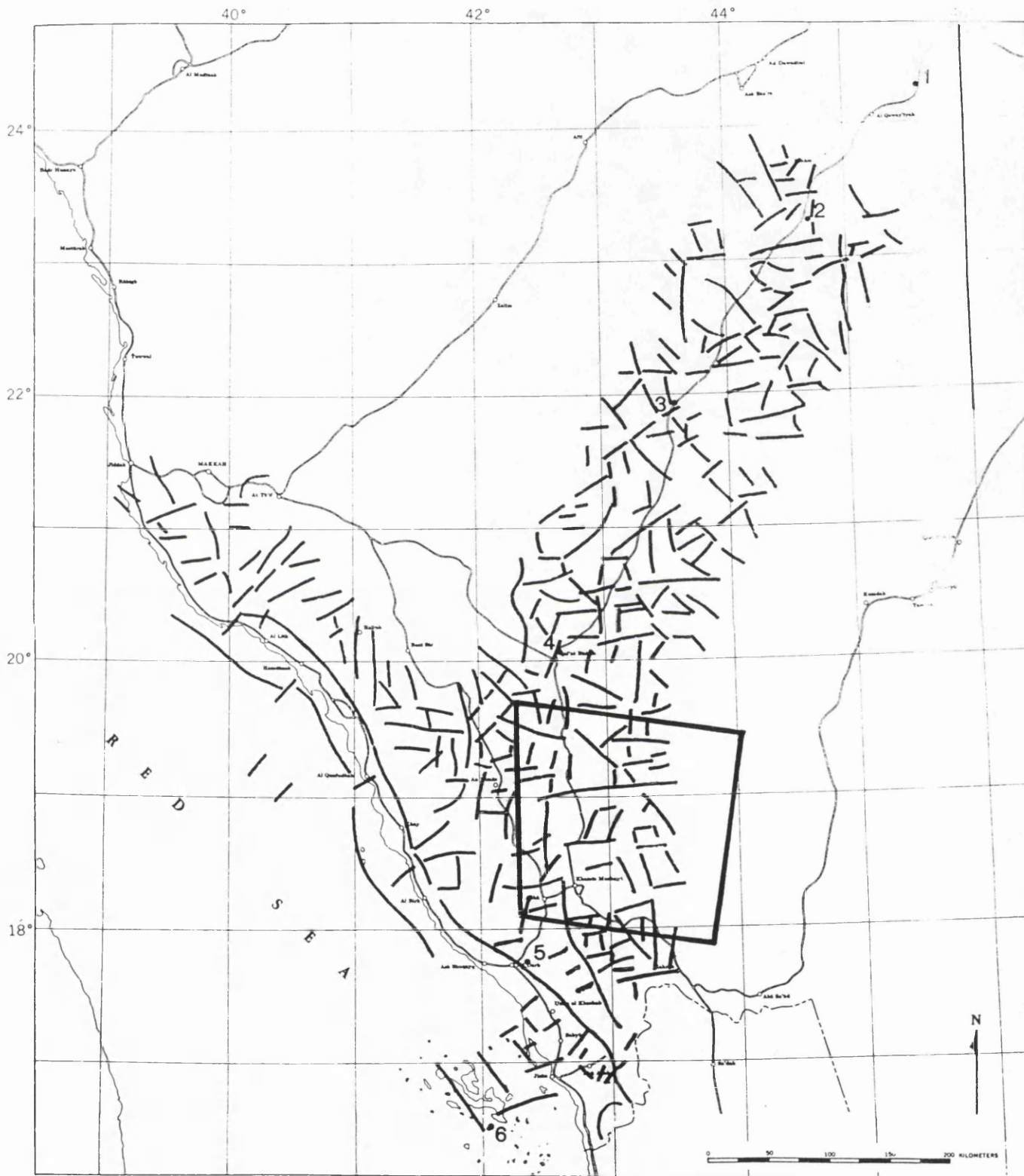
Fig. 7.3 Trend lines interpreted from the Bouguer gravity
anomaly map (after Gettings et al., 1986).

The age relationship between the east and north trend sets in unclear. Both interrupt and sometimes apparently offset each other. The east set has the least expression in the mapped geology and thus may reflect deeper crustal structure. The outcrop patterns of the large batholitic complexes appear to be influenced by both sets and thus these trends may reflect deep seated old fracture systems (Gettings et al., 1986).

Trends in the aeromagnetic map (Fig. 7.4) fall into the same four groups as in the gravity anomaly map and generally correlate well with them, although many more trend lines can be defined here because of the much higher data density and consequent increase in detail of the map. As on the gravity map, northeast and northwest trend sets on the aeromagnetic map appear to be the youngest and north and east sets seem to be the oldest. In addition, curvilinear trends appear in the southern half of the map (Fig. 7.4) which define roughly circular zones 50-100 km in diameter, and these generally correlate with the exposures of large granitic batholitic complexes (Gettings et al., 1986).

Significant trends on the aeromagnetic anomaly map are shown on a directional frequency rose diagram with a 10 degree azimuth class interval (Fig. 7.5), where there are four groups; these are E-W, N-S, NE-SW and NW-SE. Comparison of this diagram with the trends of lineaments for the whole study area shown on Figure 8.7B, indicates that the diagrams are very similar. This means that the lineament trends identified both from satellite imagery and aeromagnetic anomaly map, are probably of similar origin and correspond to important structural features identifiable on the ground.

Moore (1983) prepared a compilation based on satellite imagery interpretation of the tectonic fabric and structural control of mineralization in the southern Arabian Shield, where he demonstrated the magnetic structure of the southern Arabian Shield which is characterized by pervasive east-trending sets of magnetic features that are cut by north-northeast-trending belts of low magnetic relief that correspond to geologically well defined volcano-sedimentary belts (i.e. Asir Terrane of this study). He also defined several groups of linear features from his aeromagnetic interpretation, these are:

1- North-northwest to northwest trend in the Red Sea coastal strip (outside this study area).

2- Northwest trend which are faults of the Najd fault system (outside this study area).

3- North to north-northeast trend which are boundary faults of Proterozoic
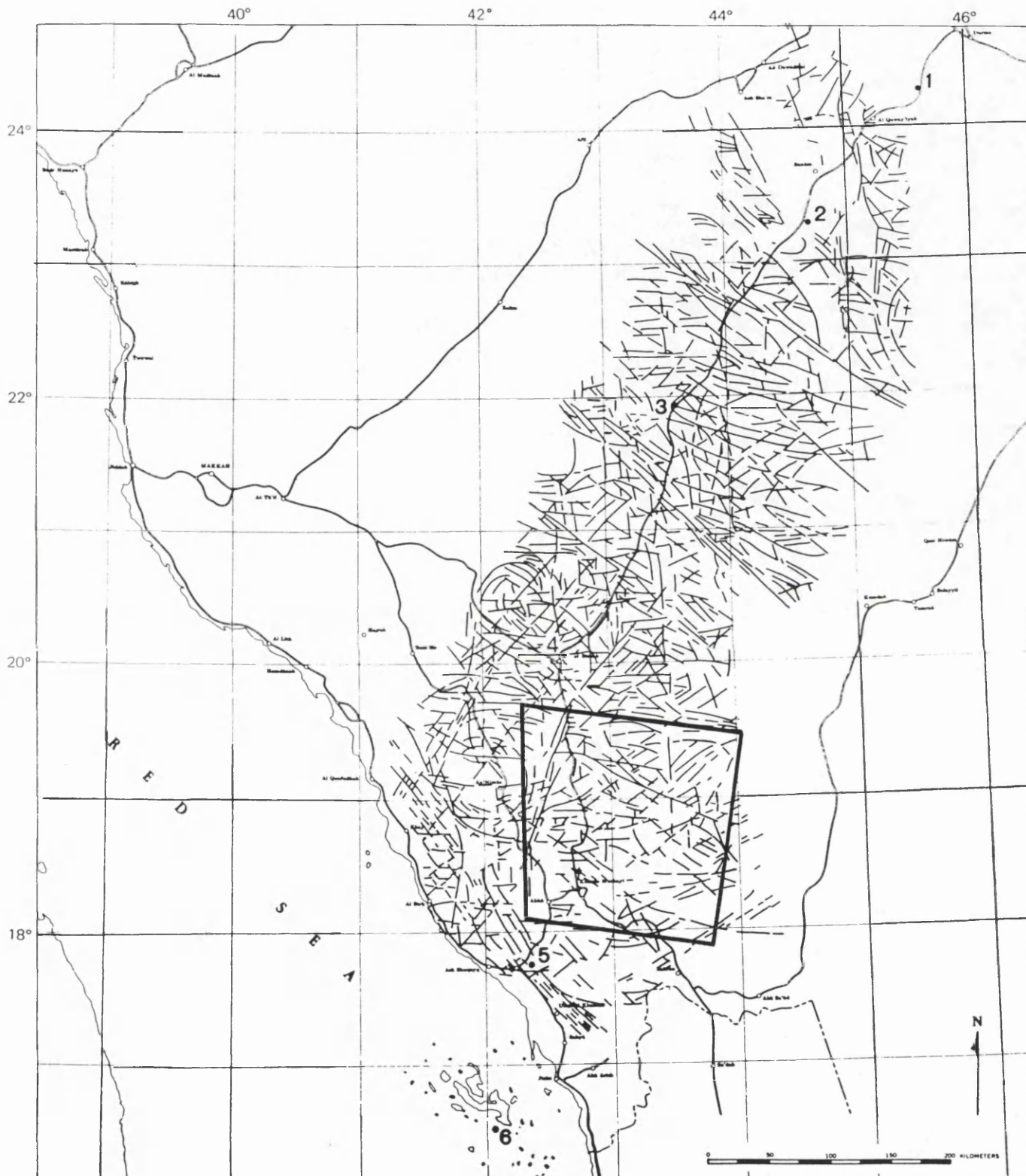
Fig. 7.4 Trend lines interpreted from the aeromagnetic map
(after Gettings et al., 1986).
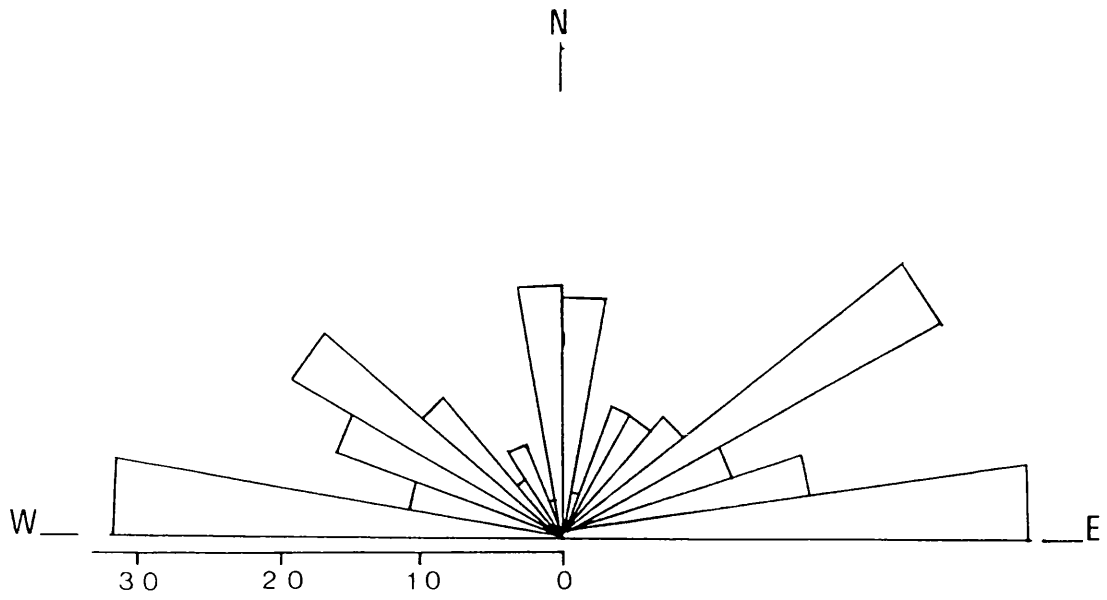
Fig. 7.5 Rose diagram summarising strike-frequency
distribution of 272 aeromagnetic lineaments
in Fig. 7.4.

volcano-sedimentary belts and serpentine belts.

4- Northeast-trending arrays of magnetic features which are discontinuous fault arrays of various ages that truncate or traverse older structures.

These linear features demonstrate, in simplified form, all the major fault groups. The northeast-trending structures are perhaps the most enigmatic (Moore, 1983).

Moore (1983) also postulated an older east-west trending tectonic fabric in the tectonically more complex and possibly older parts of the shield and proposed a structural interpretation model of the southern Arabian Shield (Fig. 7.6).

Study of the lineaments (Chapter 8) and aeromagnetic anomaly trends supports Moore's identification of E-W trending structures. Hence, the southern Arabian Shield has been affected by the following events:

1- E-W structural trend,

2- N-S trend which resulted from E-W compression,

3- NW-SE trend resulted from the Najd faulting system,

4- NE-SW trend, presumably the signature of a conjugate set of fractures, developed at the same time as the Najd system.

Younger north-trending volcano-sedimentary belts (synclines)

East-trending greenschist and amphibolite synclines

Plutonic terrain containing relics of high-grade metamorphic rocks (circled symbols)
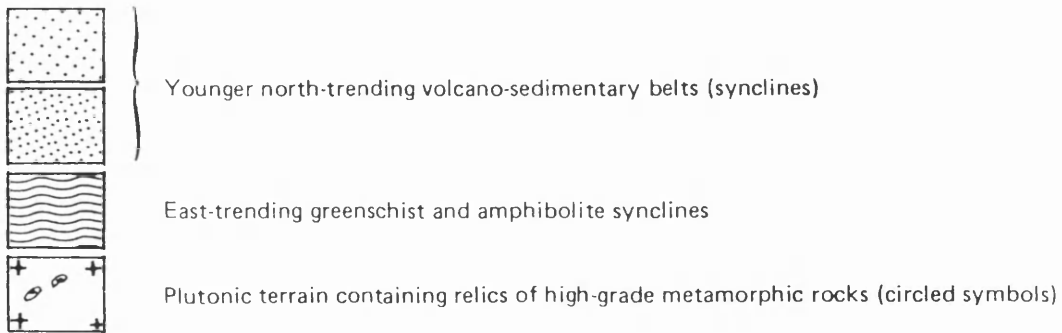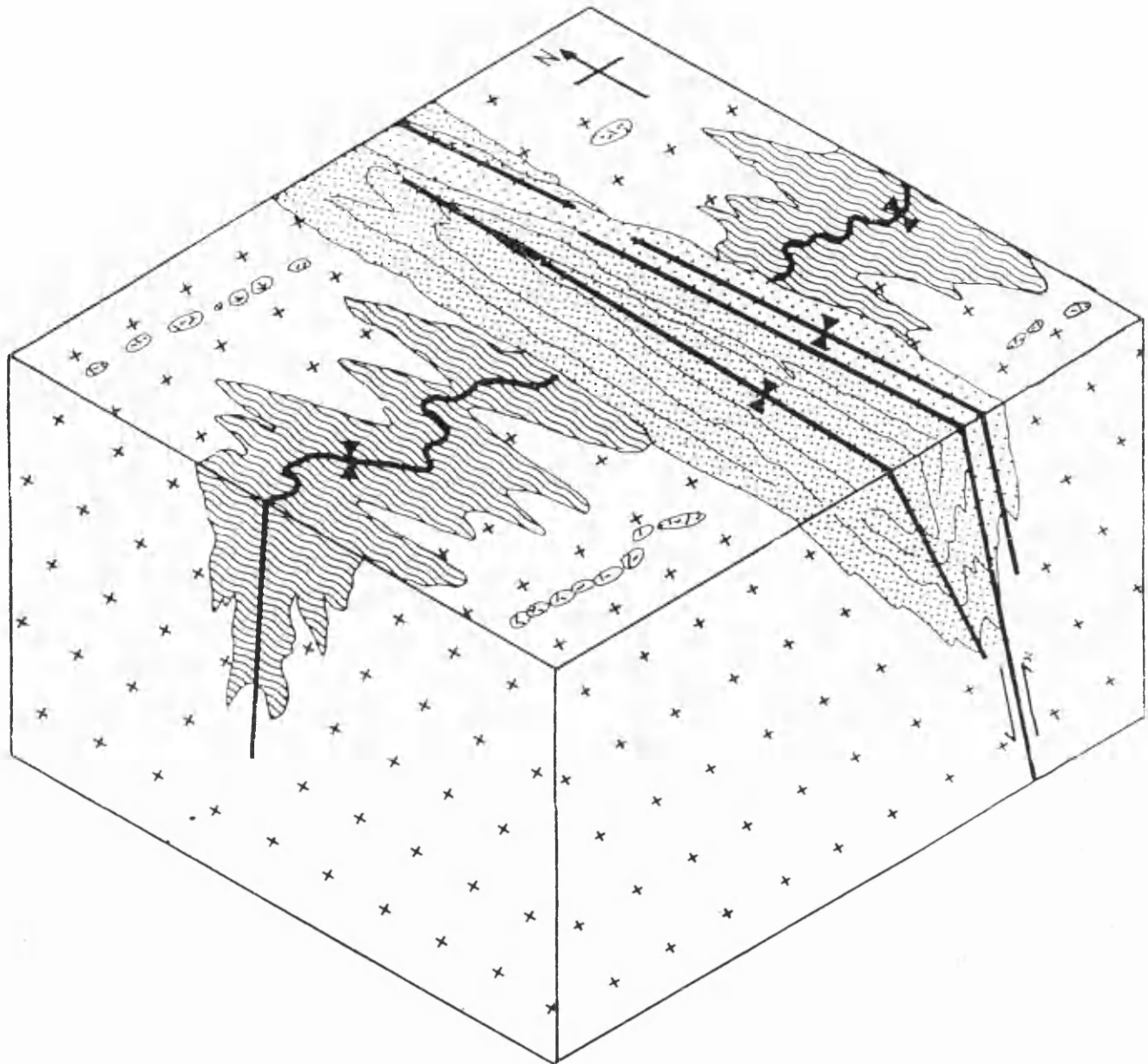
Fig. 7.6 Block diagram showing structural interpretation of the southern Arabian Shield (after Moore, 1983).

CHAPTER EIGHT REGIONAL ENHANCEMENT USING LANDSAT MSS

8.1 LANDSAT MSS IMAGES

8.2 COLOUR COMPOSITING RESULTS

8.3 PRINCIPAL COMPONENTS ANALYSIS RESULTS

8.4 EDGE ENHANCEMENT RESULTS

      (a) Image enhancement

      (b) Lineament interpretation of Landsat image

      (c) Conclusion

8.5 SUMMARY

8.1 LANDSAT MSS IMAGES

The Landsat Multi-Spectral Scanner (MSS) system has been carried on board all five Landsats since 1972. It uses an oscillating mirror to scan the earth from west to east. The total coverage area of the ground is 185x185 km. The MSS scanner records four bands of the reflected visible (green and red) and infrared spectrum designated as 1, 2, 3 and 4 (Table 8.1), which were previously (Landsats 1-3) designated 4, 5, 6 and 7, the ground resolution of which is 79x79 m (Sabins, 1987).

MSS Band	Wavelength, μm	Colour
1	0.5 - 0.6	Green
2	0.6 - 0.7	Red
3	0.7 - 0.8	Reflected Infrared
4	0.8 - 1.1	Reflected Infrared

Table 8.1 Landsat 4/5 MSS bands.

Digital Landsat-5 MSS scanner imagery from the Arabian winter season (2 Feb 1987) was obtained for the purpose of this regional complementary study.

The full MSS scene of the study area (Path 167, Row 047) is composed of 2984 lines and 3728 pixels, which is difficult to display on the CRT monitor available at the image analysis laboratory. To display the entire study area on the 512-by-512 pixels monitor, the data is sub-sampled, by showing only every sixth line and seventh pixel of the MSS data. Despite the reduction of data, sufficient detail is visible on the monitor to apply some selected image processing techniques. Because Landsat MSS scenes are skewed on both sides, the blank area on both sides when the scene is displayed on the monitor is found to affect the results, particularly the statistical based techniques. Hence, the subsampled scene was clipped from left and right sides to show only 512 pixels across. So, the subsampled scene used throughout this regional study is 512x497 pixels (Fig. 8.1A). Figure 8.1B shows the comtrast stretched scene of the study area.

Fig. 8.1 A:Landsat-5 MSS band 4 subsampled and clipped scene
for the study area; B:the linearly contrast stretched
image (Path 167, Row 047).

8.2 COLOUR COMPOSITING RESULTS

The two colour composites used in this regional study of the Landsat MSS 167/047 image were (1) colour composite of individually contrast-enhanced MSS bands and (2) contrast-enhanced band ratios.

False Colour Composite (FCC) was created using Landsat MSS bands 4,2,1 in red, green and blue and was found to give the best results; the image is shown in Figure 8.2A. A very general lithological discrimination could be carried out. For example, the dark areas in the FCC indicate areas of rocks rich in dark minerals such as amphibole and olivine (e.g. sections C7, F9 and H8, Fig. 8.2A). In contrast, granitoid rocks are presented as light greyish colour in the FCC (e.g. sections C6, F6 and G8, Fig. 8.2A). Areas of wadi alluvium are shown as saturated white hues (e.g. sections D1 and I5, Fig. 8.2A), whereas wadis filled by pure sand are shown as yellow hues in the northeastern part of the study area where Wajid Sandstone caps the shield rocks. The circular/oval shapes of numerous igneous intrusions which characterize the southern Arabian Shield are also identifiable in the FCC (e.g. sections B2 and C5, Fig. 8.2A).

To further increase contrast among surface features, Landsat MSS data can be ratioed prior to false colour compositing. The best combination for rock discrimination in the Arabian Shield combined the MSS bands 3/4,2/3,1/2 in red,green,blue into a Colour Ratio Composite (CRC) image (Blodget and Brown, 1982; Blodget et al., 1978).

The ratio colour composite image (Fig. 8.2B) was first analyzed by comparing it to the compiled geological map of the study area (Plate 2), which provided considerable detailed information. This comparative study helped to identify mapped rock units that could be correlated with MSS ratio data expressed as unique colour signatures on the ratio colour composite image.

The monzogranites and the granodiorites are shown as medium-orange colours in the CRC (e.g. sections C4 and C5, Fig. 8.2B), whereas the tonalites are shown as dark orange hues in the CRC, particularly in the southeastern corner of the image (e.g. section G8, Fig. 8.2B). Wadis with alluvium appear as a bright orange colour (e.g. sections E1, H1 and I5, Fig. 8.2B). The As-Sarat Tertiary basalt is shown as cyan hues (sections F8 and G9, Fig. 8.2B), whereas all metamorphic layered rocks of the Asir Terrane to the west of the study area are identifiable as areas of different blue hues
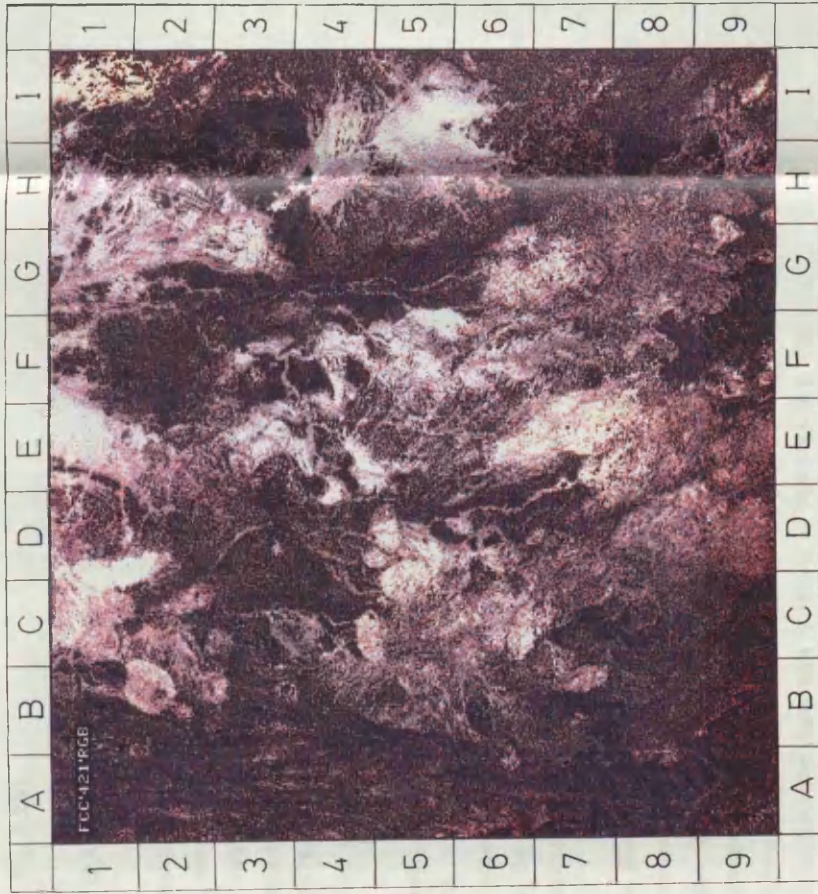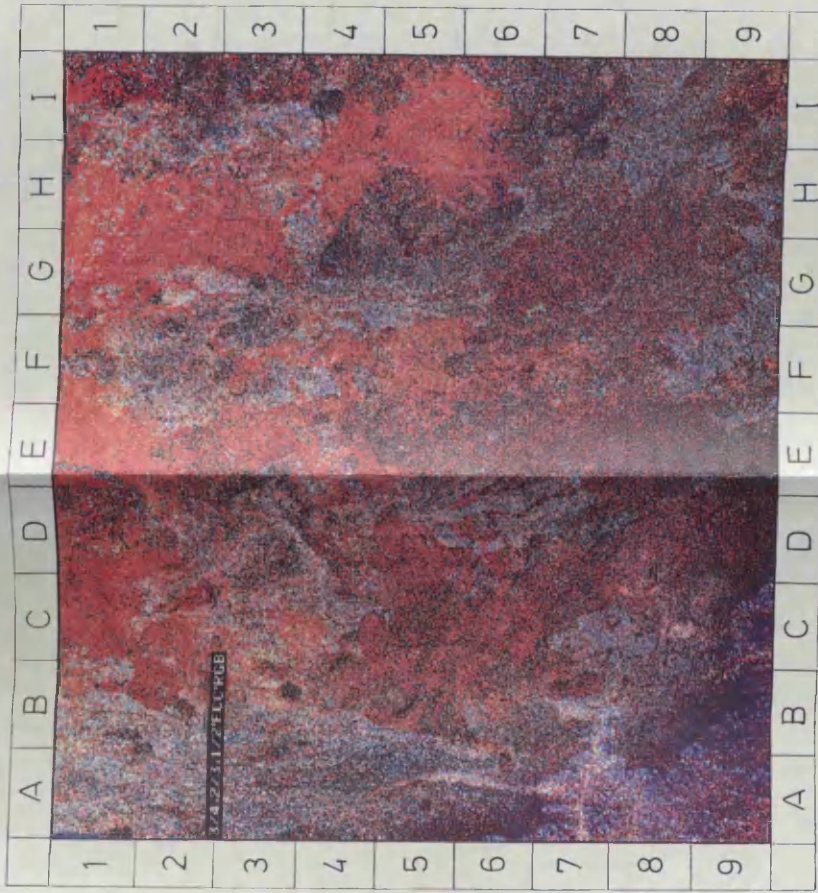
Fig. 8.2 Landsat MSS colour composite images for the study area. A:bands 4,2,1 in red, green and blue FCC; B:ratio image composite of bands 3/4,2/3,1/2 in red, green and blue.

(e.g. sections A1, A5, B8 and C9, Fig. 8.2B). The wadi sand alluvium within Wajid Sandstone outcrops (northeastern part of the study area) are shown as a reddish colour (section I1, Fig. 8.2B).

8.3 PRINCIPAL COMPONENTS ANALYSIS RESULTS

Principal components analysis/transformation (PCA) is a widely used method to calculate n new statistically independent components of n input bands, based on the covariance matrix. Three of the resulting components (PC's) may be displayed as a colour composite or used for decorrelation stretching before retransformation (Soha and Schwartz, 1978). Application of PCA in the southern Arabian Shield using the Landsat MSS was first performed by Blodget et al. (1978).

A visual inspection of the PC's colour composites indicated the Landsat MSS bands 4,3,2 in red, green and blue to be the most informative. Figure 8.3 shows the PC colour composite for the study area. The first PC image was assigned to red component; the second PC image, the green component; and the third PC image, the blue component. The colour composite was scaled using a linear-stretching algorithm.

Most of the granitoid rocks in the study area (Plate 2) are shown as cyan-to-blue hues in the PC colour composite (e.g. sections C1, C5, C6, E7 and H1, Fig. 8.3). The As-Sarat basaltic field is shown as a golden colour (section G9, Fig. 8.3), whereas the layered metamorphic rocks to the west of the study area are shown as a mixture of yellow, magenta and light blue hues (e.g. sections A1-A9 and B8, Fig. 8.3). The wadi alluvium throughout the study area is shown as blue hues (e.g. sections D6 and H5), except in the northeastern part where it is composed of Wajid Sandstone, and appears as a very dark blue colour.

8.4 EDGE ENHANCEMENT RESULTS

(a) Image enhancement

Landsat MSS images have been used extensively for purposes of structural mapping because of the synoptical and equal-illumination view provided by the Landsat system, which is ideal for examining the regional fabric of an area. A winter scene (2 Feb 1987) with low sun elevation (38°) was selected to enhance lineaments in the study area, which comprises about one-third of the southern Arabian Shield.

Fig. 8.3 Landsat MSS principal components colour composite of bands 4,3,2 in red, green and blue for the study area.

Lineaments are considered to be manifestations of geological structure. Although geological meaning of individual image lineaments is usually obscure, many have been identified as topographic expressions of faults, fault zones or zones of jointing.

As described earlier in Chapter 3 (section 3.3.4), edge enhancement was achieved by high-pass filtering in order to emphasize higher spatial frequencies. The Landsat-5 MSS band 4 (0.8 - 1.1 μm) digital image of the whole study area was selected for the application of the method in this regional study using three high-pass directional filters to enhance linear features oriented in north, northeast and northwest directions. The resulting filtered images are shown in Figure 8.4 and the addition and scaling of these filtered images is shown in Fig. 8.4D. This product was appropriate for visual definition of lineaments or fractures, but a better image was obtained by adding it to the original MSS image. This product is shown in Fig. 8.4E which was used for the identification and tracing of lineaments (similar results could be obtained following the procedure described in Appendix B). These lineaments are the most important linear features recognizable because of the coarse resolution of the Landsat MSS imagery.

The lineaments were identified initially utilizing the interactive image analysis system, where lineaments were drawn on the CRT video monitor and a map (MAP A) was produced (Fig. 8.5). Later, a thorough examination of Fig. 8.4E to identify lineaments by visual inspection and to record lineaments on transparent overlay as ruled straight lines was carried out, and a different map (MAP B) was obtained (Fig. 8.6). This map is the basis for the discussion of lineaments and/or fractures.

(b) Lineament interpretation of Landsat image

The significance of the lineament trends interpreted from images was analyzed by using directional frequency rose diagrams with a 10 degree azimuth class interval.

Initially, the rose diagram produced by the image analysis system's map (MAP A)(Fig. 8.5) was plotted (Fig. 8.7A). The following trends stand out above the background: E-W, NE-SW and NW-SE. Study of the detailed fracture map (Fig. 8.6), shows that lineament frequency is very evenly distributed within the study area. A rose diagram (Fig. 8.7B) was plotted for the detailed map (MAP B), where two distinct trends were observed; these are N-S and general E-W. NE-SW and NW-SE trends are also observed but not as significant as the N-S and E-W trends.
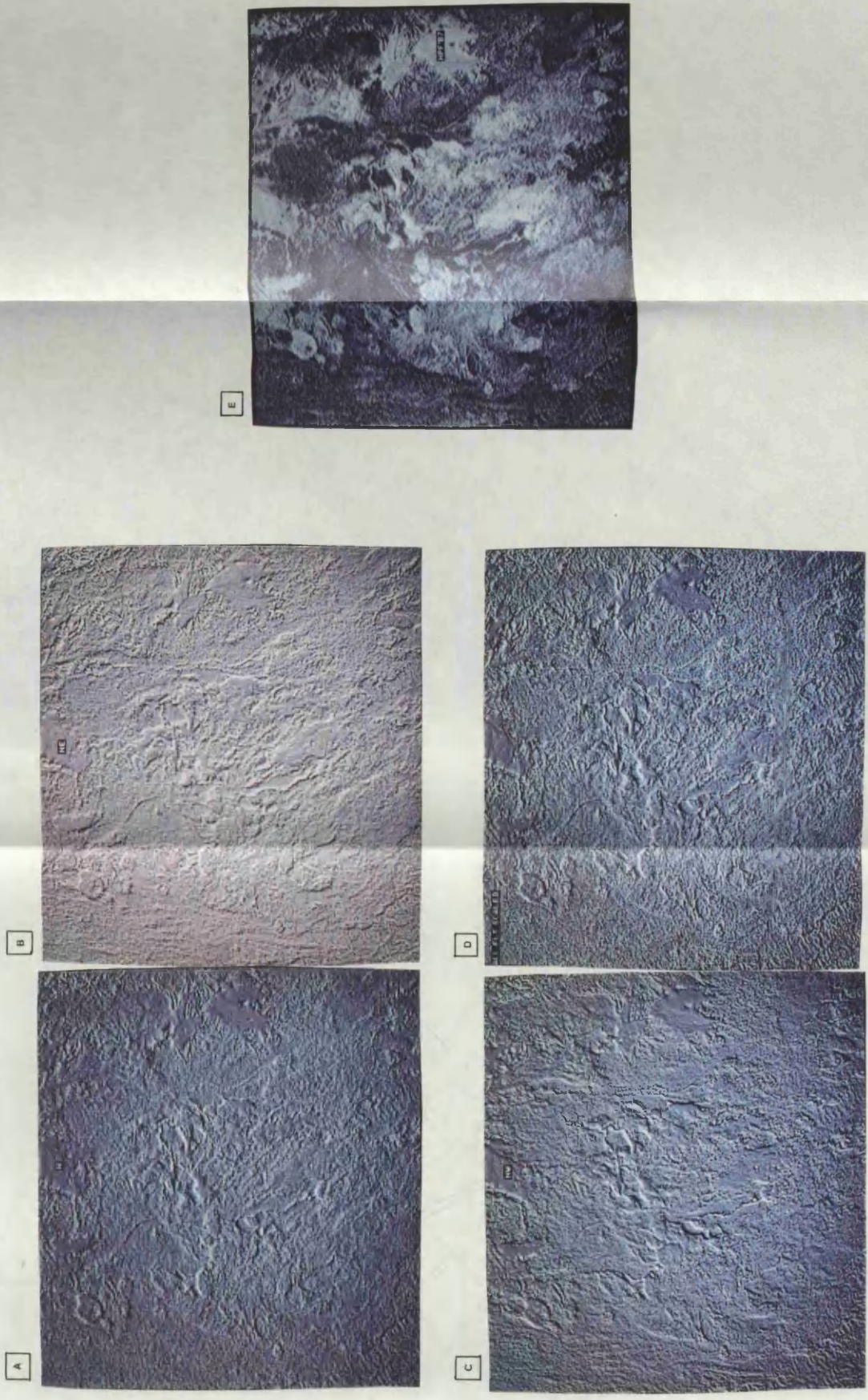
Fig. 8.4 Edge enhancement techniques images for the study area. A:north directional high-pass filtered image; B:north-eastern directional high-pass filtered image; C:north-western directional high-pass filtered image; D:all these three filtered images added together and scaled; E:directionally enhanced image superimposing MSS band 4.

N
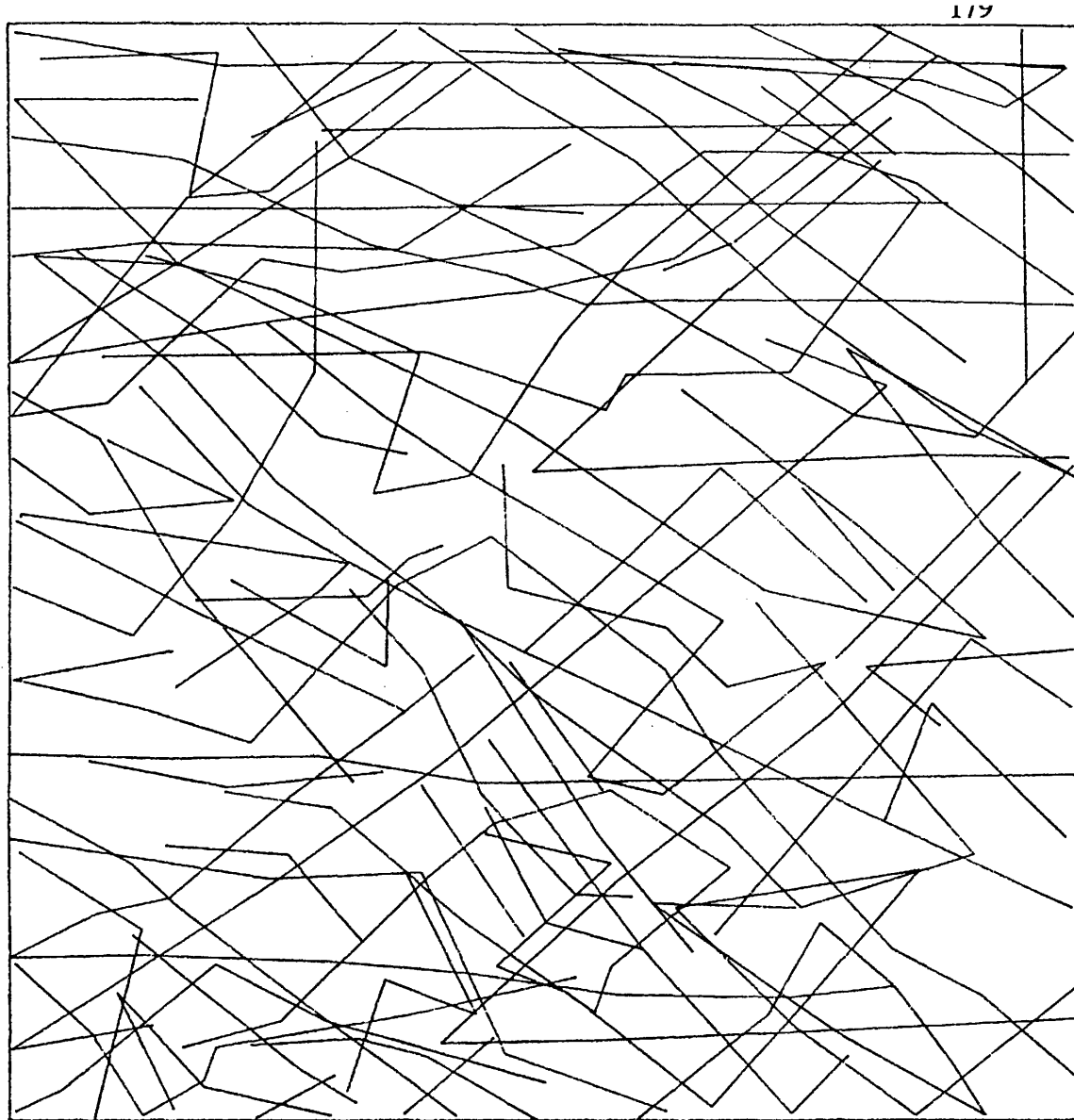
0   20   40km

⸺ Lineament (mainly joint)

Fig. 8.5 Initial lineament map for the entire study
         area (MAP A).

N

0   20   40 km
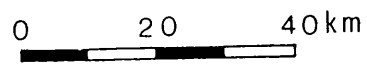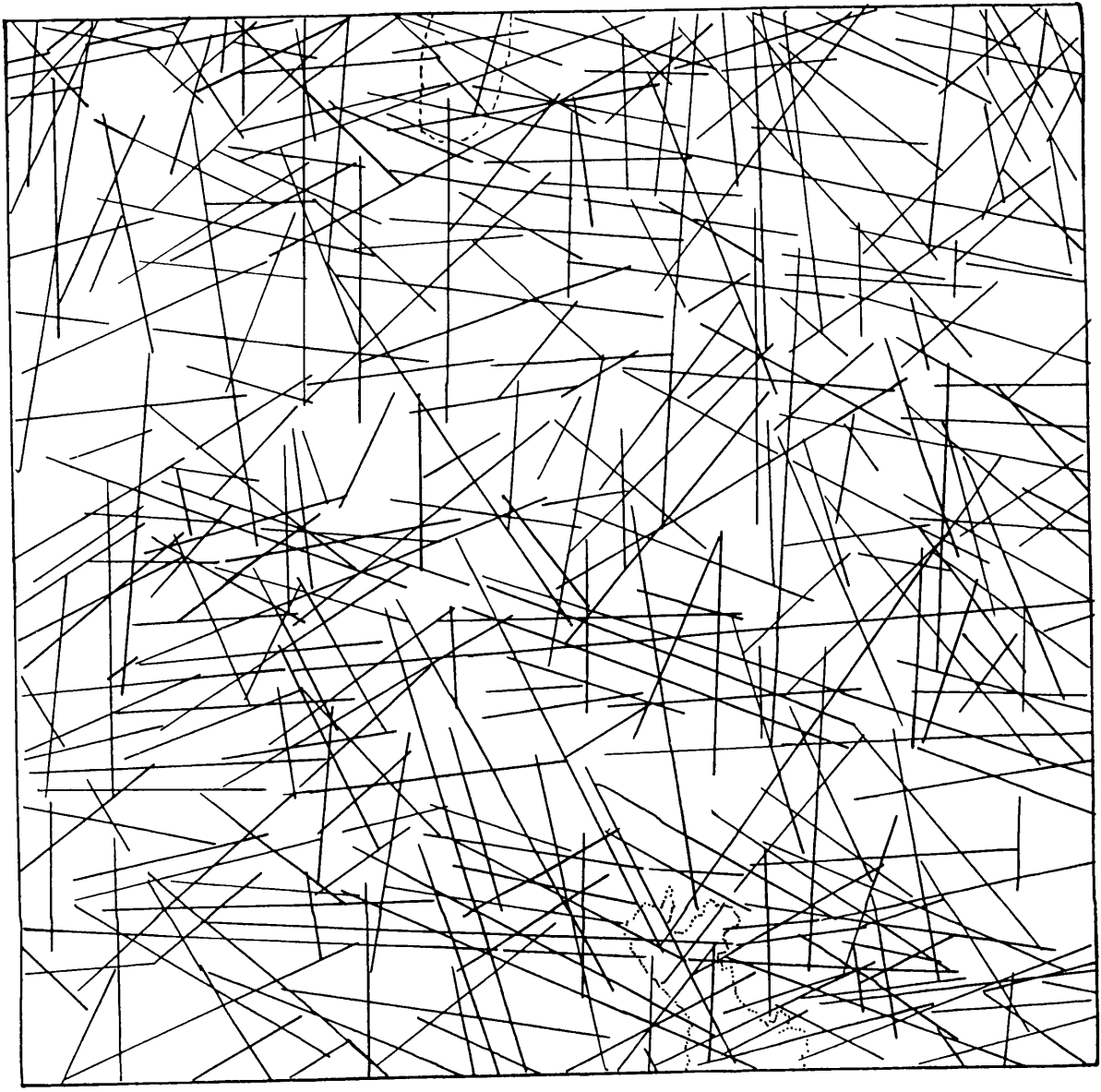
——— Lineament (mainly joint)
As-Sarat Basaltic Flow
Jabal Al-Hasir Granite

Fig. 8.6 Remotely sensed geological fracture map for
        the entire study area (MAP B).
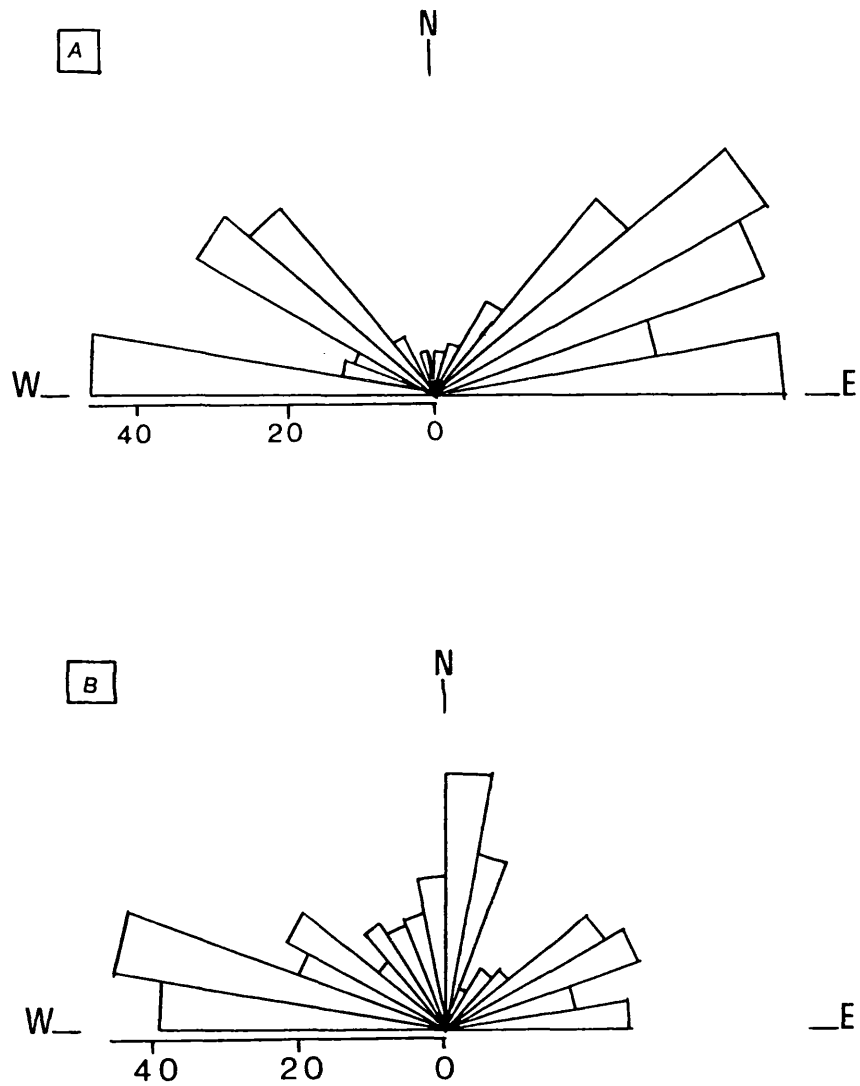
Fig. 8.7 Rose diagrams summarising strike-frequency
distribution. A:250 lineaments of Fig. 8.5;
B:394 lineaments of Fig. 8.6.

As previously mentioned (Chapter 3, section 3.3.4(c)), Norman (1980a) studied the statistics of the orientations of straight lineaments in the Arabian Shield based on unenhanced Landsat MSS band-7 1:2,000,000 mosaic. His directional frequency rose diagram of lineaments in the basement area of Saudi Arabia (Arabian Shield) was shown in Fig. 3.15. Comparing the rose diagrams obtained from this study (Fig. 8.7) with that of Norman, one can not say that results are identical, because some trends appear in one and not in the other. For example, the E-W trend which is recorded in this study was not as prominent in Norman's study. However, if we compare Norman's rose diagram with the detailed map rose diagram (Fig. 8.7B), it seems that the two show a good correspondence except in the E-W and NNE-SSW trends. This is again because Norman was dealing with the entire shield area, mostly concentrating in the central part, whereas the study area here is small compared to that of Norman. In addition, the study area lies in the southern Arabian Shield where the structural grain (fabric) may well be different from the central part of the shield. To conclude, the most prominent trends shown in the rose diagram (Fig. 8.7B) are: N-S and E-W; less marked concentrations with NE-SW and NW-SE trends were also observed.

In order to evaluate lineament occurrences which were mapped utilizing edge enhancement techniques, the following figures were created. The 394 lineaments (Fig. 8.6) were plotted as histograms both for frequency distribution and length, respectively (Fig. 8.8A and B). These two histograms are combined, and the resultant diagram shown in Figure 8.8C. Finally, Figure 8.8C was replotted in percentage terms and Figure 8.8D was obtained; this shows a nice correspondence between the length and frequency of the 394 lineaments mapped within this regional study. Frequency and length of these lineaments were plotted against each other, and the points scatter about diagonal line (Fig. 8.9), indicating a good positive correlation.

An attempt to correlate lineaments of the 3 test-sites (Chapters 3, 4 and 5) with the lineaments mapped from the Landsat MSS for the whole study area was carried out, and it was very clear that the results from both are comparable. Figure 8.10 shows the percentage histograms of both areas, i.e. the entire study area and the sum of the 3 test-sites. Although the 3 test-sites form only small parts of the whole study area, they are representative of the whole area as far as lineaments are concerned.

An attempt was also made to correlate the observed lineaments (Fig. 8.6) and mapped
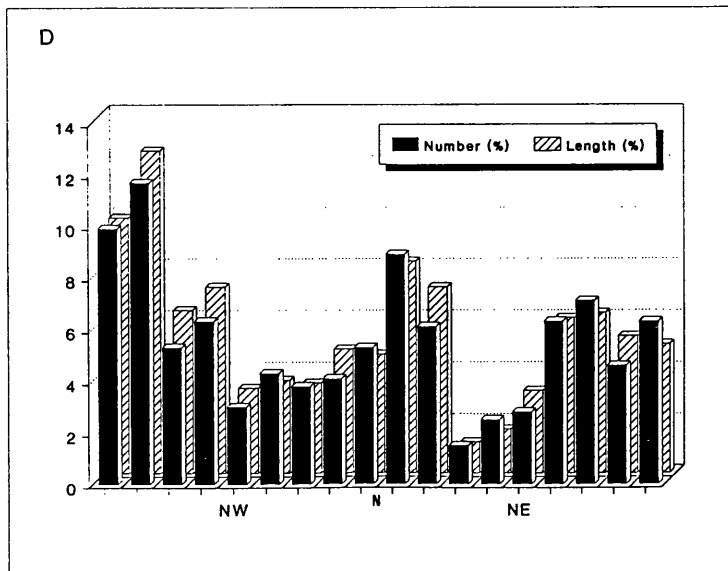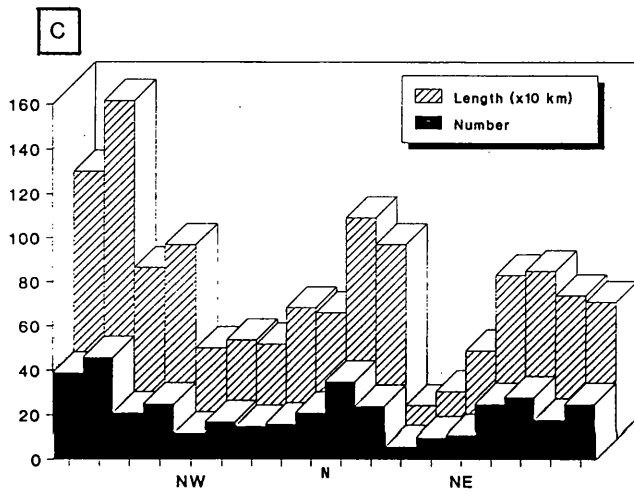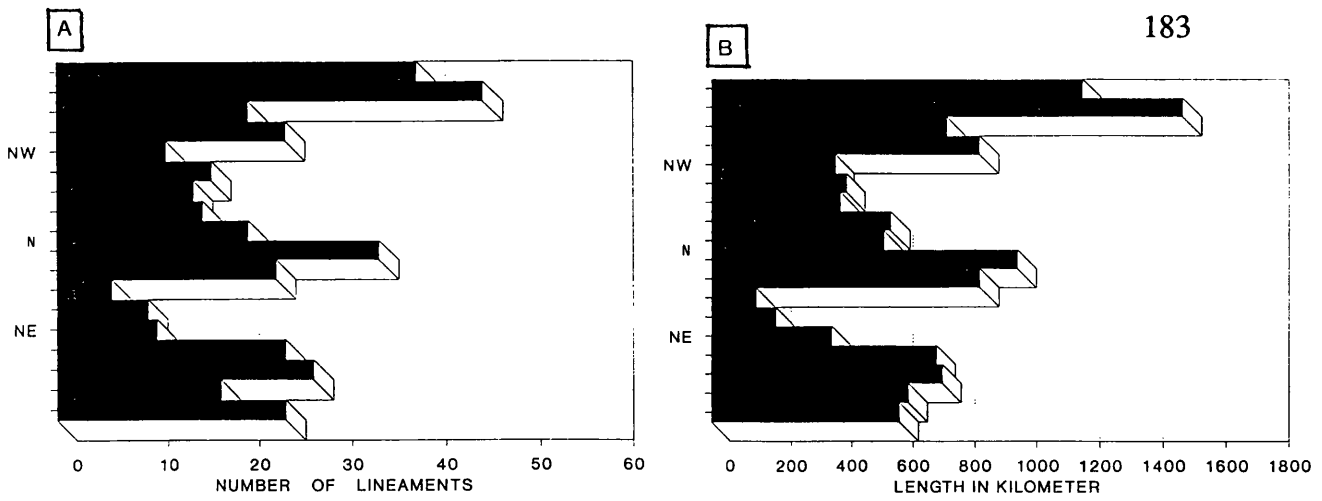
Fig. 8.8 Histograms summarising the 394 lineaments in
Fig. 8.6. A:frequency of distribution; B:length;
C:combined distribution and length; D:combined
distribution and length plotted as percentage
of total.
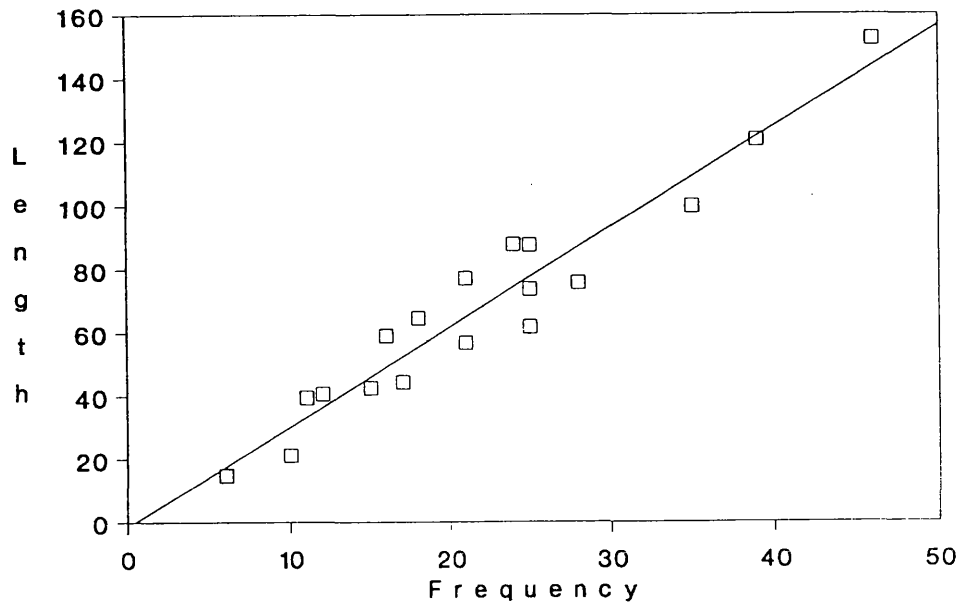
Fig. 8.9 Cross-plot of frequnecy versus length for lineaments
in the entire study area.
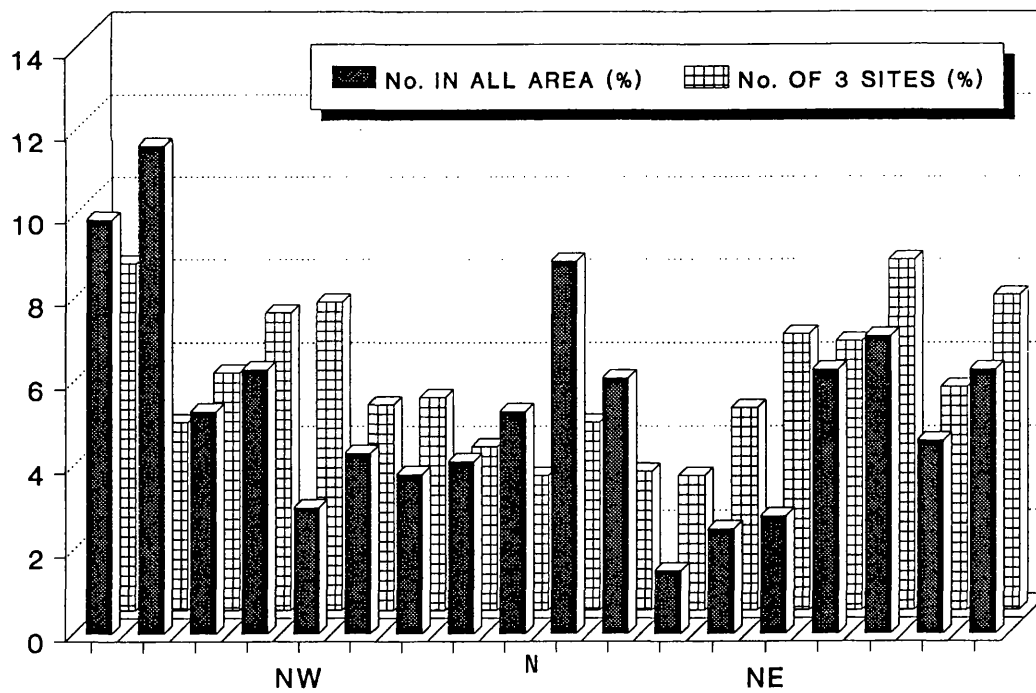
Fig. 8.10 Diagram summarising strike-frequency distribution
of 394 lineaments of the entire study area and 1183
lineaments of the 3 test-sites (see text for
details).

faults (Plate 2). Many lineaments were found to accord with mapped faults, and field work indicates that other lineaments correspond to joint sets which have not previously been mapped in the ground surveys.

(c) Conclusion

Landsat MSS imagery proved useful for revealing lineaments which can be correlated with fractures within the study area. Some of these were known, but the majority were revealed for the first time during this investigation.

Quantitative examination of the lineaments showed that the study area has several preferential directions, but the N-S and the E-W directions are the most prominent.

Correlating the lineaments mapped using the Landsat TM for the 3 test-sites and the Landsat MSS for the whole study area, indicated that the two are comparable and that these small area test-sites are in fact a reflection of what is in the whole study area.

8.5 SUMMARY

The Landsat MSS system's imagery, using a subsampled image of the full scene, was utilized for image processing and interpretation for the purpose of a regional study.

Because of the coarse spatial resolution of the Landsat MSS, and because of the subsampled imagery used, full-resolution criterion could not be maintained in this regional study (if compared with the 3 test-sites in Chapters 3, 4 and 5). However, the selected digital image processing methods performed yielded some useful results.

The false colour composite of the Landsat MSS bands 4,2,1 in red,green,blue gave a very general lithological discrimination between rock types, whereas bands 3/4,2/3,1/2 in red,green,blue ratio colour composite yield a better discrimination. The colour composite generated via principal components analysis was the best for lithological discrimination purposes.

The Landsat-5 MSS band 4 was used for the delineation of the lineaments, and the quantitative examination showed that the study area has several preferential directions.

CHAPTER NINE SUMMARY AND RECOMMENDATIONS

9.1 SUMMARY

9.2 IMPLICATIONS FOR GEOLOGICAL STUDIES IN
   THE ARABIAN SHIELD

9.3 RECOMMENDATIONS FOR FURTHER WORK

9.1 SUMMARY

The aims and objectives of this study were to test the capability and ability of Landsat multispectral remote sensing data for geological mapping (section 1.6, Chapter 1).

A study area in southwestern Saudi Arabia was selected because of the geological features it included. A wide variety of rock types is exposed in the area. This wide range provided an ideal opportunity to discriminate different lithologies using remote sensing techniques. The structural complexity of the study area provided an opportunity to evaluate the use of remote sensing for structural studies at different scales. Regional tectonic patterns were examined from synoptic scale images, i.e. MSS imagery; smaller structural features were studied using larger scale images, i.e. TM imagery.

The multispectral remote sensing data used in this study were Landsat-4 TM and Landsat-5 MSS data. The TM data has 30m spatial resolution, whereas MSS data has 79m spatial resolution. Landsat MSS, with its coarse resolution, has been used to give a general overview of the type of terrain and the general geology of the study area. The Landsat TM has been used for more precise study of the three test-sites selected within the study area. The high resolution of the TM data, along with its narrow bands, helped in the discrimination between different lithologies.

Results can be summarized as follows:

1- Landsat TM images have been used to make the first comprehensive study of three test-sites in the southern Arabian Shield, one of the best exposed terrains on Earth.

2- Landsat TM data could be used as a very effective exploration tool in the entire Arabian Shield and comparable areas.

3- The spatial and spectral resolutions of TM data is adequate for geological studies, and geological maps at scale of 1:70,000 were created reliably in this study.

4- TM bands 7/5,5/4,4/2 in red, green and blue provided the best colour composite for lithological discrimination using the ratio technique. However, TM bands 5/7,5/1,5/4x3/4 in red, green and blue can be useful

in areas rich in dark coloured igneous and metamorphic rocks.

5-   The decorrelation stretching colour composite of TM bands 7,5,4 in red, green and blue is also useful for lithological discrimination.

6-   For the first time, at least in the Arabian Shield, a migmatitic zone and the contact between two tectonic assemblages in the southern Arabian Shield was mapped using TM data.

7-   The three-step procedure for lineament enhancement implemented in this study revealed lineaments which can be correlated with fractures, many of which were mapped for the first time.

8-   Lithological information derivable from the low spatial resolution Landsat MSS data was examined using two techniques, which are colour ratio composites and principal components analysis, then compared with geological maps. The principal components analysis colour composite was the best for lithological discrimination.

9-   Landsat MSS data were processed and analyzed for both structural and lithological information. A statistical lineament analysis was performed on a full-scene; results were compared with results of other studies, such as aeromagnetic mapping. Two principal lineament trends were seen. These correlated well with the results of full-resolution analysis of the three test-sites in this study using TM data.

10-   Some of known faults in the study area appear to be of greater regional extent on Landsat imagery than shown on previous geological maps.

11-   Rocks of the southern Arabian Shield were affected by at least three successive phases of deformation. The third phase, which resulted from an east-west compression, is the most dominant.

9.2 IMPLICATIONS FOR GEOLOGICAL STUDIES IN THE ARABIAN SHIELD

Results obtained from this study should be viewed as an example of the use of Landsat

data for geological studies, particularly for lithological mapping in well-exposed arid regions with little or no vegetation cover.

Using Landsat data, particularly TM, in any geological mapping programme of the vast Arabian Shield should give good results and reduce the need for long and expensive field work. Concentrating on mineral exploration studies in some parts of the shield will facilitate future plans for locating target areas for further investigations.

Applying simple techniques described earlier in large areas should give an indication of lithologies in the early stages of planning, and hence aid the choice of appropriate technique(s) for the area under investigation.

Various geological authorities in the Kingdom of Saudi Arabia are asked to implement and utilize remote sensing technology for the benefit of their researches and programmes. The application of this technology should save time and costs in many aspects of their work.

9.3 RECOMMENDATIONS FOR FURTHER WORK

Based on the results of this work, several ideas for further study can be recommended:

1- Selection of new interesting (there are so many) test-sites within the southern Arabian Shield, particularly within the Landsat Path 167/Row 047 (study area) for full-resolution studies as described in Chapters 3, 4 and 5.

2- Extrapolating the results obtained in this study to the surrounding regions is advisable in order to broaden the understanding of the geology.

3- In addition to lithological mapping of the southern Arabian Shield, mineral prospecting studies searching for target areas should consider the use of remote sensing technology.

4- Tectonic studies utilizing remote sensing technology covering the entire Arabian Shield will facilitate comparisons with the Nubian Shield of Egypt and Sudan.

5- Comparison between the current space-borne imagery with the higher resolution sensor imagery of the SPOT satellite in lithological mapping, and testing of the stereo-imagery obtainable from SPOT in geological studies.

6- Field spectral measurements should be used for establishing lithological mapping in the vast Precambrian Shield of Saudi Arabia, which allow mapping in a short time.

7- The digitally processed images should be made available for field studies, together with aerial photographs and published maps, in order to aid interpretation, targeting and location during fieldwork.

8- Adoption of the following sequence of procedures is advisable when conducting geological remote sensing studies in the Arabian Shield and comparable areas, as follows:

     -selection of the area,

     -literature review of published maps, reports, ...

     -acquisition of available aerial photographs and digital images,

     -preliminary image processing and interpretation,

     -preliminary field work,

     -selection of test-sites,

     -final image processing and improved interpretation,

     -final field check.

REFERENCES

Abrams, M.J., Conel, J.E. and Lang, H.R., 1985. The joint NASA/ Geosat test case project, Final report. American Assoc. of Petroleum Geologists.

Abrams, M.J., Ashley, R.P., Rowan, L.C., Goetz, A.H.F. and Kahle, A.B., 1977. Mapping of hydrothermal alteration in the cupprite mining district, Nevada, using aircraft scanner images for the spectral region 0.46 to 2.36 µm. Geology, 5:713-718.

Agar, R.A., 1986. Structural geology of felsic plutonic rocks in the Arabian Shield; styles, modes and levels of emplacement. J. African Earth Sciences, 4:105-121.

Al-Hinai, K.G., 1988. Quaternary aeolian sand mapping in Saudi Arabia using remotely sensed imagery. Unpubl. Ph.D. thesis, Univ. of London.

Al-Khatieb, S.O., 1981. Detection of surface evidence of sub-surface structures by interpretation methods of Landsat imagery in the sedimentary rocks of central Saudi Arabia. Unpubl. Ph.D. thesis, Univ. of London.

Al-Khatieb, S.O. and Norman, J.W., 1982. A possibly extensive crustal failure system of economic interest. J. Petroleum Geology, 4:319-327.

Al-Sari, A.M., 1989. A Geological investigation of multispectral remote sensing data for the Mahd Adh Dhahab and Jabal Said districts, western Saudi Arabia. Unpubl. Ph.D. thesis, Univ. of Durham.

Al-Shanti, A.M. and Gass, I.G., 1983. The Upper Proterozoic ophiolite melange zones of the easternmost Arabian Shield. J. Geol. Soc. London, 140:867-876.

Almond, D.C., 1986. Geological evolution of the Afro-Arabian dome. Tectonophysics, 131:301-332.

Amlas, M.M.A., 1983. Geology and structures of the Precambrian rocks north of Khamis Mushayt, southern Arabian Shield. Unpubl. M.Sc. thesis, Faculty of Earth Sciences, King Abdulaziz Univ., Jeddah, Saudi Arabia.

Anderson, R.E., 1977. Geology of the Wadi Tarj quadrangle, Kingdom of Saudi Arabia. Saudi Arabian Directorate General of Mineral Resources Geologic Map GM-29.

Anderson, R.E., 1979. Geology of the Wadi 'Atf and Mayza' quadrangles, Kingdom of Saudi Arabia. Saudi Arabian Directorate General of Mineral Resources Bull. 25.

ARGAS, 1977. Geophysical synthesis report, eastern part of the Central Red Sea. Saudi Arabian Deputy Ministry for Mineral Resources, Jeddah, Saudi Arabia.

Bakor, A.R., Gass, I.G. and Neary, C.R., 1976. Jabal al Wask, northwest Saudi Arabia: an Eocambrian back-arc ophiolite. Earth and Planetary Science Letters, 30:1-9.

Bayer, H.-J. and Kaufmann, H., 1986. New geologic aspects based on comparative analysis of advanced satellite- and field-data in the NE Gulf of Aqaba area. GeoJournal, 12:33-42.

Blank, H.R., Gettings, M.E. and Andreasen, G.E., 1980. Total-intensity aeromagnetic

map of the Precambrian Arabian Shield, Kingdom of Saudi Arabia. Saudi Arabian Directorate General of Mineral Resources, USGS-TR-6.

Blodget, H.W., 1977. Lithologic mapping of crystalline shield test sites in western Saudi Arabia using computer manipulated multispectral satellite data. Ph.D. thesis, George Washington Univ., Washington, D.C., U.S.A.

Blodget, H.W. and Brown, G.F., 1982. Geological mapping by use of computer enhanced imagery in western Saudi Arabia. U. S. Geological Survey Professional Paper 1153.

Blodget, H.W., Gunther, F.J. and Podwysocki, M.H., 1978. Discrimination of rock classes and alteration products in southwestern Saudi Arabia with computer-enhanced Landsat data. NASA Technical Paper 1327, NASA scientific and technical information office.

Blom, R.G., Abrams, M.J. and Adams, H.G., 1980. Spectral reflectance and discrimination of plutonic rocks in the 0.45- to 2.45-μm region. J. Geophy. Res., V.85, N.B5:2638-2648.

Bohannon, R.G., 1986. Tectonic configuration of the western Arabian continental margin, southern Red Sea. Tectonics, 5:477-499.

Bokhari, F.Y. and Kramers, J.D., 1981. Island arc character and later Precambrian age of volcanics at Wadi Shwas, Saudi Arabia: geochemical and Sr and Nd isotopic evidence. Earth and Planetary Science Letters, 54:409-422.

Brown, G.F., 1972. A Tectonic map of the Arabian Peninsula. Saudi Arabian Directorate General of Mineral Resources Arabian Peninsula Map AP-2.

Brown, G.F. and Coleman, R.G., 1972. The tectonic framework of the Arabian Peninsula: XXIV Int. Geol. Cong. Montreal, part III:300-305.

Brown, G.F. and Jackson, R.O., 1959. Geologic map of the Asir quadrangle, Kingdom of Saudi Arabia. Saudi Arabian Directorate General of Mineral Resources Miscellaneous geologic investigation map I-217A.

Brown, G.F. and Jackson, R.O., 1960. The Arabian Shield. XXI Int. Geol. Cong. Copenhagen (Norden), part IX:69-77.

Brown, G.F. and Jackson, R.O., 1963. Geologic map of the Arabian Peninsula. U. S. Geological Survey and Arabian American Oil Company.

Brown, G.F., Schmidt, D.L. and Huffman, A.C., 1989. Geology of the Arabian Peninsula. Shield area of western Saudi Arabia. U. S. Geological Survey Professional Paper 560-A.

Camp, V.E., 1984. Island arcs and their role in the evolution of the western Arabian Shield. Geol. Soc. America Bull., 95:913-921.

Chayes, F., 1949. Statistical analysis of three dimensional fabric diagrams, in: Fairbairn, H.W., Structural petrology of deformed rocks. Addison-Wesley Press, Cambridge, Mass., 308-326.

Claesson, S., Pallister, J.S. and Tatsumoto, M., 1984. Samarium-Neodymium data on two late Proterozoic ophiolites of Saudi Arabia and implications for crustal and mantle evolution. Contrib. Mineral. Petrol., 85:244-252.

Coleman, R.G., 1973a. Reconnaissance geology of the Khaybar quadrangle, Kingdom of Saudi Arabia. Saudi Arabian Directorate General of Mineral Resources Geologic Map GM-4.

Coleman, R.G., 1973b. Reconnaissance geology of the Khamis Mushayt quadrangle, Kingdom of Saudi Arabia. Saudi Arabian Directorate General of Mineral Resources Geologic Map GM-5.

Coleman, R.G., Fleck, R.J., Hedge, C.E. and Ghent, E.D., 1977. The volcanic rocks of southwest Saudi Arabia and the opening of the Red Sea, Red Sea research 1970-1975. Saudi Arabian Directorate General of Mineral Resources Bull. 22:D1-D30.

Condit, C.D. and Chavez, P.S., 1979. Basic concepts of computerized digital image processing for geologists. U. S. Geol. Surv. Bull. 1462.

Cornwall, H.R., 1973. Geology of the Wadi Harjab quadrangle, Kingdom of Saudi Arabia. Saudi Arabian Directorate General of Mineral Resources Geologic Map GM-3.

Darbyshire, D.P.F., Jackson, N.J., Ramsay, C.R. and Roobol, M.J., 1983. Rb-Sr isotope study of latest Proterozoic volcano-sedimentary belts in the central Arabian Shield. J. Geol. Soc. London, 140:203-213.

Delfour, J., 1979. L'orogenese Pan-Africaine dans le partie nord du Bouclier Arabe (Royaume d'Arabie Seoudite). Bull. Soc. Geol. France 7:449-456.

Dietrich, R.V. and Mehnert, K.R., 1960. Proposal for the nomenclature of migmatites and associated rocks. XXI Int. Geol. Cong. Copenhagen (Norden), suppl. vol. sect., 1-21, 56-57.

Drury, S.A., 1987. Image interpretation in geology. Allen & Unwin, London.

Duyverman, H.J., Harris, N.B.W. and Hawkesworth, C.J., 1982. Crustal accretion in the Pan African: Nd and Sr isotope evidence from the Arabian Shield. Earth and Planetary Science Letters, 59:315-326.

Engel, A.E.J., Dixon, T.H. and Stern, R.J., 1980. Late Precambrian evolution of Afro-Arabian crust from ocean arc to craton. Geol. Soc. America Bull., 91:699-706.

Engel, C.G. and Sharp, R.P., 1958. Chemical data on desert varnish. Geol. Soc. America Bull., 69:487-518.

Fairbairn, H.W., 1949. Structural petrology of deformed rocks. Addison-Wesley Press, Cambridge, Mass., U.S.A.

Fairer, G.M., 1985. Geologic map of the Wadi Baysh quadrangle, Sheet 17F, Kingdom of Saudi Arabia. Saudi Arabian Deputy Ministry for Mineral Resources Geoscience Map GM-77A.

Fleck, R.J., Greenwood, W.R., Hadley, D.G., Anderson, R.E. and Schmidt, D.L., 1980.

Rubidium-strontium geochronology and plate-tectonic evolution of the southern part of the Arabian Shield. U. S. Geological Survey Professional Paper 1131.

Flinn, D., 1958. On tests of significance of preferred orientation in three-dimensional fabric diagrams. J. Geol., V.66.

Frisch, W. and Al-Shanti, A.M.S., 1977. Ophiolite belts and the collision of island arcs in the Arabian Shield. Tectonophysics, 43:293-306.

Gass, I.G., 1977. The evolution of the Pan African crystalline basement in N.E. Africa and Arabia. J. Geol. Soc. London, 134:129-138.

Gass, I.G., 1979. Evolutionary model for the Pan-African crystalline basement. Evolution and mineralization of the Arabian-Nubian Shield, King Abdulaziz Univ., Institute of Applied Geology Bull.3, V.1:11-20.

Gettings, M.E., 1983. A simple Bouguer gravity anomaly map of southwestern Saudi Arabia and an initial interpretation: Saudi Arabian Deputy Ministry for Mineral Resources Open-File Report USGS-OF-03-94.

Gettings, M.E., Blank, H.R., Mooney, W.D. and Healy, J.H., 1986. Crustal structure of southwestern Saudi Arabia. J. Geophy. Res., V.91, N.B6:6491-6512.

Gillespie, A.R., 1980. Digital techniques of image enhancement. Chapter 6, in: Remote Sensing in Geology, Siegal & Gillespie (eds.). John Wiley & Sons, New York.

Gillespie, A.R., Kahle, A.B. and Walker, R.E., 1986. Color enhancement of highly correlated images. I. Decorrelation and HSI contrast stretches. Remote Sensing of Environment, 20:209-235.

Goetz, A.F.H. and Rowan, L.C., 1981. Geologic remote sensing. Science, 211:781-791.

Greenwood, W.R., 1979a. Geology of the An-Nimas quadrangle, Kingdom of Saudi Arabia. Saudi Arabian Directorate General of Mineral Resources Geologic Map GM-37.

Greenwood, W.R., 1979b. Geology of the Khadra quadrangle, Kingdom of Saudi Arabia. Saudi Arabian Directorate General of Mineral Resources Geologic Map GM-38.

Greenwood, W.R., 1980. Reconnaissance geology of the Wadi Malahah quadrangle, Kingdom of Saudi Arabia. Saudi Arabian Directorate General of Mineral Resources Geologic Map GM-39.

Greenwood, W.R., 1985a. Geologic map of the Bir-Idamah quadrangle, Sheet 18G, Kingdom of Saudi Arabia. Saudi Arabian Deputy Ministry for Mineral Resources Geoscience Map GM-79A.

Greenwood, W.R., 1985b. Geologic map of the Jibal Al-Qahr quadrangle, Sheet 19G, Kingdom of Saudi Arabia. Saudi Arabian Deputy Ministry for Mineral Resources Geoscience Map GM-76A.

Greenwood, W.R., 1985c. Geologic map of the Abha quadrangle, Sheet 18F, Kingdom of Saudi Arabia. Saudi Arabian Deputy Ministry for Mineral Resources

Geoscience Map GM-75C.

Greenwood, W.R., Anderson, R.E., Fleck, R.J. and Roberts, R.J., 1980. Precambrian geologic history and plate tectonic evolution of the Arabian Shield. Saudi Arabian Directorate General of Mineral Resources Bull. 24.

Greenwood, W.R., Jackson, R.O. and Johnson, P.R., 1986. Geologic map of the Jabal Al-Hasir quadrangle, Sheet 19F, Kingdom of Saudi Arabia. Saudi Arabian Deputy Ministry for Mineral Resources Geosience Map GM-94C.

Greenwood, W.R., Hadley, D.G., Anderson, R.E., Fleck, R.J., and Schmidt, D.L., 1976. Late Proterozoic cratonization in southwestern Saudi Arabia. Phil. Trans. R. Soc. London, A280:517-527.

Greenwood, W.R., Stoeser, D.B., Fleck, R.J. and Stacey, J.S., 1982. Late Proterozoic island-arc complexes and tectonic belts in the southern part of the Arabian Shield, Kingdom of Saudi Arabia. U. S. Geological Survey Open-File Report USGS-OF-02-8.

Hemer, D.O., 1968. Diagnostic palynologic fossils from Arabia: American Inst. of Mining Engineers Regional Tech. Sympos., 2d, Dhahran, Saudi Arabia, 1968 Report, 311-315.

Hunt, G.R. and Ashley, R.P., 1979. Spectra of altered rocks in the visible and near infrared. Economic Geology, 74:1613-1629.

Hunt, G.R. and Salisbury, J.W., 1970. Visible and near-infrared spectra of minerals and rocks: I. Silicate minerals. Modern Geology, 1:283-300.

Hunt, G.R. and Salisbury, J.W., 1976b. Visible and near infrared spectra of minerals and rocks: XII. Metamorphic rocks. Modern Geology, 5:219-228.

Hunt, G.R., Salisbury, J.W. and Lenhoff, C.J., 1971. Visible and near-infrared spectra of minerals and rocks: III. Oxides and Hydroxides. Modern Geology, 2:195-205.

Hunt, G.R., Salisbury, J.W. and Lenhoff, C.J., 1973a. Visible and near infrared spectra of minerals and rocks: VI. Additional Silicates. Modern Geology, 4:85-106.

Hunt, G.R., Salisbury, J.W. and Lenhoff, C.J., 1973b. Visible and near-infrared spectra of minerals and rocks: VII. Acidic Igneous rocks. Modern Geology, 4:217-224.

Hunt, G.R., Salisbury, J.W. and Lenhoff, C.J., 1974. Visible and near infrared spectra of minerals and rocks: IX. Basic and Ultrabasic Igneous rocks. Modern Geology, 5:15-22.

Johnson, P.R., 1983. A preliminary lithofacies map of the Saudi Arabian Shield--Explanatory notes. Saudi Arabian Deputy Ministry for Mineral Resources Technical Record RF-TR-03-2.

Kamb, W.B., 1959. Ice petrofabric observations from blue glacier, Washington, in relation to theory and experiment. J. Geophy. Res., V.64:1891-1909.

Karpoff, R., 1957a. Esquisse geologique de l'Arabie Seoudite. Bull. Soc. Geol. France,

6:653-697.

Karpoff, R., 1960. L'Antecambrien de la Peninsule arabique. XXI Int. Geol. Cong. Copenhagen (Norden), part IX:78-94.

Kaufmann, H. and Pfeiffer, B., 1988. Image optimization versus classification-An application oriented comparison of different methods by use of Thematic Mapper data. Photogrammetria, 42:311-324.

Kennedy, W.Q., 1964. The structural differentiation of Africa in the Pan-African (±500 m.y.) tectonic episode. Research Institute of African Geology, Univ. of Leeds, 8th Annual Report:48-49.

Kroner, A., 1985. Ophiolites and the evolution of tectonic boundaries in the late Proterozoic Arabian-Nubian Shield of northeast Africa and Arabia. Precambrian Res., 27:277-300.

Kroner, A., Roobol, M.J., Ramsay, C.R. and Jackson, N.J., 1979. Pan African ages of some gneissic rocks in the Saudi Arabian Shield. J. Geol. Soc. London, 136:455-461.

Loughlin, W.P. and Tawfiq, M.A., 1985. Discrimination of rock types and alteration zones from airborne MSS data: the Samran-Shayban and Mahd Adh-Dhahab areas of Saudi Arabia. Proc. of Int. Symp. on remote sensing of Environment, 4th Thematic Conf., Remote Sensing for Exploration Geology, San Francisco, California.

Mehnert, K.R., 1968. Migmatites and the origin of granitic rocks. Elsevier, Amsterdam.

Moore, G.K. and Waltz, F.A., 1983. Objective procedures for lineament enhancement and extraction. Photogrammetric Engineering and Remote Sensing, 49:641-647.

Moore, J.McM., 1976. A major lineament in the Arabian Shield and its relationship to mineralization. Mineral. Deposita, 11:323-328.

Moore, J.McM., 1979. Tectonics of the Najd transcurrent fault system, Saudi Arabia. J. Geol. Soc. London, 136:441-454.

Moore, J.McM., 1983. Tectonic fabric and structural control of mineralization in the southern Arabian Shield: a compilation based on satellite imagery interpretation. Saudi Arabian Deputy Ministry for Mineral Resources Open-File Report USGS-OF-03-105.

Naseef, A.O. and Gass, I.G., 1980. Arabian Shield granite traverse. Evolution and mineralization of the Arabian-Nubian Shield, King Abdulaziz Univ., Institute of Applied Geology Bull.3, V.4:77-82.

Norman, J.W., 1980a. Second Progress Report on the regional tectonic structure of the cover rocks. Open-File Report CRC-IC2. Ministry of Petroleum and Mineral Resources, Jeddah, Saudi Arabia.

O'Leary, D.W., Friedman, J.D. and Pohn, H.A., 1976. Lineament, linear, lineation: Some proposed new standards for old terms. Geol. Soc. America Bull., 87:1463-1469.

Overstreet, W.C., 1978. A geological and geochemical reconnaissance of the Tathlith one-degree quadrangle, Kingdom of Saudi Arabia. U. S. Geological Survey, Saudi Arabian Project Report 230.

Overstreet, W.C., Stoeser, D.B., Overstreet, E.F. and Goudarzi, G.H., 1977. Tertiary laterite of the As Sarat mountains, Asir province, Kingdom of Saudi Arabia. Saudi Arabian Directorate General of Mineral Resources Bull. 21.

Pallister, J.S., Stacey, J.S., Fischer, L.B. and Premo, W.R., 1987. Precambrian ophiolites of Arabia: a summary of geologic settings, U-Pb geochronology, lead isotope characteristics, and implications for microplate accretion, Kingdom of Saudi Arabia. Saudi Arabian Deputy Ministry for Mineral Resources Open-File Report USGS-OF-07-10.

Pontual, A., 1990. Lithological information in remotely sensed images and surface weathering in arid regions. Unpubl. Ph.D. thesis, The Open Univ.

Potter, R.M. and Rossman, G.R., 1977. Desert varnish: The importance of clay minerals. Science, 196:1446-1448.

Powers, R.W., Ramirez, L.F., Redmond, C.D. and Elberg, E.L., Jr., 1966. Geology of the Arabian Peninsula--sedimentary geology of Saudi Arabia. U. S. Geological Survey Professional Paper 560-D.

Prinz, W.C., 1975. Reconnaissance geology of the Jabal 'Aya quadrangle, Kingdom of Saudi Arabia, with a section on aeromagnetic studies by G.E. Andreasen. Saudi Arabian Directorate General of Mineral Resources Geologic Map GM-17.

Qari, M.Y.H.T., 1985. Structural analysis of the Proterozoic rocks near Janfoor village (northwest of Khamis Mushayt), southern Arabian Shield. Unpubl. M.Sc. thesis, Faculty of Earth Sciences, King Abdulaziz Univ., Jeddah, Saudi Arabia.

Qari, M.Y.H.T., 1989. Lithological mapping and structural analysis of Proterozoic rocks in part of the southern Arabian Shield using Landsat images. Int. J. Remote Sensing, 10:499-503.

Ratte, J.C. and Andreasen, G.E., 1974. Reconnaissance geology and magnetic intensity map of the Jabal Sawdah quadrangle, Kingdom of Saudi Arabia. Saudi Arabian Directorate General of Mineral Resources Geologic Map GM-16.

Richter-Bernburg, G. and Schott, W., 1954. Geological researches in western Saudi Arabia. Saudi Arabian Directorate General of Mineral Resources Open-File Report 38.

Roobol, M.J., Ramsay, C.R., Jackson, N.J. and Darbyshire, D.P.F., 1983. Late Proterozoic lavas of the central Arabian Shield--evolution of an ancient volcanic arc system. J. Geol. Soc. London, 140:185-202.

Rothery, D.A., 1987a. Improved discrimination of rock units using Landsat Thematic Mapper imagery of the Oman ophiolite. J. Geol. Soc. London, 144:587-597.

Rothery, D.A., 1987b. Decorrelation stretching as an aid to image interpretation. Int. J. Remote Sensing, 8:1253-1254.

Rothery, D.A., 1988. MOMS-01 used synergistically with Landsat TM. 4th Int. Symp. on spectral signatures of objects in remote sensing, Aussois, France.

Sabins, F.F., 1978. Remote Sensing Principles and Interpretation, 1st edition. W.H. Freeman & Co., New York.

Sabins, F.F., 1987. Remote Sensing Principles and Interpretation, 2nd edition. W.H. Freeman & Co., New York.

Sable, E.G., 1985. Geologic map of the Najran quadrangle, Sheet 17G, Kingdom of Saudi Arabia. Saudi Arabian Deputy Ministry for Mineral Resources Geoscience Map GM-78A.

Scheibner, E., 1986. A preliminary review of the structural framework of the Arabian Shield. Saudi Arabian Deputy Ministry for Mineral Resources Open-File Report RF-OF-06-19.

Schmidt, D.L. and Brown, G.F., 1982. Major-element chemical evolution of the late Proterozoic shield of Saudi Arabia. Saudi Arabian Deputy Ministry for Mineral Resources Open-File Report USGS-OF-02-88.

Schmidt, D.L., Hadley, D.G., Greenwood, W.R., Gonzalez, L., Coleman, R.G. and Brown, G.F., 1972. Stratigraphy and tectonism of the southern part of the Precambrian shield of Saudi Arabia. U. S. Geological Survey, Saudi Arabian Project Report 139.

Schmidt, D.L., Hadley, D.G., Greenwood, W.R., Gonzalez, L., Coleman, R.G. and Brown, G.F., 1973. Stratigraphy and tectonism of the southern part of the Precambrian shield of Saudi Arabia. Saudi Arabian Directorate General of Mineral Resources Bull. 8.

Schmidt, D.L., Hadley, D.G. and Stoeser, D.B., 1979. Late Proterozoic crustal history of the Arabian Shield, southern Najd province, Kingdom of Saudi Arabia. Evolution and mineralization of the Arabian-Nubian Shield, King Abdulaziz Univ., Institute of Applied Geology Bull.3, V.2:41-58.

Schowengerdt, R.A., 1983. Techniques for Image Processing and Classification in Remote Sensing. Academic Press, Inc., London.

Shackleton, R.M., 1979. Precambrian tectonics of northeast Africa. Evolution and mineralization of the Arabian-Nubian Shield, King Abdulaziz Univ., Institute of Applied Geology Bull.3, V.2:1-5.

Simmons, G.C., 1980. Reconnaissance geology of the Madha quadrangle, Kingdom of Saudi Arabia. Saudi Arabian Directorate General of Mineral Resources Geologic Map GM-55.

Soha, J.M. and Schwartz, A.A., 1978. Multispectral histogram normalization and contrast enhancement. Proc. 5th Canadian Symp. on remote sensing, Victoria, B.C., 86-93.

Stacey, J.S. and Agar, R.A., 1985. U-Pb isotopic evidence for the accretion of a continental microplate in the Zalm region of the Saudi Arabian Shield. J. Geol. Soc. London, 142:1189-1203.

Stacey, J.S. and Hedge, C.E., 1984. Geochronologic and isotopic evidence for early Proterozoic crust in the eastern Arabian Shield. Geology, 12:310-313.

Stacey, J.S. and Stoeser, D.B., 1983. Distribution of oceanic and continental leads in the Arabian-Nubian Shield. Contrib. Mineral. Petrol., 84:91-105.

Stacey, J.S., Roberts, R.J., Doe, B.R., Delevaux, M.H. and Gramlich, J.W., 1981. A lead-isotope study of mineralization in the Saudi Arabian Shield, Contrib. Mineral. Petrol., 74:175-188.

Stoeser, D.B., 1984. Reconnaissance geology of the Wadi Tarib quadrangle, Kingdom of Saudi Arabia. Saudi Arabian Deputy Ministry for Mineral Resources Technical Record USGS-TR-04-4.

Stoeser, D.B. and Camp, V.E., 1985. Pan-African microplate accretion of the Arabian Shield. Geol. Soc. America Bull., 96:817-826.

Stoeser, D.B., Fleck, R.J. and Stacey, J.S., 1982. Geochronology and origin of an early tonalite gneiss of the Wadi Tarib batholith and the formation of syntectonic gneiss complexes in the southeastern Arabian Shield, Kingdom of Saudi Arabia. Saudi Arabian Deputy Ministry for Mineral Resources Open-File Report USGS-OF-02-62.

Stoeser, D.B. and Stacey, J.S., 1988. Evolution, U-Pb geochronology, and isotope geology of the Pan-African Nabitah Orogenic Belt of the Saudi Arabian Shield, Chapter 9. In: El-Gaby and Greiling (eds.), 1988, The Pan-African belt of northeast Africa and adjacent areas. Frieder. Vieweg & Sohn, Braunschweig/Wiesbaden. 227-288.

Stoeser, D.B., Stacey, J.S., Greenwood, W.R. and Fisher, L.B., 1984. U/Pb zircon geochronology of the southern part of the Nabitah mobile belt and Pan-African continental collision in the Saudi Arabian Shield. Saudi Arabian Deputy Ministry for Mineral Resources Technical Record USGS-TR-04-5.

Sultan, M., Arvidson, R.E., Duncan, I.J., Stern, R.J. and El-Kaliouby, B., 1988. Extension of the Najd shear system from Saudi Arabia to the central eastern desert of Egypt based on integrated field and Landsat observations. Tectonics, 7:1291-1306.

Sultan, M., Arvidson, R.E., Sturchio, N.C. and Guinness, E.A., 1987. Lithologic mapping in arid regions with Landsat thematic mapper data: Meatiq dome, Egypt. Geol. Soc. America Bull., 99:748-762.

Vail, J.R., 1985. Pan-African (late Precambrian) tectonic terrains and the reconstruction of the Arabian-Nubian Shield. Geology, 13:839-842.

von-Gartner, H.R. and Schurenberg, H., 1954. Geological researches in western Saudi Arabia. Saudi Arabian Directorate General of Mineral Resources Open-File Report 40.

Warden, A.J., 1982. Reconnaissance geology of the Markas quadrangle, Kingdom of Saudi Arabia. Saudi Arabian Deputy Ministry for Mineral Resources Open-File Report USGS-OF-02-41.

APPENDIX   A

PREPARATION OF ORIENTATION-DENSITY DIAGRAMS, After Kamb (1959)

The primary question in interpreting any fabric diagram is whether or not the diagram shows statistically significant preferred orientation. Statistical methods of testing significance of preferred orientation have been discussed by Chayes (1949) and Flinn (1958). However, instead of using numerical methods, Kamb has taken a simpler and more graphic approach that utilizes the orientation-density diagram to exhibit directly the statistical significance of the data. The density diagram is treated not simply as a means of portraying the original orientation data, as is done in conventional contouring procedures (Fairbairn, 1949, pp. 285-290). Instead, the actual data are presented as scatter diagrams, which contain the information that would be needed for a statistical test by numerical methods, and the density diagrams are prepared in such a way as to abstract from the scatter diagrams the orientation information that is of statistical significance.

The measure of statistical significance is the probability that the observed orientation density could have resulted from random sampling of a population that lacks preferred orientation. To control this probability, the area A of the conventional (Schmidt) contouring procedure is so chosen that, if the population lacks preferred orientation, the number of points E expected to fall within a given area A is three times the standard deviation of the number of points n that will actually fall within the area under random sampling of the population. This insures that the observed orientation densities, if obtained by random sampling of a non-preferentially oriented population, will not fluctuate wildly from the expected density E/A. Observed densities that differ from E/A by more than two or three times the standard deviation σ (for random orientation) are then likely to be significant, and the more so if the significantly higher densities are clustered in one portion of the diagram. The observed densities are therefore contoured in intervals 2σ, at the values 0, 2σ, 4σ, etc., the expected density E for no preferred orientation being 3σ.

For a given area A, expressed as its fraction of the area of the hemisphere, the distribution of n values for random samples of size N is binomial, and for a population without preferred orientation Kamb found

$$\sigma/E = (1-A)/N \ A$$

where $E=NA$.

Setting $\sigma/E = 1/3$, the appropriate area A of the counter to be used in preparing the density diagram is computed for a given fabric with N points. The pertinent values accompany each density diagram presented.

Diagrams prepared in this way have a considerably smoothed appearance in comparison with conventional density diagrams. This is because most of the irregular detail visible in conventional diagrams is of no statistical significance, the conventional choice $A=0.01$ being usually much too small. With the choice of A used, the difference between the Schmidt and Mellis contouring methods (Flinn, 1958) can lead to no statistically significant differences in the positions of contours and may therefore be disregarded; the Schmidt method is, of course, much easier to use.

APPENDIX   B

THREE-STEP PROCEDURE

At a late stage in this work, analysis of the edge enhancement techniques showed that the result of:

(a) adding the three filters used in the edge enhancement techniques before doing the filtering and deriving a directional component from original TM band 5 or MSS band 4,

is the same as

(b) adding the three filtered images (which was the procedure used throughout this study). The following three-step procedure should be applied instead.

Step 1:   Derive directional component from original TM band 5 or MSS band 4. Each pixel in the window is multiplied by the digital value, the final value for the central pixel being the sum of these products.

3	3	3
1	-6	1
-1	-3	-1

Step 2:   Apply linear stretching (scaling) to the resultant directionally derived component (filtered image). Scaling is a procedure where the lowest digital value is set at 0, and the highest at 255, all intermediate values being distributed through this range.

Step 3:   Superimpose (add) directional component of Step 2 on the original TM band 5 or MSS band 4 image for display and interpretation.

APPENDIX   C

PUBLISHED WORK

UTILIZATION OF REMOTE SENSING TECHNOLOGY IN GEOLOGICAL MAPPING - A CASE STUDY IN PART OF 'ASIR', SOUTHERN ARABIAN SHIELD*

MOHAMMED YOUSEF H. T. QARI**
DEPT. OF GEOLOGICAL SCIENCES, UNIV. COLLEGE LONDON,
GOWER ST., LONDON WC1E 6BT, ENGLAND.

ABSTRACT

The Landsat Thematic Mapper (TM) scanner records six bands of reflected visible and infrared spectrum and one thermal infrared band, the data from which are available in photographic and digital form. A study area of 225 km^2 in the southern Arabian Shield, was selected to demonstrate the utility of the Landsat TM sensor digital imagery for lithological mapping and structural analysis. The selected area is complex due to poly-phase deformation, which has resulted in interference fold patterns and faulting. The major lithologies are: granites, gneisses, metasediments, metavolcanics, and gabbroic rocks.

Several image processing techniques were applied to the TM data, following which visual interpretations and map constructions were performed employing the resulting images. These processing techniques included: band ratioing, decorrelation stretching, and edge enhancement. The results demonstrate that TM data can be used for lithological mapping and structural analysis in well exposed arid regions, and to generate detailed geological maps over large areas by using quantitative remote sensing methods, where prior knowledge is available for part of the area.

Lithological mapping and structural analysis of Proterozoic rocks in part of the southern Arabian Shield using Landsat images

MOHAMMED YOUSEF H. T. QARI

Department of Geological Sciences, University College London,
Gower Street, London WC1E 6BT, England

Abstract. The geology of a structurally complex part of the Arabian Shield which has been subjected to four successive phases of deformation over a considerable period of time, has been extended by Landsat image analysis. The lithologies are Proterozoic metavolcanics, metasediments, gneisses and granites. Their macroscopic structures, identified on the ground by traditional geological mapping methods, have been extrapolated and hence new information about the regional tectonics has been obtained. Thus the use of multispectral satellite sensor image data has proved to be an excellent tool for geological mapping on a regional scale in crystalline basement terrains.

1. Introduction

Structural analysis and ground-based geological mapping of the area (figure 1), was originally carried on in partial fulfilment on an M.Sc. degree in structural Geology (Qari 1985). The area of this primary mapping is composed of Proterozoic metavolcanics, metasediments, gneisses and granites. These rocks were regionally metamorphosed under low to medium amphibolite facies conditions. They are part of
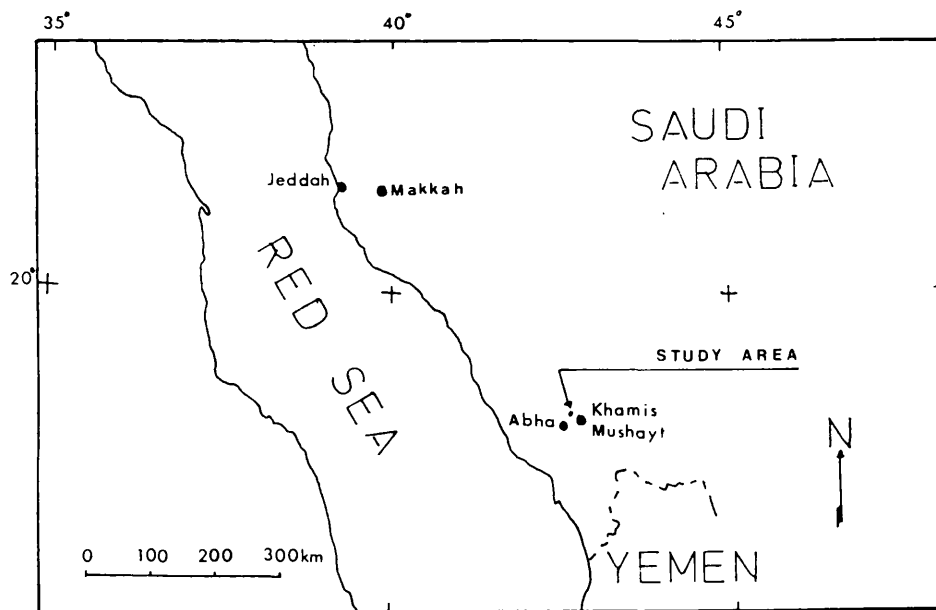

Figure 1. Location map of the study area.

the Precambrian of the southern Arabian Shield which has been divided into a number of stratigraphic units, based on lithology, degree of metamorphism and structural complexity (Schmidt *et al.* 1973). These units are intruded by mafic to felsic igneous rocks and are unconformably overlain by Ordovician sedimentary rocks.

2. Lithology

The area consists almost exclusively of metamorphic rocks which are intruded by various igneous bodies. The outcrop patterns of these rocks are complex because of the repeated folding which affected them. Based on field relationships and structural character, the following major lithological units could be delineated, numbered from youngest to oldest (Qari 1985): (1) dykes, (2) granites, (3) migmatites, (4) granitic gniess, (5) metasediments and (6) metavolcanics.

The metavolcanic rocks are composed of amphibolites, which occur as bands extending for several kilometres and are the most widespread rock types in the area. The finer grained metasedimentary rocks are composed of semi-pelitic schist, quartz-hornblende schist and quartz-muscovite schist. The contact between the metasediments and the metavolcanics is conformable. The granitic gneiss, which is locally migmatitic, has an intrusive relationship with the metavolcanic and metasedimentary units, as it contains xenoliths of amphibolite and semi-pelitic schist. Two types of granite are present; syn- and post-tectonic granites. Numerous dykes cut the metamorphic rocks, including pegmatites, granitic dykes and quartz veins. The age of the metamorphic rocks is considered to be Precambrian (Coleman 1973 b).

3. Structures

The metamorphic rocks in the study area are affected by four phases of deformation, D1, D2, D3 and D4, which produced F1, F2, F3 and F4 folds, S1, S2, S3 and S4 foliations and L1, L2, L3 and L4 lineations, respectively.

All the rock units exhibit well developed S1 to S2 foliation. Two large-scale F2 folds have been identified. They are tight to isoclinal, and could be extended in the northern and southern part of the study area. The D3 structures are the most prominent and widespread throughout the entire area. F3 folds are found on meso and macro scales in the form of open to tight asymmetrical folds with steep, N–S axial planes. The D4 structures, of lesser significance, occur as open warps observed on the meso and macro scales, with sub-vertical axial planes striking in an E–W directions. The last two phases of deformation (D3 and D4) define the outcrop patterns observed in the area. Since folding there has been some faulting.

Major and minor interference structures have been formed by the four phases of deformation. It is probable that the four deformational phases occured successively during one tectonic cycle, because all the lithologies were affected by all four phases and unconformities between lithological units are absent within the area (Qari 1985).

4. Remote sensing study

It is well established that interactive digital image processing can augment and complement traditional field techniques in geological mapping in arid regions (e.g. Blodget and Brown 1982, Loughlin and Tawfiq 1985, Rothery 1987, Sultan *et al.* 1986, 1987).

A Landsat-5 Thematic Mapper (TM) band 4. 3. 2–red, green, blue, standard false-colour composite image of a part of the southern Arabian Shield was acquired on 2 February 1987 (Path 167, Row 047). The delineation and extraction of relevant
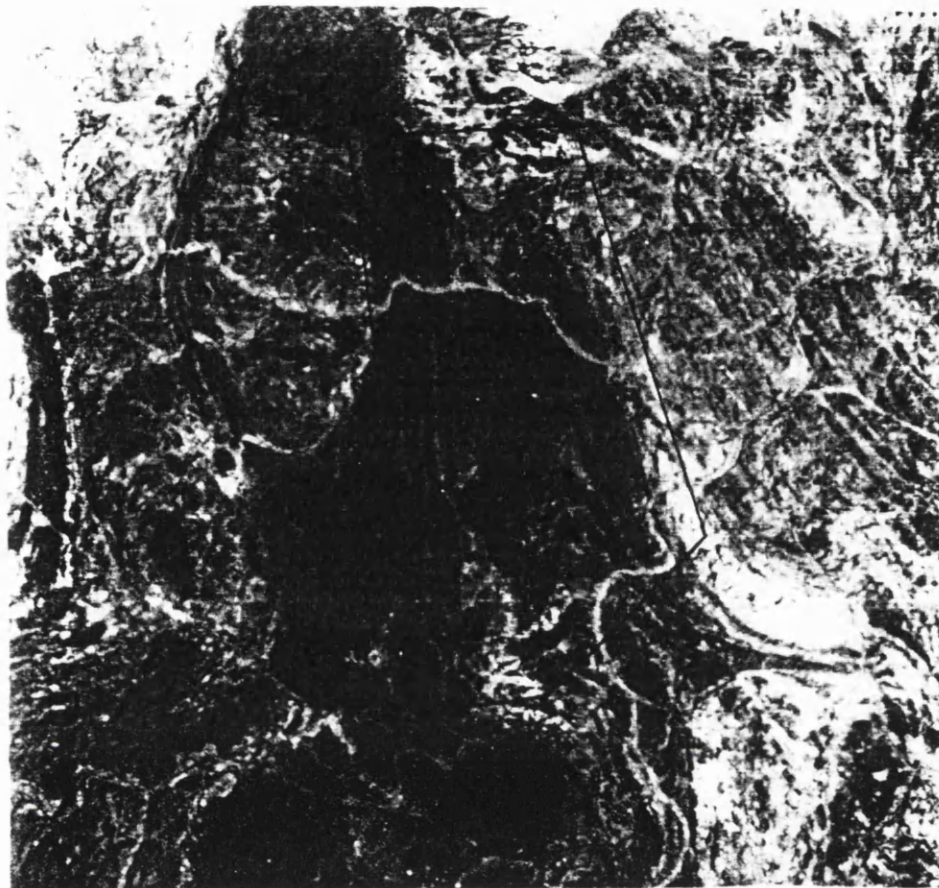
Figure 2.   1:125 000-scale enlargement of the study area.

information from the image data through human visual analysis was carried out on a 1 : 125 000 scale enlarged print (figure 2) for the study area only. The methodology used was akin to photogeological interpretation.

It was found that amphibolites and metasediments could be mapped on the basis of their chracteristic tonal characters, the darker tones indicating the amphibolites. Similar mineralogical granitoid rocks could be mapped as a group, depending on their tonal and fracturing character, but they could only be subdivided by using the ground field survey results (Qari 1985). The boundaries between these units were easily located.

The F2, F3 and F4 phases of folding were clearly detectable in the interference folding patterns visible in the TM imagery. Two F2 antiformal fold axial traces (figure 3, sections D2 and F8), and several F3 antiformal and synformal fold axial traces were extended throughout the entire area. The F3 traces strike approximately N–S. Five F4 fold axial traces, striking E–W, were detected in the western part of the study area. F2 and F3 axial traces were more easily located than F4, which was the lesser significance phase of deformation (Qari 1985). F1, F2, F3 and F4 micro and meso scale folds were not detectable or extendable on TM imagery because their wavelengths are less than the resolution of the image. The criteria on which these

502

Legend

Wadi with alluvium	
Granitic rock	
Foliated granite	
Granitic gneiss	
Amphibolites	
Metasediments	
Amphibolites intercalated with metasedimentary rocks	
Lithological contact	
Fault	
Strike and dip direction of foliation	
F2 Antiform	
F3 Antiform	
F3 Synform	
F4 Antiform	
F4 Synform	

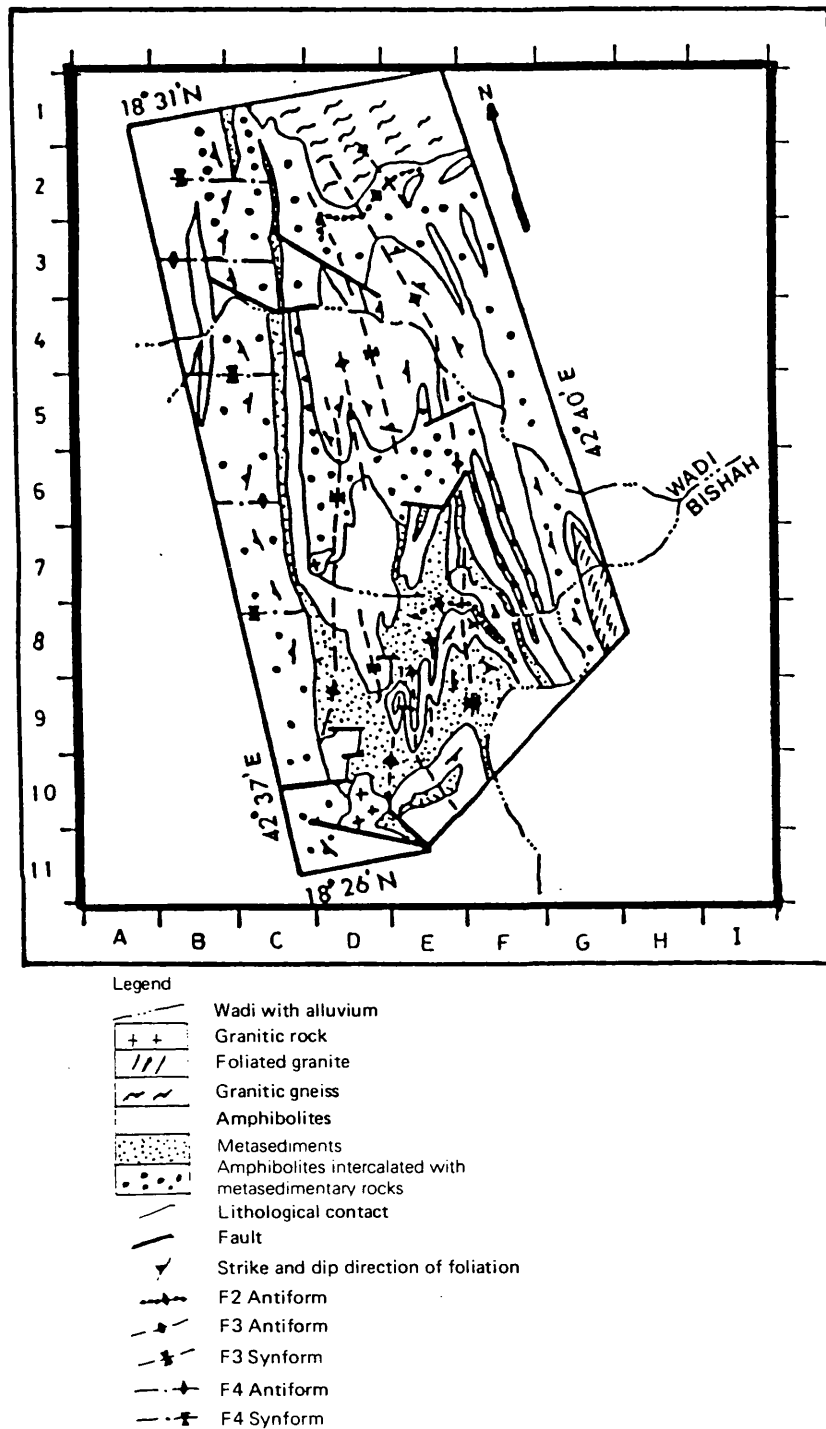Figure 3. Geological and structural map of the study area.

folds and their axial traces were studied is based on the change of the geometry of the rock units' banding (foliation planes). The resulting geological and tectonic map is presented in figure 3. This simple method can be applied to portray and construct quickly geological and tectonic maps of large areas of the well exposed Arabian Shield and comparable areas.

5. Conclusion

Lithological mapping as well as structural analysis has been conducted effectively on metamorphic rocks with polyphase deformation patterns in this part of the Arabian Shield, using a simple image interpretation technique, human visual analysis. This technique has considerable potential for supplementing and extending ground-based geological surveys in Precambrian gneiss terrains, if *a priori* knowledge is provided for such rugged terrains and a selection of appropriate false-colour composites were envisaged.

Acknowledgments

References

BLODGET, H. W., and BROWN, G. F., 1982, Geological mapping by use of computer enhanced imagery in western Saudi Arabia. United States Geological Survey Professional Paper No. 1153, U.S. Geological Survey, Washington, D.C., U.S.A.

COLEMAN, R. G., 1973, Reconnaissance geology of the Khamis Mushayt quadrangle, Kingdom of Saudi Arabia: Saudi Arabian Directorate General of Mineral Resources Geologic Map GM-5. Ministry of Petroleum and Mineral Resources, Jeddah, Kingdom of Saudi Arabia.

LOUGHLIN, W. P., and TAWFIQ, M. A., 1985, Discrimination of rock types and alteration zones from airborne MSS data: the Samran-Shayban and Mahd Adh-Dhahab areas of Saudi Arabia. *Proceedings of the International Symposium on Remote Sensing of Environment, 4th Thematic Conference, Remote Sensing for Exploration Geology, held in San Francisco, California, in 1985.* (Ann Arbor: Environmental Research Institute of Michigan).

QARI, M. Y. H. T., 1985, Structural analysis of the Proterozoic rocks near Janfoor village (northwest of Khamis Mushayt), southern Arabian Shield. M.Sc. thesis, Faculty of Earth Sciences, King Abdulaziz University, Jeddah, Kingdom of Saudi Arabia.

ROTHERY, D. A., 1987, Improved discrimination of rock units using Landsat Thematic Mapper imagery of the Oman ophiolite. *Journal of the Geological Society of London,* **144,** 587–597.

SCHMIDT, D. L., HADLEY, D. G., GREENWOOD, W. R., GONZALEZ, L., COLEMAN, R. G., and BROWN, G. F., 1973, Stratigraphy and tectonism of the southern part of the Pre-cambrian Shield of Saudi Arabia. *Saudi Arabian Directorate General of Mineral Resources, Bulletin,* No. 8, (Jeddah, Kingdom of Saudi Arabia: Ministry of Petroleum and Mineral Resources).

SULTAN, M., ARVIDSON, R., and STURCHIO, N. C., 1986. Mapping of serpentinites using Landsat thematic mapper data in the Eastern Desert of Egypt. *Geology,* 14, 995–999.

SULTAN, M., ARVIDSON, R., STURCHIO, N. C., and GUINNESS, E. A., 1987, Lithologic mapping in arid regions with Landsat thematic mapper data: Meatiq dome, Egypt. *Geological Society of America Bulletin,* **99,** 748–762.

APPLICATION OF LANDSAT TM DATA TO LITHOLOGICAL AND LINEAMENT STUDIES, SOUTHERN ARABIAN SHIELD.

Mohammed Yousef H. T. Qari

Dept. of Geological Sciences. Univ. College London
Gower Street, London WC1E 6BT, England.

A test-area of 512x512 picture-elements, corresponding to 225 square kilometres within the Nabitah Mobile Belt, southern Arabian Shield, was selected for the application of full-resolution LANDSAT Thematic Mapper (TM) data to lithological and lineament studies. The area was selected because of the interesting structural character, diverse lithologies and history of igneous activity. The major lithologies are volcanic rocks, layered metamorphic rocks and plutonic rocks. Most of these rocks are of late Proterozoic age. The outcrop pattern in the area is complex due to multiple episodes of folding and faulting.

The volcanic rocks are located in the west of the area above tonalite gneiss. They are Tertiary alkali-olivine basalt flows of the As-Sarat mountains. The base of the basalt sequence is marked by a well-developed sub-lateritic paleosol. The Precambrian layered metamorphic rocks are well-foliated metavolcanic and metasedimentary rocks assigned to the Halaban Group, and they occur between and/or within the plutonic rocks. The plutonic rocks include granite, tonalite and gneiss. A major group of right-lateral east-west trending faults were mapped, commonly having mafic dyke rocks emplaced along portions of their length.

Several techniques of image processing were applied, visual interpretations were made and several different types of geological map were constructed. Image processing techniques included Principal Component Analysis (PCA), Decorrelation Stretching and Edge Enhancement. TM bands 7,5, and 4 were selected for the application of PCA and also used to produce images of both Principal Component and Decorrelation Stretching techniques. Edge Enhancement was achieved by high-pass filtering of the TM band 5 following a three-step procedure involving filtering and addition of images. Lithological contacts were easily detected on colour composites produced by Principal Component and Decorrelation Stretching techniques. Structural syntheses have been incorporated in maps. Several concentrations of lineament orientations are shown on a directional frequency rose diagram. These principal concentrations are in the E-W, NE-SW and NW-SE directions. The resulting interpretations were checked by geological field-work in the test-area.

Results show that TM data can be used reliably for lithological and lineament studies in well exposed arid regions. The combination of image processing techniques and fieldwork permits the construction of geological maps for this region of much greater accuracy and with greater detail than those previously published. Geological understanding of the complex evolution of the Arabian Shield will be much improved by employing remote sensing techniques and will allow much faster and accurate geological assessment of this vast region.

In Press in:

PHOTOGRAMMETRIC ENGINEERING AND REMOTE SENSING

MOHAMMED YOUSEF H. T. QARI[*]

DEPT. OF GEOLOGICAL SCIENCES, UNIVERSITY COLLEGE LONDON,

GOWER STREET, LONDON WC1E 6BT, U.K.

APPLICATION OF LANDSAT TM DATA TO GEOLOGICAL STUDIES,

AL-KHABT AREA, SOUTHERN ARABIAN SHIELD

[*]Permanent address: Faculty of Earth Sciences, King Abdulaziz University, P.O.Box
1744, Jeddah 21441, Saudi Arabia.

ABSTRACT

Al-Khabt test-area of 225 km² within the Nabitah Mobile Belt, southern Arabian Shield, was selected for application of Landsat TM data to geological studies. The major lithologies are granites, metavolcanics, metasediments, and mafic dyke rocks. Most of these rocks are of late Proterozoic age. The outcrop pattern in the area is complex due to multiple episodes of folding and faulting.

The geology of a structurally complex area which has been subjected to at least three phases of deformation, has been extended by applying various image processing techniques. Visual interpretations were made and several different types of geological maps were constructed. Image processing techniques included principal components analysis, decorrelation stretching, and edge enhancement. Lineament analysis revealed directions which can be related to regional tectonics of the Arabian Shield. The resulting interpretations were checked by geological fieldwork in the test-area.

Geological understanding of the complex evolution of the Arabian Shield will be much improved by employing remote sensing techniques and will allow much faster and accurate geological assessment of this vast region.

1) STUDY AREA

The study area (Fig. 1) of 225 km² is located to the east of Abha city in the southern Arabian Shield. It was selected to test the utility of the Landsat Thematic Mapper (TM) sensor digital imagery to lithological and structural studies. The area has excellent exposure of a diverse suite of igneous and metamorphic rocks.

2) GEOLOGICAL SETTING

The exposed outcrop pattern of the area is complex due to folding, intense faulting and intrusions. The major lithologies are Tertiary volcanic rocks, and Precambrian metamorphic and plutonic rocks. The area was mapped by Stoeser (1984) and an extract from this map, covering the study area, is shown in Figure 2.

The volcanic rocks are situated in the west of the area overlying the Suwaydah tonalite gneiss. They are Tertiary alkali-olivine basalt flows of the As-Sarat mountains. The base of the basalt sequence is marked by a well-developed sub-lateritic paleosol. The metamorphic rocks occupy a small area and are well-foliated Upper Proterozoic metasedimentary rocks assigned to the Halaban Group. The plutonic rocks include granite, tonalite, gneiss, and gabbro.

A major group of east-west striking faults is shown on this map, and individual faults extend in some cases for distances over 20 km. These are mostly right-lateral strike-slip faults and commonly have mafic dykes emplaced along portions of their length. The dykes are fine grained hornblende dolerites (Stoeser, 1984).

3) LANDSAT DIGITAL DATA ANALYSIS AND RESULTS

The TM scanner records six band of reflected visible and infrared light (0.45 - 2.35 µm), each picture element (pixel) measuring 30mx30m on the ground, plus one thermal infrared band (10.4 - 12.5 µm), 120mx120m on the ground. A Landsat TM scanner image from the Arabian winter season (1 Mar 1984, Path 167, Row 047) was obtained for the purpose of the present study, with a sun elevation angle of 57° and a sun azimuth angle of 101°. The sub-scene (Fig. 3A) for the selected test-area is 512x512 pixels in size, which is approximately 15x15 kilometres.

The spectral distribution of reflected sunlight from an earth material, when represented as a tone or colour in image, is invaluable for geological interpretations. The sub-scene

was analyzed using various image processing techniques which included principal components analysis, decorrelation stretching, and edge enhancement. Visual interpretations were made and several different types of geological maps were constructed. Subsequently, two-days fieldwork was carried out in the test-area to measure geological elements, characterize mapped contacts and different lithologies.

(a) Principal components analysis

Principal components analysis (PCA) is used in various applications including remote sensing (e.g. Blodget et al., 1978). Typically, for any pixel in a multispectral original image, the brightness values or Digital Numbers (DN's), are highly correlated from band to band, so that there is much redundancy in the data set.

PCA is used to compress multichannel image data by calculating a new coordinate system, so as to condense the scene variance in the original data into a new set of variables which are called principal components (PC's). These data are decorrelated and most of the image variance is confined within the first few channels. In this study, after transformation, the data were scaled or linearly contrast stretched. This procedure increases the spectral discrimination capability among terrestrial materials.

PCA of the Landsat TM data for the Al-Khabt test-area was applied on the six non-thermal bands (7,5,4,3,2, and 1), and a set of three-band PC colour composites was created. Visual inspection of the PC colour composites indicated that the composite containing the first 3 PCs was the most informative. This is shown with (-PC1)=red, (-PC2)=green, and (-PC3)=blue in Figure 3B.

The basaltic rocks in the southwestern corner of the test-area display red hues, due to high albedo in the (-PC1) image (section A8, Fig. 3B). Since these rocks are the extension of the basaltic flows of the As-Sarat volcanic field (located to the west outside the test-area, and is high in elevation), the material transported to most of the wadis in the test-area is of basaltic composition and is displayed as a red colour filling these wadis (e.g. sections A4, B7 and G7, Fig. 3B). Where the alluvium in the wadis is not of basaltic composition, the colour is not red (e.g. sections E2, G6 and I2, Fig. 3B). Obvious contacts were detected on the (-PC) colour composite image between most of the lithologies, such as the Hadabah dome granodioritic gneiss, the layered metamorphic rocks, and the northern granitic unit. The layered metamorphic rocks (LMR) were identified in the (-PC) colour composite as yellow hues, particularly in the eastern flank of the Al-Khabt synformal phacolith (e.g. sections G8 and H8, Fig. 3B). These LMR also appear in the eastern part of the Hadabah dome and in the southwestern corner of the area next to the basaltic rocks (section C8, Fig. 3B). Small patches of these LMR are easily distinguished within the northern granitic unit as yellow patches in pinkish colour (granite). The granitoid rocks in the test-area, which include granites, tonalites, granodiorite-, and tonalite-gneisses can be distinguished as two groups. The granodioritic composition (Hadabah dome and Al-Khabt synformal phacolith) display a blue colour, while the other group which displays pink hues includes the northern granite, Suwaydah tonalite gneiss, and mafic tonalites. The mafic dyke rocks filling the E-W faults are also identifiable as red colours cutting through the blue and pink colours of assorted lithologies, particularly in the Al-Khabt phacolith (e.g. sections D4 and F6, Fig. 3B). Because the Al-Khabt synformal phacolith granodioritic gneiss includes tonalite gneiss, it also can be distinguished on the (-PC) colour composite as a pink colour (section F3, Fig. 3B).

(b) Decorrelation stretching

Another way of emphasizing spectral information in an image is decorrelation stretching (DS). DS serves to exaggerate colour differences which may be very subtle in the raw

or scaled colour composite. Generally, colour saturation is increased, without significant distortion of the hue.

The DS transformation involves using the original eigen vector matrix of the PCA in order to create a DS image by transformation of the PC's back to the domain of the original variables. Displaying the manipulated variables in red, green, and blue colour space retains the colour appearance of the original 3-channel false colour image and the useful topographic information (e.g. Gillespie et al., 1986; Rothery, 1987).

The TM band 7,5,4 red, green, and blue DS colour composite image of the Al-Khabt test-area is shown in Figure 3C. The basaltic rocks in the southwestern corner of the test-area display blue hues (section A8, Fig. 3C), which should not be confused with the blue colour along some wadis which are material transported from the As-Sarat volcanic flow to the west of the test-area. The sub-lateritic paleosol is easily identifiable in the DS colour composite as light-blue colour rims of the basaltic rocks (e.g. section B8, Fig. 3C). The granitoid rocks are shown mostly in bright-white hues mixed with a brown colour, although one can distinguish the Hadabah dome- and the Al-Khabt synformal phacolitic-granodioritic gneisses from other granitoid lithologies. The layered metamorphic rocks are not as easily identifiable as in the (-PC) colour composite, though brownish in colour (e.g. section G8, Fig. 3C). The mafic dyke rocks which intrude the E-W faults are also very distinctive (e.g. sections G6 and H4, Fig. 3C).

A detailed geological map of the Al-Khabt test-area was constructed (Fig. 4) from the DS colour composite taking advantage also of information from principal components analysis composite image. Field observations were used extensively to supplement remote sensing interpretations, particularly in the northern granitic unit. Comparing with the geological information contained in the earlier map (Fig. 2), it is clear that although there is a good correspondence between the two maps, there is more detail in the TM-based map. The area which was mapped as Al Fayd tonalite in the previous map can be resolved into two lithologies, which are the Al Fayd tonalite and the northern granitic unit. In addition, the schistose rocks were mapped easily within the granitic unit in the NE quarter of the map (Fig. 4).

The Al Fayd tonalite and the northern granitic unit are showing as greenish and pinkish hues in the (-PC) composite image, respectively. In the field, the tonalite is gneissose uniform body rich in hornblende and light- to medium-grey in colour, whereas granite is rich in biotite and pinkish in colour. The tonalite is locally migmatised near the contact with the granite.

(c) Edge enhancement

Edge enhancement was achieved by high-pass filtering, emphasizing higher spatial frequencies, using a convolution operation to increase lineament contrast. TM band 5 (1.55-1.75 μm) was selected, and a simple unsymmetrical weighted kernel of size 3x3 pixels was applied. The resultant filtered image is shown in Figure 3D, which allowed the drawing of the lineaments or fractures. However, an even better image was obtained by adding this scaled image to the original TM band 5 image which is shown in Figure 5.

The lineaments were identified by visual inspection and recorded on transparent overlay as ruled lines. A remotely sensed lineament map was constructed (Fig. 6) based on the total knowledge compiled from edge enhancement, principal components, and decorrelation stretched images together with ground study. In identifying lineaments, what remains relatively constant represents the azimuth and the length of a line rather than its precise location. The fracture map shows that lineament frequency is generally

constant within the test-area. The significance of the interpreted lineaments was analyzed using histograms (Fig. 7). Figure 7A shows strike-frequency distribution and length of lineaments in the test-area. There is a single dominant preferred orientation of lineaments in the west direction, however, there are general concentrations at NW-SE and ENE-WSW directions. There is a good correspondence between the length of these lineaments and their distribution, but when both distribution and length were plotted to percentage (Fig. 7B), one can compare the distribution of lineaments with their length, except in the west direction where length of lineaments is much higher which represents the long faults which were filled with mafic dyke rocks in the test-area. Frequency and length of these lineaments were plotted against each other, the scatter of points is confined to the lower diagonal half of the diagram (Fig. 8), though a positive good correlation is obtainable.

The lineaments shown on Figure 6 were counted on a 2.5x2.5 km grid and the total density contoured (Fig. 9) to examine the pattern of concentration. The number of lineaments/6.25 km^2 varies from 3 to 21. Several concentrations of lineaments are quite apparent throughout test-area, particularly in the Al-Khabt synformal phacolith area.

Comparison of observed lineaments with previously mapped features showed that many of them coincide with mapped faults. However, about 60% correspond to joint sets that have not previously been mapped in ground surveys.

4) STRUCTURES

An attempt to construct a structural map (Fig. 10) was based on colour composites, field studies, correlation with detailed ground studies of comparable areas (Amlas, 1983; Qari, 1985), and the available work of Stoeser (1984).

As in other regions nearby (Amlas, 1983; Qari, 1985 and 1989), all rock units and in particular the layered metamorphic rocks exhibit well developed S_1 to S_2 foliation. This axial planar foliation is strongly developed fabric and easily distinguishable as schistosity or fracture cleavage across minor F_2 fold hinges. The foliation is broadly parallel to the contacts between the lithologies throughout the test-area. This foliation is almost parallel to S_1 foliation and thus difficult to distinguish from S_1 foliation. The S_2 foliation generally strikes between north and northeast and it is folded around the hinges of later fold generations.

The F_2 folds present in the limbs of the F_3 major folds, particularly in the layered metamorphic rocks in the SE quarter of the test-area. The F_2 phase is represented by tight, upright asymmetrical folds where the axial planes are parallel to the S_2 foliation.

F_3 folds are the most dominant and widespread structures and defining the major structures of Al-Khabt test-area. This phase is found as tight- to open-asymmetrical folds with variable geometry. Three major antiforms and synforms with steep, generally N-S axial planes, and plunging towards south in the test-area are assigned to F_3 folds (Fig. 10). The Hadabah dome is the result of two antiforms found plunging in opposite directions. Linear structures associated with F_3 folding were observed around the hinge of Al Khabt synform as strong mineral lineation in the schistose rocks trending mostly towards south with low to moderate plunges, which is in correspondence with the plunge of the synform.

Faults are very prominent in the Al-Khabt test-area. They are easily detectable on the colour composites. Most of these E-W faults are right-lateral strike-slip faults intruded by mafic dyke rocks. Some of these faults can be traced into the Tertiary As-Sarat volcanic field which suggests that they may have been rejuvenated during the Tertiary

(Stoeser, 1984).

5) <u>CONCLUSIONS</u>

The Al-Khabt test-area within the southern Arabian Shield was selected for the evaluation of the Landsat TM data for geological studies. Principal components analysis, decorrelation stretching, and edge enhancement techniques were used for mapping different lithologies and for the structural analysis of this rugged terrain. Sharp lithological boundaries based on colour composites were easily detectable which was checked by fieldwork, and hence utilized in preparing the geological map of the test-area.

At least three phases of deformation (D_1, D_2, and D_3) have affected the area, however, the dominant and major structures in the test-area are the D_3 structures. This third phase of folding is asymmetrical, tight-to-open, and plunging generally towards south. L_3 lineation is developed, in general, parallel to the fold axes of F_3. Faulting is also very prominent.

Quantitative examination of the lineaments showed that the test-area has several significant preferred directions, these are E-W, NW-SE, and ENE-WSW. Length of these lineaments is comparable with their distribution, except in the west direction where it is reflecting the obvious long E-W faults filled with mafic dyke rocks.

The NW-SE direction is proposed to be part of the Najd fault system which had affected the Arabian Shield at about 530-630 Ma (Moore, 1979), whereas the E-W direction is conformable with the older east-trending tectonic fabric in the tectonically more complex and possibly older parts of the shield which was postulated by Moore (1983). The general NE-SW or ENE-WSW direction is postulated to be the youngest, possibly the extension of transform faults identified in the Red Sea by several geophysical surveys (ARGAS, 1977), or the signature of a conjugate set of fractures developed at the same time with the Najd system.

Results show that TM data can be used reliably for lithological and structural studies in well exposed arid regions. The combination of image processing techniques and fieldwork permits the construction of better geological maps.

References

Amlas, M.M.A., 1983. Geology and structures of the Precambrian rocks north of Khamis Mushayt, southern Arabian Shield. M.Sc. thesis, Faculty of Earth Sciences, King Abdulaziz Univ., Jeddah, Saudi Arabia.

ARGAS, 1977. Geophysical synthesis report, eastern part of the Central Red Sea. Saudi-Sudanese Commission for the Exploitation of the Red Sea Resources.

Blodget, H.W., F.J. Gunther, and M.H. Podwysocki, 1978. Discrimination of rock classes and alteration products in southwestern Saudi Arabia with computer-enhanced Landsat data. NASA Technical Paper 1327.

Gillespie, A.R., A.B. Kahle, and R.E. Walker, 1986. Color enhancement of highly correlated images. I. Decorrelation and HSI contrast stretches. Remote Sensing of Environment, 20:209-235.

Moore, J.M., 1979. Tectonics of the Najd transcurrent fault system, Saudi Arabia. J. Geol. Soc. London, 136:441-454.

Moore, J.M., 1983. Tectonic fabric and structural control of mineralization in the southern Arabian Shield: a compilation based on satellite imagery interpretation. Saudi Arabian Deputy Ministry for Mineral Resources Open-File Report USGS-OF-03-105.

Qari, M.Y.H.T., 1985. Structural analysis of the Proterozoic rocks near Janfoor village (northwest of Khamis Mushayt), southern Arabian Shield. M.Sc. thesis, Faculty of Earth Sciences, King Abdulaziz Univ., Jeddah, Saudi Arabia.

Qari, M.Y.H.T., 1989. Lithological mapping and structural analysis of Proterozoic rocks in part of the southern Arabian Shield using Landsat images. Int. J. Remote Sensing, 10:499-503.

Rothery, D.A., 1987. Improved discrimination of rock units using Landsat Thematic Mapper imagery of the Oman ophiolite. J. Geol. Soc. London, 144:587-597.

Stoeser, D.B., 1984. Reconnaissance geology of the Wadi Tarib quadrangle, Kingdom of Saudi Arabia. Saudi Arabian Deputy Ministry for Mineral Resources Technical Record USGS-TR-04-4.
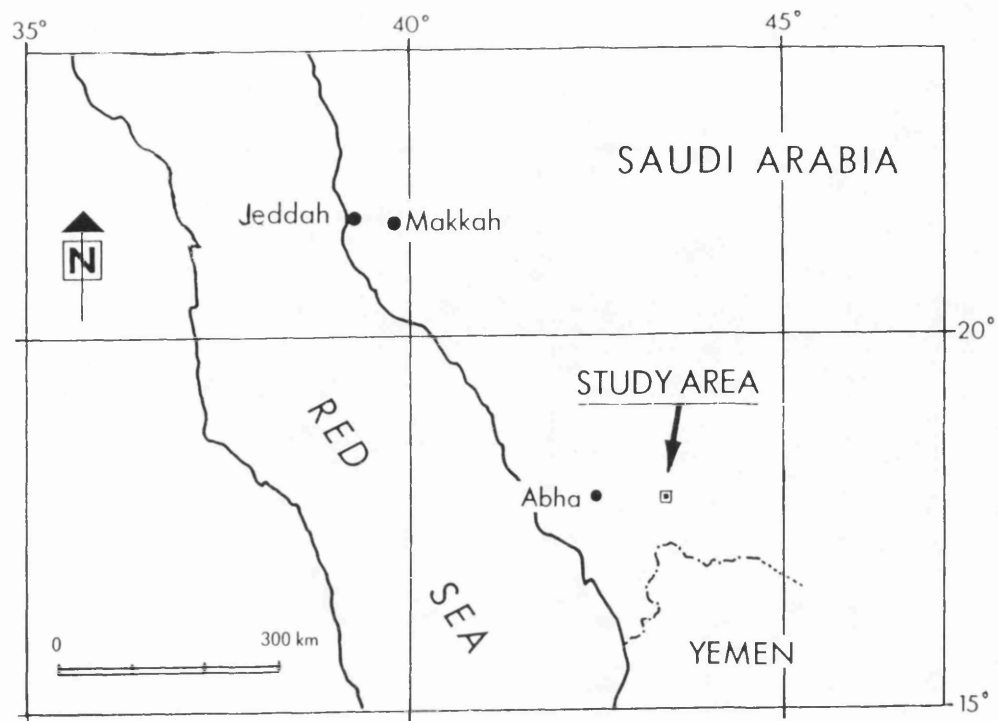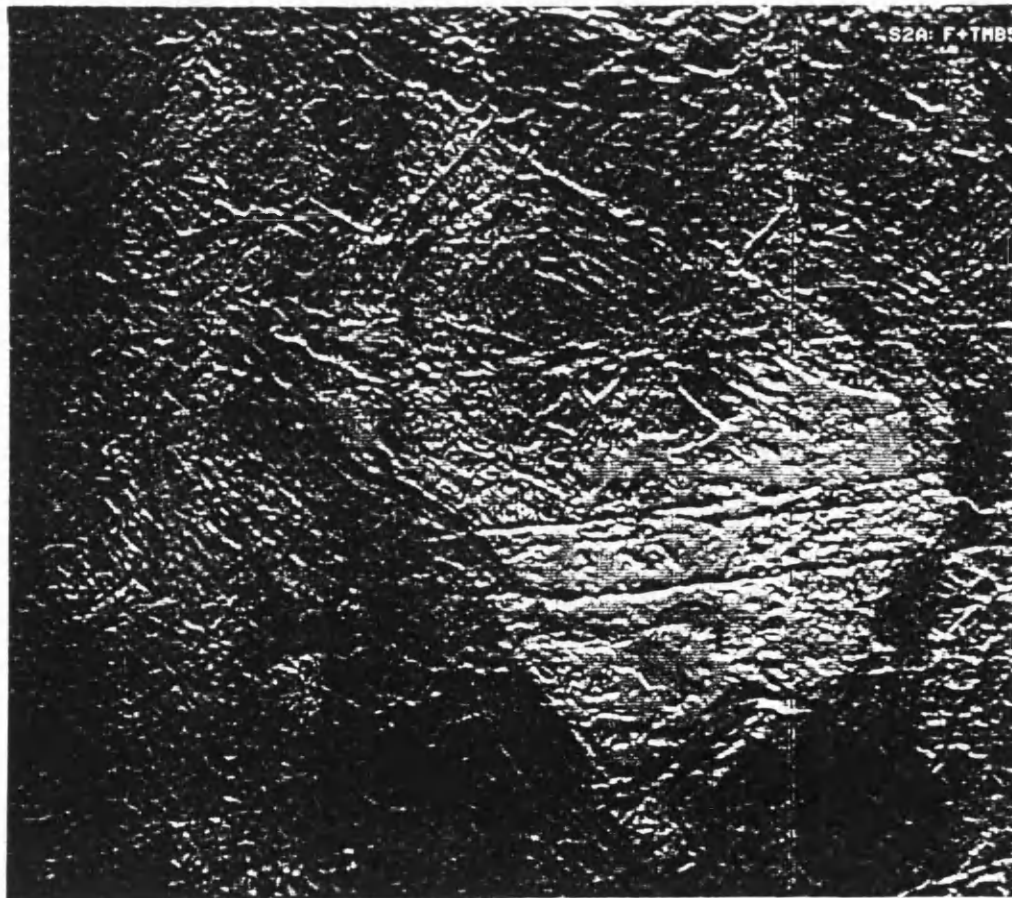
Fig. 1 Location map of the study area.

Fig. 5 Directionally enhanced image superimposing TM-band 5 for the study area.
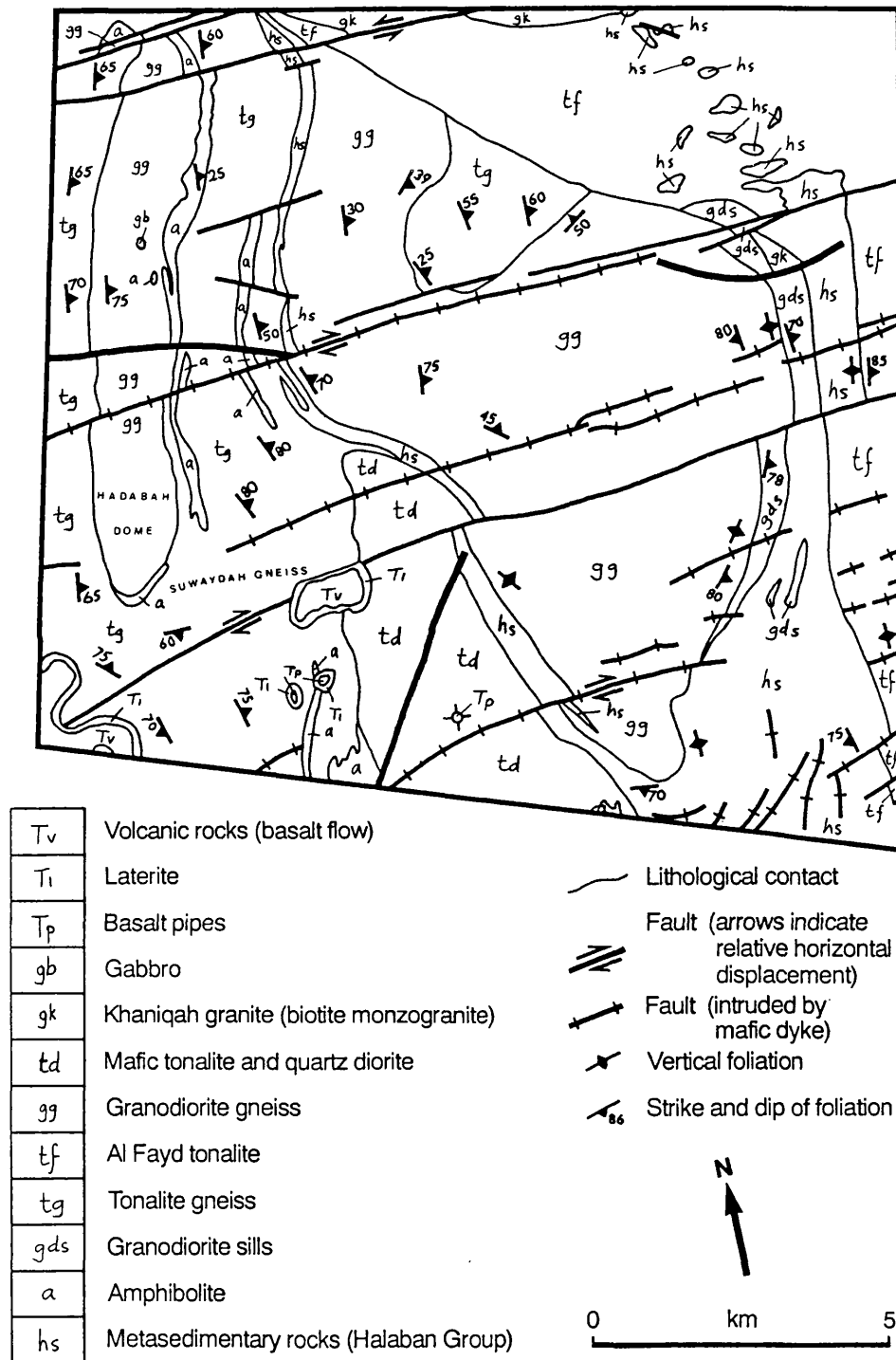
Tv	Volcanic rocks (basalt flow)
Ti	Laterite
Tp	Basalt pipes
gb	Gabbro
gk	Khaniqah granite (biotite monzogranite)
td	Mafic tonalite and quartz diorite
gg	Granodiorite gneiss
tf	Al Fayd tonalite
tg	Tonalite gneiss
gds	Granodiorite sills
a	Amphibolite
hs	Metasedimentary rocks (Halaban Group)

Lithological contact

Fault (arrows indicate relative horizontal displacement)

Fault (intruded by mafic dyke)

Vertical foliation

Strike and dip of foliation

N

0   km   5

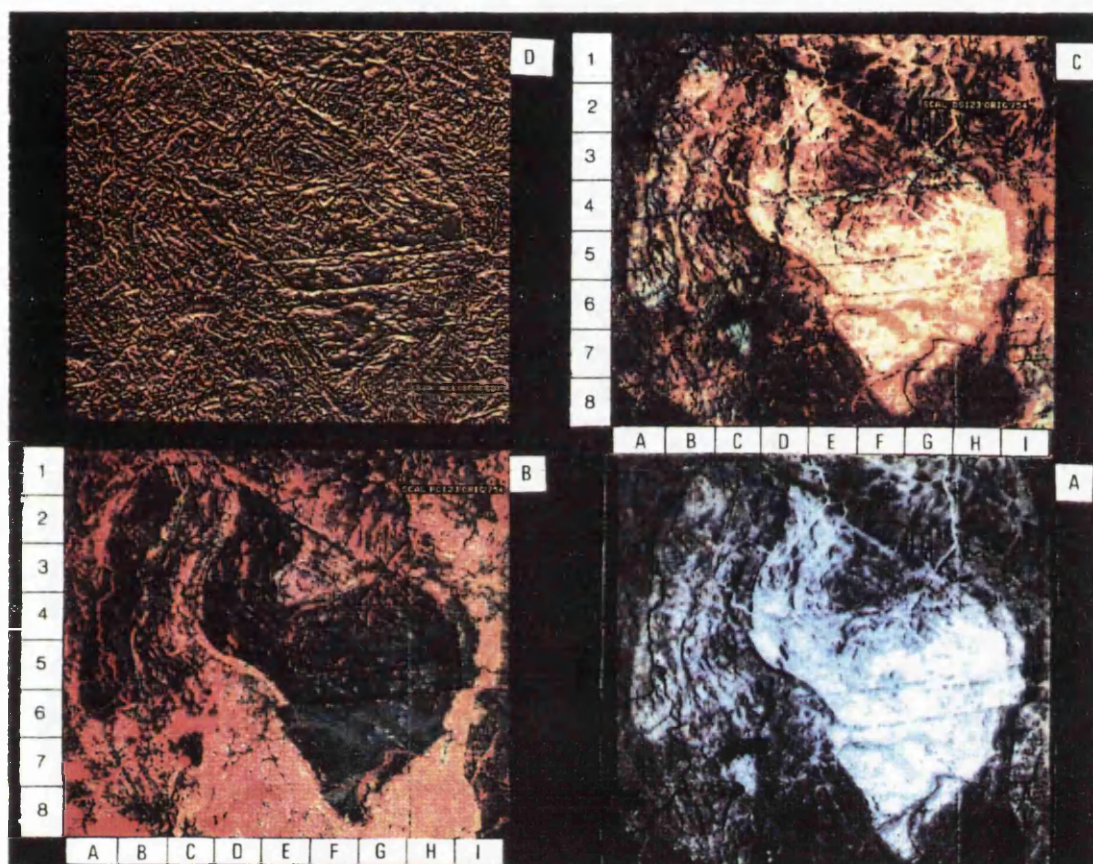Fig. 2 Geological map (after Stoeser, 1984).

Fig. 3 A:TM-band 5 sub-scene for the study area (15x15 km across), B:(-PC) colour composite, C:DS colour composite, D:High-pass filtered image, (see text for details).
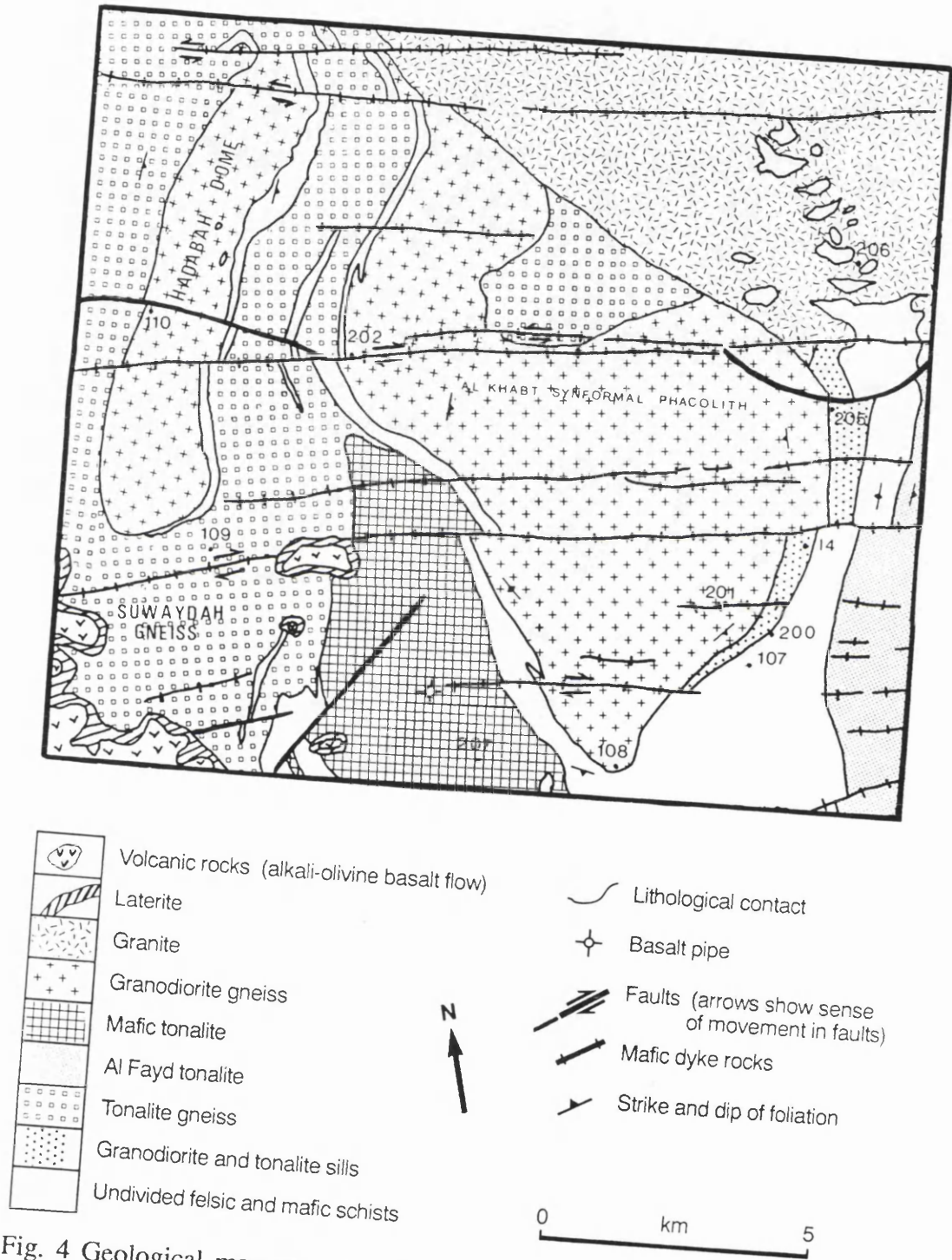
Fig. 4 Geological map constructed from the colour composites. Number indicate eleven localities visited.
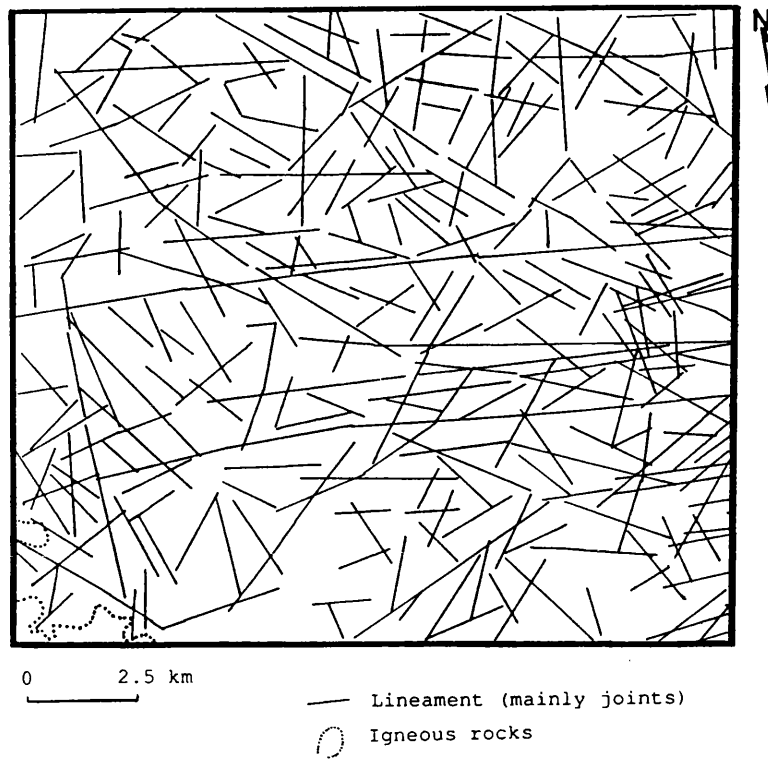
0   2.5 km

——— Lineament (mainly joints)

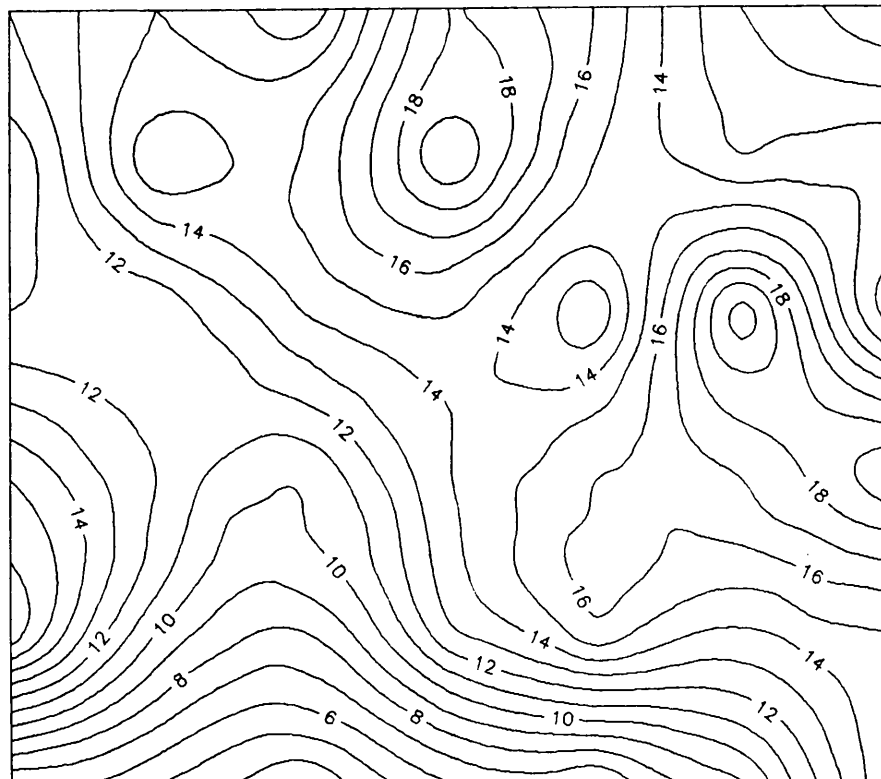Igneous rocks

Fig. 6 Remotely sensed lineament map.

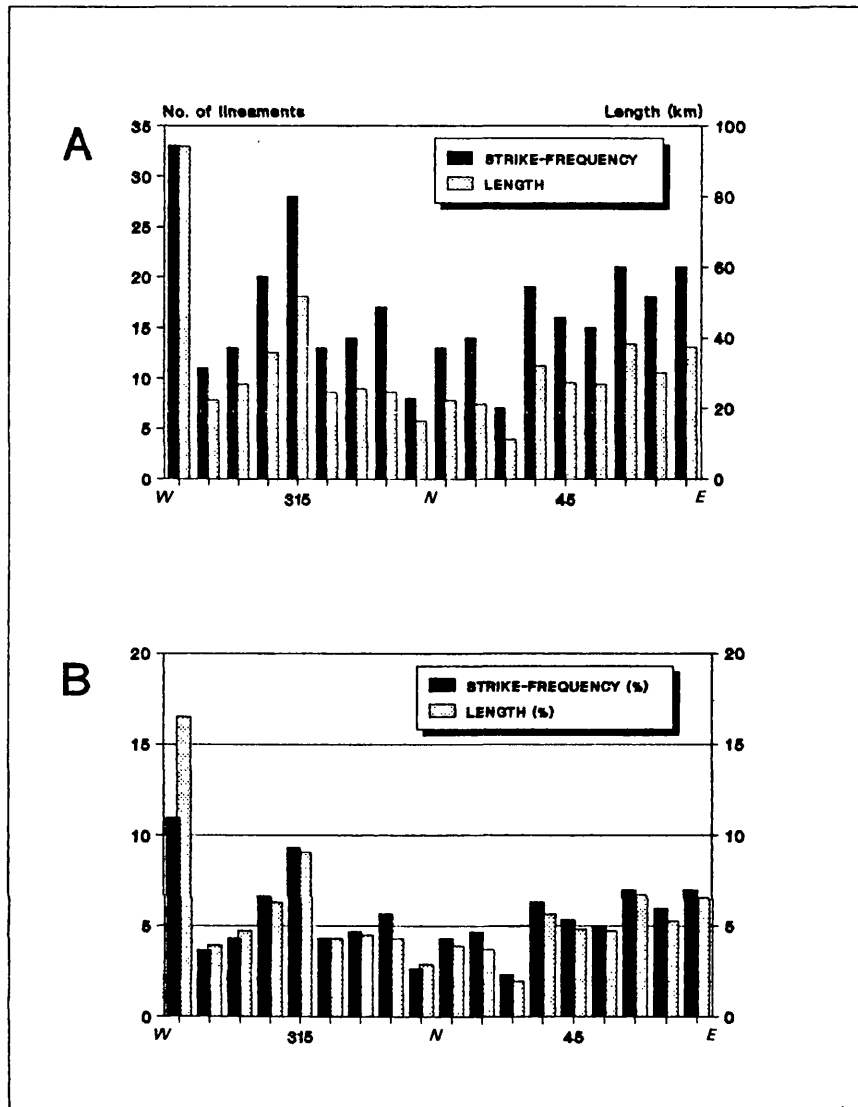Fig. 9 Fracture density isopleth map. Fracture density is expressed in number of fractures/6.25 km^2.

Fig. 7 Histograms summarizing 301 lineaments in Fig. 6, (see text for details).
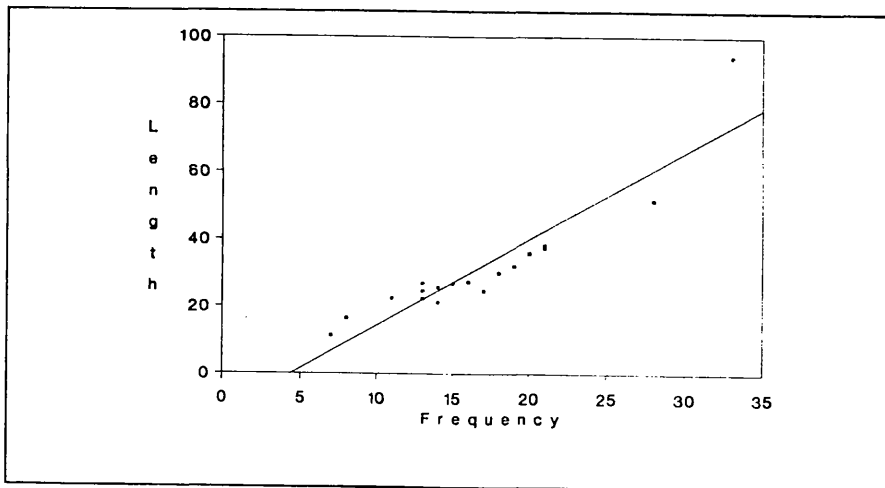

Fig. 8 Cross-plot of frequency versus length for lineaments in the study area.
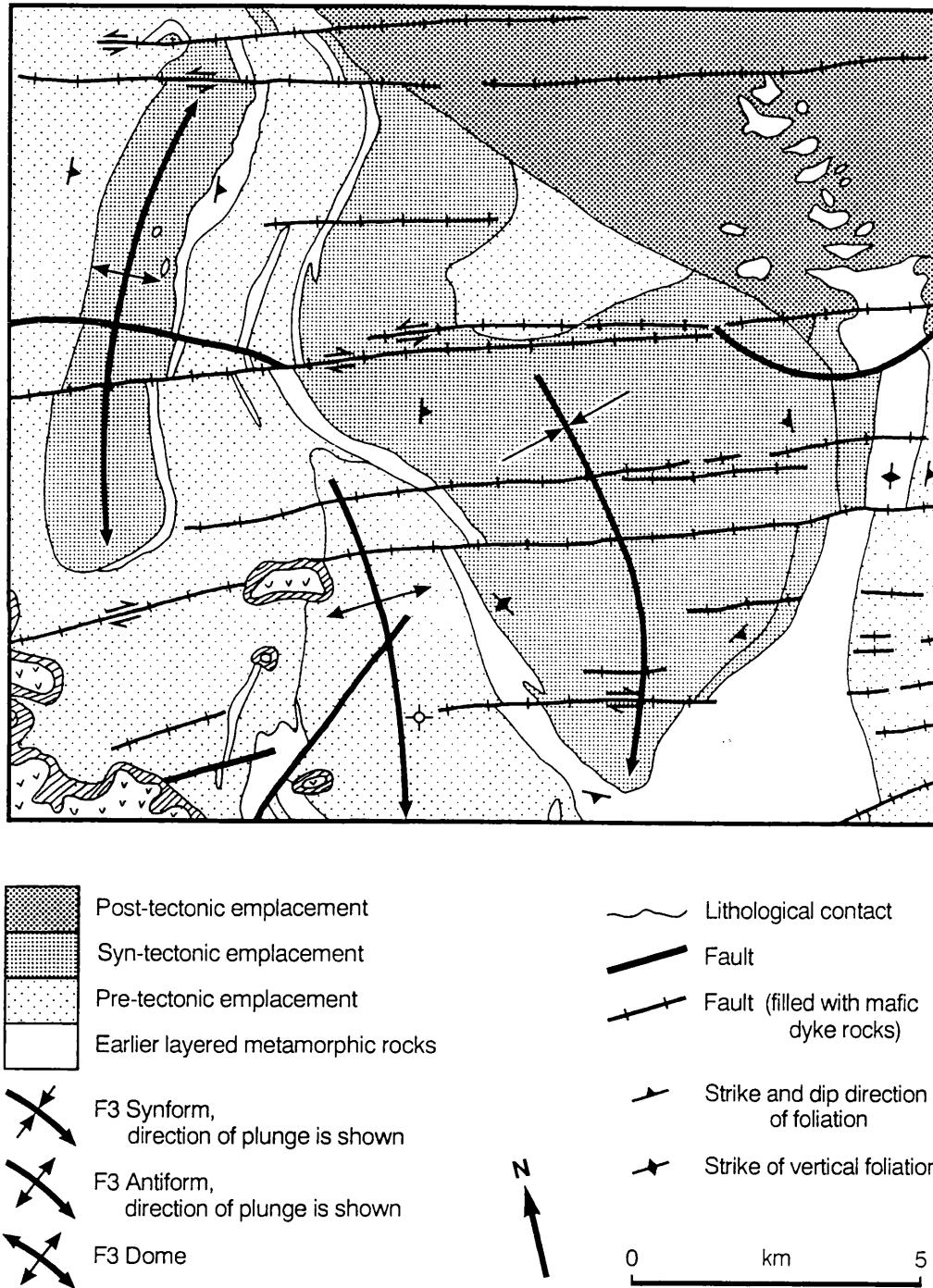
Fig. 10 Structural map constructed from the colour composites, field work, and Stoeser (1984).

GEOLOGICAL MAP OF A PART OF
SOUTHERN ARABIAN SHIELD

N

ASIR TERRANE

NABITAH

MOBILE BELT

TERRANE

PLATE 1

DRAINAGE MAP

SCALE   1 : 500 000

LEGEND

ABHA   City
              Village
              Jabal (mountain(s)
              Wadi
    x   Ancient working or
              mineral locality
              Watershed

LOCATION MAP

N

LEGEND

City   **ABHA'**

Town/village   • TAREEB

Location of observation site   • 153

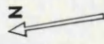Jabal (mount)   × J. HIBR

Mount chain   JIBA'L AL HA'SIR

Asphalt road

Wadi

Elevation (meters)   • 2144

RED SEA

TO BISHAH

TO TATHLEETH   TO RIYADH

J. JANDUF ×

JIBA'L AL HA'SIR

AL HAMDAH

AL AMWAH

W. TATHLEETH

JASH

SUBAYKHAH

AL HAGIRA

AL KHANIQAH

SAMAKH

AL JAZIRAH

AL QADDAH

KHAYBAR AL JANUB

J. SHA'IX

RAGHWAH

AL AREEN (BILAD QAHTAN)

J. HIBR ×

AL MADDAH

KHULAYL

W. BISHAH

AL HAYMAH

WADI BIN HASHBAL

ALMIKTA

KHAMIS MUSHAYT

W. TAREEB

TAREEB

AL JAWF

JIBA'L AS SIRAT

SARAT ABIDAH

AL WAHHABAH

INDANAH

AHAD RUFAYDAH

DALAGHAN

TO NAJRAN

TO AL JAWWAH

TO AL QARA

AL MAHA'ILAH

ABHA'

DILA DESCENT

ASH SHA'AF DESCEN

J. A SOODA

ASH SHI'BAYN

JAZAT AL THULATHA

ASIR ESCARPMENT

TO AL DARB & JIZAN

TO BAHAH

TO MUHAYIL